5 µm

5 µm

Julia C. Singer

Controlling the Morphology of Supramolecular Nano- and Microfibers by Self-Assembly and Electrospinning

Dissertation
Universität Bayreuth, 2014

MV-WISSENSCHAFT

Julia C. Singer

Controlling the Morphology of Supramolecular Nano- and Microfibers by Self-Assembly and Electrospinning

Dissertation

Universität Bayreuth, 2014

MV WISSENSCHAFT

Controlling the Morphology
of Supramolecular Nano- and Microfibers
by Self-Assembly and Electrospinning

Dissertation

zur Erlangung des akademischen Grades
eines Doktors der Naturwissenschaften (Dr. rer. nat.)
im Promotionsprogramm „Polymer Science"
der Bayreuther Graduiertenschule für Mathematik und Naturwissenschaften

vorgelegt von

Julia Christa Singer

geboren in Fürth, Deutschland

Bayreuth, 2014

Die vorliegende Arbeit wurde in der Zeit von Dezember 2010 bis Juli 2014 am Lehrstuhl Makromolekulare Chemie I der Universität Bayreuth unter der Betreuung von Herrn Prof. Dr. Hans-Werner Schmidt angefertigt.

Vollständiger Abdruck der von der Bayreuther Graduiertenschule für Mathematik und Naturwissenschaften (BayNAT) der Universität Bayreuth genehmigten Dissertation zur Erlangung des akademischen Grades eines Doktors der Naturwissenschaften (Dr. rer. nat.).

Dissertation eingereicht am: 22. Juli 2014

Zulassung durch das Leitungsgremium: 27. Juli 2014

Wissenschaftliches Kolloquium: 25. September 2014

Amtierender Direktor: Prof. Dr. Franz Xaver Schmid

Prüfungsausschuss

Prof. Dr. Hans-Werner Schmidt (Erstgutachter)

Prof. Dr. Sema Agarwal (Zweitgutachter)

Prof. Dr. Andreas Fery (Vorsitz)

Prof. Dr. Jürgen Senker

Meiner lieben Familie

«Les choses ne sont pas ce qu'elles sont,
elles sont ce qu'on les fait.»

„Die Dinge sind nie so, wie sie sind.
Sie sind immer das, was man aus ihnen macht."

Jean Anouilh (französischer Dramatiker, 1920-1987)

Table of contents

Summary

This thesis focuses on the preparation, characterization and comparison of supramolecular nano- and microfibers of 1,3,5-benzene- and 1,3,5-cyclohexane-trisamides using two routes: self-assembly from solution as bottom-up approach and melt electrospinning as top-down approach.

The design and the controlled fabrication of fibrous structures from self-assembling molecules have gained increasingly interest in material and life science. Network structures (nonwovens) based on supramolecular materials exhibit intriguing properties. In addition to the high surface area to volume ratio well-defined surfaces are present. A large amount of natural materials are made out of fibrous structures with hierarchical organization.

In this context the *Introduction* summarizes the background of supramolecular chemistry, which is the common *bottom-up approach*. Small molecules self-assemble on the nano- and mesoscale in well-defined structures by the formation of noncovalent bonds. Detailed information of secondary interactions necessary to build up such self-assembled constructs is described. Selected examples from nature and other supramolecular materials are presented. A prominent class of self-assembling molecules are 1,3,5-benzene- and 1,3,5-cyclohexanetrisamides. Since these organic molecules present the key structure of this thesis, a deeper insight of their self-assembly behavior in solution and the resulting solid state is provided. Trisamides self-assemble predominantly into columnar structures via the formation of strong and directed triple hydrogen bonds. In case of 1,3,5-benzenetrisamides, the columnar construct is further stabilized by π-π-interactions. The thermotropic behavior and the formation of a macrodipole within a column can be utilized to manipulate and align those supramolecular structures within an electrical field.

A modern *top-down approach* to prepare fibers is electrospinning of polymers from solution and melt. The electrospinning process is well-studied for the fabrication of polymeric fibers. A polymer solution or melt is subjected to an electrical field, and any droplet is deformed into a cone-like shape (Taylor cone) due to electrostatic repulsion of generated charges at the droplet surface. At stronger electrical fields a jet is ejected from the cone and then accelerated towards a collector. The experimental conditions, such as applied electrical field strength, flow rate or shape of the collector, exhibit parameters to optimize and influence the fiber formation.

A very recent research area focuses on electrospinning of self-assembling small molecules without the addition of a polymer. Only a few examples have been reported on solution electrospinning, and only one molecule was electrospun from melt so far.

The *Objective of this thesis* is the fabrication, characterization and comparison of supramolecular nano- and microfibers based on 1,3,5-benzene- and 1,3,5-cyclohexane-trisamides using the two approaches: self-assembly from solution as bottom-up approach and electrospinning from melt as top-down approach. An objective was the development of structure-property relations concerning the formation of supramolecular nano- and micro fibers, and the mechanical properties of the fibers. Therefore, the chemical structures of 1,3,5-benzene- and 1,3,5-cyclohexanetrisamides was systematically varied. The morphology of obtained fibers was studied and compared in detail and the fiber stiffness was determined.

In the *first chapter*, the influence of the molecular structure of 1,3,5-benzenetrisamides on the mechanical properties of their supramolecular fibers is investigated. Three compounds with different alkyl substituents and varying in the connectivity of the amide linkage to the core were selected. From all compounds, well-defined, self-assembled fibers were obtained by controlled recrystallization from 2,2,4,4,6,8,8-heptamethylnonane (HMN), a high boiling nonpolar solvent, which can be evaporated after fiber formation. The average diameter of the fibers varied from 200 nm to 2 μm depending on the molecular structure. In collaboration with the group of Prof. Andreas Fery, Physical Chemistry II, University of Bayreuth, the flexural rigidities of the fibers were determined using atomic force microscopy (AFM) bending experiments. The corresponding Young's moduli E were calculated to average values of 2.1 to 3.3 GPa. Their values are comparable to semi crystalline, non-orientated polymers. The flexural rigidity of the fibers shows a difference up to three orders of magnitude, however, the Young's modulus of each fiber type is similar. Consequently, the flexural rigidity of the fibers is a pure size effect allowing to tune the rigidity of the fibers by adjusting their diameter.

In the *second chapter*, it was demonstrated for the first time that 1,3,5-benzene- and 1,3,5-cyclohexanetrisamides could be shaped into fibers by melt electrospinning. From the thermotropic nematic phase and, surprisingly, also from the optical isotropic phase, just above the clearing temperature, homogenous and long nano- and microfibers were collected. The fact that fibers are obtained from these low molecular weight substances is a consequence of the supramolecular structure of trisamides. The optical isotropic melt still consists of very small columnar aggregates; thus, it is assumed that their macrodipoles are acting with the electrical field and contribute to the formation of fibers. The influence of the spinning temperature and the applied electrical field strength were studied in detail. An increasing temperature resulted in an augmented sphere formation, whereas, long and thinner fibers were obtained with increasing field strength.

The focus of the *third chapter* is on melt electrospinning of small molecules. A more detailed structure-property relation of trisamides and other self-assembling molecules was investigated. The amount and type of secondary interactions were systematically investigated to gain more information about the applicability of this new top-down approach. Different sets of compounds, including 1,3,5-benzene- and 1,3,5-cyclohexanetrisamides varying in substituents and in the connectivity of the amide linkage to the core, bisamides with benzene-, naphtyl- and cyclohexane moieties, sorbitol derivates and perylenebisimide derivates were selected. Also 1,3,5-benzenetrisamides incapable of forming hydrogen bonds were investigated. The electrospun morphology was correlated with the molecular structure. 1,3,5-benzene- and 1,3,5-cyclohexanetrisamides form most often and reliable fibers during melt electrospinning. Electrospinning of bisamides and sorbitol derivates resulted mostly in the formation of spheres due to insufficient strong secondary interactions. Due to the fast cooling of the melt during the process, supramolecular fiber formation has no time to develop. For the first time, it was shown that perylenebisimide can be shaped into fibers, since sufficient π-π-interactions are present. By melt electrospinning of tertiary 1,3,5-benzenetrismaides, it was surprisingly found that hydrogen bonds are not absolutely necessary to collect fibers.

The *fourth chapter* connects and compares the self-assembly and melt electrospinning approach. Therefore, melt electrospun and self-assembled 1,3,5-benzene-tricarboxamide fibers were characterized on different length scales including crystal structure, fiber morphology and mechanical properties. From one compound, fibers with significantly different morphologies were obtained by the top-down and the bottom-up approach. Melt electrospun fibers offered a smooth and homogenous surface, whereas self-assembled fibers were hierarchically structured by a bundle-like structure. On the Ångström scale, X-ray diffraction revealed the same crystal structure of both fiber types. However, despite the morphological differences, nanomechanical bending experiments show that the Young's modulus (E= 3.6-4.7 GPa) is comparable for self-assembled and melt electrospun fibers. The results are in the same range as further supramolecular 1,3,5-benzenetrisamide fibers presented in the first chapter.

The results of this thesis reveal that 1,3,5-benzene- and 1,3,5-cyclohexanetrisamides can be shaped into nano- and microfibers using powerful bottom-up and top-down approaches. Their interesting morphology combined with their mechanical properties make this class of low molecular weight substances suitable for constructing new materials, such as hierarchically structured nonwovens for efficient filter applications.

Zusammenfassung

Im Fokus dieser Arbeit steht vor allem die Herstellung und Charakterisierung von supramolekularen Nano- und Mikrofasern aus 1,3,5-Benzol- und 1,3,5-Cyclohexantrisamiden. Zur Faserherstellung wurden zwei bekannte Prozesse untersucht: Als sogenannter Bottom-up-Ansatz wurde die Selbstassemblierung aus Lösung und als Top-down-Methode Schmelzelektrospinnen gewählt.

In den Materialwissenschaften sowie im Life-Science-Bereich hat das Design sowie die gezielte Herstellung von faserigen Strukturen ein zunehmendes Interesse geweckt. Diese Fasern werden vor allem durch ihre definierte Oberflächenmorphologie charakterisiert. Netzwerke und Gewebe bestehend aus solchen feinen, definierten Strukturen zeichnen sich daher besonders durch ihre außergewöhnlichen Eigenschaften wie ein hohes Oberflächen-zu-Volumen-Verhältnis. Viele natürlichen Materialen sind zudem aus Fasern, Fibrillen und hierarchisch strukturieren Bausteinen aufgebaut.

In diesem Zusammenhang werden in der *Einleitung* zuerst die Grundlagen der supramolekularen Chemie, angewendet als typische *Bottom-up-Methode*, zusammengefasst. Einzelne Moleküle ordnen sich durch die Ausbildung von gerichteten und reversiblen, nichtkovalenten Wechselwirkungen zu nanoskaligen Strukturen an. Mögliche sekundäre Wechselwirkungen, die zum Aufbau definierter, selbstassemblierter Gebilde nötig sind, werden im Weiteren detailliert erläutert. Ebenso werden ausgewählte Beispiele aus der Natur sowie weitere supramolekulare Fasern diskutiert. Zu den prominenten Vertretern selbstassemblierender Moleküle zählen 1,3,5-Benzol- und 1,3,5-Cyclohexantrisamide, welche die Hauptverbindungsklasse dieser Arbeit darstellen. Es wird vor allem ihre Selbstorganisation im festen und flüssigen Zustand näher betrachtet. Trisamide organisieren sich über die Ausbildung von starken und gerichteten Wasserstoffbrückenbindungen zu kolumnaren Strukturen. Diese kolumnaren Gebilde werden im Fall von 1,3,5-Benzoltrisamiden zusätzlich durch π-π-Wechselwirkungen stabilisiert. 1,3,5-Benzol- und 1,3,5-Cyclohexantrisamide zeigen oftmals ein thermotropes, flüssigkristallines Verhalten. Zudem bildet sich entlang der Kolumnenachse ein Makrodipol aus. Dieser kann dazu genutzt werden, die gebildeten supramolekularen Strukturen im elektrischen Feld auszurichten und zu manipulieren.

Eine typische *Top-down-Methode* zur Herstellung von Fasern ist Elektrospinnen aus Lösung oder Schmelze. Für Polymerfasern ist der Elektrospinnprozess bereits sehr gut untersucht. Eine Polymerlösung oder –schmelze wird kontinuierlich aus einer Düse in ein angelegtes elektrisches Feld transportiert. Jeder Tropfen, der sich am Düsenende bildet, wird durch die elektrostatischen Abstoßungen der an der Tropfenoberfläche

induzierten Ladungen in Längsrichtung deformiert (Taylor-Kegel). In einem genügend starken elektrischen Feld wird aus dem Kegel ein Strahl ausgestoßen, der im elektrischen Feld in Richtung eines Kollektors beschleunigt wird. Die experimentellen Bedingungen, wie die angelegte elektrische Feldstärke, die Flussrate oder die Form des Kollektors, haben einen enormen Einfluss auf die Faserbildung.

Ein neues, vielversprechendes Forschungsgebiet umfasst das Elektrospinnen von kleinen, selbstassemblierten Molekülen, ohne den Einsatz einer Polymermatrix. Bisher sind nur sehr wenige Verbindungen bekannt, aus denen Fasern durch Lösungselektrospinnen gebildet werden können. Zudem ist bisher nur ein Beispiel über Schmelzelektrospinnen publiziert.

Das Ziel und die Motivation der vorliegenden Arbeit war die Herstellung, die Charakterisierung und der Vergleich supramolekularer 1,3,5-Benzol- und 1,3,5-Cyclohexantrisamid-Fasern. Zur Faserherstellung wurden sowohl der Bottom-up- als auch der Top-down-Ansatz gewählt. Ein wichtiges Ziel war die Entwicklung von Struktur-Eigenschafts-Beziehungen. Dafür wurde die Molekülstruktur der Trisamide systematisch geändert, die Morphologie der entstandenen selbstassemblierten und schmelzelektrogesponnenen Fasern eingehend untersucht und verglichen, sowie deren Biegesteifheit in Kooperation mit der Gruppe von Prof. Andreas Fery, Physikalische Chemie II, Universität Bayreuth, bestimmt.

Im *ersten Kapitel* wurde der Einfluss der molekularen Struktur von 1,3,5-Benzoltrisamiden auf die mechanischen Eigenschaften der supramolekularen Fasern untersucht. Drei Verbindungen wurden ausgewählt, welche sich in der Auswahl der Alkyl-Substituten sowie in der Verknüpfung der Amidbindungen zum zentralen Kern unterscheiden. Aus allen Verbindungen konnten durch kontrollierte Selbstorganisation (Bottom-up-Methode) aus 2,2,4,4,6,8,8-Heptamethylnonan (HMN), einem hochsiedenden, unpolaren Lösungsmittel, definierte Fasern hergestellt werden. Der mittlere Faserdurchmesser lag, abhängig von der Molekülstruktur, zwischen 200 nm und 2 µm. Mittels Rasterkraftmikroskopie (AFM) konnte die Biegesteifigkeit der selbstassemblierten Fasern erfasst, sowie die entsprechenden Elastizitätsmoduli mit E= 2.1-3.3 GPa berechnet werden. Die Elastizitätsmoduli sind vergleichbar mit denen von teilkristallinen, nicht orientierten Polymerfasern. Obwohl sich die Werte der Biegesteifigkeiten um bis zu drei Größenordnungen unterschieden, waren die Elastizitätsmoduli der Fasern ähnlich. Der Unterschied in den Biegesteifigkeiten der Fasern ist somit auf einen reinen Größeneffekt zurückzuführen. Durch ein gezieltes Moleküldesign kann der Faserdurchmesser eingestellt werden und ermöglicht so die genaue Einstellung und Vorhersage der Biegesteifigkeiten.

Im *zweiten Kapitel* konnte zum ersten Mal gezeigt werden, dass sich 1,3,5-Benzol- und 1,3,5-Cyclohexantrisamide durch Schmelzelektrospinnen zu Fasern im Nano- und Mikrometerbereich verarbeiten lassen (Top-down-Methode). Lange und einheitliche Fasern wurden sowohl aus der thermotropen nematischen Phase als überraschender-weise auch aus der optisch isotropen Schmelze gewonnen. Dass es gelang diese niedermolekularen Verbindungen zu Fasern zu verarbeiten, lässt sich auf die supra-molekularen Eigenschaften der Trisamide zurückführen. Da sich in der optisch isotropen Schmelze immer noch sehr kleine, kolumnare Aggregate befinden, wird vermutet, dass die vorhandenen Makrodipole mit dem angelegenen elektrischen Feld wechselwirken. Die verbleibenden sekundären Wechselwirkungen in den Kolumnen müssen gleichzeitig stark genug sein, um das Zerreißen des Elektrospinnstrahls zu Tröpfchen zu verhindern. Darüber hinaus wurde der Einfluss der Temperatur und der elektrischen Feldstärke eingehend untersucht. Mit ansteigender Temperatur wurde eine vermehrte Kugelbildung beobachtet, wohingegen mit einer höheren elektrischen Feldstärke lange und dünnere Fasern erzeugt werden konnten.

Das *dritte Kapitel* befasst sich intensiv mit dem Schmelzelektrospinnen niedermolekularer, selbstassemblierender Moleküle. Die Anzahl und die Art der sekundären Wechselwirkungen wurden dabei systematisch variiert und detailliert untersucht, um diesen neuartigen Top-Down-Ansatz besser zu verstehen. Zu den für die Studie ausgewählten Substanzklassen gehören 1,3,5-Benzol- und 1,3,5-Cyclohexan-trisamide, die sich sowohl in ihrer Peripherie als auch in der Verknüpfung der Amidbindungen zum zentralen Kern unterscheiden. Des Weiteren wurden Bisamide mit Benzol, Naphtyl oder Cyclohexan als zentrale Einheit, Sorbitol- und Perylenbisimid-Derivate gewählt. Zudem wurden tertiäre 1,3,5-Benzoltrisamide, welche keine Wasserstoffbrücken-Bindungen ausbilden können, ausgesucht. Alle aus dem Schmelzelektrospinnen erhaltenen Morphologien wurden mit der Molekülstruktur korreliert. Vor allem aus 1,3,5-Benzol- und 1,3,5-Cyclohexantrisamides konnten zuverlässig schmelzelektrogesponnene Nano- und Mikrofasern hergestellt werden. Beim Elektrospinnen von Bisamiden und Sorbitol-Derivaten wurden fast ausschließlich Kugeln mit einigen Mikrometern im Durchmesser erzeugt. Die sekundären Wechselwirkungen, die sich ausbilden während die Schmelze im Elektrospinnprozess sehr schnell abgekühlt wird, sind nicht stark genug, um das Zerreißen des Elektrospinnstrahls in Tröpfchen zu verhindern. Dagegen konnte zum ersten Mal gezeigt werden, dass Perylenbisimid-Derivate zu Fasern verarbeitet werden können, da auch in der Schmelze noch ausreichend starke π-π-Wechselwirkungen zwischen den Molekülen vorhanden sind. Dass Wasserstoffbrückenbindungen nicht unbedingt nötig sind, um Fasern aus niedermolekularen Substanzen durch Schmelzelektrospinnen herzustellen,

wurde durch das erfolgreiche Verspinnen von tertiäre 1,3,5-Benzoltrisamiden bewiesen. Durch eine sorgfältige Auswahl der niedermolekularen Substanzen ist es möglich, gewünschte elektrogesponnenen Morphologien, wie Fasern, perlschnurähnliche Fasern und Kugeln, vorherzusagen und einzustellen.

Im *vierten Teil* der Arbeit wurden alle Ergebnisse dieser Arbeit miteinander verknüpft und verglichen. Dafür wurden schmelzelektrogesponnene und selbstassemblierte 1,3,5-Benzoltrisamid-Fasern einer Verbindung auf verschiedenen Längenskalen charakterisiert und miteinander verglichen. Im Fokus standen dabei die Kristallstruktur, die Fasermorphologie sowie die mechanischen Eigenschaften. Über den Top-down-bzw. den Bottom-up-Ansatz wurden deutlich verschiedene Fasern erzeugt. Die schmelzelektrogesponnenen Fasern zeichneten sich durch eine glatte und defektfreie Oberfläche aus. Die selbstassemblierte Fasern hingegen waren hierarchisch strukturiert und durch eine bündelartige Struktur, bestehend aus vielen einzelnen Fibrillen, charakterisiert. Mittels Röntgenbeugung wurden die Fasern auf der Ångström-Skala untersucht und es wurde für beide Fasertypen die gleiche Kristallstruktur gefunden. Obwohl sich die Fasernmorphologie derart unterscheidet, wurde durch nanomechanische Biegeexperimente bewiesen, dass die Elastizitätsmoduli beider Fasertypen im selben Bereich liegen (E= 3.6-4.7 GPa). Die mechanischen Eigenschaften waren somit auch mit den Ergebnissen anderer selbstassemblierter Trisamid-Fasern vergleichbar (siehe erstes Kapitel).

Mit den Forschungsergebnissen, die im Rahmen der vorliegenden Arbeit gewonnen werden konnten, wurde gezeigt, dass 1,3,5-Benzol- und 1,3,5-Cyclohexantrisamide zu Fasern mit einem Durchmesser im Nano- und unteren Mikrometerbereich (200 nm bis 10 μm) verarbeitet werden können. Zur Faserherstellung konnten sowohl der Bottom-up- als auch erstmals der Top-Down-Ansatz als kraftvolle Methoden etabliert werden. Die interessante Morphologie der Fasern sowie ihre hervorragenden mechanischen Eigenschaften machen es dieser niedermolekularen Substanzklasse möglich, in neuen Materialien, wie beispielsweise in hierarchisch strukturierten Vliesen für effiziente Filteranwendungen, eingesetzt zu werden.

1   Introduction

In our daily routine we are surrounded by diverse technical equipments, high-tech products and further countless objects facilitating, supporting and maintaining our life. A tremendous amount of these applications are made of fibers or are based on fibrous materials. Fibers are one-dimensional, flexible structural elements characterized by an outstanding ratio of length to diameter of at least 3:1 and up to more than 1000:1.[1,2] Natural and synthetic fibers accompany us in textiles ranging from home textiles, street wear over active wear to protective clothes. They are present in hygiene and sanitary products as well as in filter applications for liquids and air as found in normal coffee filters, vacuum cleaners or air conditioners. Particularly, nature itself takes the advantage of mechanically robust fibers to build successful biological materials. These mostly hierarchical structures cover many length scales and are found in flora, fauna as well as in human bodies in form of e.g. wood, leaves, stalks, bones, blood vessels and nerves.[3] A benefit of nanofibers, in particular, is the achieved high surface area to volume ratio, thousand times higher than human hair and desired for a wide variety of applications. Proposed uses of nanofibers include biomedical applications such as wound dressing, vascular grafts, artificial skin and tissue engineering, drug delivery systems as well as technical areas like (breathable) textiles, sensors, filters and membranes.[4,5]

To realize a sustainable, safe and healthy society, scientists focus more and more on the controlled fabrication of well-defined one-dimensional structures.[6] There are two approaches leading to micro- and nanofibers, denoted as *bottom-up* and *top-down approach* (Figure 1). Typical bottom-up approaches cover the self-assembly and the self-organization of smaller units such as single molecules or polymeric building blocks, forming hierarchically structured fibers.[7,8] The most prominent top-down approaches in industry are dry spinning, wet spinning, melt spinning and other techniques to manufacture synthetic fibers.

Industrial fiber spinning starts from solution or bulk, and desired shaped fibers with a diameter range from 2 μm to 500 μm are produced in these pressure driven extrusions of a viscous polymer solution or melt. Multiple dies are used to produce simultaneously a large amount of fibers. The polymeric fibers are collected on a rotating drum inducing additional stretching to increase strength and orientation.
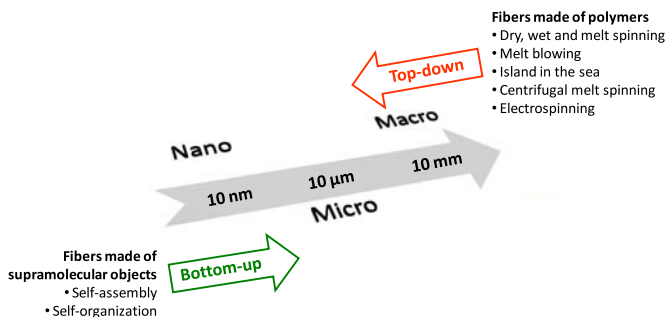
Figure 1. Preparation of micro-and nanofibers by bottom-up and top-down approaches. [Modified from reference 9.]

Dry spinning is the technique of choice when polymers have to be dissolved in a solvent to be spun. The solidification of the fibers occurs by evaporation of the solvent during the spinning process facilitated by an air or inert gas stream.[10] Also for wet spinning the polymer has to be dissolved. The polymer solution gets spun directly into a liquid bath filled with a non-solvent and fibers are obtained by precipitation or coagulation.[11,12] Melt spinning utilizes the polymer melt to spin fibers.[13,14] In melt blowing equipments polymer melts of low viscosity are blown towards the collector using a high velocity air stream, and fibers with diameters below 1 μm can be achieved.[15,16] The solidification of the fibers occurs for both melt extrusion processes simply by cooling, quickened by an air or inert gas stream. Other industrial techniques to produce submicron fibers are island in the sea[17] and centrifugal melt spinning.[18]

An interesting top-down approach to gain nonwovens with sub-micron diameters is electrospinning from solution or melt. The fibers produced by electrospinning are usually one to two magnitudes smaller than fibers gained by most conventional techniques.[19]

This thesis focus addresses both types of fiber formation, self-assembly and electrospinning. Self-assembly processes are based on supramolecular chemistry, and many fibers are formed simultaneously from solution. Moreover, the size of the batch can easily be up-scaled. Usually, self-assembled fibers have limited lengths. Electrospinning results in nonwovens with infinite long fibers, which can be easily aligned and orientated.[20] In the following, both approaches are discussed in more detail.

1.1 Supramolecular chemistry

Supramolecular chemistry is a typical bottom-up approach. Early work in the field of supramolecular chemistry concerned just two components, a host and a guest. In 1894 Emil Fischer defined the "lock-and-key" model for enzyme-substrate interactions.[21] The host and the guest components interact in a non-covalent fashion. The host is made of a large cyclic molecule or aggregate forming an intrinsic molecular cavity. Into this central hole of convenient size the guest molecule, a small molecule or ion, can be integrated. In any case, the bond of the guest in the host must be selective and involves a special mutual attraction of lock and key (Figure 2). Recent research works concerning host-guest-complexes focus especially on metal-organic frameworks (MOFs) and on inorganic hosts, e.g. zeolites.[22,23]
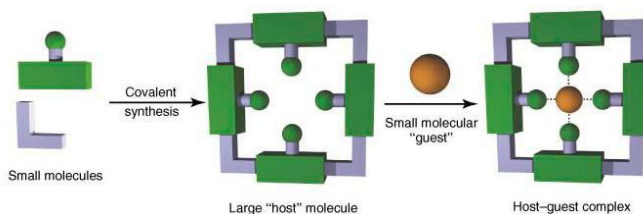
Figure 2. Schematic model of the molecular host-guest chemistry. [Scheme modified with permission from reference 22. Copyright © 2012, John Wiley & Sons. Ltd.]

In its modern sense supramolecular chemistry includes, besides host-guest chemistry, all aspects of self-assembly. This extended supramolecular concept was defined by Jean-Marie Lehn in 1978 as "*the chemistry of molecular assemblies and intermolecular bonds*".[24] Further explanations refer to "*the chemistry beyond the molecule*", "*the chemistry of the noncovalent bond*" or the "*chemistry of the intermolecular bond*".[7] In a supramolecular approach which is a common bottom-up method, single molecules or smaller units self-assemble spontaneously and reversible into nanoscale constructions by the formation of additive and cooperative noncovalent bonds. The small building blocks with carefully chosen shape, size, functional groups and consequently defined properties, such as solubility and melting point, determine the shape, size and properties of the dynamic supramolecular construct.

The supramolecular approach comprises the study, the intelligent design as well as discrete functions and properties of intermolecularly bonded molecules. In contrast to molecular chemistry which is the chemistry of covalent bonds, the self-assembly concept creates self-assembled aggregates (Figure 3). For their pioneer contributions to supramolecular chemistry, Jean-Marie Lehn, Charles Pedersen and Donald Cram were honored with the Nobel Prize in 1987.[7,23-28]
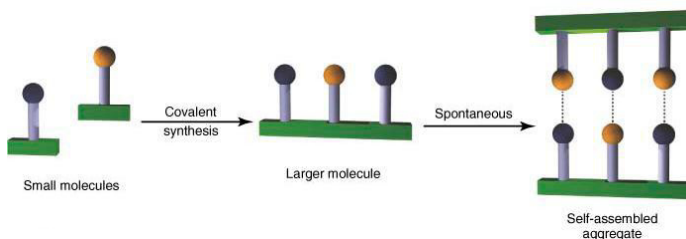
Figure 3. Schematic illustration of self-assembly concept. [Scheme modified with permission from reference 22. Copyright © 2012, John Wiley & Sons. Ltd.]

The concepts of self-assembly and self-organization are often mixed. However, they are distinguished in their thermodynamic behavior. In contrast to self-organization processes self-assembly systems reach their equilibrium without any outside force. In the case of self-organization processes energy is required to achieve a nonequilibrium state.[29]

1.1.1   Supramolecular interactions

The formation of noncovalent forces and interactions, the key element in supramolecular chemistry, encompasses ion-ion, ion-dipole, dipole-dipole, van-der-Waals, metal-metal, π-π, cation-π and anion- π interactions, as well as coordination, halogen and hydrogen bonds. These interactions can be nondirectional, slightly directional or directional by constructing molecular assemblies. [30]

Simple inorganic salts, as sodium chloride, are built of ion-ion forces, forming a well-defined isotropic lattice. These electrostatic interactions have extreme bond strengths of 100-350 kJ·mol^{-1}. In contrast, van-der-Waals bond energies are below 5 kJ·mol^{-1}. Closed-shell metal-metal interactions, known from agentophilic and aurophilic cation systems e.g. Ag(I) and Au(I), are in the range of 5 kJ·mol^{-1} to 60 kJ·mol^{-1}. All three interactions are of nondirectional nature.[23,30] Covalent carbon-carbon single bonds are typically 348 kJ·mol^{-1}.

Slightly directional forces result from ion-dipole and dipole-dipole interactions formed due to electrostatic attractions by an ion and a neutral molecule with a dipole or by two molecules with dipoles, respectively. The bond energies are 5-50 kJ·mol^{-1} for dipole-dipole interactions and for ion-dipole forces in the range of 50 kJ·mol^{-1} to 200 kJ·mol^{-1}.[30]

The supramolecular interactions discussed in the following are directional. Widely used in supramolecular chemistry are coordination bonds of complexes of transition-metal-ions with ligands, such as metal-pyridine complexes. Coordination bonds are reversible and form reasonable bond energies of 100 kJ·mol^{-1} to 300 kJ·mol^{-1}.[30]

If an electron-deficient halogen atom (Lewis acid) interacts with an electron-rich atom (neutral or anionic Lewis base), an attractive halogen bond is formed in the order of 10 kJ·mol^{-1} to 50 kJ·mol^{-1}.[30,31]

Hydrogen bonds and π-π interactions are assigned to be the the most important interactions in supramolecular chemistry. Hydrogen bonds are present in various length, strength (4-120 kJ·mol^{-1}) and geometries. They were firstly described by Linus Pauling in 1931.[32] In general, a hydrogen bond bridges two atoms A and B and is drawn as A-H···B. The donor bond is A-H. Thus, atom B has to bring a lone pair of electrons or polarizable π-electrons to act as acceptor, and so a reversible hydrogen bond can be formed. A strong hydrogen bond on an almost covalent level is formed, for example, by HF complexes or strong acids and bases. Moderate bond energies are reached by acids, alcohols and several biomolecules by a mostly electrostatic character of the hydrogen bonds. C-H···O interactions are comparable weak as they are of pure electrostatic nature.[23,30,33]

Examples of π-π-stacking compounds are common organic compounds such as benzene. The bond energies reach values of 2 to 50 kJ·mol^{-1}. Regarding a benzene dimer as important consideration, five possible structures can be formed. Figure 4 shows the a) face-to-face parallel stacked, b) offset parallel stacked, c) T-shaped edge to edge and d) and e) two tilted T-geometries. σ-π attraction forces have to balance π-π-electronic repulsions, dominating in structure a), to result in a favorable electrostatic interaction. In solid states, the π-surfaces self-assemble in a stacked or herringbone structure shape.[23,30,34,35]
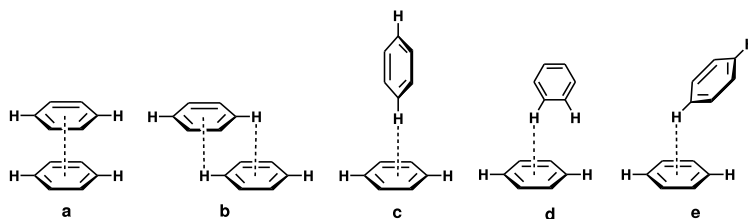

Figure 4. Possible structures of a benzene dimer: a) face-to-face parallel stacked, b) offset parallel stacked, c) T-shaped edge to edge, d) and e) tilted T-geometry.[35]

If organic ions or alkali-metal cations show affinities for aromatic structures, cationic-π and anionic-π-interactions are formed. The electrostatic forces occur within bond strengths of 5 to 80 kJ·mol^{-1}.[23,30]

1.1.2 Self-assembly in nature and further examples of supramolecular fibers

The main challenge in supramolecular chemistry is to understand, design and apply the noncovalent interactions in an intelligent fashion to construct functional supramolecular architectures. Some important facts can be learned and adopted from nature.

Our human body is made of several self-assembled nanofibers of different dimensions. Thereby, collagen is the major building unit of tissues, tendons and bones, and provides mechanical stability, elasticity, and strength to organisms. In the extracellular matrix, the stiffness of the collagen fibers is responsible for structural and biochemical support. Collagen molecules are made of covalent bonded amino acids. These polypeptides of 300 nm in length and 1.6 nm in diameter develop a triple helix stabilized by hydrogen bonds. Always three of the helices self-assemble into a several micrometer long and 100 nm thin collagen fibril. The fibrils self-assemble in lateral and longitudinal directions into collagen fibers up to several millimeters in length and diameter of 10 μm. Those supramolecular collagen fibers are the basis material of the construction of tissues, like tendons and bones.[36] This complex, but for the human being crucial, self-assembly mechanism is represented in Figure 5.
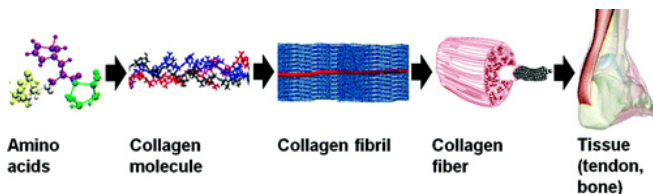
Figure 5. Hierarchical structure of collagen protein materials forming tendons and bones. [Reprinted with permission from reference 36. Copyright (2011) American Chemical Society.]

The list of supramolecular assemblies in nature is long and can also be found in most diverse fields of flora and fauna. For instance, the self-assembly of peptides is also essential for viruses. In the tobacco mosaic virus (TMV) 2130 identical protein molecules self-assemble in a regular helical array around an RNA strand forming a rod structure with around 300 nm in length and 18 nm in diameter.[37]

The self-assembly of amphiphiles in aqueous or organic media is well-studied. Amphiphiles carry a polar head group and a hydrophobic tail and can form, besides nanofibers, a broad variety of geometries, such as vesicles, tubes, disks, lamellas and helices, depending on molecular shape and concentration. The self-assembled amphiphiles form secondary and tertiary structures by interacting with the surrounding environment similarly to protein folding. Amphiphiles, which are applied as organo- and

hydrogelators, as surfactants, emulsifiers or as phospholipids, are a major building block in cell membranes.[38,39]

More and more research groups focus on the well-defined design of self-assembled, one-dimensional nanofibers, especially designed for applications in nanodevices.[7] In supramolecular organic semiconductors the molecules are stacked via π-π-interactions forming wire-like units, sometimes additionally stabilized by hydrogen bonds. The often disc-shaped aromatic core units show thermotropic behavior and form discotic liquid crystalline phases. In electronic devices the molecules have to stack in an accurate way to allow an optimal charge carrier transport along the columnar axis. Often used are perylene bisimide, porphyrin, triphenylene or carbazol units. For solar cells, systems containing p- and n-type nanofibers might be an encouraging approach for the generation of a photocurrent. Further promising examples are summarized in works from Spiess[40] and González-Rodríguez and Schenning.[41]

Also polymers can self-assemble in even lager entities by noncovalent interactions. This special class is denoted as supramolecular polymers.[42] For example, block-co-polymers self-assemble in hierarchical ordered structures, such as spheres, cylinders, lamellae and vesicles.[43,44] Recently, a DNA-based oligothymidine was utilized to guide the self-assembly of dyes in water. π-stacked diaminotriazine derivates anchor to the single strand of the oligonucleotide via complementary hydrogen bonds forming a right-handed helical arrangement.[45] In Figure 6 this templated self-assembly process is represented. More helical arranged self-assembled nanofibers formed by small molecules or polymers are reviewed by Lee *et al*..[46]
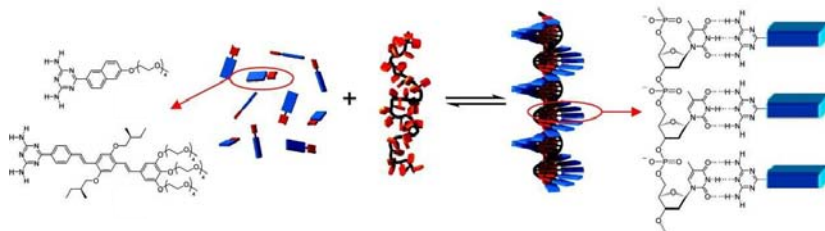

Figure 6. Schematic representation of the supramolecular polymerization of a single strand DNA unit and diaminotriazine derivates. This templated self-assembly process is stabilized by hydrogen bonds and π-π-interactions. [Adapted with permission from reference 41. Copyright (2011) American Chemical Society.]

Nowadays, supramolecular chemistry is a major, interdisciplinary research field containing the cooperation and professional knowledge of chemists, biologists, physicists and material scientists to develop new materials with unique functions for advanced materials.

1.2 Benzene- and cyclohexanetrisamides

One of the most investigated and easiest motif of self-assembling small molecules are 1,3,5-benzene- and 1,3,5-cyclohexanetrisamides. The central core, benzene respectively cyclohexane, is responsible for symmetry and planarity of the molecule. Amide groups at the 1, 3 and 5-position of the central core are the moieties forming hydrogen bonds and forcing the one-dimensional self-assembly as well as the crystal growth. The attachment of the amide moiety at the central core can be either accomplished with the carbonyl groups (C-centered) or the nitrogen side (N-centered) of the amide groups. Also molecules with mixed amide connectivity are known. By an intelligent choice of the peripheral substituents R the dissolution and self-assembly behavior can be tailored. The nature of the substituents can be aliphatic, aromatic, charged or neutral, polar, apolar, chiral or achiral.[47-50] The concept of the molecular structure of 1,3,5-benzene- and 1,3,5-cyclohexanetrisamides is shown in Figure 7.


I (a) I (b) II (a) II (b)
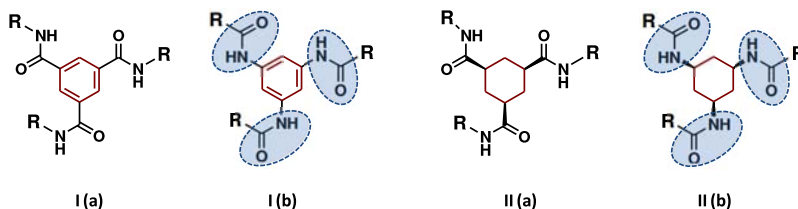
Figure 7. Concept of the molecular structure of 1,3,5-benzene- (I) and 1,3,5-cyclohexanetris-amides (II). The amide bonds can be tailored with C- (a) or N-centered (b) amide connectivity.

Since this representing class of supramolecular building blocks can be designed easily and versatile, 1,3,5-benzene- and 1,3,5-cyclohexanetrisamides become more and more important in many research fields.

1,3,5-benzene- and 1,3,5-cyclohexanetrisamides are widely investigated as organo-[50-54] and (pH-sensitive) hydrogelators.[55-59] Moreover, well-defined 1,3,5-benzenetrisamides fibers, formed *in situ*, can act reliable as nucleating agents for poly(vinylidene fluoride)[61] and poly(therephthalate)[62] and additionally, as clarifier for isotactic polypropylene.[63,64] Further application fields for 1,3,5-benzenetricarboxamides are as additives to improve the electret performance of isotactic polypropylene[65], they serve as supramolecular materials with thermoplastic and elastic properties[66], and can form a supramolecular nanofiber web inside of a nonwoven scaffold to be used as filter media.[67] This class is, furthermore, suitable for coordinating metal ions[68-71] for example applicable in asymmetric catalysis[72] or as sensors.[73]

### 1.2.1 Benzenetrisamides based on trimesic acid
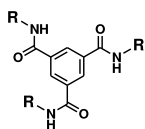
1,3,5-Benzenetrisamides based on trimesic acid contain three carbonyl group centered amid bonds. Depending on subtle changes of the peripheral substituents, different packing, crystal structures and self-assembly behavior in solution have been observed.

Benzenetrisamides based on trimesic acid in the solid state

Table 1 summarizes the packing structures and space groups for several 1,3,5-benzenetricarboxamides. Lightfoot *et al.* proved in 1999 via crystallographic investigations that N,N',N''-tris-(2-methoxyethyl)-1,3,5-benzenetricarboxamide self-assembles into columnar structures by forming strong, three-fold hydrogen bonds between adjacent molecules and crystallizes in the monoclinic space group $P2_1$ (Table 1, entry 1).[48] The resulting aggregates are stabilized additionally by the π-π-stacking of the phenyl units, indicated by an interdisc distance of 3.62 Å. To form strong hydrogen bonds the amide groups has to turn into a favorable 90° position with respect to the central core. However, the extend of the turn is limited since the amide groups are conjugated with the phenyl core, and consequently, the amide units turn with angles of 36.8° to 45.5° just slightly out of the coplanarity. Thereby, all amide groups point in the same direction. Moreover, the adjacent discs undergo a 60° turn to strengthen the hydrogen bonds resulting in a helical arrangement of the hydrogen bonds.[48]
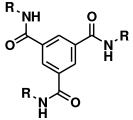
Equipped with three bulky *tert*-butyl substituents, 1,3,5-benzenetricarboxamides form also columnar structures, organized in a hexagonal fashion within the space group $P6_3/m$ (Table 1, entry 2). A directional triple-helical bonding pattern was found along the column axis. Depending on the orientation of the oxygen atoms in the column, two helical assemblies, the up- and the down-configuration, can be formed. To lower the energy of the supramolecular structure adjacent columns arrange in an antiparallel fashion.[74] The one-dimensional self-assembly concept of trialkyl-substituted 1,3,5-benzenetrisamides is illustrated in Figure 8.
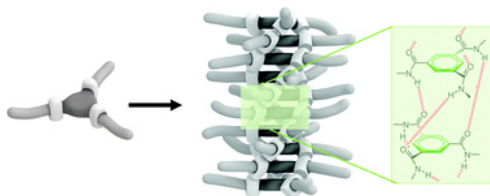
Figure 8. Schematic illustration of the self-assembly behavior of C-centred trialkyl-substituted 1,3,5-benzenetrisamides. Single molecules self-assemble into a columnar structure by triple-helical hydrogen bonds and π-π-stacking of the phenyl units. This concept applies also for N-centered representatives (Ib, **Figure 7**). [Reproduced from reference 49 with permission from The Royal Society of Chemistry.]

However, 1,3,5-benzenetricarboxamides can also crystallize in a two-dimensional fashion, when heteroaromatic or short aliphatic side chains are introduced. Surprisingly, a nanosheet structure was also reported for *N,N',N''*-tris(*n*-octyl)-1,3,5-benzene-tricarboxamide.[75] This finding is an absolute exception for trisamides with long, linear alkyl chains and can maybe be attributed to the mild conditions used to obtain the analyzed powder. Two-dimensional structures are in contrast with the columnar molecular packing of 1,3,5-benzenetricarboxamides with longer[48] or more bulky[74] trialkyl substituents. It is revealed that the nature of the side chains has an enormous influence on the crystal structure, as well as the solvent used to obtain these powders.

Table 1. Packing structures and space groups for 1,3,5-benzenetricarboxamides **1-7**. 2D: two-dimensional; 3D: three-dimensional packing.

Entry	Molecular structure: with substituent R	Packing structure	Space group	Ref.
1	R=	3D, columnar	monoclinic, $P2_1$	48
2	R=	3D, columnar	hexagonal, $P6_3/m$.	74
3	R=	2D, rosette-like	trigonal, $P\bar{3}$	76
3		2D, T-shaped	orthorhombic, $Pbca$	77
4	R=	2D, T-shaped	orthorhombic, $Pbca$	77
5	R= • —CH_3	2D, sheet	monoclinic, $P2_1$	51
6	R=	2D, sheet	orthorhombic, $P2_12_12_1$	79
7	R=	3D, network	trigonal, $R3c$	79

Carrying three 3- or 4-pyridyl substituents (Table 1, entry 3 and 4), the pyridyl nitrogens form intermolecular hydrogen bonds with the amide groups of the neighboring molecules resulting in a macrocycle out of six molecules. This rosette-like structure forces the creation of an infinitive two-dimensional honeycomb network. The bilayer structure itself is packed in a three-dimensional porous superstructure with all macrocycles located exactly on top of each other. To stabilize the structure, pyridyl-substituted 1,3,5-benzenetrisamides include solvent molecules in the crystal lattice.[76,77] In general, trisamides developing intramolecular hydrogen bonds have a flatter

geometry in comparison to trisamides with three amides groups forming intermolecular hydrogen bonds with adjacent molecules.[78]

In 2009 Ruiz-Pérez *et al.* compared the crystal structures of methyl-,[51] ethyl- and propyl-substituted 1,3,5-benzenetricarboxamides (Table 1, entry 5-7). Supramolecular sheets are formed by intermolecular hydrogen bonds of the methyl- and ethyl- substituted representative.[79] 1,3,5-Tripropyl-benzenetricarboxamide packs in a primitive cubic supramolecular three-dimensional network stabilized by amide hydrogen bonds.[79]

For 1,3,5-tricarboxamides equipped with three 4-halogen-phenyl substituents the role of solvent in crystallization process was studied. In the presence of tetrahydrofuran (THF) the molecules tend to form triple-helical hydrogen bonds in columnar fashion. Interestingly, a blocking of the formation of hydrogen bonds occurred when cyclohexanone was used as solvent, resulting in a two-dimensional packing of the halogenated benzenetrisamide molecules.[80]

For 1,3,5-benzenetricarboxamides with long alkyl substituents different crystalline, plastic crystalline and liquid crystalline phases were found. The presence of three-fold intermolecular hydrogen bonds between neighboring trisamides is responsible for the formation of stable, columnar mesophases in a wide temperature range.[47,81,82] Ordered hexagonal columnar mesophases were reported starting from a linear *n*-hexyl side chain. Benzenetricarboxamides substituted with linear butyl or pentyl side chains provide plastic crystalline phases, but no liquid crystalline mesophases.[82] The introduction of branched side chains further stabilizes the aggregation in the mesophase and has a major impact on the transition temperatures. As closer the branching point is moved to the amide group, the higher the clearing temperatures and corresponding enthalpies.[82,83]

Recently, Timme *et al.* investigated the stepwise loss of order during heating. Columnar hexagonal or rectangular mesophases are formed at higher temperatures when starting at the well-defined crystalline state. With increasing temperature the lateral order, thus the intercolumnar interaction, becomes weaker while maintaining the strong intermolecular three-fold hydrogen bonds along the column axis. At even higher temperatures the lateral order is completely lost. Depending on the strength of the hydrogen bonds, the columns break into smaller pieces. Although if short columnar aggregates still exist above the clearing temperature of the melt, the phase appears optical isotropic. By further increase of the temperature, a molecular isotropic phase is obtained.[82]

Self-Assembly of benzenetrisamides based on trimesic acid in solution

Since years, the self-assembly behavior of achiral and chiral 1,3,5-benzenetrisamides based on trimesic acid depending on the solvent has been intensively studied. Main contributions are made by the research group of E.W. Meijer.

Derived from the crystal structures, it is evidently that C-centered 1,3,5-benzene-trisamides self-assemble in solution into one-dimensional, columnar aggregates by strong, helically arranged intracolumnar hydrogen bonds.[49] The presence and formation of hydrogen bonds in dilute solutions can be detected by Ultraviolet-visible (UV-Vis) spectroscopy. An absorption maximum is observed at 193 nm. In more polar solution 1,3,5-benzenetricarbxamides are molecularly dissolved, so that the UV-Vis absorption maximum shifts to 208 nm. This was exemplarily shown for 1,3,5-trioctyl-benzenetricarboxamide in acetonitrile at room temperature.[84] As it was discussed before, in the solid state *N,N',N''*-tris(*n*-octyl)-1,3,5-benzene-tricarboxamide crystallizes under mild conditions into a nanosheet structure.[75] However, the self-assembly in dilute *n*-heptan solution yielded columnar aggregates by helically arranged hydrogen bonds.[84]

Investigations by circular dichroism spectroscopy revealed a stable helical arrangement of 1,3,5-benzenetricarboxamide columns in nonpolar alkane solutions.[85] For achiral trisamides right-handed (*P*) and left-handed (*M*) helices are formed in equal amounts. Chiral side chains introduce a preferred helicity of the columns. If a mixture of achiral and chiral trisamides in dilute solutions is investigated, the chiral compound determines the preference in handness of the mixed aggregates. Thereby *P*- or *M*- helices can be formed.[84,86,87] The sense of the helical columns, *P* or *M*, depends strongly on the choice of the solvent. As it was shown for a in the α-position deuterated trioctyl-benzenetricarboxamide, leading to a (*S,S,S*)-benzenetrisamide motif, right-handed helices were formed in methylcyclohexane, whereas in *n*-heptan left-handed columns were achieved. The solvent also influences the amide torsion angle, leading to two different conformations having an angle of 35° or 45° with respect to the central core, and causes a larger interdisc distance by intercalating solvent molecules between the trisamide molecules within a stack. At higher temperatures this intercalation is facilitated.[87,88] A computational study of the helical-sense bias of this (*S,S,S*)-enantiomer shows that a right-handed helical aggregate is preferred when the solvent influence is not considered. These calculations were carried out with a simplified molecular structure by replacing the *n*-octyl side chains by ethyl groups.[89]

Moreover, even the introduction of chiral information by a methyl group in one of the three aliphatic side chain of 1,3,5-benzenetricarboxamides results in a preference of the helical conformation of the self-assembled stacks in *iso*-octane. If the methyl group is introduced to the α-position of the chain, a left-handed helix with an amide-benzene-angle of 45° is preferred. A methyl group in β-position leads to right-handed helices with a torsion angle of the amide group of 35°. Interestingly, if *n*-heptane is used as solvent, the torsion angle is 45° independent of the position of the methyl group in the asymmetrical substituted molecule. This is due to the intercalation of the solvent molecules between the alkyl chains of the stacked trisamides. Anyway, for all investigated compounds, intermolecular, helical arranged hydrogen bonds are present.[90,91]

In a recently published work of the Meijer group, the co-self-assembly of dye-labeled and non dye-labeled 1,3,5-benzenetricarboxamides is followed by stochastic optical reconstruction microscopy (STORM). This super-resolution microscopy method allows the visualization of the molecular exchange pathways of these one-dimensional aggregates and reveals a homogenous exchange along the trisamide stack.[92]

To study the role of the π-conjugated core, an oligo(phenylene ethynylene) unit was introduced to the tricarboxamides. It is shown that this larger π-conjugated system also self-assembles into helical, columnar stacks primarily via π-π-stacking. The stability of these supramolecular assemblies is comparable to columns of conventional 1,3,5-benzenetricarboxamides. Moreover, it was shown that solvents, such as chloroform, can interact faster with the columns of the larger π-conjugated molecules weakening the self-assembling process.[93]

With a precise design of the peripheral substituents, 1,3,5-benzenetricarboxamides can become water soluble and self-assemble into fibers. Thereby, the aggregation is stabilized in addition to hydrogen bonds by ionic[94,95] or hydrophobic[96] effects. By the introduction of fully rigid substituents a lyotropic liquid crystal phase was observed in aqueous solutions. These hexagonal supramolecular columnar phases are formed by helical rosette nanotubes.[97] By alignment of the channels anisotropic ionic conductivity is achieved.[98]

A lot of investigation was made concerning the mechanism of the self-assembly process. By temperature depended CD- and UV-Vis analysis the self-assembly mechanism was determined to be highly cooperative. This nucleation-elongation self-assembly model, also called nucleating-growth model, includes two regimes: The nucleation regime is present at high enough temperatures, depending on molecular structure, concentration and solvent in which all molecules are molecularly dissolved. Upon cooling, large

enough nuclei are formed promoting the further one-dimensional growth of the aggregate. By further cooling out of the solution the elongation regime sets in in which the aggregates are formed before they rapidly grow.[83]

Density Functional Theory (DFT) electronic structure calculations show that the cooperative mechanism is caused by electrostatic interactions. With increasing number of monomers in one stack the average electronic interaction energy decreases, indicating that larger aggregates are more favorable than smaller ones. Moreover, the intermolecular hydrogen bonds become stronger with an increasing length of the column.[99,100] Molecular dynamics simulations show, that the formation of the stack occurs within tens of nanoseconds.[101]

For chiral compounds the growing aggregates are better stabilized by the branched side chains resulting in larger stacks compared to achiral 1,3,5-benzenetricarboxamides.[84] Furthermore, this cooperative self-assembly mechanism is also valid for partially fluorinated 1,3,5-benzenetricarboxamides.[102]

The nucleation-elongation self-assembly model is shown schematically in Figure 9.
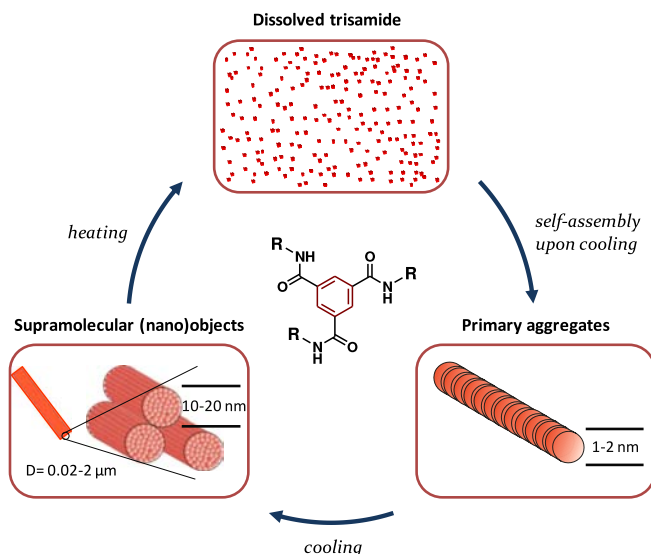
Figure 9. Schematic concept of the cooperative self-assembly mechanism of 1,3,5-benzene-tricarboxamides in dilute nonpolar solutions. Dissolved trisamide molecules self-assemble upon cooling into primary aggregates via strong hydrogen bonds. Upon further cooling supramolecular bundles are formed. This self-assembly process is thermally reversible.
[Scheme modified from reference 9 and 103.]

1,3,5-Benzenetricarboxamides with substituents forming intramolecular hydrogen bonds prefer an isodesmic growth pattern as it was shown for 3,3'-diamino-2,2'-bipydridine substituents.[104,105] The isodesmic growth is characterized by the independence of the stack length from the strength of association between two monomers.[106]

Formation of macrodipoles in benzenetrisamides based on trimesic acid

Due to the fixed direction of hydrogen bonds of the supramolecular aggregates in solid state as well as in solution a macrodipole arises along the columnar aggregate. This macrodipole consists at least of the sum total of individual dipole moments generated of each molecule within a column. A dipole moment of 8 to 14 Debye of the three amide bonds is discussed. Even if the helically arranged columns come along with a preferred helicity, a macrodipole develops in right- as well as in left-handed helices.[107,108]

Columnar liquid crystal phase behavior of several 1,3,5-benzenetricarboxamides can induce polar order in the mesophase by ferroelectric switching. The uniform alignment and switching of columnar phases in an electrical field was possible. This polar order can be frozen by crystallization of the 1,3,5-benzenetrisamide producing thin film with stable, remnant polarization.[109-111] Albuquerque *et al.* carried out calculations on a semi-empirical level to describe the relation between macrodipole and properties of the columnar aggregates in 1,3,5-benzenetrisamides. The dipole moment per molecule increases with increasing molecules self-assembled within one supramolecular column. Consequently, the generated macrodipole of a large column is larger than the sum of the monomer units and the one-dimensional growth is favored.[112]

These findings support the self-assembly mechanism of cooperative growth in of 1,3,5-benzenetrisamides caused by electrostatic interactions, proposed by *Greef et al*. for diluted solutions.[99]

1.2.2 Benzenetrisamides based on triaminobenzene
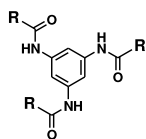
Another class of 1,3,5-benzenetrisamides is based on triaminobenzene instead of trimesic acid. Here, all three amide groups are N-centered with respect to the central core.

Benzenetrisamides based on triaminobenzene in the solid state
and the formation of macrodipoles

Recently, Marko Schmidt *et al*. determined the crystal structure of 1,3,5-tris(2,2,-dimethylpropionylamino)benzene (Figure 10, left), an highly efficient clarifier for isotactic polypropylene, by combining powder X-ray diffraction and solid-state NMR spectroscopy. The trisamide crystallizes in the orthorhombic metric $P2_12_12_1$, wherein the molecules arrange in a pseudohexagonal columnar packing via moderate hydrogen bonds and π-π-stacking of adjacent molecules. The amide bonds turn out of the benzene core plane with torsion angles of 31.36°, 31.46° and 34.56° to form hydrogen bonds. The distance between two benzene cores is between 3.37 Å and 3.42 Å.[113] Even for this molecule it was found that all three oxygen atoms of the amide groups point in the same direction, as it was already shown for alkyl-substituted C-centered 1,3,5-benzenetrisamides.[48,74] Within the individual columns of 1,3,5-tris(2,2,-dimethylpropionylamino)benzene a macrodipole is postulated. To cancel the net dipole of the structure neighboring columns arrange here in an antiparallel fashion (Figure 10).[113] This was also shown for the structural analogues with three C-centered amid bonds.[74]
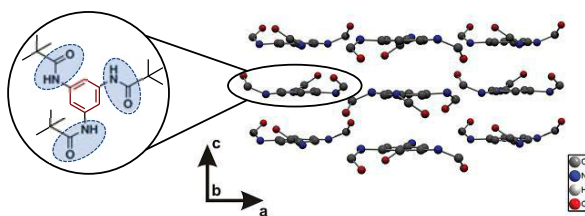
Figure 10: Left: molecular structure of 1,3,5-tris(2,2,-dimethylpropionylamino)benzene. Right: insight of the crystal structure with view along the *b*-axis. The columns arrange anti-parallel to compensate the generated macrodipole of each rod.
[Reprinted with permission from reference 113. Copyright (2012) American Chemical Society.]

In comparison to C-centered representatives, the amide groups are more planarized with the central benzene core and weaker hydrogen bonds are formed, thus leading to a decrease of the macrodipole as indicated by theoretical calculations.[112]

Additionally, Marko Schmidt *et al*. investigated the nucleating mechanism of 1,3,5-tris(2,2,-dimethylpropionylamino)benzene in isotactic polypropylene. Even in very low concentrations the molecules form long, needle-like objects in the polymer melt and provide sufficient surface area to initiate a heteronuclear nucleation of polypropylene. The packing of these trisamide molecules in columns leads to a surface modulation with comparable distances (6.8 Å) as characteristic for isotactic polypropylene (6.5 Å).[114]

Spiess *et al*. studied the impact of the amide connectivity of 1,3,5-benzenetrisamides on the self-assembly behavior in solid states via solid-state NMR experiments and Car-Parinello Molecular Dynamics simulations. As model substances, a C-centered trisamide equipped with (*S*)-dimethyloctyl and a N-centered trisamide carrying (*S*)-dimethylhephtyl substituents were chosen. Asignificantly different molecular packing was found. For simplicity reasons the simulations were carried out with leaving just methyl groups as alkyl side chains.[115] The researchers revealed that the molecular organization of N-centered compound showed a symmetry breaking. The amide bonds of the N-centered representative are asymmetrically arranged, meaning two amide bonds point in one direction, whereas the third one is turned and points in the opposite direction. To form at least quasi-helically formed hydrogen bonds, a simple coplanar arrangement of the central core, as it is known for C-centered trisamides, is not possible. The discussion includes also the symmetric arrangement of the amide bonds, generally valid for C-centered 1,3,5-benzenetrisamides. The asymmetric array is slightly more stable than the symmetric one. However, these energy differences are too small to predict the packing of N-centered trisamides directly. A more favorable packing of the side chains within the asymmetric packing model is mentioned as deciding fact. At higher temperatures a transition into the symmetric configuration is discussed.[115]

The above presented studies of Schmidt and Spiess show impressively that the amide connectivity in combination with the peripheral substituents may have remarkable influence on the supramolecular organization. At least, a strong influence on the generated macrodipole is evident.

A nanosheet instead of a columnar structure was obtained under mild conditions from a N-centered 1,3,5-benzenetrisamide carrying three 3-cyclopentylpropan substituents[75] identifying another possible arrangement of the molecules in the solid state.

Self-assembly of benzenetrisamides based on triaminobenzene in solution

Only a few studies are available dealing with the self-assembly behavior of 1,3,5-benzenetrisamides based on triaminobenzene in dilute solutions.

The stacking of N-centred benzenetrisamides in dilute alkan solutions into one-dimensional aggregates via helical hydrogen bonds was proved via UV-Vis and CD spectroscopy. In polar solvents as methanol the molecules are molecularly dissolved.[116] Compared to C-centered 1,3,5-benzenetrisamides, the columns formed by 1,3,5-benzenetrisamides based on triaminobenzene are less stable. This fact can be attributed to the difference in hydrogen-bonding strength. DFT calculations indicate that the amide groups in N-centred trisamides are more planarized with the benzene core resulting in weaker intermolecular hydrogen bonds.[116] The introduction of chiral substituents results in aggregates with preferred helicity, similar to C-centered benzenetrisamides, even if just one of the three side chains carries a chiral center. The last case highlights that the amplification of chirality is present in both, C- and N-centered representatives.[116] The self-assembly mechanism takes place in highly cooperative fashion.[116] Consequently, the mechanism shown in Figure 9 can also be transferred to 1,3,5-benzenetrisamides based on triaminobenzene.

Among others[74], the self-assembly of 1,3,5-tris(2,2,-dimethylpropionylamino)benzene was investigated in high boiling hydrocarbon solvents. Supramolecular fibers with exceptional aspect ratios (>1000:1) were obtained by the controlled recrystallization from 2,2,4,4,6,8,8-heptamethylnonane (HMN) at defined concentrations between 50 and 600 ppm. Abraham *et al*. demonstrated that with decreasing trisamide concentration, but constant cooling rate, the lateral dimension of the fibers becomes smaller and the fiber diameter distribution gets more and more narrow down to the nanometer range. Moreover, the influence of the cooling rate on the self-assembled morphology was investigated by keeping the trisamide concentration in solution the same. With a slower cooling rate a broader fiber diameter distribution is observed for all investigated concentrations.[117]

The nanomechanical properties of supramolecular fibers of 1,3,5-tris(2,2,-dimethylpropionylamino)benzene obtained from a concentration of 600 ppm in HMN with a cooling rate of 10 K/min were investigated via atomic force microscopy (AFM) bending experiments (Prof. A. Fery, Physical Chemistry II, University of Bayreuth). Kluge *et al*. found a Young's modulus of 3.2 ± 1.4 GPa, which is similar to those of semicrystalline polymers and consequently impressive due to the lack of covalent bonds within the aggregates.[118]
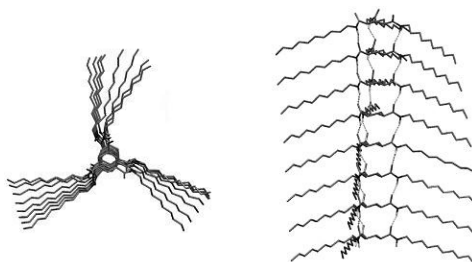
1.2.3 Cyclohexanetrisamides
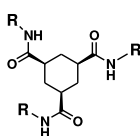
1,3,5-Cyclohexanetrisamides are based on an alicyclic core. The different core structure has a significant influence on the solid state properties and self-assembly behavior in solutions compared to 1,3,5-benzenetrisamides. 1,3,5-Cyclohexane-trisamides with C-centered amid bonds have been studied and are summarized in the following.

Cyclohexanetrisamides in the solid state

In 1995 Hilton *et al*. reported on the crystal structure of *cis,cis*-cyclohexane-tricarboxamide carrying three 6-picoline substituents.[119] The compound crystallizes in the trigonal space group *R*3c. The amide bonds can rotate freely since they are not linked to a conjugation with the core, as it is the case for 1,3,5-benzenetrisamides. Thus, almost linear hydrogen bonds are formed by tilting the amide group nearly perpendicular to the ring. All amide groups point in the same direction. The side chains are arranged on top of each other. A turn of the molecule of 60° is not necessary to strengthen the hydrogen bonds. Thus, a rigid supramolecular nonhelical column is formed (Figure 11).[48,119] The interdisc spacing is 41 Å and, therefore, larger than the distance in 1,3,5-benzenetrisamides with 35 Å. The reasons for the wider spacing are the almost 90° turned amide bonds filling more space in between two adjacent cyclohexane cores. Moreover, the columns pack closer compared to aromatic analogues, due to a smaller column distance, revealed from XRD investigations.[82]

Carrying branched side chains, the packing structures of the columns are more compact as for 1,3,5-cyclohexanetrisamides with linear substituents, which are more equally distributed around the alicyclic core.[120]

Figure 11. Top and side view of *N,N',N''*-octyl-1,3,5-cyclohexanetricarboxamide. The geometry was calculated using a PM6 approximation. [Modified with permission from reference 112. Copyright © 2013 WILEY-VCH Verlag GmbH & Co. KGaA, Weinheim.]

The thermotropic phase behavior of symmetric 1,3,5-cyclohexanetrisamides equipped with several linear and branched substituents was intensively investigated by Sijbesma *et al*.[120] and Timme *et al*.[82] Starting from *n*-hexyl side chains,

1,3,5-cyclohexanetrisamides form columnar rectangular plastic mesophases. A relatively rare columnar nematic phase was found for this substance class with alkyl chains longer as *n*-heptyl. The nematic phase is an intermediate state between the higher ordered columnar mesophase and the isotropic phase. With branched side chains pseudorectangular lattices and columnar hexagonal ordered phases were observed. In general, the transition temperatures are higher than those of analogous 1,3,5-benzenetrisamides, since 1,3,5-cyclohexanetrisamides form stronger hydrogen bonds within a columnar stack resulting in highly stable aggregates.[82,120]

Concerning the transition from the mesophase into the optical isotropic phase, weaker lateral interactions are lost first while maintaining the hydrogen bonds, as it is already known from 1,3,5-benzenetricarboxamides. 1,3,5-Cyclohexanetrisamides carrying branched alkyl chains are transferred into a nematic phase, which is optically anisotropic. With increasing temperature the hydrogen bonds get weaker, the columns break into smaller pieces and the melt appears optically isotropic, even if there are still columnar aggregates present. Just by further heating single molecules are obtained in the molecular isotropic phase.[82]

Self-assembly of cyclohexanetrisamides in solution and the formation of macrodipoles

1,3,5-Cyclohexanetrisamides are widely used as organo- and hydrogelators. They form enormous long supramolecular aggregates, resulting in a dramatic increase of the solution viscosity.[51,53] The self-assembled columns are remarkable straight and stabilized by strong hydrogen bonds[121] as seen from the structural elucidation in solid state.

Due to the fixed direction of the amide groups in one direction, a macrodipole is generated along the stiff columns in solid state and in solution.[121] Theoretical investigations show that the macrodipoles formed in cyclohexanetrisamides (~170 D) are much stronger than those of benzenetrisamides (~110 D). This fact can be attributed to the different strength of the hydrogen bonds of these two substance classes. The macrodipole itself is higher than the sum of the dipole moments of the individual monomers within one column, indicating cooperativity among hydrogen bonds pushing the one-dimensional growth.[112] Consequently, the self-assembly mechanism shown in Figure 9 is also valid for 1,3,5-cyclohexanetrisamides.

Samori *et a*l. proved that supramolecular 1,3,5-cyclohexanetrisamide fibers can be aligned and manipulated in an electric field due to the presence of the macrodipole.[122]

1.3 Electrospinning

Electrospinning, or electrostatic fiber spinning, is an easy, versatile, and inexpensive technique to produce fibers with diameters down to several nanometers by subjecting a fluid jet into an electrical field. The collected nonwovens are formed of quasi infinitively long fibers; fiber ends are barely observable.[19,123]

Electrospinning of solutions, as typical top-down approach was already observed by Rayleigh in 1897. The first patent was granted to Formhals in 1934, followed by several others dealing with the experimental set-up to produce polymer fibers using an electrostatic force. In the past 80 years an enormous amount of publication and patents have been published about electrospinning of polymer solution and melts.[124] Over a hundred natural and synthetic polymers have been electrospun into fibers. The variety of investigated polymers ranges from commercial ones, such as polyethylene, polypropylene, polystyrene and poly(methyl methacrylate), to biopolymers, such as collagen, gelatin and silk fibroin, and liquid-crystalline[125] representatives, just to mention a few.[126,127]

Worldwide more than 200 universities and research institutes are examining the electrospinning process in its detail and all the various aspects of fiber formation by using electrostatic forces.[128] Away from the academic investigations, the technique is already well-established in many technological areas.[126] Besides a tremendous amount of available review articles, a very good overview of electrospinning is given in the recently published text books from Wendorff *et al.*[19.] and Ramakrishna *et al.*.[129]

Most research topics and articles about electrospinning deal with the fabrication of polymeric fibers from solution[19,128,126] Nevertheless, just a few studies are available for melt electrospinning since polymer melts are intrinsically nonconductive and their viscosity is much higher compared to solutions. The fiber formation of solution electrospinning is based on the evaporation of the solvent, whereas the fiber formation gained by melt electrospinning relies on the cooling of the melt.[130]

The first study about electrostatic fiber spinning from polymer melts was done by Larrondo and St. John Manley in 1981. Their melt electrospinning process resulted in large fibers with diameters above 50 μm, related to the high viscosity of the polymer melt.[131-133] Recent studies demonstrate that homogenous melt electrospun fibers with a diameter below one micron are accessible by applying higher voltages and increasing the spinning temperature.[128,130,134,135] Increasing the conductivity of the polymer melt by addition of conductive additives such as antistatic agents, ammonium salts, sodium oleate and sodium chloride, is another possibility to achieve more narrow fiber diameter distributions. In the case of polypropylene[136,137] and polyamide-6[138]

electrospun fibers with average diameters in the range of 500 nm were obtained. Therefore, the benefits of the easy and inexpensive generation of nanofibers are ensured by avoiding problems known from solution electrospinning, such as (harmful) solvent residuals in nonwovens.[139] Moreover, melt electrospinning offers the access to many polymers being limited in fiber production due to their low solubility, often just in scarce and expensive solvents.[138] A severe drawback of electrospinning arise e.g. from the lower fiber output compared to melt blowing techniques.

1.3.1   Electrospinning set-up and the influence of the parameters

A typical experimental set-up of a solution or melt electrospinning apparatus is shown in Figure 12. For an electrospinning experiment a syringe equipped with a metal needle capillary, which is filled with (polymer) solution or melt is required. The fluid or melt is pumped through the needle capillary to ensure a homogenous flow and maintain material supply during the spinning process. A high voltage source is applied between the metal needle capillary and the collector plate serving as counter electrode. For a melt electrospinning apparatus additional heating around the syringe is required.
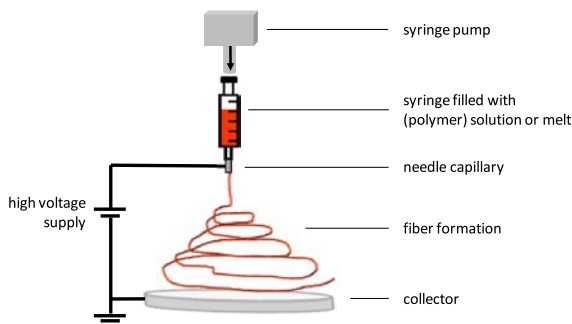
Figure 12. Schematic set-up of an electrospinning unit.

Usually a metering syringe pump is used to transport the solution or melt at a continuous and stable rate through the capillary into the electrical field. The flow rate is usually in the range from 5 µL/h up to 100 mL/h. The diameter of the capillary needle used depends on the application: For melt electrospinning the inner needle diameter is restricted by the viscosity of the melt because a sufficient flow has to be ensured. Usually, the inner spinneret diameter is around 0.5 mm.

In many experiments the distance between needle tip and collector is between 3 cm and 25 cm. Since fast solvent evaporation respectively fast cooling of the melt is important for solidification of the jet, the collector distance has to be set sufficiently

large to avoid the collection of coalesced fibers. An exception is near field electrospinning using reduced distances in the range of 500 μm to 3 mm.[140]

There are variations on the collector geometries and collection configuration to fabricate desired fiber patterns, such as a nonwoven fiber mesh, aligned fibers, huge fiber mats or the production of individual fibers. Set-ups with e.g. a rotation drum, parallel electrodes, rotating wire drum disc collectors, an array of counter-electrodes and yarn collection using a water bath represent a selection of various approaches to obtain ordered electrospun fiber assemblies.[141-143]

The applied electric field is determined by the needle tip to collector distance and the applied voltage. Typically the electrical fields are between 100 kV/m to 500 kV/m. The required high voltage, mostly in the range of 7 kV to 50 kV, can either be applied at the needle tip or at the collector. The corresponding counterpart is either grounded or oppositely charged. E.g., when a positive voltage is applied at the needle tip, the melt is positively charged before accelerated towards the collector. Most studies of solution or melt electrospinning of polymers are based on an electrical field direction from needle tip to collector. In some cases the direction of the electrical field can be reversed.[19,126,127,130,144]

The morphology and diameter of the electrospun fibers depends strongly on the electrospinning parameters, such as applied voltage, distance between needle tip to collector, configuration of the electrodes, flow rate and inner needle diameter. Additionally, intrinsic parameters such as electrical conductivity of the polymer, surface free energy, viscous and elastic properties and, in case of solution electrospinning, on solution and solvent properties are crucial for the electrospinning process. Experimental and theoretical studies show that changes in solvent purity respectively applied temperature, molecular weight of the polymer, flow rate and electrical field strength have significant influence on the diameter.[127,130,145-148] Moreover, charge-bearing additives such as surfactants, cationic or anionic agents are widely used to enhance the electrospinnability due to a better conductivity of solution or melt and, consequently, to end up with thinner electrospun fibers[125,137,138,144,149]

The fiber formation during the electrospinning process from solution or melt can be divided into four parts: (1) droplet formation at the tip of the needle capillary; (2) initiation of the jet; (3) elongation of the jet due to instabilities; (3) solidification of the jet into fibers.[150] On the first glance this top down approach looks quite simple, but the physical process behind is very complex.[151-153]

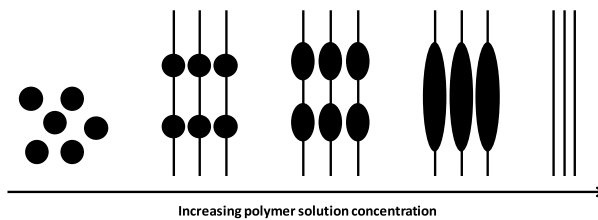### 1.3.2   Fiber formation by solution electrospinning

In solution electrospinning a drop is formed at the tip of the capillary die and begins to deform from a hemispherical to a cone-like shape, when the drop gets electrostatically charged in the presence of the electrical field. A so called Taylor cone[154] with a half angle around 30° is formed by electrostatic repulsion of the charges into the droplet.[126,155,156] The induced charges are positive in case of an electrical field direction from needle to collector, whereas a reversed field direction leads to oppositely charged charges. When the applied electrical field is higher than a critical value, the repulsive electrostatic forces overcome the surface tension and a fluid jet is ejected towards the collector.[126,128,142,150,157] The formation of the Taylor cone and the initiation of the jet are shown in Figure 13.
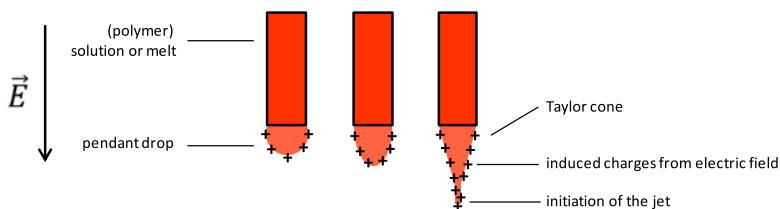
Figure 13. Schematic illustration of the formation of the Taylor cone. In this case the electrical field direction is from needle to collector. Left: pendant drop, formed at the needle tip; center: elongation of the drop from hemispherical to a cone-like shape due to the repulsion of the induced charges; right: formation of the Taylor cone and the initiation of the jet, if a high enough electric field is applied. [Adapted from reference 142.]

In solution electrospinning instabilities occur about 1 cm under from the capillary tip. Thereby, the diameter of the filament gets extremely reduced by stretching, bending, further acceleration, and the evaporation of the solvent. These instabilities strongly influence the size, geometry, and morphology of the electrospun fibers. The first upcoming instability is axisymmetric and known as Rayleigh instability. It occurs when the applied electric field is too low or when the viscosity of the solution is below an optimum value. Apart from the Rayleigh instability, the straight part of the jet is also controlled by two further instabilities. These instabilities are bending (axisymmetric) and whipping (non-axisymmetric), and arise from the charge-charge repulsion of the excess charges present in the jet. The axisymmetrical instabilities, Rayleigh and bending, can be avoided by applying higher electrical fields, resulting in a larger charge density, or by working with higher solution concentrations. In this case whipping instabilities are enhanced. Often, the whipping instability occurs in such a high frequency that the jet appears to be split into multiple filaments.[142,156-163]

The solution concentration and the molecular weight of the polymer, consequently the solution viscosity, is a parameter for the extent of chain entanglement which plays a crucial role in the formation of fibers. If the chain entanglement is lower than a critical value, often denoted as concentration for entanglements C_e, the electrospinning jet breaks up and electrosprayed beads are obtained instead of electrospun fibers. This happens at very low concentrations even if high molecular weight polymers are used. Beaded fibers are collected, if the extend of chain overlap is not high enough, even if the chains starts to interact with each other ($C \leq C_e$). First at concentrations above C_e, fiber formation in electrospinning will proceed. [147,142,164,165] The schematic sketch in Figure 14 draws possible morphologies being formed by solution electrospinning.

Increasing polymer solution concentration

Figure 14. Schematic representation of the influence of the solution viscosity on the electrospun morphology obtained by solution electrospinning of polymers as parameter for chain entanglement. [Adapted from reference 147.]

1.3.3   Fiber formation by melt electrospinning

The physical process for the jet formation during melt electrospinning is similar to solution electrospinning. A pendant drop of a polymer melt, hanging at the spinneret, is first extended (Taylor cone) when exposed to a high electric field. The electrostatic charges, introduced by the applied electrical field acting on the fluid have to overcome the surface tension and viscoelastic properties of the melt to form a single fluid jet out of the Taylor cone. This jet is accelerated towards to the collector when a sufficient field strength is reached.[130,135,166] Compared to solutions, the viscoelastic jet obtained from melt is thicker because of the higher elongational viscosity.[167] As the molecular weight of a polymer increases, the increasing chain entanglement resists the stretching process and, consequently, a higher electrical field is required to stretch the cone into a fiber form.[130] Even at high electric fields it was not possible to form a Taylor cone for a high molecular weight polypropylene. Due to the high viscosity of the melt, it is rather extruded through the spinneret than electrospun.[166]

On its way to the collector the jet gets accelerated in the electrical field, internal stresses caused by charge repulsion result in an alignment of the polymer chains along the fiber axis and a thinning of the jet is observed.[130,168] Within the initial region the jet

stays straight for a long distance, about 10 cm at a nozzle-collector distance of 15 cm, before instabilities occur and the jet begins to coil and to buckle.[135,169] This so called "late coiling" was also demonstrated for other melt electrospun polymers such as polylactic acid.[167] This agrees with early studies performed by Taylor, pointing out that the jet stability increases with a high viscous material.[170,171] If excessive surface charges overcome the surface tension, an area of instabilities occurs resulting in buckling and, consequently, whipping of the jet, whereby the diameter of the jet decreases by orders of magnitudes.[130] The jet thinning rate decreases, if the jet temperature comes close to the melting point of the polymer.[168]

Low conductive and viscous fluid materials, such as silicone oil and ethylene glycol, form stable jets without buckling instabilities. Coalesced fibers were collected in this case. Consequently, the low conductivity of polymer melts might be the reason that melt electrospun fibers are often thicker than solution electrospun fibers because buckling instabilities of the jet are suppressed.[130]

In general, the chain entanglement increases with increasing molecular weight of the polymer which is crucial to obtain homogenous fibers without beads. At low viscosities of the polymer melt, for example by selecting higher temperatures of the melt electrospinning process, the jets breaks up during acceleration and droplets are formed.[164,172]

Since bending and buckling of the molten polymer jet occurs close to the collector, elongated jets from polymer melt have been exploited to "write" direct lines of electrospun fibers (near field electrospinning).[139,173,174] Melt electrospinning offers a stable jet allowing a rather good prediction over the position of electrospun fibers, when the needle-collector distance is reduced.[130] Especially for tissue engineering, it is important to place electrospun fibers into discrete patterns on a collector/substrate. For example, fibroblast cells were seeded onto a melt electrospun biodegradable polymeric fiber mesh and they start to adhere within the scaffold in a three dimensional fashion.[174,175]

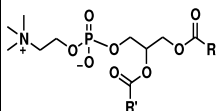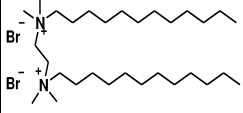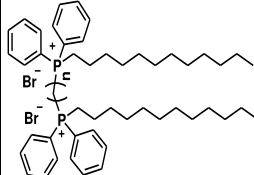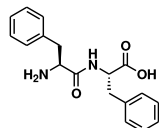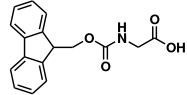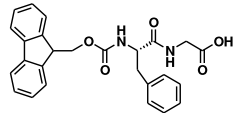### 1.3.4 Electrospinning of small molecules from solution and melt

When a liquid of a low molecular weight substance is subjected to an electric field, a jet is formed out of the elongated droplet. Due to the electrical forces, the jet breaks up when it is accelerated in the electrical field. The jet disrupts into droplets due to the lack of chain entanglement and electrospraying occurs.[176] Therefore, polymers have been tailored with additives like drugs,[177] enzymes, bacteria, inorganic particles[178-180] or for example liposomes[181] to act as supporting material during the electrospinning process.[126,150]

However, Long *et al.* proved in 2006 that homogenous electrospun fibers from solution can also be obtained from lecithin, a mixture of phospholipids and neutral lipids derived from soybean, thus a non-polymeric, low molecular weight substance (Table 2, entry 1). Required are solely sufficient intermolecular interactions acting similar to the chain entanglements in polymeric systems.[182] This low molecular mass amphiphile could be electrospun due to the formation of cylindrical micelles growing in a one-dimensional fashion upon an increase in amphiphile concentration. At higher concentrations these formed "wormlike" lecithin micelles overlap and undergo entanglement, comparable to polymer chains in semi-dilute solutions. At 35 wt% in a 70/30 chloroform/N,N'-dimethylformamid solution beaded fibers were obtained, identifying the critical entanglement concentration (C=C_e). At lower concentrations only droplets were formed (C<C_e). Above 35 wt% lecithin (C>C_e), electrospun fibers within a diameter range of 1 μm to 5 μm were formed due to sufficient entangled properties of the wormlike micelles. [164,182,183]
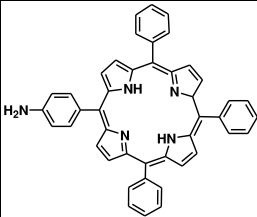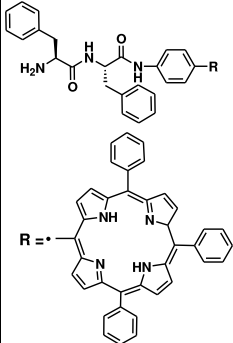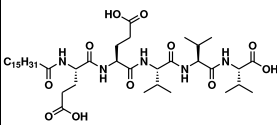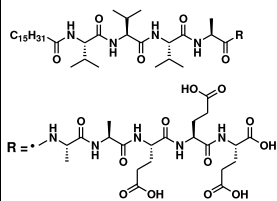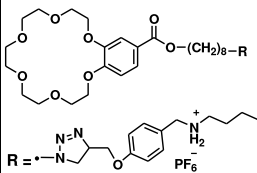
In the last years some publications appeared dealing with successful electrospinning of self-assembling molecules from solution into a uniform nonwoven. The investigated substances are summarized in Table 2.

Long *et al.* examined also another class of amphiphiles on their electrospinnability. The ammonium gemini surfactant, *N,N'*-didodecyl-*N,N,N',N'*-tetramethyl-*N,N'*-ethandiyldi-ammonium dibromide (12-2-12), self-assembles into threadlike micelles in solution. Thus, an important factor required for electrospinning is given. Electrospun fibers were obtained from a 50/50 water/methanol mixture above a concentration of 22 wt% (C>C_e). At lower concentrations (C<C_e) beads were formed and beaded fibers were obtained at C=C_e (Table 2, entry 2).[184] Moreover, also phosphonium gemini surfactants (Table 2, entry 3) were recently electrospun into fibers (d= ~1 μm) from methanol (52wt%).[185] Consequently, Long *et al.* demonstrated once again that the electrospinning jet is stabilized by the entanglement of the wormlike micelles being required for the formation of electrospun fibers from this low molecular weight amphiphile.

Table 2. Overview of small molecules investigated by solution electrospinning with molecular structure, used solvent, solution concentration and morphology of the electrospun material.

Entry	Molecular structure	Solvent	Conc. [wt%]	Morphology/ fiber diameter	Ref.
1	R, R': fatty acid residues	CHCl$_3$/DMF 70/30	< 35	beads	164, 182, 183
			35	beaded fibers	
			> 35	fibers / ~ 5 µm	
2		Water/MeOH 50/50	< 22	beads	184
			22	beaded fibers	
			> 22	fibers /~ 5 µm	
3	n=2-3	MeOH	< 52	beads and beaded fibers	185
			≥ 52	fibers /~ 1 µm	
4		HFIP	< 13.2	beads	186
			13.2	beaded fibers	
			> 13.2	fibers /~ 0.7 µm	
		n.n.	> 15	fibers	187
5		n.n.	> 15	fibers	187
6		HFIP	≥ 18	fibers/ ~0.3-10 µm	187, 188

Continuation of **Table 2**: Overview of small molecules investigated by solution electrospinning.

Entry	Molecular structure	Solution parameters	Conc. [wt%]	Morphology/ fiber diameter	Ref.
7		HFIP	9.1	fibers/ 0.8 ± 0.6 µm	189
8		HFIP	9.1	fibers/ 0.4 ± 0.3 µm	189
9		Water	3	fibers/ 3.8 ± 0.4 µm	190
10		Water	3	fibers/ 3.9 ± 1.3 µm	190
11		CHCl$_3$	13	fibers/ ~0.4-4 µm	191

Continuation of **Table 2**: Overview of small molecules investigated by solution electrospinning.

Entry	Molecular structure	Solution parameters	Conc. [wt%]	Morphology/ fiber diameter	Ref.
12	n=6: α-cyclodextrin n=7: β-cyclodextrin n=8: γ-cyclodextrin	Water, DMF or DMAC	< 100	beads	192-195
			~100	beaded fibers	
			~140	fibers/ ~0.2-2 µm	
13		CHCl$_3$	18.1	fibers/ ~0.3-3 µm	199

Kern *et al.* reported the electrospinnability of diphenylalanine (Phe-Phe) nanotubes from 1,1,1,3,3,3-hexafluoro-2-propanol (HFIP) above 13.2 wt% (Table 2, entry 4). At lower concentrations (6 wt%) beads or a mixture of beads and fibers (13.2 wt%) were obtained due to the absence of entanglement respectively low entanglement of the assembled molecules. It is pointed out that strong interactions acting similar to sufficient entanglement, are essential for the fiber formation, and are only achieved with high concentrated solution. It was assumed that above 13.2 wt% the phenyl molecules start to interact in the Taylor cone, before a jet is ejected into the electrical field. As driving force for the formation of beadless fibers the evaporation of the solvent is mentioned forcing the diphenylalanine molecules into an ordered structure, at least along the surface of the jet. The surface of the fibers seems to be totally hydrophobic and is probably completely composed of phenyl moieties. The mechanical properties of the electrospun fibers were investigated in comparison to self-assembled fibers via atomic force microscopy (AFM) tests showing that the self-assembled fibers are much stronger.[186]

Further self-assembling aromatic peptide derivates, Fmoc-glycine (Table 2,entry 5) and Fmoc-phenylalanyl-glycine (Table 2, 5) were electrospun into fibers from various solvents with a concentration above 15 wt%.[187] Fmoc-phenylalanyl-glycine was electrospun from a 18 wt% solution in HFIP into short fibers with diameters from 300 nm to 10 µm (Table 2, entry 6).[187,188]

Also tetraphenylporphyrin (TPP) is a self-assembling, small molecule (Table 2, entry 7). Electrospinning from a 9.1 wt% HFIP solution resulted in fibers with an average diameter of 0.8 ± 0.6 μm. Furthermore, diphenylalanine (Phe-Phe) was coupled with TPP (Phe-Phe-TPP) and electrospun from HFIP (Table 2, entry 8). Nanofibers with a diameter distribution of 0.4 ± 0.3 μm were obtained. Additionally, a mixture of Phe-Phe and Phe-Phe-TPP (1:9 mol%) was electrospun from a 9.1 wt% HFIP solution into fibers (0.5 ± 0.2 μm).[189]

At a very low concentration of 3 wt%, two bioactive peptide amphiphiles were electrospun from water (Table 2, entry 9 and 10). Due to the achieved, already sufficient high enough solution concentration and solution conductivity, electrospun fibers with average diameters of around 4 μm were collected.[190]

A heteroditopic monomer was successfully electrospun from solution by Huang *et al.*. Benzo-21-crown-7 forms with a dialkylammonium salt a host-guest interaction which self-assembles in chloroform into a rod-like fiber at high concentrations (Table 2, entry 11). The electrospinning from chloroform in a concentration of 250 mM resulted in a nonwoven with a broad fiber diameter distribution in the range from 200 nm to 4 μm. Huang *et al.* argue that the formation of the required stable electrospinning jet is stabilized by the formation and entanglement of the supramolecular structure. Moreover, the increase of the solution viscosity caused by the good association of the host-guest complex in chloroform is important to generate fibers. Using Acetonitril instead of chloroform as electrospinning solvent solely beads were obtained. The choice of solvent is crucial in the electrospinning process since it affects the bond strength between the molecules as well as the solution viscosity.[191]

The class of cyclodextrins is the most published representative of electrospinable low molecular weight substances. Cyclodextrines are cyclic oligosaccharides with a ring-shaped molecular structure. If the chemical structure is built up of six, seven or eight glucopyranose units, α-, β- or γ-cyclodextrins are formed, respectively. Like the heteroditopic monomer, also cyclodextrins can form host-guest complexes with various small molecules and self-assemble via intermolecular hydrogen bonding into intriguing structures. The ring-shaped cyclodextrin structure acts thereby as hydrophobic cavity.

In 2010 Uyar *et al.* reported on electrospun cyclodextrin nanofibers obtained from very high concentrated solutions for the first time.[192] Bead-free nanofibers from β- and γ-cyclodextrins were collected from water, dimethylformamide (DMF), and dimethyl-acetamide in concentrations of 140 and 160 (w/v) (Table 2, entry 12). Note that more substance than solvent was used. The obtained fibers were in the range of 20 nm to

2.0 µm. At concentration around 100-120 % (w/v) beaded fibers were obtained and electrospraying occurred from the three solvents.[192-194]

Similar observations were made for α-cyclodextrin when it was electrospun from a 10 % (w/v) NaOH aqueous solution.[195] β-Cyclodextrins can also be electrospun from water at concentrations between 60 wt% to 70 wt% with an improved electrospinning set-up, which was published by Khan *et al.* in 2012.[196] An additional study of electrospinning of β-cyclodextrins from DMF was done by Diao *et al.*. The electrospun cyclodextrin nanofibers were decorated afterwards in an adsorption experiment with a red dye to show their potential in separation applications of organic pollutants or drug delivery.[197]

Also γ-cyclodextrin was electrospun from a DMSO/water system without using a carrying polymeric matrix. Furthermore, the nanofibers were successfully used for the entrapment of aniline and toluene by inclusion complexation opening the way for functional filter materials.[198]

These studies prove that at high concentrations cyclodextrin molecules are able to form sufficient hydrogen bonded aggregates and efficiently acting as chain entanglement and necessary overlap in electrospinning by stabilizing the electrified jet.

Also, the addition of urea to the water based electrospinning solutions was investigated because urea acts chaotropic and can break the hydrogen bonds between self-assembled molecules. Due to the lowered viscosity of the solution the jet was more stretched during the electrospinning process. Thinner fibers were obtained when up to 10 wt% urea were added to the 140 % (w/v) and 160 % (w/v) cyclodextrin solutions.

A higher amount of urea (17.5-20 wt%) led to the formation of beads, because the electrified jet broke up due to the lack of a sufficient amount of cyclodextrin aggregates.[192-196]

In a different work, a cyclodextrin inclusion complex with triclosan, an antibacterial and antifungal agent, was investigated in electrospinning. As the host-guest complex was not soluble in water, the dispersion was electrospun into homogenous fibers with an average fiber diameter distribution of 380 ± 200 nm. The addition of 20 wt% urea to the inclusion complex resulted also in beads, due the depressed self-assembly of the cyclodextrin molecules.[193]

Very recently, Yang *et al.* reported on a photoresponsive supramolecular substance in electrospinning. A blue fluorescent nonwoven of a stiff stilbene with two ureidopyrimidinone moieties in (Z)-configuartion was obtained by electrospinning from chloroform (Table 2, entry 13). The stiff stilbene derivate self-assembles in ring-chain supramolecular fashion due to the quadruple hydrogen-bonding unit 2-ureido-4[1H]-pyrimidinone. It is the first published work on photoresponsive quadruple hydrogen-bonded supramolecular substances.[199]

When lecithin, a phospholipid mixture, was investigated in melt electrospinning, the process failed and ended up in electrosprayed beads. Long *et al.* speculate that the electrospinning process occurs too fast for the different molecules interacting, included in the phospholipid mixture. Another phospholipid, 1-palmitoyl-2-oleoyl-*sn*-glycerol-3-phosphoethanol-amine (POPE, Figure 15), was successfully melt electrospun at 200 °C into fibers with an average fiber diameter of 6.5 ± 2.0 µm by this research group. They argue that POPE molecules associate fast enough during the electrospinning process due to its well-defined chemical structure and the existing long range aggregates in melt.[164,200]
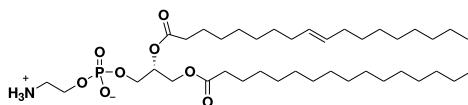
Figure 15. Chemical structure of 1-palmitoyl-2-oleoyl-*sn*-glycerol-3-phosphoethanol-amine (POPE). It is the only investigated small molecule yielding fibers by melt electrospinning.[200]

This novel solution and melt electrospinning approach using low molecular weight substances offers a promising access to self-assembling molecules. The necessary requirements to obtain electrospun nano- and microfibers have to be further investigated.

1.4 References

[1]   Anton Schenek*; Lexikon Garne und Zwirne: Eigenschaften und Herstellung textiler Fäden*, **2006**, Deutscher Fachverlag GmbH, Frankfurt a.M., Germany.

[2]   Guozhong Cao; *Nanostructures & Nanomaterials*, Synthesis, Properties & Applications, **2004**, Imperial College Press, London, UK.

[3]   John W. C. Dunlop, Richard Weinkamer, Peter Fratzl; *Mater. Today*, **2011**, *14*, 70-78.
Artful interfaces within biological materials.

[4]   Seema Agarwal, Joachim H. Wendorff, Andreas Greiner; *Polymer*, **2008**, *49*, 5603-5621.
Use of electrospinning technique for biomedical applications.

[5]   Ping Lu, Bin Ding; *Recent Pat. Nanotechnol*., **2008**, *2*, 169-182.
Application of electrospun fibers.

[6]   Younan Xia, Peidong Yang,Yugang Sun, Yiying Wu, Brian Mayers, Byron Gates, Yadong Yin, Franklin Kim, Haoquan Yan; *Adv. Mat.*, **2003**, *15*, 353-389.
One-dimensional nanostructures: synthesis, characterization, and applications.

[7]   Jean-Marie Lehn; *Angew. Chem. Int. Ed. Engl.*, **1988**, *27*, 89-112.
Supramolecular chemistry – Scope and perspectives; molecules, supermolecules, and molecular devices (Nobel Lecture).

[8]   Nobuo Kimizuka; *Adv. Polym. Sci.,* **2008**, *219*, 1-26.
Self-assembly of supramolecular nanofibers.

[9]   Macromolecular Chemistry I, University of Bayreuth, Germany.

[10]   Emily B. Anderson, Denis Ingildeev, Frank Hermanutz, Alexandra Müller, Michael Schweizer, Michael R. Buchmeiser; *J. Mater. Chem*., **2012**, *22*, 11851-11860.
Synthesis and dry-spinning fibers of sulfinyl-based poly(p-phenylene vinylene) (ppv) for semi-conductive textile applications.

[11]   A. L. Kalabin, E. A. Pakshver, N. A. Kukushkin; *Theor. Found. Chem. Eng*., **1996**, *30*, 295-301.
Modeling the filament formation in the wet spinning of synthetic fiber from polymer solutions.

[12]   Edith Mathiowitz, Danya M. Lavin, Richard A. Hopkins; *Therapeutic Delivery*., **2013**, *4*, 1075-1077.
Wet spun microfibers: potential in the design of controlled-release scaffolds?

[13]   K. Katayama, T. Amano, K. Nalcamura; *Kolloid-Zeitschrift, Zeitschrift für Polymere*, **1968**, *226*, 125-134.
Structural formation during melt spinning process.

[14]   John C. Slattery, Sangheon Lee; *J. Non-Newtonian Fluid Mech*., **2000**, *89*, 273-286.
Analysis of melt spinning.

[15]   Randall R. Bresee, Wen-Chien Ko; *International Nonwovens Journal INJ*, **2003**, *12*, 21-29.
Fiber formation during melt blowing.

[16]   Wanli Han, Xinhou Wang, Gajanan S. Bhat; *J. Nanomater. Mol. Nanotechnol*., **2013**, *2*.
Structure and air permeability of melt blown nanofiber webs.

[17]   http://www.hillsinc.net; 21.07.2014.

[18]   Ralf T. Weitz, Ludger Harnau, Stephan Rauschenbach, Marko Burghard, Klaus Kern; *Nano Lett.*,
         2008, *8*, 1187-1191.
         Polymer nanofibers via nozzle-free centrifugal spinning.

[19]   Joachim H. Wendorff, Seema Agarwal, Andreas Greiner (**2012**) *Electrospinning: Materials,*
         Processing and Applications, Wiley-VCH Verlag GmbH & Co. KGaA, Weinheim, Germany.

[20]   Yuris Dzenis; *Science*, **2004**, *304*, 1917-1919.
         Spinning continuous fibers for nanotechnology.

[21]   Emil Fischer; *Ber. Dtsch. Chem. Ges.*, **1894**, *27*, 2985-2993.
         Einfluss der Configuration auf die Wirkung der Enzyme.

[22]   Joanathan W. Steed, Jerry L. Atwood, Philip A. Gale; *Definition and Emergence of Supramolecular*
         Chemistry; published in *Supramolecular Chemistry: From Molecules to Nanomaterials, 8 Volume*
         Set in **2012** by John Wiley & Sons, Ltd; p. 3-8.

[23]   Dushyant B. Varshey, John R.G. Sander, Tomislav Friščić, Leonard R. MacGillivray; *Supramolecular*
         Interactions; published in *Supramolecular Chemistry: From Molecules to Nanomaterials, 8*
         Volume Set in **2012** by John Wiley & Sons, Ltd; p. 9-24.

[24]   Jean-Marie Lehn; *Pure Appl. Chem.*, **1978**, *50*, 851-892.
         Cryptates: inclusion complexes of macropolycyclic receptor molecules.

[25]   Jean-Marie Lehn; *Angew. Chem. Int. Ed. Engl.*, **1990**, *29*, 1304-1319.
         Perspectives in supramolecular chemistry – From molecular recognition towards molecular
         information processing and self-organization.

[26]   Jean-Marie Lehn; *Macromol. Symp.*, **2001,** *174*, 5-6.
         Supramolecular polymer chemistry.

[27]   Jean-Marie Lehn; *Polym. Int.*, *51*, **2002**, 825-839.
         Supramolecular polymer chemistry – Scope and perspectives.

[28]   Jean-Marie Lehn; *Chem. Soc. Rev.*, **2007**, *36*, 151-160.
         From supramolecular chemistry towards constitutional dynamic chemistry and adaptive
         chemistry.

[29]   Michael F. Geer, Linda S. Shimizu; *Self-Assembly and Self-Organization*; published in
         Supramolecular Chemistry: From Molecules to Nanomaterials, 8 Volume Set in **2012** by
         John Wiley & Sons, Ltd; p. 167-180.

[30]   Jonathan W. Steed, Jerry L. Atwood; *Supramolecular Chemistry*, 2nd Edition, John Wiley & Sons,
         Ltd.; Chichester, UK; **2009**.

[31]   Pierangelo Metrangolo, Hannes Neukirch, Tullio Pilati, Giuseppe Resnati; *Acc. Chem. Res*., **2005**,
         38, 386-395.
         Halogen bonding based recognition processes: A world parallel to hydrogen bonding.

[32]   Linus Pauling; *JACS*, **1931**, *53*, 1367-1400.
        The nature of the chemical bond. Application of results obtained from the quantum mechanics and from a theory of paramagnetic susceptibility to the structure of molecules.

[33]   George A. Jeffrey; *An Introduction to Hydrogen Bonding*; Oxford University Press: New York, **1997**.

[34]   Christoph A. Hunter, Jeremy K.M. Sanders; *JACS*, **2009**, *112*, 5525-5534.
        The nature of π- π interactions.

[35]   W. Brian Jennings, Brid M. Farrell, John F. Malone; *Acc. Chem. Res.*, **2001**, *34*, 885-894.
        Attractive intramolecular edge-to-face aromatic interactions in flexible organic molecules.

[36]   Alfonso Gautieri, Simone Vesentini, Alberto Redaelli, Markus J. Buehler; *Nano Lett*., **2011**, *11*, 757-766.
        Hierarchical structure and nanomechanics of collagen microfibrils from the atomistic scale up.

[37]   Aaron Klug; *Angew. Chem. Int. Ed. Engl*.; **1983**, *22*, 565-582.
        From macromolecules to biological assemblies (Nobel Lecture).

[38]   Nobuo Kimizuka; *Soluble Amphiphilic Nanostructures and Potential Applications*; published in *Supramolecular Polymers, Second Edition* in **2005** by CRC Press; p. 481.

[39]   Martin J. Greenall, Carlos M. Marques; *Phys. Rev. Lett.*, **2013**, *110*, 88301-1-4.
        Can amphiphile architecture directly control vesicle size?

[40]   Hans Wolfgang Spiess; *Macromolecules*, **2010**, *43*, 5479-5491.
        Interplay of structure and dynamics in macromolecular and supramolecular systems.

[41]   David González-Rodríguez; Albert P.H.J. Schenning, *Chem. Mater.*, **2011**, *23,* 310-325.
        Hydrogen-bonded supramolecular π-functional materials.

[42]   Luc Brunsveld, B.J.B. Folmers, E.W. Meijer, Rint P. Sijbesma; *Chem. Rev*., **2001**, *101*, 4071-4097.
        Supramolecular polymers.

[43]   Frank S. Bates, Glenn H. Fredrickson; *Physics Today*, **1999**, *52*, 32-38.
        Block copolymers-designer soft materials.

[44]   Yiyong Mai, Adi Eisenberg; *Chem. Soc. Rev*., **2012**, *41*, 5969-5985.
        Self-assembly of block copolymers.

[45]   Pim G. A. Janssen, Sara Jabbari-Farouji, Mathieu Surin, Xavier Vila, Jeroen C. Gielen, Tom F. A. de Greef, Matthijn R. J. Vos, Paul H. H. Bomans, Nico A. J. M. Sommerdijk, Peter C. M. Christianen, Philippe Leclere, Roberto Lazzaroni, Paul van der Schoot, E.W. Meijer, Albertus P. H. J. Schenning; *JACS*, **2009**, *131*, 1222-1231.
        Insights into templated supramolecular polymerization: Bond of naphthalene derivatives to ssDNA templates of different lengths.

[46]   Cameron C. Lee, Christoph Grenier, E.W. Meijer, Albertus P.H.J. Schenning; *Chem. Soc. Rev.*, **2009**, *38*, 671-683.
        Preparation and characterization of helical self-assembled nanofibers.

[47]   Yoshio Matsunaga, Nobuhiko Miyajima, Yuichi Nakayasu, Satoshi Sakai, Michihiro Yonenaga; *Bull. Chem. Soc. Jpn*, **1988**, *61*, 207-210.
        Design of novel mesomorphic compounds: N,N',N''-trialkyl-1,3,5-benzene-tricarboxamides.

[48]   Matthew P. Lightfoot, Francis S. Mair, Robin G. Pritchard, John E. Warren; *Chem. Commun.*, **1999**, 1945-1946.
        New supramolecular packing motifs: π-stacked rods encased in triply-helical hydrogen bonded amide strands.

[49]   Seda Cantekin, Tom. F.A. de Greef, Anja R.A. Palmans; *Chem. Soc. Rev.*, **2012**, *41*, 6125-6137.
        Benzene-1,3,5-tricarboxamide: a versatile ordering moiety for supramolecular chemistry.

[50]   Maaike de Loos, Jan H. van Esch, Richard M. Kellogg, Ben L. Feringa; *Tetrahedron*, **2007**, *63*, 7285-7301.
        C_3-Symmetric, amino acid based organogelators and thickeners: a systematic study of structure-property relations.

[51]   Kenji Hanabusa, Chiemi Koto, Mutsumi Kimura, Hirofusa Shirai, and Akikazu Kakehi; *Chem. Lett*., **1997**, *5*, 429-430.
        Remarkable viscoelasticity of organic solvents containing trialkyl-1,3,5-benzenetricarboxamides and their intermolecular hydrogen bonding.

[52]   Yoshiaki Yasuda, Eiichi Iishi, Hiroshi Inada, Yasuhiko Shirota; *Chem. Lett*., **1996**, *4*, 575-576.
        Novel low-molecular-weight organic gels: N,N',N''-tristearyltrimesamide/organic solvent system.

[53]   Toshiyuki Shikata, Yuichi Kuruma, Aiko Sakamoto, Kenji Hanabusa; *J. Phys. Chem*. B, **2008**, *112*, 16393-16402.
        Segment sizes of supramolecular polymers of N,N',N''-tris(3,7-dimethyloctyl)benzene-1,3,5-tricarboxamide in n-decane.

[54]   Hai Cao, Pengfei Duan, Xuefeng Zhu, Jian Jiang, Minghua Liu; *Chem. Eur. J.*, **2012**, *18*, 5546-5550.
        Self-assembled organic nanotubes through instant gelation and universal capacity for guest molecule encapsulation.

[55]   Naien Shi, Hao Dong, Gui Yin, Zheng Xu, Shuhua Li; *Adv. Funct. Mater.*, **2007**, *17*, 1837-1843.
        A smart supramolecular hydrogel exhibiting pH-modulated viscoelastic properties.

[56]   Andreas Bernet, Rodrigo Q. Albuquerque, Marina Behr, Sebastian T. Hoffmann, Hans-Werner Schmidt; *Soft Matter*, **2012**, *8*, 66-69*.*
        Formation of supramolecular chromophore: a spectroscopic and theoretical study.

[57]   Hendrik Frisch, Jan Patrick Unsleber, David Lüdeker, Martin Peterlechner, Gunther Brunklaus, Mark Wallner, Pol Besenius; *Angew. Chem. Int. Ed.*, **2013**, *52*, 10097-10101.
        pH-switchable ampholytic supramolecular copolymers.

[58]   Maximilian von Gröning, Isja de Feijter, Marc C.A. Stuart, Ilja K. Voets, Pol Besenius; *J. Mat. Chem. B,* **2013**, *1*, 2008-2012.
        Tuning the aqueos self-assembly of multistimuli-responsive polyanionic peptide nanorods.

[59]   Feng Li, Ganesan Palaniswamy, Menno R. de Jong, Andreas Åslund, Peter Konradsson, Antonius T. M. Marcelis, Ernst J. R. Sudhölter, Martien A. Cohen Stuart, Frans A. M. Leermakers; *Chem. Phys. Chem.*, **2010**, *11*, 1956-1960.
        Nanowires formed by the co-Assembly of a negatively charged low-molecular weight gelator and a zwitterionic polythiophene.

[60]   Christianus M.A. Leenders, Tristan Mes, Matthew B. Baker, Marcel M.E. Koenigs, Pol Besenius, Anja A.R. Palmans, E.W. Meijer; *Mater. Horiz.*, **2014**, *1*, 116-120.
        From supramolecular polymers to hydrogel materials.

[61]   Frank Abraham, Hans-Werner Schmidt; *Polymer*, **2010**, *51*, 913-921.
        1,3,5-Benzenetrisamide based nucleating agents for poly(vinylidene fluoride).

[62]   Florian Richter, Hans-Werner Schmidt; *Macromo. Mater. Eng.*, **2013**, *298*, 190-200.
        Supramolecular nucleating agents for poly(butylene terephthalate) based on 1,3,5-benzenetrisamides.

[63]   Frank Abraham, Sandra Ganzleben, Doris Hanft, Paul Smith, Hans-Werner Schmidt;
        Macromol. Chem. Phys., **2010**, *211*, 171-181.
        Synthesis and structure-efficiency relations of 1,3,5-benzenetrisamides as nucleating agents and clarifiers for isotactic poly(propylene).

[64]   Markus Blomenhofer, Sandra Ganzleben, Doris Hanft, Hans-Werner Schmidt; *Macromolecules*, **2005**, *38*, 3688-3695.
        „Designer" nucleating agents for polypropylene.

[65]   Nils Mohmeyer, Nico Behrendt, Xiaoquing Zhang, Paul Smith, Volker Altstädt, Gerhard M. Sessler, Hans-Werner Schmidt; *Polymer*, **2007**, *48*, 1612-1619.
        Additives to improve the electret properties of isotactic polypropylene.

[66]   Jorg Roosma, Tristan Mes, Philippe Leclère, Anja R. A. Palmans, E. W. Meijer; *JACS*, **2008**, *130*, 1120-1121.
        Supramolecular materials from benzene-1,3,5-tricarboxamide-based nanorods.

[67]   Holger Misslitz, Klaus Kreger, Hans-Werner Schmidt; *Small*, **2013**, *9*, 2053-2058.
        Supramolecular nanofiber webs in nonwoven scaffolds as potential filter media.

[68]   Vassili N. Dokorou, Annie K. Powell, George E. Kostakis; *Polyhedron*, **2013**, *52*, 538-544.
        Two pseudopolymorphs derived from alkaline earth metals and the pseudopeptidic ligand trimesoyl-tris-glycine.

[69]   Xu-Zhong Luo, Xin-Jian Jia, Ji-Hua Deng, Jin-Lian Zhong, Hui-Jin Liu, Ke-Jun Wang, Di-Chang Zhong; *JACS*, **2013**, *135*, 11684-11687.
        A microporous hydrogen-bonded organic framework: Exceptional stability and high selective adsorption of gas and liquid.

[70]   Shi-Meng Wang, Ling Qian, Hong-Ye Bai, Wei-Qiang Fan, Chun-Bo Liu, Guang-Bo Che;
        Transition Met. Chem., **2013**, *38*, 157-163.
        Synthesis, structures, and photoluminescence properties of three metal(II) coordination polymers derived from a flexible tripodal ligand and 2,6-pyridinedicarboxylic acid.

[71]   Sung Ho Jung, Jiwon Jeon, Hyungjun Kim, Justyn Jaworski, Jong Hwa Jung; *JACS*, **2014**, *136*, 6446-6452.
        Chiral arrangement of achiral Au nanoparticles by supramolecular assembly of helical nanofiber templates.

[72] Matthieu Raynal, François Portier, Piet W. N. M. van Leeuwen, Laurent Bouteiller; *JACS*, **2013**, *135*, 17687-17690.
Tunable asymmetric catalysis through ligand stacking in chiral rigid rods.

[73] Perumal Rajakumar, Ramasamy Anandhan, Devaraj Manoj, Jayadevan Santhanalakshimi; *RSC Adv.*, **2014**, *4*, 4413-4419.
Synthesis, $H_2PO_4^-$ and Pd^{2+} ion sensing and gold nanoparticles encapsulation of ferrocenyldendrimers by a green chemistry approach.

[74] Magnus Kristiansen, Paul Smith, Henri Chanzy, Christian Baerlocher, Volker Gramlich, Lynne McCusker, Thomas Weber, Philip Pattison, Markus Blomenhofer, Hans-Werner Schmidt; *Cryst. Growth Des.*, **2009**, *9*, 2556-2558.
Structural aspects of 1,3,5-benzenetrisamides–A new family of nucleating agents.

[75] Xiaodong Hou, Matthew Schober, Qianli Chu; *Cryst. Growt. Des.*, **2012**, *12*, 5159-5163.
A chiral nanosheet connected by amide hydrogen bonds.

[76] Anja R.A. Palmans, Jef A.J.M. Vekemans, Huub Kooijman, Anton L. Spek, E.W. Meijer; *Chem. Comm.*, **1997**, 2247-2248.
Hydrogen-bonded porous solid derived from trimesic amide.

[77] Lalit Rajput, Kumar Biradha; *J. Mol. Struct.*, **2011**, *991*, 97-102.
Crystalline forms of 1,3,5-benzene-tri(pyridinyl)carboxamides: Isolated site hydrates as polymorphs and solvates.

[78] Alain Rochefort, Étienne Bayard, Salah Hadj-Messaoud; *Adv. Mater.*, **2007**, *19*, 1992-1995.
Competitive hydrogen bonding in π-stacked oligomers.

[79] Claudio A. Jiminéz, Julio B. Belmar, Leandro Ortíz, Paulina Hidalgo, Oscar Fabelo, Jorge Pasán, Catalina Ruiz-Pérez; *Cryst. Growth Des.*, **2009**, *9*, 4987-4989.
Influence of the aliphatic wrapping in the crystal structure of benzene tricarboxamide supramolecular polymers.

[80] Lalit Rajput, Gargi Mukherjee, Kumar Biradha; *Cryst. Growth Des.*, **2012**, *12*, 5773-5782.
Influence of solvents in assembling tris(4-halophenyl)benzene-1,3,5-tricarboxamides: Interplay of N-H···O and Halogen···Halogen interactions.

[81] Yukimasa Harada, Yoshio Matsunaga; *Bull. Chem. Soc. Jpn*, **1988**, *61*, 2739-2741.
New mesomorphic compounds: N,N',N''-trialkanoyl-2-4-6-trimethyl-1,3,5-benzenetriamines.

[82] Andreas Timme, Roman Kress, Rodrigo Albuquerque, Hans-Werner Schmidt; *Chem. Eur. J.*, **2012**, *18*, 8329-8339.
Phase behavior and mesophase structures of 1,3,5-benzene- and 1,3,5-cyclohexanetricarbox-amides: Towards an understanding of the losing order at the transition into the isotropic phase.

[83]   Patrick J.M. Stals, Maarten M.J. Smulders, Rafael Martín-Rapún, Anja R.A. Palmans, E.W. Meijer; *Chem. Eur. J.,* **2009**, *15*, 2071-2080.
Assymetrically substituted benzene-1,3,5-tricarboxamides: Self-assembly and odd-even effects in the solid state and in dilute solutions.

[84]   Maarten M.J. Smulders, Albertus P.H.J. Schenning, E.W. Meijer; *JACS*, **2008**, *130*, 606-611.
Insights into the mechanism of cooperative self-assembly: The "sergeants-and-soldiers" principle of chiral and achiral C_3-symmetrical discotic trisamides.

[85]   Tristan Mes, Maarten M.J. Smulders, Anja R.A. Palmans, E.W. Meijer; *Macromolecules*, **2010**, *43*, 1981-1991.
Hydrogen-bond engineering in supramolecular polymers: Polarity influence on the self-assembly of benzene-1,3,5-tricarboxamides.

[86]   Daisuke Ogata, Toshiyuki Shikata, Kenji Hanabusa; *J. Phys. Chem. B*, **2004**, *108*, 15503-15510.
Chiral amplification of the structure and viscoelasticity of a supramolecular polymeric system consisting of N,N',N''-tris(3,7-dimethyloctyl)benzene-1,3,5-tricarboxamide and n-decane.

[87]   Seda Cantekin, Yoko Nakano, Jeffery C. Everts, Paul van der Schoot, E.W. Meijer, Anja A.R. Palmans; *Chem. Comm.*, **2012**, *48*, 3803-3805.
A stereoselectively deuterated supramolecular motif to probe the role of solvent during self-assembly processes.

[88]   Yoko Nakano, Albert J. Markvoort, Seda Cantekin, Ivo A.W. Filot, Huub M.M. ten Eikelder, E.W. Meijer, Anja A.R. Palmans; *JACS*, **2013**, *135*, 16497-16506.
Conformational analysis of chiral supramolecular aggregates: Modeling the subtle difference between hydrogen and deuterium.

[89]   Ivo A.W. Filot, Anja A.R. Palmans, Peter A.J. Hilbers, Emiel J.M. Hensen, Tom F.A. de Greefs, Evgeny A. Pidko; *Phys. Chem. Chem. Phys*, **2012**, *14*, 13997-4002.
The origin of isotope-induced helical-sense bias in supramolecular polymers of benzene-1,3,5-tricarboxamides.

[90]   Yoko Nakano, Takashi Hirose, Patrick J.M. Stals, E.W. Meijer, Anja R.A. Palmans; *Chem. Sci.*, **2012**, *3*, 148-155.
Conformational analysis of supramolecular polymerization processes of disc-like molecules.

[91]   Maarten M. Smulders, Patrick J.M. Stals, Tristan Mes, Tim F.E. Paffen, Albertus P.H.J. Schenning, Anja A.R. Palmans, E.W. Meijer; *JACS*, **2010**, *132*, 620-626.
Probing the limits of the majority-rules principle in a dynamic polymer.

[92]   Lorenzo Albertazzi, Daan van der Zwaag, Christianus M. A. Leenders, Robert Fitzner, Remco W. van der Hofstad, E. W. Meijer; *Science*, **2014**, *344*, 491-495.
Probing exchange pathways in one-dimensional aggregates with super-resolution microscopy.

[93]   Fátima García, Peter A. Korevaar, Arno Verlee, E.W. Meijer, Anja A.R. Palmans, Luis Sánchez; *Chem. Comm.*, **2013**, *49*, 8674-8676.
The influence of π-conjugated moieties on the thermodynamics of cooperatively self-assembling tricarboxamides.

[94]   Agnieszka Iwan, Henryk Janeczek, Bozena Kaczmarczyk, Jan Jurusik, Zbigniew Mazurak,
         Danuta Sek, Patrice Rannou, Jean-Pierre Bonnet, Adam Pron; *Synth. Met.*, **2009**, *159*, 282-291.
         *Supramolecular associations of poly(ketanil)s with sulfonic acid derivatives of
         benzenetricarboxamide via Brönsted acid–base interactions: Preparation, spectroscopic
         morphological and thermal investigations.*

[95]   Isja de Feijter, Pol Besenius, Lorenzo Albertazzi, E.W. Meijer, Anja A.R. Palmans, Ilja K. Voets; *Soft
         Matter*, **2013**, *9*, 10025-10030.
         Mechanistic control over morphology: self-assembly of a discotic amphiphile in water.

[96]   Christianus M.A. Leenders, Lorenzo Albertazzi, Tristan Mes, Marcel M.E. Koenigs,
         Anja A.R. Palmans, E.W. Meijer; *Chem. Comm.*, **2013**, *49*, 1963-1965.
         *Supramolecular polymerization in water harnessing both hydrophobic effects and hydrogen bond
         formation.*

[97]   Daoliang Wang, Youju Huang, Junjun Li, Lu Xu, Mingming Chen, Jiaojiao Tao, Liangbin Li; *Chem.
         Eur. J.*, **2013**, *19*, 685-690.
         *Lyotropic supramolecular helical columnar phases formed by C_3-symmetric and unsymmetric rigid
         molecules.*

[98]   Youju Hang, Yuanhua Cong, Junjun Li, Daoliang Wang, Jingtuo Zhang, Lu Xu, Weili Li, Liangbin Li,
         Guoqiang Pan, Chuanlu Yang; *Chem. Comm.*, **2009**, 7560-7562.
         Anisotropic ionic conductivities in lyotropic supramolecular liquid crystals.

[99]   Ivo A.W. Filot, Anja A.R. Palmans, Peter A.J. Hibers, Rutger A. van Santen, Evgeny A. Pidko,
         Tom F.A. de Greef; *J. Phys. Chem. B.*, **2010**, *114*, 13667-13674.
         *Understanding cooperativity in hydrogen-bond-induced supramolecular polymerization: A density
         functional theory study.*

[100]   Chidambar Kulkarni, Sandeep Kumar Reddy, Subi J. George, Sundaram Balasubramanian;
         Chem. Phys. Let., **2011**, *515*, 226-230.
         Cooperativity in the stacking of benzene-1,3,5-tricarboxamides: The role of dispersion.

[101]   Karteek K. Bejagam, Giacomo Fiorin, Michael L. Klein, Sundaram Balasubramanian; *J. Phys. Chem.
         B.*, **2014**, *118*, 5218-5228.
         *Supramolecular polymerization of benzene-1,3,5-tricarboxamide: A molecular dynamics
         simulation study.*

[102]   Patrick J.M. Stals, Peter A. Korevaar, Martijn A.J. Gillissen, Tom F.A. de Greef, Carel F.C. Fitié,
         Rint P. Sijbesma, Anja R.A. Palmans, E.W. Meijer; *Angew. Chem. Int. Ed.*, **2012**, *51*, 1-6.
         Symmetry breaking in the self-assembly of partially fluorinated benzene-1,3,5-tricarboxamides.

[103]   Marieluise Stumpf, Andreas Spörrer, Hans-Werner Schmidt, Volker Altstädt; Journal of Cellular
         Plastics, **2011**, *47*, 519-534.
         Influence of supramolecular additives on foam morphology of injection-molded i-PP.

[104]   Thorsten Metzroth, Anke Hoffmann, Rafael Martín-Rapún, Maarten M.J. Smulders, Koen Pieterse, Anja A.R. Palmans, Jef A.J.M. Vekemans, E.W. Meijer, Hans W. Spiess, Jürgen Gauss; *Chem. Sci.*, **2011**, *2*, 69-76.
Unravelling the fine structure of stacked bipydridine diamine-derived C₃-discotics as determined by X-ray diffraction, quantum-chemical calculations, Fast-MAS NMR and CD spectroscopy.

[105]   Martijn A.J. Gillissen, Tom T. Hoeben, A.J.H. Spiering, Jef A.J.M. Vekemans, Anja R.A. Palmans, E.W. Meijer; *Isr. J. Chem.*, **2011**, *51*, 118-1127.
Supramolecular chirality using both cooperative and isodesmic self-assembly: Hierarchical growth through competition.

[106]   Chidambar Kulkarni, Sundaram Balasubramanian, Subi J. George; *Chem. Phys. Chem.*, **2013**, *14*, 661-673.
What molecular features govern the mechanism of supramolecular polymerization?

[107]   Thuc-Quyen Nguyen, Mark L. Bushey, Louis E. Brus, Colin Nuckolls; *JACS*, **2002**, *124*, 15051-15054.
Tuning intermolecular attraction to create polar order and one-dimensional nanostructures on surfaces.

[108]   Aiko Sakamoto, Daisuke Ogata, Toshiyuki Shikata, Osamu Urakawa, Kenji Hanabusa; *Polymer*, **2007**, *47*, 956-960.
Large macro-dipoles generated in a supramolecular polymer of N,N',N''-tris(3,7-dimethyloctyl)benzene-1,3,5-tricarboxamide in n-decane.

[109]   Mark L. Bushey, Thuc-Quyen Nguyen, Colin Nuckolls; *JACS*, **2003**, *125*, 8264-8269.
Synthesis, self-assembly, and switching of one-dimensional nanostructures from new crowded aromatics.

[110]   Carel F.C. Fité, W.S. Christian Roelofs, Martijn Kemerink, Rint P. Sijbesma; *JACS,* **2010***, 132, 6892-6893.*
Remnant polarization in thin films from a columnar liquid crystal.

[111]   Carel F.C. Fité, W.S. Christian Roelofs, Pieter C.M.M. Magusin, Michael Wübbenhorst, Martijn Kemerink, Rint P. Sijbesma; *J. Phys. Chem. B,* **2012**, *116*, 3928-3937.
Polar switching in trialkylbenzene-1,3,5-tricarboxamides.

[112]   Rodrigo Q. Albuquerque, Andreas Timme, Roman Kress, Jürgen Senker, Hans-Werner Schmidt; *Chem. Eur. J.*, **2013**, *19*, 1647-1657.
Theoretical investigation of macrodipoles in supramolecular columnar stackings.

[113]   Marko Schmidt, Johannes J. Wittmann, Roman Kress, Denis Schneider, Stefan Steuernagel, Hans-Werner Schmidt, Jürgen Senker; *Cryst. Growth Des.*, **2012**, *12*, 2543-2551.
Crystal structure of a highly efficient clarifying agent for isotactic polypropylene.

[114]   Marko Schmidt, Johannes J. Wittmann, Roman Kress, Hans-Werner Schmidt, Jürgen Senker; *Chem. Comm.*, **2013**, *49*, 267-269.
Probing self-assembled 1,3,5-benzenetrisamides in isotactic polypropylene by ¹³C DQ solid-state NMR spectroscopy.

[115]   Martin Wegner, Dmytro Dudenko, Daniel Sebastiani, Anja A.R. Palmans, Tom F.A. de Greef, Robert Graf, Hans W. Spiess; *Chem. Sci.*, **2011**, *2*, 2040-2049.
The impact of the amide connectivity on the assembly and dynamics of benzene-1,3,5-tricarboxamides in the solid state.

[116]   Patrick J.M. Stals, Jeffery C. Everts, Robin de Bruijn, Ivo A.W. Filot, Maarten M.J. Smulders, Rafael Martín-Rapún, Evgeny A. Pidko, Tom F.A. de Greef, Anja R.A. Palmans, E.W. Meijer; *Chem. Eur. J.*, **2010**, *16*, 810-821.
Dynamic supramolecular polymers based on benzene-1,3,5-tricarboxamides: The influence of amide connectivity on aggregate stability and amplification of chirality.

[117]   Frank Abraham; *Synthesis and structure-property relations of 1,3,5-benzenetrisamides as nucleating agents for isotactic polypropylene and poly(vinylidene fluoride)*; **2009**, dissertation, University of Bayreuth, Germany.

[118]   Daniel Kluge, Frank Abraham, Stephan Schmidt, Hans-Werner Schmidt, Andreas Fery; *Langmuir*, **2010**, *26*, 3020-3023.
Nanomechanical properties of supramolecular self-assembled whiskers determined by AFM force mapping.

[119]   Erkang Fan, Ji Yang, Steven J. Geib, Timothy C. Stoner, Michael D. Hopkins, Andrew D. Hamilton; *J. Chem. Soc., Chem. Comm.*, **1995**, 1251-1252.
Hydrogen-bonding control of molecular aggregation: Self-complementary subunits lead to rod-shaped structures in the solid state.

[120]   Itsuro Tomatsu, Carel F.C. Fitié, Dmytro Byelov, Wim H. de Jeu, Pieter C.M.M. Magusin, Michael Wübbenhorst, Rint P. Sijbesma; *J. Phys. Chem. B,* **2009**, *113*, 14158-14164.
Thermotropic phase behavior of trialkyl cyclohexanetriamides.

[121]   Aiko Sakamoto, Daisuke Ogata, Toshiyuki Shikata, Kenji Hanabusa; *Macromoleucles*, **2005**, *38*, 8983-8986.
Controlled large macrodipoles in a supramolecular polymer of tri-3,7-dimethyloctyl-cis-1,3,5-cyclohexanetricarboxamide in n-decane.

[122]   Laura Sardone, Vincenzo Palermo, Eloïse Devaux, Dan Credgington, Maaike de Loos, Giovanni Marletta, Franco Cacialli, Jan van Esch, Paolo Samorì; *Adv. Mater.*, **2006**, *18*, 1276-1280.
Electric-field-assisted alignment of supramolecular fibers.

[123]   B. Sun, Y.Z. Long, H.D. Zhang, M.M. Li, J.L. Duvail, X.Y. Jiang, H-L. Yin; *Prog. Polym. Sci.*, **2014**, *39*, 862-890.
Advances in three-dimensional nanofibrous macrostructures via electrospinning.

[124]   Nick Tucker, Jonathan J. Stanger, Mark P. Staiger, Hussam Razzaq, Kathleen Hofman; *Journal* of Engineered Fibers and Fabrics *JEFF*, **2012**, *Special Issue: Fibers*, 63-73.
The history of the science and technology of electrospinning from 1600-1995.

[125]   Yiguang Wu, Qi An, Jingxiang Yin, Tao Hua, Huiming Xie, Guangtao Li, Hong Tang; *Colloid Polym Sci.*, **2008**, *286*, 897-905.
Liquid crystal fibers produced by using electrospinning technique.

[126]   Andreas Greiner, Joachim H. Wendorff; *Angew. Chem. Int. Ed.*, **2007**, *46*, 5670-5703.
         Electrospinning: A fascinating method for the preparation of ultrathin fibers.

[127]   Thandavamoorthy Subbiah, G. S. Bath, R. W. Tock, S. Parameswaran, S.S. Ramkumar;
         J. Appl. Polmy. Sci., **2005**, *96*, 557-569.
         Electrospinning of nanofibers.

[128]   Nandana Bhardwaj, Subhas C. Kundu; *Biotech. Adv.*, **2010**, *28*, 325-347.
         Electrospinning: A fascinating fiber fabrication technique.

[129]   Seeram Ramakrishna, Kazutoshi Fujihara, Wee-Eong Teo, Teik-Cheng Lim, Zuwei Ma (**2005**)
         An Introduction to Electrospinning and Nanofibers, World Scientific Publishing Co. Pte. Ltd.,
         Singapore.

[130]   Dietmar W. Hutmacher, Paul D. Dalton; *Chem. Asian J.*, **2011**, *6*, 44-56.
         Melt electrospinning.

[131]   L. Larrondo, R. St. John Manley; *J. Polym. Sci. Polym.Phys Ed*, **1981**, *19*, 909-920.
         *Electrostatic fiber spinning from polymer melts. I. Experimental observations on fiber formation
         and properties.*

[132]   L. Larrondo, R. St. John Manley; *J. Polym. Sci. Polym.Phys Ed*, **1981**, *19*, 921-932.
         *Electrostatic fiber spinning from polymer melts. II. Examination of the flow field in an electrically
         driven jet.*

[133]   L. Larrondo, R. St. John Manley; *J. Polym. Sci. Polym.Phys Ed*, **1981**, *19*, 933-940.
         *Electrostatic fiber spinning from polymer melts. III. Electrostatic deformation of a pendant drop of
         polymer melt.*

[134]   Xiao-fei Wang, Zheng-ming Huang; *Chin. J. Polym. Sci*, **2010**, *28*, 45-53.
         Melt-electrospinning of PMMA.

[135]   Paul D. Dalton, Dirk Grafahrend, Kristina Klinkhammer, Doris Klee, Martin Möller; *Polymer*, **2007**,
         48, 6823-6833.
         Electrospinning of polymer melts: Phenomenological observations.

[136]   Cosima Freiin von Salis-Soglio; *Struktur-Eigenschaftsbeziehungen von Additiven zur Verbesserung
         der Elektreteigenschaften und der Schmelzelektrospinnbarkeit von Polypropylen;* **2010**,
         dissertation, University of Bayreuth, Germany.

[137]   Rajkishore Nayak, Ilias Louis Kyratzis, Yen Bach Truong, Rajiv Padhye, Lyndon Arnold; *J. Mater.
         Sci.*, **2012**, *47*, 6387-6396.
         Melt-electrospinning of polypropylene with conductive additives.

[138]   S. N. Malakhov, A. Yu. Khomenko, S. I. Belousov, A. M. Prazdnichnyi, S. N. Chvalun,
         A. D. Shepelev, A. K. Budyka; *Fibre Chemistry*, **2009**, *41*, 355-359.
         Method of manufacturing nonwovens by electrospinning from polymer melts.

[139]   Paul D. Dalton, Kristina Klinkhammer, Jochen Salber, Doris Klee, Martin Möller;
         Biomacromolecules, **2006***, 7*, 686-690.
         Direct in vitro electrospinning with polymer melts.

[140]   Changhai Ru, Jie Chen, Zhushuai Shao, Ming Pang, Jun Luo; *AIP* Advance, 2014, *4*, 017108-1-11.
         A novel mathematical model for controllable near-field electrospinning.

[141]   Wee-Eong Teo, Seeram Ramakrishna; *Nanotechnology*, **2006**, *17*, R89-R106.
         A review on electrospinning design and nanofibre assemblies.

[142]   Avinash Baji, Yiu-Wing Mai, Shing-Chung Wong, Mojtaba Abtahi, Pei Chen; *Compos. Sci. Technol*.,
         2010, *70*, 703-718.
         *Electrospinning of polymer nanofibers: Effects on oriented morphology, structures and tensile
         properties.*

[143]   António M. dos Santos, Joris Dierck, Marc Troch, Mario Podevijin, Etienne Schacht; *Macromol.
         Mater. Eng.*, **2011**, *296*, 637-644.
         Production of continuous electrospun mats with improved mechanical properties.

[144]   Ho-Wang Tong, Min Wang; *Nano LIFE*, **2012**, *2*, 1250004-1-16.
         *Negative voltage electrospinning and positive voltage electrospinning of tissue engineering
         scaffolds: A comparative study and charge retention on scaffolds.*

[145]   Chris J. Thompson, Gorge G. Chase, Alexander L. Yarin, Darell H. Reneker; *Polymer*, **2007**, *48*,
         6913-6922.
         Effects of parameters on nanofibers diameter determined from electrospinning model.

[146]   Jason Lyons, Christopher Li, Frank Ko; *Polymer*, **2004**, *45*, 7597-7603.
         Melt-electrospinning part I: Processing parameters and geometric properties.

[147]   Joeseph M. Deitzel, James Kleinmeyer, D. Harris, Nora C. Beck Tan; *Polymer*, **2001**, *42*, 261-272.
         The effect of processing variables on the morphology of electrospun nanofibers and textiles.

[148]   Nicole E. Zander; *Polymers*, **2013**, *5*, 19-44.
         Hierarchially structured electrospun fibers.

[149]   Hidetoshi Matsumoto, Akihiko Tanioka; *Membranes*, **2011**, *1*, 249-264.
         *Functionalty in electrospun nanofibrous membranes based on fiber's size, surface area, and
         molecular orientation.*

[150]   Seema Agarwal, Andreas Greiner, Joachim H. Wendorff; *Prog. Poly. Sci.*, **2013**, *6*, 963–991.
         Functional materials by electrospinning of polymers.

[151]   George Collins, John Frederici, Yuki Imura, Luiz H. Catalani; *J. Appl. Phys*., **2012**, *111*, 044701-1-
         18.
         *Charge generation, charge transport, and residual charge in the electrospinning of polymers:
         A review of issues and complications.*

[152]   Darell H. Reneker, Alexander L. Yarin; *Polymer*, **2008**, *49*, 2387-2425.
         Electrospinning jets and polymer nanofibers.

[153]   Darell H. Reneker, Alexander L. Yarin, Eyal Zussman, Hongde *Xu*; *Adv. Appl. Mech.,* **2007**, *41*,
         43-195 and 345-346.
         Electrospinning of nanofibers from polymer solutions and melts.

[154]   Geoffrey I. Taylor; *Proc. R. Soc. Lond. A.*, **1964**, *280*, 383-397.
         Disintegration of water drops in an electric field.

[155]   Alexander L. Yarin, Sureeporn Koombhongse, Darell H. Reneker; *J. Appl. Phys.*, **2001**, *90*, 4863-4846.
         Taylor cone and jetting from liquid droplets in electrospinning of nanofibers.

[156]   Andreas Greiner, Joachim H. Wendorff; *Adv. Polym. Sci*, **2008**, *219*, 107-171.
         Functional self-assembled nanofibers by electrospinning.

[157]   Gregory C. Rutledge, Sergey V. Fridrikh; *Adv. Drug Deliv. Rev.*, **2007**, *59*, 1384-1391.
         Formation of fibers by electrospinning.

[158]   Moses M. Hohman, Michael Shin, Gregory Rutledge, Michael P. Brenner; *Phys. Fluids*, **2001**, *78*, 1149-1151.
         Electrospinning: A whipping fluid jet generates submicron polymer fibers.

[159]   Moses M. Hohman, Michael Shin, Gregory Rutledge, Michael P. Brenner; *Phys. Fluids*, **2001**, *13*, 2201-2220.
         Electrospinning and electrically forced jets. I. Stability theory.

[160]   Moses M. Hohman, Michael Shin, Gregory Rutledge, Michael P. Brenner; *Phys. Fluids*, **2001**, *13*, 2221-2236.
         Electrospinning and electrically forced jets. II. Applications.

[161]   Y. Michael Shin, Moses M. Hohman, Michael P. Brenner, Gregory C. Rutledge; *Polymer*, **2001**, *42*, 9955-9967.
         Experimental characterization of electrospinning: the electrically forced jet and instabilities.

[162]   Tao Han, Darrell H. Reneker, Alexander L. Yarin; *Polymer*, **2007**, *48*, 6064-6076.
         Buckling of jets in electrospinning.

[163]   A.V. Subbotin, V.G. Kulichikhin; *Polym. Sci., Ser. A.*, **2014**, *56*, 213-221.
         Dynamics of a conducting polymer jet in an electric field

[164]   Matthew T. Hunley, Matthew G. McKee, Pankaj Gupta, Garth L. Wilkes, Timothy E. Long; *Mater. Res. Soc. Symp. Proc.*, **2006**, *948*, 0948-B02-03.
         Taking advantage of supramolecular structure in melt and solution electrospinning.

[165]   Suresh L. Shenoy, W. Douglas Bates, Harry L. Frisch, Gary E. Wnek; *Polymer*, **2005**, *46*, 3372-3384.
         Role of chain entanglements on fiber formation during electrospinning of polymer solutions: Good solvent, non-specific polymer-polymer interaction limit.

[166]   Chitrabala Subramanian, Samuel C. Ugbolue, Steven B. Warner, Prabir K. Patra; *Mater. Res. Symp. Proc.*, **2008**, *1134*, 1134-BB08-18.
         The melt electrospinning of polycaprolactone (PCL) ultrafine fibers.

[167]   Huajun Zhou, Thomas B. Green, Yong Lak Joo; *Polymer*, **2006**, *47*, 7497-7505.
         The thermal effects on electrospinning of polylactic acid melts.

[168] Eduard Zhmayev, Daehwan Cho, Yong Lak Yoo; *Polymer*, **2010**, *51*, 274-290.
Modeling of melt electrospinning for semi-crystalline polymers.

[169] Eduard Zhmayev, Huajun Zhou, Yong Lak Yoo; *J. Non-Newtonian Fluid Mech.*, **2008**, *153*, 95-108.
Modeling of non-isothermal polymer jets in melt electrospinning.

[170] Geoffrey Taylor; *Proc. R. Soc. Lond. A.*, **1969**, *313*, 453-475.
Electrically Driven Jets.

[171] Bin Ding, Hak-Yong Kim, Se-Chul Lee, Douk-Rae Lee, Kyung-Ju Choi; *Fiber Polym*., **2002**, *3*, 73-79.
Preparation and characterization of nanoscaled poly(vinyl alcohol) fibers via electrospinning.

[172] Paul D. Dalton, Júlia Lleixà Calvet, Ahmed Mourran, Doris Klee, Martin Möller; *Biotechnol. J.*, **2006**, *1*, 998-1006.
Melt electrospinning of poly-(ethylene glycol-block-ε-caprolactone).

[173] Toby D. Brown, Paul D. Dalton, Dietmar W. Hutmacher; *Adv. Mater.*, **2011**, *23*, 5651-5657.
Direct writing by way of melt electrospinning.

[174] Toby D. Brown, Anna Slotosch, Laure Thibaudeau, Anna Taubenberger, Daniela Loessner, Cedryck Vaquette, Paul D. Dalton, Dietmar W. Hutmacher; *Biointerphases*, **2012**, *7*, 1-16.
Design and fabrication of tubular scaffolds via direct writing in a melt electrospinning mode.

[175] Paul D. Dalton, Nanna T. Jörgensen, Jürgen Groll, Martin Möller; *Biomed. Mater.,* **2008**, *3*, 034109-1-11.
Patterned melt electrospun substrates for tissue engineering.

[176] A. Jaworek, A.T. Sobczyk; *Journal of Electrostatics*, **2008**, *66*, 197-219.
Electrospraying route to nanotechnology: An overview.

[177] Attila Balogh, Gábor Drávavölgyi, Kornél Faragó, Attila Farkas, Tamás Vigh, Péter Lajos Sóti, István Wagner, János Madarász, Hajnalka Pataki, György Marosi, Zsombor Kristóf Nagy; *J. Pharm. Sci.*, **2014**, *103*, 1278-1287.
Plasticized drug-loaded melt electrospun polymer mats: Characterization, thermal degradation, and release kinetics.

[178] Luca Lanotte, Claudio Bilotti, Luigi Sabetta, Giovanna Tomaiuolo, Stefano Guido; *Polymer*, **2013**, *54*, 1295-1297.
Dispersion of sepiolite rods in nanofibers by electrospinning.

[179] Cong-Ju Li, Guo-Rong Xu; *e-Polymers*, **2011**, *12*,1-9.
Electrospinning technique in the nano-photocatalyst research.

[180] Madhab Prasad Bajgai, Daman Chandra Parajuli, Soo-Jin Park, Hyung-Sub Kang, Kong Hee Chu, Hak Yong Kim; *Bioceram Dev. Appl.*, **2011**, *1*, 1-4.
Hydroxyapatite particulate nanofiber modified titanium: In-vitro bioactivity.

[181] Deng-Guang Yu, Christopher Branford-White, Gareth R. Williams, S. W. Annie Bligh, Kenneth White, Li-Min Zhu, Nicholas P. Chatterton; *Soft Matter,* **2011**, *7*, 8239-8247.
Self-assembled liposomes from amphiphilic electrospun nanofibers.

[182]   Matthew G. McKee, John M. Layman, Matthew P. Cashion, Timothy E. Long; *Science*, **2006**, *311*, 353-355.
        Phospholipid nonwoven electrospun membranes.

[183]   Matthew T. Hunley, Matthew G. McKnee, Timothy E. Long; *J. Mater. Chem*., **2007**, *17*, 605-608.
        Submicron functional fibrous scaffolds based on electrospun phospholipids.

[184]   Matthew P. Cashion, Xiaolin Li, Yan Geng, Matthew T. Hunley, Timothy E. Long; *Langmuir*, **2010**, *26*, 678-683.
        Gemini surfactant electrospun membranes.

[185]   Sean T. Hemp, Amanda G. Hudson, Michael H. Allen, Jr., Sandeep S. Pole, Robert B. Moore, Timothy E. Long; *Soft Matter*, **2014**, **DOI:** 10.1039/C4SM00271G.
        Solution properties and electrospinning of phosphonium gemini surfactants.

[186]   Gurvinder Singh, Alexander M. Bittner, Sebastian Loscher, Nikola Malinowski, Klaus Kern; *Adv. Mater.*, **2008**, *20*, 2332-2336.
        Electrospinning of diphenylalanine nanotubes.

[187]   Wiwat Nuansing, Amaia Rebollo, Jose Maria Mercero, Javier Zumiga, Alexander M. Bittner; *J. Raman Spectrosc.*, **2012**, *43*, 1397-1406.
        Vibrational spectroscopy of self-assembling aromatic peptide derivates.

[188]   Wiwat Nuansing, Daniela Frauchiger, Florian Huth, Amaia Rebollo, Rainer Hillenbrand, Alexander M. Bittner; *Faraday Discuss.*, **2013**, *166*, 209-221.
        Electrospinning of peptide and protein fibres: Approaching the molecular scale.

[189]   Wiwat Nuansing, Evangelos Georgilis, Thales V.A.G. de Oliveira, Georgios Charalambidis, Aitziber Eleta, Athanassios G. Coutsolelos, Anna Mitraki, Alexander M. Bittner; *Part. Part. Syst. Charact.*, **2014**, *31*, 88-93.
        Electrospinning of tetraphenylporphyrin compounds into wires.

[190]   Alok S. Tayi, E. Thomas Pashuck, Christina J. Newcomb, Mark T. McClendon, Samuel I.Stupp; *Biomacromolecules,* **2014**, *15*, 1323-1327.
        Electrospinning bioactive supramolecular polymers from water.

[191]   Xuzhou Yan, Mi Zhou, Jianzhuang Chen, Xiaodong Chi, Shengyi Dong, Mingming Zhang, Xia Ding, Yihua Yu, Shuang Shao, Feihe Huang; *Chem. Comm.*, **2011**, *47*, 7086-7088.
        Supramolecular polymer nanofibers via electrospinning of a heteroditopic monomer.

[192]   Asli Celebioglu, Tamer Uyar; *Chem. Comm.*, **2010**, *46*, 6903-6905.
        Cyclodextrin nanofibers by electrospinning.

[193]   Asli Celebioglu, Tamer Uyar; *Langmuir*, **2011**, *27*, 6218-6226.
        Electrospinning of polymer-free nanofibers from cyclodextrin inclusion complexes.

[194]   Asli Celebioglu, Tamer Uyar; *Nanoscale*, **2012**, *4*, 621-631.
        *Electrospinning of nanofibers from non-polymeric systems: polymer-free nanofibers from cyclodextrin derivat*es.

[195]   Asli Celebioglu, Tamer Uyar; *J. Colloid Interface Sci.*, **2013**, *404*, 1-7.
         Electrospinning of nanofibers from non-polymeric systems: Electrospun nanofibers from native cyclodextrins.

[196]   Joshua L. Manasco, Carl D. Saquin, Christina Tang, Saad A. Khan; *RSC Adv.*, **2012**, *2*, 3778-3784.
         Cyclodextrin fibers via polymer-free electrospinning.

[197]   Wang Zhang, Ming Chen, Binbin Zha, Guowang Diao; *Phys. Chem. Chem. Phys.*, **2012**, *14*, 9729-9737.
         Correlation of polymer-like solution behaviors with electrospun fiber formation of hydroxypropyl-β-cyclodextrin and the adsorption study on the fiber.

[198]   Asil Celebioglu, Tamer Uyar; *RSC Adv.*, **2013**, *3*, 22891-22895.
         Electrospun gamma-cyclodextrin (γ-CD) nanofibers for the entrapment of volatile organic compounds.

[199]   Jiang-Fei Xu, Yu-Zhe Chen, Dayong Wu, Li-Zhu Wu, Chen-Ho Tung, Qing-Zheng Yang; *Angew. Chem*., **2013**, *125*, 9920-9924.
         Photoresponsive hydrogen-bonded supramolecular polymers based on a stiff stilbene unit.

[200]   Matthew T. Hunley, Afia S. Karikari, Matthew G. McKnee, Brian D. Mather, John M. Layman, Ann R. Fornof, Timothy E. Long; *Macromol. Symp.*, **2008**, *270*, 1-7.
         Taking advantage of tailored electrostatics and complementary hydrogen bonding in the design of nanostructures for biomedical applications.

2 Objective of this thesis

The main objective of this thesis is the preparation, characterization and comparison of supramolecular nano- and microfibers based on 1,3,5-benzene- and 1,3,5-cyclohexanetrisamides using self-assembly from solution as bottom-up and electrospinning from melt as top-down approaches.

The *first objective* is the establishment of structure-property relations concerning the mechanical properties of nano- and microfibers prepared by self-assembly. Supramolecular 1,3,5-benzenetrisamide fibers should be prepared from nonpolar solvents within a fiber diameter range of 200 nm to 2 µm. The molecular structure of the trisamides (connectivity of the amide linkage to the central core, peripheral substituents) and the self-assembly conditions (concentration, cooling rate) should be varied to investigate the influence on the morphology. Suitable methods have to be applied to characterize the fiber structure. The mechanical properties of the supramolecular fibers should be determined in collaboration with the group of Prof. Andreas Fery, Physical Chemistry II, University of Bayreuth.

As top-down approach, electrospinning, which is well-studied for polymers, is a suitable method. In contrast, electrospinning of small molecules from melt has only been described for one phospholipid. Therefore, the *second objective* is to establish melt electrospinning of 1,3,5-benzene- and 1,3,5-cyclohexanetrisamides without utilizing a polymeric carrier material. The conditions of the melt electrospinning process such as spinning temperature, electrical field strength and electrical field direction should be varied to gain a deep understanding in the electrospinnability of this class of low molecular weight substances.

In case of a successful preparation of supramolecular nano- and microfibers, a systematic study of the influence of the molecular structure of 1,3,5-benzene- and 1,3,5-cyclohexanetrisamides on their electrospinnability should be performed in more detail. Additionally, the gained experience should be used to shape small molecules of other self-assembling compound classes into fibers by melt electrospinning (*third objective*).

To connect all previous findings, the *fourth objective* of this thesis is concerned with the comparison of the crystal structure, the morphology and the nanomechanical properties of 1,3,5-benzenetrisamides fibers obtained by self-assembly from nonpolar solvent and melt electrospinning. Further structure-property relations should be established.

3   Synopsis

Four publications are the basis of this thesis, which have already been published. Three of them are published as full article and one as feature article. They are presented in chapter 4, section 3 to 6.

The objective of this thesis is the formation, characterization and comparison of nano- and microfibers consisting of 1,3,5-benzene- and 1,3,5-cyclohexanetrisamides fabricated by self-assembly from a nonpolar solvent and by electrospinning from melt. The chemical structure of these low molecular weight substances was systematically varied to study the influence on their self-assembly behavior and melt electrospinnability. In addition, the mechanical properties of the supramolecular fibers obtained by a typical bottom-up and by a top-down approach were investigated in collaboration with the group of Prof. Andreas Fery, Physical Chemistry II, University of Bayreuth. The findings were compared to establish new structure-property relations. A schematically representation of the focus of the thesis is shown in Figure 16.
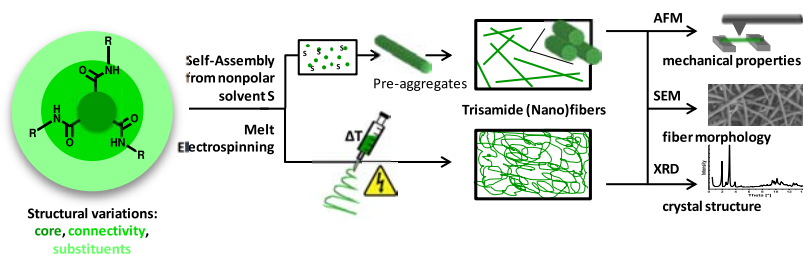
Figure 16. Schematic illustration of objectives of the publications and manuscripts of this thesis. Fibers are produced from 1,3,5-benzene- and 1,3,5-cylohexanetrisamides by using self-assembly and melt electrospinning techniques. The molecular structure is systematically varied to gain insights to structure-property relations concerning fiber morphology, mechanical properties and molecular orientation.

The 1,3,5-benzene- and 1,3,5-cyclohexanetrisamides discussed in this thesis were synthesized via established synthesis procedures using commercially available starting materials. In general, the substances were synthesized from the amine reacting with the corresponding acid chloride. The synthesis routes of 1,3,5-benzene- and 1,3,5-cyclohexanetrisamides and other investigated self-assembling molecules can be found in detail in the corresponding publications and manuscripts. The characterization of the materials was carried out by standard techniques. The purity of the materials was analyzed by nuclear magnetic resonance spectroscopy (NMR) and mass spectroscopy.

The thermal behavior was characterized by thermogravimetric analysis (TGA) and differential scanning calorimetry (DSC). Image techniques such as polarized optical microscopy (POM), scanning electron microscopy (SEM) and transmission electron microscopy (TEM) were applied to characterize the morphology of the formed fibrous materials. The crystal structure was investigated using X-ray diffraction.

The *first part* of this thesis deals with the influence of the molecular structure of 1,3,5-benzenetrisamides on fiber morphology and on mechanical properties of the fibers. Three compounds were selected varying in the connectivity of the amide group to the benzene core and carrying different alkyl substituents. Well-defined, self-assembled nano- and microfibers were obtained from all substances by controlled recrystallization from 2,2,4,4,6,8,8-heptamethylnonane (HMN) as nonpolar solvent, as a typical bottom-up approach. Using atomic force microscopy (AFM) bending experiments, the flexural rigidities and the Young's moduli of the supramolecular fibers were determined.

In the *second part*, the possibility to shape 1,3,5-benzene- and 1,3,5-cyclo-hexanetrisamides into fibers by using melt electrospinning, a typical top-down approach, is demonstrated for the first time. Long and homogenous fibers in the (sub)micron diameter range were obtained from the thermotropic nematic phase, and, as well, from the isotropic phase. In particular, the influence of the spinning temperature and the applied electrical field strength were investigated in detail.

In the *third part* of this thesis, the melt electrospinning approach was extended besides further trisamides to other self-assembling molecules such as bisamides, sorbitol and perylene bisimides derivatives. By a selection of several sets of compounds, the number of hydrogen bonds was systematically decreased or even prevented and the influence of the π-conjugated core was taken into account. The electrospinning process, in particular the formation of the Taylor cone, was investigated. With this work melt electrospinning of small molecules into nanofibers was established.

The *fourth part* connects and compares all results obtained in this thesis. Therefore, the focus is on the characterization on multiple length scales of supramolecular fibers obtained by bottom-up and top-down approaches. Self-assembled and melt electrospun microfibers were fabricated using the same 1,3,5-benzenetricarboxamide. On the Ångström scale, X-ray diffraction was performed to investigate the resulting crystal structure of both fiber types. The microscopic fiber morphologies were observed using SEM and the Young's modulus of self-assembled and melt electrospun fibers was determined by nanomechanical bending experiments.

In the following, the major findings, applied procedures and experimental set-ups of the four topics are summarized. No literature references are given in the synopsis, but they can be found in the attached publications and manuscripts (chapter 4).

3.1 Influence of the Molecular Structure and Morphology of Self-Assembled 1,3,5-Benzenetrisamide Nanofibers on their Mechanical Properties*

The first part of this thesis focuses on the self-assembly of different 1,3,5-benzenetrisamides into fibers. To establish structure-property relations, the mechanical properties were determined as function of the molecular structure and fiber morphology.

Three compounds (**1a**, **1b**, **2a**) were selected varying in connectivity of the amide moieties to the central core and the structure of the substituents. The morphology of the supramolecular assemblies obtained by a controlled recrystallization from 2,2,4,6,8,8-heptamethylnonane (HMN), a high boiling nonpolar solvent, depending on concentration and cooling rate was investigated in detail. The chemical structures of the compounds are shown in Figure 17.
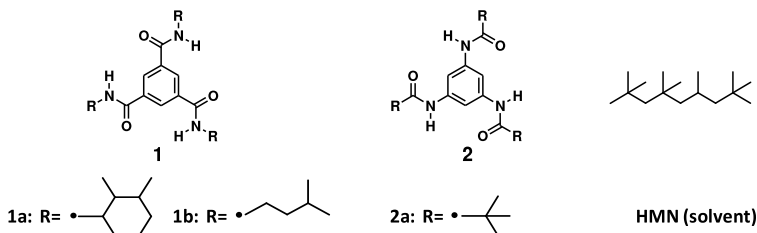
Figure 17. Chemical structures of 1,3,5-benzenetrisamides based on trismesic acid (**1**) and 1,3,5-triaminobenzene (**2**). As solvent 2,2,4,4,6,8,8-heptamethylnonane (HMN) was used.

For the controlled recrystallization, compounds **1a** (600 ppm), **1b** (500 ppm) and **2a** (600 ppm) were dissolved in a closed cup in HMN at 240 °C using a drop point cell. The self-assembly into fibers was achieved by cooling the samples to room temperature applying a cooling rate of 20 K/min for **1a** and **2b** and 5 K/min for compound **1b**. The morphology of the supramolecular fibers was investigated by scanning electron microscopy (SEM, Figure 18). All fibers exhibited large aspect ratios of more than 500:1. Over the whole length of the fiber, the uniform and linear structure, and, the fiber diameter are maintained. Nanofibers with a narrow average diameter of 200 nm were obtained from **1a**. Compound **1b** self-assembles into nanofibers with an average diameter 400 nm. Fibers with a significantly larger diameter are generated by compound **2a** (d= 2000 nm). Thus, the influence of the peripheral substituents and the amide connectivity to the benzene core on the self-assembly behavior resulting in different fiber morphologies was established.
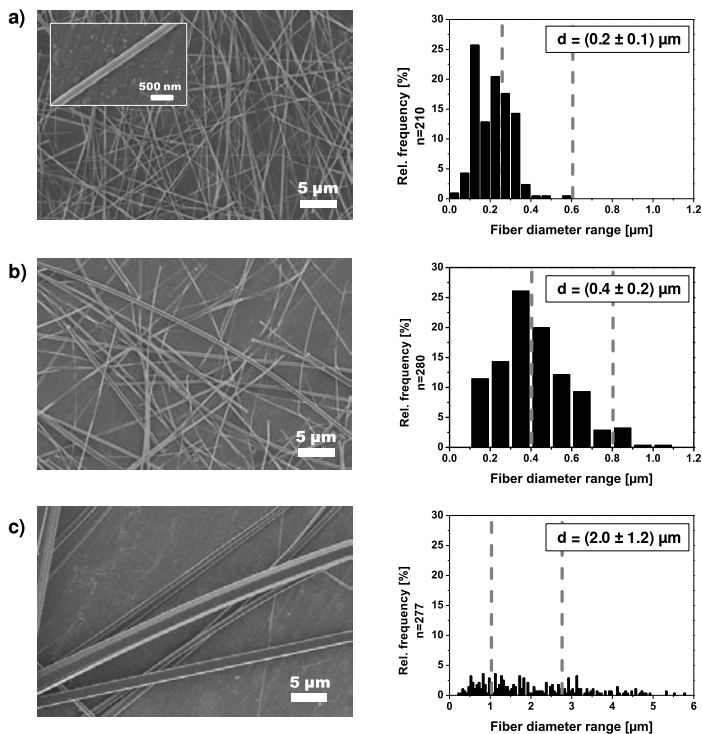
Figure 18. a) SEM image and size distribution of nanofibers of **1a**. The average diameter *d* is 0.2±0.1 μm. The SEM overview image and the inset highlight the narrow size distribution and homogeneous structure of the nanofibers. b) SEM image and size distribution of nanofibers of **1b** (d = 0.4±0.2 μm). c) SEM image and size distribution of fibers of **2a** (d = 2±1 μm). The vertical dashed lines in the histograms indicate the minimal and maximal size of each fiber type for which successful AFM bending measurements were performed. [Modified with permission from *Small*, **2012**, *8*, 2563-2570. Copyright © 2012 WILEY-VCH Verlag GmbH & Co. KGaA, Weinheim.]

The mechanical properties of the supramolecular fibers were determined by nanomechanical bending experiments using atomic force microscopy (AFM) in collaboration with the research group of Prof. Dr. Andreas Fery, Physical Chemistry II, University of Bayreuth. For that purpose, the fibers were transferred to glass substrates structured with channels (width: 10-40 μm) to achieve a freestanding configuration (Figure 19a). The deformation setup is schematically shown in Figure 19b. Recorded force-deformation curves on the supported segments of the fibers reveal no significant deformation of the fibers influencing the nanomechanical bending experiments (Figure 19c). Afterwards, force-distance measurements were performed on several positions x along the freestanding fiber segments. From the slope of the force-distance curve the

stiffness k of the fiber at the respective position x was calculated. An obtained stiffness profile of a supported fiber segment of **1a** is shown in Figure 19d.
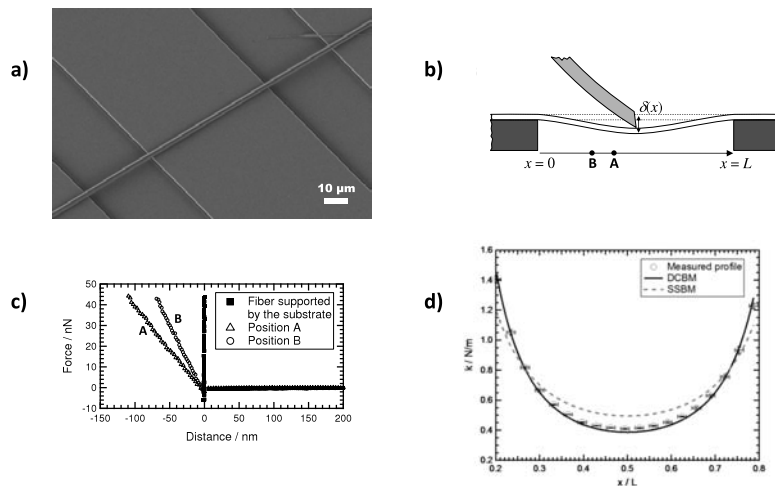
Figure 19. a) Freestanding configuration of a fiber on a structured glass substrate. b) Sketch of the experimental setup. c) Force-deformation curves obtained on the bare substrate, around the middle of the supported segment (A), and at an intermediate position between edge and midpoint (B). From the slope of the curves the stiffness k at the respective position is calculated. d) Stiffness profile of a freestanding segment of **1a** along position x. The data were obtained by averaging over six measurements on the same segment and were fitted with the double-clamped beam model (DCBM; solid line) and the supported beam model (SSBM; dashed line). The DCBM allows the better fit. [Modified with permission from *Small*, **2012**, *8*, 2563-2570. Copyright © 2012 WILEY-VCH Verlag GmbH & Co. KGaA, Weinheim.]

From the shape of the profiles, the boundary condition and the fiber modulus was determined. There are two commonly applied models describing the boundary conditions: The fiber ends are firmly fixed in the double-clamped beam model (DCBM), whereas the fiber ends can rotate freely in the supported beam model (SSBM). For the herein investigated fiber data both models were tested. Since the DCBM allowed the better fit, only segments corresponding to the DCBM were used for the calculation of the flexural rigidity and the modulus. The Young's modulus of **1a** was calculated to 2.3±0.3 GPa, for **1b** a modulus of 2.1±0.1 GPa and for **2a** of 3.3±0.4 GPa was determined. The values are comparable with those found for electrospun poly(trimethyl hexamethylene terephthalamide) (PA 6(3)T).

For the comparison of the three 1,3,5-benzenetrisamides the stiffness of the freestanding fiber segments was considered (Figure 20a). The rigidity of **1b** was two orders of magnitude higher than for **1a**. For compound **2a**, the flexural rigidity was three orders of magnitude higher. Since rigidity is proportional to the cross section, this increase is a pure size effect.

In addition, it was found that the distribution of the individual moduli is comparable for all systems (Figure 20b). Consequently, the influence of the investigated molecular structures of 1,3,5-benzenetrisamides on the Young's modulus is less pronounced.
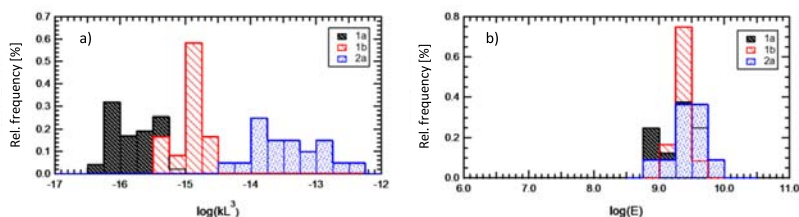
Figure 20. a) Apparent flexural rigidity of all investigated nanofiber segments. The stiffness was measured at the midpoint of the freestanding segments. Please note that the x axis has a logarithmic scaling. The rigidity of **1b** is one to two, and of **2a** is up to three orders of magnitude higher than that of **1a**. b) Distribution of the calculated modulus E for all three investigated systems. The results for all systems are comparable. [Adapted with permission from *Small*, **2012**, *8*, 2563-2570. Copyright © 2012 WILEY-VCH Verlag GmbH & Co. KGaA, Weinheim.]

Via a defined molecule design and carefully chosen recrystallization conditions the morphology of the nano- and microfibers can be altered and their flexural rigidity can be tuned while maintaining the Young's modulus.

3.2 Shaping Self-Assembling Small Molecules into Fibres by Melt Electrospinning*

Usually, a liquid drop of a low molecular weight substance disrupts into droplets when subjected to an electric field due to the lack of chain entanglement. Recently, it was shown by Long *et al.* that secondary interactions in small molecules can act similar to chain entanglement in polymers necessary to form fibers by solution and melt electrospinning. That 1,3,5-cyclohexane- and 1,3,5-benzenetrisamides self-assemble into supramolecular structures from solution was well-investigated in the first chapter of this thesis. Their mesophase behaviour and the existence of a macrodipole along the columnar stacking axis which can be utilized to align self-assembled fibers in an electrical field is the motivation to investigate these small molecules in melt electrospinning.

In this chapter, for the first time , the fiber formation from 1,3,5-cyclohexane- and 1,3,5-benzenetrisamides using melt electrospinning technique as top-down approach was described. It was demonstrated that quasi-endless and homogenous fibers were obtained from the liquid crystal nematic and from the isotropic phase of 1,3,5-cyclohexane- and 1,3,5-benzenetrisamides. It is assumed that even in the optical isotropic melt sufficient secondary interactions are present to prevent the electrospinning jet from disruption. In particular, the influence of the spinning temperature and the applied electrical field strength on the morphology of the electrospun material was studied.

Three compounds, 1,3,5-cylohexane- (**1**) and two 1,3,5-benzenetrisamides (**2**-**3**), were chosen, their molecular structure differing in core structure, connectivity of the amide groups to the central core, and the length of the linear aliphatic substituents (Figure 21-23). Compound **1** and **2** form liquid crystalline phases: 1,3,5-cylohexanetrisamide **1** exhibits a columnar rectangular plastic mesophase followed by a nematic phase before the transition into the isotropic state is observed. Compound **2** exhibits a hexagonal plastic phase transforming into a columnar hexagonal ordered phase before reaching the isotropic state. Compound **3** is characterized by a melting point without forming any mesophases.

The obtained fiber morphologies of **1**-**3** were investigated as function of spinning temperature and applied electrical field strength. The used electrospinning set-up is a custom designed machine. The syringe needle and all attached electronic components

were earthed and the high voltage power supply was attached to the collector plate. For comparable electrospinning parameters, the needle to collector distance (6 cm) and the flow rate (200 μL·h^{-1}) was kept constant for all experiments.

Compound **1**, a 1,3,5-benzenetrisamide based on trimesic acid, was electrospun from its nematic phase since this phase is less viscous than columnar phases. From the columnar phase at 200 °C electrospinning failed due to the high viscosity of the melt. Moreover, fibers were also collected by melt electrospinning from the optical isotropic melt, even if secondary interactions are not expected anymore (Figure 21).
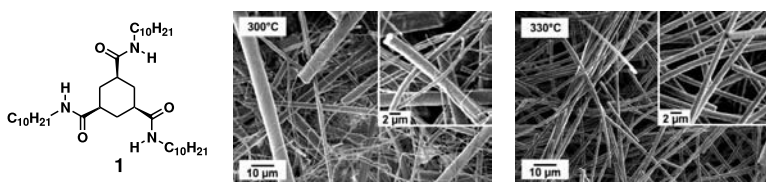
Figure 21. Left: chemical structure of **1**. Comparison of SEM images of melt electrospun fibers of **1** from the nematic phase at 300°C (center) and optical isotropic phase at 330°C (right). [Modified from *Soft Matter*, **2012**, *8*, 9972-9976 with permission from The Royal Society of Chemistry.]

A more heterogeneous spinning process was observed for electrospinning from the nematic phase due to the relatively high melt viscosity resulting in fiber with a broader diameter distribution (d=1.1±1.2 μm). Long and homogenous fibers with a size distribution of d=1.3±0.2 μm were obtained from the isotropic melt.

For compound **2** the fiber formation was studied as function of the spinning temperature (Figure 22).
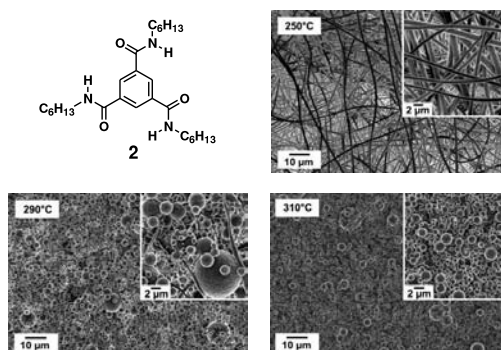
Figure 22. Chemical structure of **2** and the SEM images of melt electrospun fibers and spheres of **2** as a function of the spinning temperature. Spinning conditions: voltage: -30 kV, flow-rate: 200 μL h^{-1}, distance needle tip–ground plate: 6 cm, needle ID: 0.6 mm. [Modified from *Soft Matter*, **2012**, *8*, 9972-9976 with permission from The Royal Society of Chemistry.]

Electrospinning from the columnar phase at 200 °C was not possible due to the high melt viscosity. However, at 32 K above its transition into the isotropic phase (250°C) homogenous and quasi-endless fibers were obtained with a diameter distribution of 0.9±0.2 μm. By further increasing the temperature (290 °C) a fiber thinning to d=0.3±0.2 μm and the formation of spheres was observed. At an even higher spinning temperature (310°C) solely spheres were collected.

Compound **3**, based on 1,3,5-triaminobenzene, was electrospun from its isotropic melt at 200 °C, and the influence of the applied electrical field strength was studied (Figure 23). At a voltage of -25 kV (E=4.2 kV·cm^{-1}) thick fiber fragments with an average diameter of 12.0±2.0 μm were obtained. With increasing electric field strength, respectively voltage, an elongation of the fragments to homogenous and quasi-endless fibers was observed. Fibers with an average size distribution of d=2.2±0.4 μm were collected at -45 kV (E=7.5 kV·cm^{-1}). A stronger electrical field induces additional charges to the melt droplet and facilitates the formation of long and homogenous fiber by melt electrospinning.
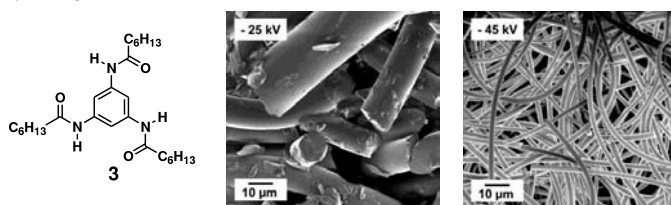
Figure 23: Left: chemical structure of **3**. SEM images of melt electrospun fibers of **3** from the isotropic phase as function of the electrical field strength E: center: -25 kV (E=4.2 kV·cm^{-1}); right: -45 kV (E=7.5kV·cm^{-1}). Spinning conditions: temperature: 200 °C, flow-rate: 200 μL h^{-1}, distance needle tip–ground plate: 6 cm, needle ID: 0.6 mm. [Modified from *Soft Matter*, **2012**, *8*, 9972-9976 with permission from The Royal Society of Chemistry.]

A unique consequence of the supramolecular properties of trisamides is the fiber formation during melt electrospinning even from the isotropic phase. It is assumed that in the optical isotropic phase columnar aggregates are still present. Due to these pre-aggregates forming a macrodipole, it is proposed that the columns can interact with the electrical field and fiber formation is favored. The disruption of the electrospinning jet into spheres is prevented in the same manner. At higher temperatures sphere formation is observed due to the decreasing hydrogen bonds interactions between the molecules within a column and the resulting length reduction of the pre-aggregates down to molecular isotropic phase where single molecules are present.

3.3   Melt Electrospinning of Small Molecules*

In the third part of this thesis the field of melt electrospinning of low molecular weight compounds was exhaustively explored. Therefore, the amount of hydrogen bonds was consciously decreased or even prevented and the influence of the π-conjugated core was investigated. Besides 1,3,5-cyclohexane- and 1,3,5-benzenetrisamides, the study was extended to bisamides, sorbitol derivates as well as to perylenebisimide derivatives and 1,3,5-benzenetrisamides incapable of forming hydrogen bonds as curiosity. The melt electrospun morphologies of 31 small molecules were explored as function of molecular structure and the parameters necessary to obtain electrospun fibers were investigated.

First of all, the study focuses on the determination of the experimental parameters using 1,3,5-cyclohexane- and 1,3,5-benzenetrisamides. The distance between needle tip to ground plate was set to 6 cm, the flow rate was adjusted to 200 mL h^{-1}, and for every experiment a needle capillary with an inner diameter of 0.6 mm was chosen. Since with increasing spinning temperature, the amount of electrosprayed beads rises by surpressing the formation of fibers, the spinning temperature was set for all experiments about 20 K above the isotropic transition. Therefore, a fully isotropic melt was ensured and progressing decomposition was handled.

In the next step, the influence of the electrical field direction on the fiber morphology was investigated. When a positive voltage was applied in the used electrospinning set-up with a grounded needle tip, the field direction pointed from ground plate to needle tip and negative charges were induced to the melt surface. In case of applying a negative voltage the field direction was reversed and, consequently, the melt was positively charged. It was found, that when a positive voltage is applied, a lower electrical field was necessary to obtain fibers. However, with negative applied voltages thinner and more uniforms fibers were collected and the melt electrospinning process was overall more homogeneous.

Finally, the influence of the electrical field strength E was tested by applying negative voltages from -25 kV to -45 kV (E = 4.2 − 7.5 kV cm^{-1}). At higher voltages solely fibers were collected, whereas at lower applied voltages mainly spheres and beaded fibers were obtained. Therefore, it was shown, similar to polymer solutions, that the net charge density on the surface of the melt droplet increases with stronger electrical field strength facilitating the formation of long and homogenous fibers.

Consequently, all further experiments were performed using a negative applied voltage of -40 kV at a distance of 6 cm (electrical field strength E = 6.7 kV/cm).

For a 1,3,5-benzenetricarboxamide equipped with *n*-hexyl substituents the Taylor cone formation and the jet ejected from the drop was studied (Figure 24). This was the first time that the electrospinning process of small molecules was investigated by high-speed imaging. A spherical fluid drop was emerged from the capillary die (0 ms) and got electrically charged in the electrical field. The interaction of the charged fluid with the electrical field resulted in a cone-like deformation of the drop shape (1.05 to 2.15 ms). The applied electric field overcame the surface tension of the drop when a half-angle of the cone of 30° was reached and, consequently, a jet was ejected towards the collector (2.35 and 2.50 ms). The ejected and accelerated jet followed a straight path before instabilities occurred and the jet performed unstable motions necessary to obtain nanofibers during electrospinning (Figure 24, right). It was visualized that a stable jet was generated by melt electrospinning and the intermolecular interactions are sufficient to prevent a breaking of the fluid jet into droplets.
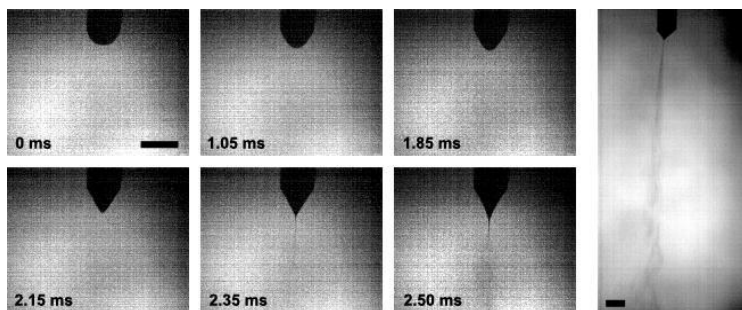
Figure 24. Images taken from a high-speed video of the formation of the Taylor cone (left) and the acceleration of the jet in the electric field (right) are shown for trihexyl-1,3,5-benzenetricarboxamide. Images were taken with a frame rate of 20,000 frames/s (left) and 10,000 frames/s (right), respectively. The scale bar indicates 1 mm. (Spinning parameters: voltage: -30 kV, distance needle tip–ground plate: 6 cm, temperature: 250 °C, flow rate: 200 mL h^{-1}, needle capillary ID: 0.6 mm). [Adapted from *Macromol. Mater. Eng*., **2015**, *300*, 259–276. Copyright © 2015 WILEY-VCH Verlag GmbH & Co. KGaA, Weinheim.]

To establish structure-property relations, the study focused on melt electrospinning of 1,3,5-benzene- and 1,3,5-cyclohexanetrisamides from the isotropic phase. A comparison of trisamides carrying linear or branched side chains indicated a strong influence of these substituents on the melt electrospun morphology. With branched side chains mainly beaded fibers and spheres were collected when electrospun. In contrast, compounds with linear side chains were shaped into long and homogenous nanofibers. 1,3,5-cyclohexanetrisamides were additionally electrospun from their nematic phase and fibers with a broader diameter distribution were collected.

Moreover, the influence of the amide connectivity to the central core was investigated in detail for 1,3,5-benzenetrisamides. When all three amide bonds were connected C- or N-centered homogenous melt electrospun nanofibers were collected. However, with mixed amide connectivity from electrospinning resulted in a heterogeneous mixture of fibers, beaded fibers, and spheres (Figure 25, left). The formation of spheres and beaded fibers was the consequence of a less stable electrospinning jet and could not been explained solely by considering the strength of the macrodipoles formed within a supramolecular column. The reason might be a weaker packing of the columnar aggregates when formed out of the melt of trisamides with mixed amide connectivity. The disturbed stability of the jet might also be caused by weaker hydrogen bonding within a column due to an asymmetric arrangement of the hydrogen bonds.

Cr 184 I; T_{Sp} = 200 °C; d_{fib}=1.7±0.9 µm/ d_{sph} =6.6±2.0 µm

Cr_1 79 Cr_2 115 Cr_3 190 Cr_4 206 I T_{Sp}= 225 °C; d_{sph} = 2.4±1.0 µm

Cr 85 I; T_{Sp} = 110 °C d_{fib} = 2.0±0.6 µm
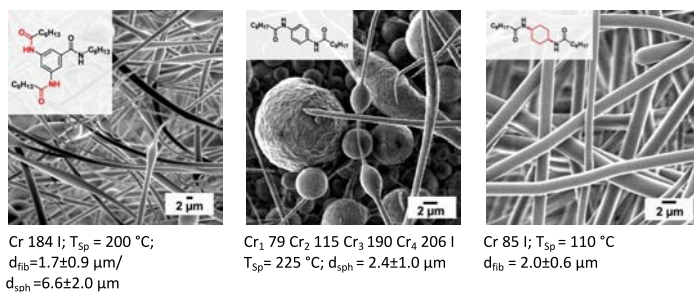
Figure 25. SEM pictures of a representative morphology obtained by the spinning experiments of a 1,3,5-benzenetrisamide (left), a 1,4-benzenebisamide (center) and a 1,4-*cis*-cyclohexane bisamide (right) is depicted in the SEM images. Their phase transitions, melt electrospinning temperatures (T_{Sp}) and fiber/sphere diameters (d_{fib}/d_{sph}) are listed. (Cr: crystalline, I: isotropic. Spinning parameters: voltage: -40 kV, distance: 6 cm, flow rate: 200 mL h^{-1}, needle capillary ID: 0.6 mm). [Modified from *Macromol. Mater. Eng*., **2015**, *300*, 259–276. Copyright © 2015 WILEY-VCH Verlag GmbH & Co. KGaA, Weinheim.]

To understand the influence of the amount of amide hydrogen bonds needed for fiber electrospinning, the amount of hydrogen bonds was successively decreased. Therefore, mono- and bisamides based on benzene-, naphthyl and cyclohexane cores were investigated. Electrospinning of these compounds resulted mainly in spheres or short and inhomogeneous fiber fragments and beaded fibers (Figure 25, center). For compounds with a low melting point undefined morphologies were collected due to an insufficient difference between spinning and ambient temperature. However, only 1,4-*cis*-cyclohexanebisamide equipped with *n*-octly substituents was found to formlong and homogenous microfibers (Figure 25, right).

In the following, sorbitol derivates were investigated in melt electrospinning, since they are known for their self-assembly behavior by another type of hydrogen bond interactions, namely between an oxygen and a hydrogen atom. For all compounds electrospraying was observed and mostly spheres were collected (Figure 26, left).

It seemed that the hydrogen bonds formed by the fast cooling of the melt during electrospinning were too weak to shape the fluid jet into fibers.

To answer the question whether hydrogen bonds are essential for fiber formation, electrospinning experiments were performed with perylenebisimide derivatives, equipped only with large, conjugated π-π-systems. For the very first time, it was demonstrated that these electron transporting materials can be shaped into fibers by melt electrospinning (Figure 26, center). The strong π-π-interactions, originated from the extended aromatic systems, are obviously sufficient to obtain electrospun fibers.

Cr 245 I; T_{Sp} = 245°C;   Cr 64 Col$_{ho}$ 123 I; T_{Sp} = 140°C;   glass, T_g=65°C; T_{Sp} = 140°C
d_{sph} = 3.1±2.9 µm d_{fib} = 3.4±1.2 µm d_{fib} = 12.9±1.3 µm
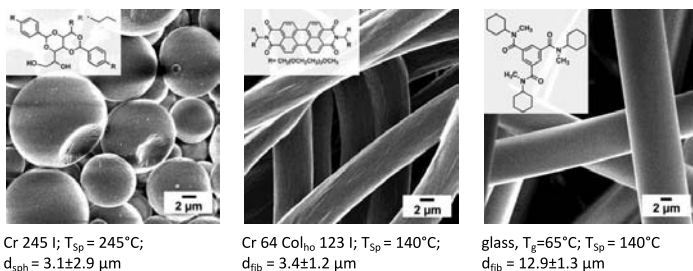
Figure 26. SEM pictures of a representative morphology obtained by the spinning experiments of the sorbitol derivative NX8000 (left), a perylenebisimide derivative (center) and a 1,3,5-benzene-trisamides incapable of forming hydrogen bonds (right) is depicted in the SEM images. Their phase transitions, melt electrospinning temperatures (T_{Sp}) and fiber/sphere diameters (d_{fib}/d_{sph}) are listed. (Cr: crystalline, Col: columnar mesophase, h: hexagonal, o: ordered liquid crystalline, I: isotropic. Spinning parameters: voltage: -40 kV, distance: 6 cm, flow rate: 200 mL h^{-1}, needle capillary ID: 0.6mm). [Modified from *Macromol. Mater. Eng*., **2015**, *300*, 259–276. Copyright © 2015 WILEY-VCH Verlag GmbH & Co. KGaA, Weinheim.]

Encouraged from the finding that hydrogen bonds were not necessarily essential to form fibers of small molecules during electrospinning, the study was extended to tertiary 1,3,5-benzenetrisamides incapable of forming hydrogen bonds. Surprisingly, fibers were collected from all three investigated tertiary 1,3,5-benzenetricarboxamides (Figure 26, right). Presumably, secondary π-π-interactions of the central benzene core are still present and, even if they are weaker than hydrogen bonds, sufficient enough to prevent the electrospinning jet from breaking into droplets.

This extensive and for the first time available study on melt electrospinning of self-assembling low molecular weight substances shows that hydrogen bonds are not necessary to collect fibers as long as sufficient π-π-interactions are present. By a carefully selection of the substance and an intelligent design of the periphery, desired electrospun morphologies such as fibers, beaded fibers and spheres, can be achieved. With this study melt electrospinning was established as powerful top-down method for the fabrication of nano- and microfibers of small molecules.

3.4   Top-Down Meets Bottom-Up: A Comparison of the Mechanical Properties of Melt Electrospun and Self-Assembled 1,3,5-Benzenetrisamide Fibers*

As it was shown in the previous chapters, supramolecular fibers of 1,3,5-benzene- and 1,3,5-cyclohexanetrisamides can be obtained by bottom-up and top-down approaches. To connect all results of this thesis, this chapter focuses on the characterization of those fibers on multiple length scales: crystal structure, fiber morphology and mechanical properties were investigated and compared.

Tripropyl-1,3,5-benzenetricarboxamide (**1**, Figure 27) was selected and fibers were prepare by controlled recrystallization from 2,2,4,4,6,8,8-heptamethylnonane (HMN), a nonpolar solvent, (denoted SA-fibers) and by melt electrospinning (ES-fibers).

At an Ångström scale, XRD measurements were performed on powdered fibers indicating the same crystal structure for SA- and ES-fibers (Figure 27).
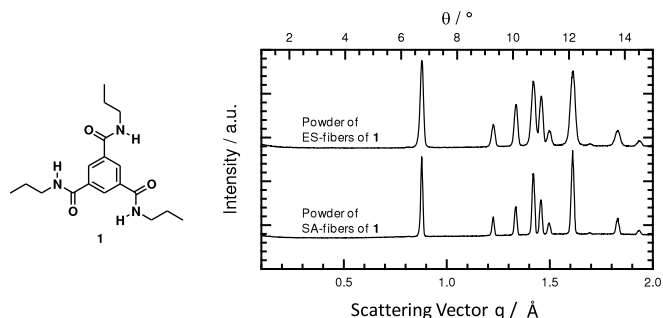
Figure 27. Left: chemical structure of tripropyl-1,3,5-benzenetricarboxamide (**1**). Right: X-ray diffractogram of self-assembled (SA) and electrospun (ES) fibers in powder form. [Modified with permission from *Polymer*, **2012**, *53*, 5754-5759. Copyright © 2012 Elsevier Ltd.]

On a microscopic scale, the morphology of the SA- and ES-fibers was investigated by SEM. SA-fibers were obtained with an average diameter of 1.2±0.7 µm and ES-fibers were fabricated with an average diameter of 0.8±0.2 µm. Even if the fiber diameters are comparable, the morphology was found to be considerably different (Figure 28). The differences in fiber morphology can be attributed to the process used to generate the two fiber types: The self-assembly process, allowing the development of defined structures, is much slower than fiber formation in electrospinning occurs. Therefore, SA-fibers consisted of bundles formed by individual, approximately 100 nm thick strands. In contrast, ES fibers are obtained with a smooth and defect-free surface.

In addition, ES-fibers are obtained from molten bulk material resulting in homogenous fiber morphology.
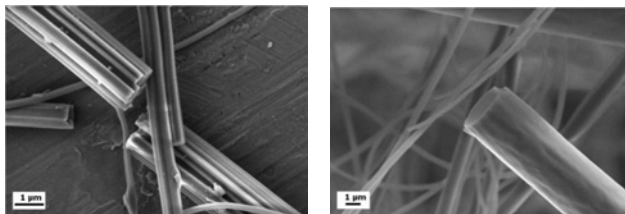
Figure 28. SEM micrograph of the fracture section of a SA fiber (left) and an ES-fiber (right). [Modified with permission from *Polymer*, **2012**, *53*, 5754-5759. Copyright © 2012 Elsevier Ltd.]

To compare the mechanical properties of both fiber types, nanomechanical bending experiments using AFM (see section 3.1) were performed. The fibers were transferred to micro-structured glass substrates to attain the required free-standing fiber segments over the gap. The stiffness profiles, obtained by bending deformation measurements, matched the double clamped beam model (DCBM). Afterwards, the Young's modulus of each investigated segment was calculated by applying the DCBM fitting conditions. The distributions are shown in Figure 29. For SA-fibers an average modulus of E=3.6±0.4 GPa and for ES-fibers a value of E=4.7±0.6 GPa was calculated. The Young's moduli of the investigated fibers are in the same range as (semi)crystalline or glassy polymers and are in good agreement with former performed bending experiments on 1,3,5-benzenetrisamides (see section 3.1).
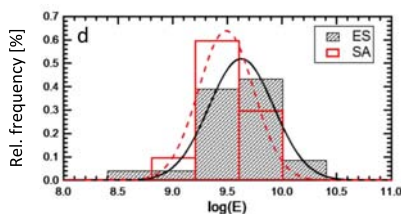
Figure 29. Distribution of the Young's moduli *E* of each individual fiber of SA-fibers (open bars, dashed line) and ES-fibers (hatched bars, solid line). [Modified with permission from *Polymer*, **2012**, *53*, 5754-5759. Copyright © 2012 Elsevier Ltd.]

Even if the fiber morphologies of SA- and ES-fibers are significantly different, both fiber types show comparable elastic properties. The determined modulus of SA-fibers is slightly lower than that for ES-fibers. This observation can be explained by the bundle structure of SA-fibers tending to defects. In summary, supramolecular fibers were obtained from tripropyl-1,3,5-benzenetricarboxamide (**1**), processed by a common bottom-up and top-down approach.

4 Publications

This chapter presents the list of publications; the individual contributions to joint publications and manuscripts are outlined and the publications and manuscripts are embedded. The corresponding author is marked with an asterisk.

4.1 List of publications

1. Daniel Kluge, Julia C. Singer, Jens W. Neubauer, Frank Abraham, Hans-Werner Schmidt and Andreas Fery*
   "Influence of the Molecular Structure and Morphology of Self-Assembled 1,3,5-Benzenetrisamide Nanofibers on their Mechanical Properties"
   published in *Small,* **2012***, 8,* 2563–2570.

2. Julia C. Singer, Reiner Giesa and Hans-Werner Schmidt*
   "Shaping Self-Assembling Small Molecules into Fibres by Melt Electrospinning"
   published in *Soft Matter*, **2012**, *8*, 9972–9976.

3. Julia C. Singer, Andreas Ringk, Reiner Giesa and Hans-Werner Schmidt*
   „Melt Electrospinning of Small Molecules"
   published in *Macromolecular Materials and Engineering*, **2015**, *300*, 259–276.

4. Daniel Kluge, Julia C. Singer, Benedikt R. Neugirg, Jens W. Neubauer, Hans-Werner Schmidt and Andreas Fery*
   „Top-Down Meets Bottom-Up: A Comparison of the Mechanical Properties of Melt Electrospun and Self-Assembled 1,3,5-Benzenetrisamide Fibers"
   published in *Polymer*, **2012**, *53*, 5754–5759.

4.2   Individual contributions to joint publications

The publications of the thesis present the experimental work and findings as result of collaborations with fellow researchers. The individual contributions of each coworker to joint publications and manuscripts are specified in the following.

My work contribution was carried out at the chair of Macromolecular Chemistry I (MC I), University of Bayreuth, and assisted by Dr. Reiner Giesa under the supervision of Prof. Dr. Hans-Werner Schmidt. The technical assistants Jutta Failner, Sandra Ganzleben, Doris Hanft and Rika Schneider, Macromolecular Chemistry I, University of Bayreuth, synthesized most of the compounds used in this thesis under my guidance.
The publications 1 and 4 were accomplished in cooperation with the research group of Prof. Dr. Andreas Fery, Physical Chemistry II, University of Bayreuth.

Publication 1:

Influence of the Molecular Structure and Morphology of Self-Assembled 1,3,5-Benzenetrisamide Nanofibers on their Mechanical Properties

Small, **2012**, *8,* 2563–2570.
Daniel Kluge, Julia C. Singer, Jens W. Neubauer, Frank Abraham, Hans-Werner Schmidt and Andreas Fery*

The first manuscript was published as a full article describing the mechanical properties of self-assembled 1,3,5-benzenetrisamides as a function of molecular structure and fiber morphology. The compounds were synthesized by Sandra Ganzleben under my guidance. I characterized all substances. Dr. Frank Abraham prepared one class of self-assembled nanofibers. All other investigated self-assembled fibers were prepared by me. I carried out the morphological characterization of all fibers by SEM investigations and evaluated the fiber diameters of all supramolecular fibers. Dr. Daniel Kluge and Jens W. Neubauer, Physical Chemistry II, University of Bayreuth, performed the nanomechanical bending experiments by AFM measurements and evaluated the AFM data.
The first draft of the manuscript was equally written by myself and Dr. Daniel Kluge. Prof. Dr. Hans-Werner Schmidt and Prof. Dr. Andreas Fery supervised the project and were involved in finalizing of the manuscript.

Publication 2:

Shaping Self-Assembling Small Molecules into Fibres by Melt Electrospinning

Soft Matter, **2012**, *8*, 9972–9976.

Julia C. Singer, Reiner Giesa and Hans-Werner Schmidt*

The second manuscript was published as a communication article demonstrates for the first time that supramolecular nano- and microfibers can be obtained by melt electro-spinning. Under my supervision, the compounds were synthesized by Sandra Ganzleben. The characterization of the substances was carried out by me. The melt electrospinning experiments were performed jointly with Dr. Reiner Giesa. I performed the morphological characterization by SEM investigations, evaluated the fiber diameters and interpreted the results.

The first manuscript draft was written by me. Dr. Reiner Giesa and Prof. Dr. Hans-Werner Schmidt were involved in the scientific discussion and finalized the manuscript.

Publication 3:

Melt Electrospinning of Small Molecules

Macromolecular Materials and Engineering, **2015**, *300*, 259–276.

Julia C. Singer, Andreas Ringk, Reiner Giesa and Hans-Werner Schmidt*

The third manuscript was published as a feature article discussing the state of the art of electrospinning of small molecules from solution and melt. Different sets of self-assembling, low molecular weight compounds varying in the amount of secondary interactions were investigated with respect to melt electrospinning. Two of the investigated compounds were synthesized by Dr. Andreas Ringk. All other substances were synthesized by Jutta Failner, Sandra Ganzleben and Doris Hanft under my guidance. I characterized all substances. The melt electrospinning experiments were performed by myself, assisted by Dr. Reiner Giesa. The electrospinning parameters were systematically investigated by me to determine the optimum process condition. The morphology and size distribution of electrospun materials was evaluated by myself and I interpreted the results. Dr. Roland Dersch, Macromolecular Chemistry II, University of Bayreuth, and I investigated the melt electrospinning process using a high speed camera.

I wrote the first draft of the manuscript, which was jointly finalized with the help of all coauthors.

Publication 4:

Top-Down Meets Bottom-Up: A Comparison of the Mechanical Properties of Melt Electrospun and Self-Assembled 1,3,5-Benzenetrisamide Fibers

Daniel Kluge, Julia. C. Singer, Benedikt R. Neugirg, Jens W. Neubauer,
Hans-Werner Schmidt and Andreas Fery*

The fourth manuscript was published as full article and describes the characterization on multiple length scales of fibers prepared by self-assembly and melt electrospinning. The compound was synthesized by Doris Hanft under my supervision. I did the characterization. The preparation and morphological characterizations of the supramolecular microfibers were performed by myself and I carried out the XRD investigations. An important step was the electrospinning directly on structured glass substrates for the mechanical evaluation, which allowed the study of a broader range of supramolecular nano- and microfibers. The AFM bending experiments and the evaluation of the AFM data were carried out by Dr. Daniel Kluge, Benedikt R. Neugirg and Jens W. Neubauer, Physical Chemistry II, University of Bayreuth.

The first draft of the manuscript was equally written by myself and Dr.Daniel Kluge. Prof. Dr. Hans-Werner Schmidt and Prof. Dr. Andreas Fery supervised the project and were involved in finalizing of the manuscript.

4.3 Influence of the Molecular Structure and Morphology of Self-Assembled 1,3,5-Benzenetrisamide Nanofibers on their Mechanical Properties*

The mechanical properties of supramolecular nanofibers are revealed by means of nanomechanical bending tests. Different molecular structures have a strong influence on the diameter and stiffness of the fibers. In contrast, the Young's modulus is surprisingly little affected by differences in the chemical structure.
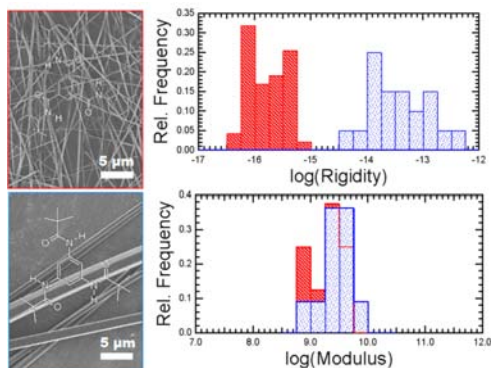
Reproduced with permission;
Copyright © 2012 WILEY-VCH Verlag GmbH & Co. KGaA, Weinheim

---

small

Nanofibers

Influence of the Molecular Structure and Morphology of Self-Assembled 1,3,5-Benzenetrisamide Nanofibers on their Mechanical Properties

Daniel Kluge, Julia C. Singer, Jens W. Neubauer, Frank Abraham, Hans-Werner Schmidt, and Andreas Fery*

The influence of molecular structure on the mechanical properties of self-assembled 1,3,5-benzenetrisamide nanofibers is investigated. Three compounds with different amide connectivity and different alkyl substituents are compared. All the trisamides form well-defined fibers and exhibit significant differences in diameters of up to one order of magnitude. Using nanomechanical bending experiments, the rigidity of the nanofibers shows a difference of up to three orders of magnitude. Calculation of Young's modulus reveals that these differences are a size effect and that the moduli of all systems are similar and in the lower GPa range. This demonstrates that variation of the molecular structure allows changing of the fibers' morphology, whereas it has a minor influence on their modulus. Consequently, the stiffness of the self-assembled nanofibers can be tuned over a wide range—a crucial property for applications as versatile nano- and micromechanical components.

1. Introduction

Functional materials with a defined nanostructure have become one of the most promising research fields for advanced applications such as tissue engineering, drug delivery, micro/nanoelectromechanical systems (MEMS/NEMS), and filtration.[1–3] In these materials, one-dimensional (1D) objects like nanofibers or nanorods play an important role since they often define or reinforce their structure—as individual rods or threads or as a part of complex hierarchical networks.[4,5]

Naturally, a lot of effort has been put into the development and efficient preparation of 1D nanostructures and structured materials in general.[5–7] However, regardless of their preparation, the macroscopic properties of these materials are always determined by their structure on much smaller length scales. As a consequence, there is an ever-growing interest in systems where, on the molecular level, structure–property correlations can be understood and controlled.

Recently, 1,3,5-benzenetrisamides (BTAs) have attracted great research interest because of their supramolecular aggregation into helical columnar stacks with enormous aspect ratios.[8,9] In general, the growth of BTA molecules into an ordered 1D structure is stabilized by threefold hydrogen bonding.[10–12] The specific self-assembly behavior, however, strongly depends on the connectivity of the amide moieties to the central core. Thus, we must differentiate between BTA based on trimesic acid **1** and 1,3,5-triaminobenzene **2** (**Scheme 1**). All amide functions of type **1** are pointing in the same direction, which results in helically arranged, strong hydrogen bonds.[13] Compared to type **1**, the hydrogen-bond length in columns formed by BTA molecules of type **2** are longer and hence weaker. Solid-state NMR experiments combined with Car–Parrinello molecular dynamics simulations showed that

D. Kluge, J. W. Neubauer, Prof. A. Fery
Physical Chemistry II and Bayreuth Center
for Colloids and Interfaces
University of Bayreuth
Universitaetsstrasse 30, 95440 Bayreuth, Germany
E-mail: andreas.fery@uni-bayreuth.de

J. C. Singer, Dr. F. Abraham, Prof. H.-W. Schmidt
Macromolecular Chemistry I and Bayreuth Institute of
Macromolecular Research
University of Bayreuth
Universitaetsstrasse 30, 95440 Bayreuth, Germany

full papers

D. Kluge et al.
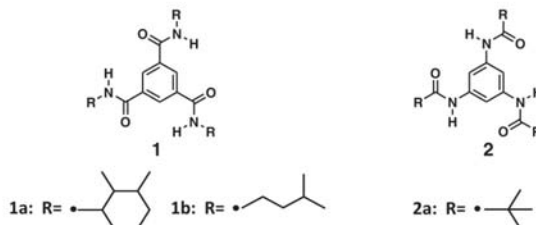
Scheme 1. Chemical structure of BTAs based on trimesic acid (**1**) and 1,3,5-triaminobenzene (**2**).

in the solid state, the amide functions within the column of **2** are asymmetrically arranged, thus leading in total to a weaker aggregation.[13]

The self-assembly behavior in solution and the solid-state properties of BTAs also depend dramatically on the constitution of the peripheral groups.[14] Even subtle changes of the side chains can influence the aggregation behavior and properties of BTA. Starting with a linear C_6-alkyl chain, **1** shows discotic liquid-crystalline behavior.[15–19] The aggregation in the mesophase is stabilized utilizing branched side chains.[14,15] BTAs of type **2** show thermotropic liquid-crystal behavior only with chiral substituents.[11]

Consequently, BTAs offer the possibility to tailor desired properties. Well-defined BTA fibers were tailored to serve as organo-[19–23] and hydrogelators,[24–27] supramolecular materials,[28,29] nucleating agents for polyvinylidenefluoride,[30] and were designed to improve the properties of electret materials.[31–35] Both BTAs based on trimesic acid and on 1,3,5-triaminobenzene were intensively studied as polymer processing aids[36] and nucleating agents for isotactic polypropylene (i-PP).[9,37–39] Varga et al. recently used **1a** as a new type of β-nucleating agent for i-PP.[38]

While there are many studies on the application of BTAs, only a little is known about their mechanical properties. In a previous study we showed that fibers obtained from **2a** self-assembled from 2,2,4,4,6,8,8-heptamethylnonane (HMN) possess a significant mechanical stability.[40] The reported stability and the possibility to tailor their properties makes BTA nanofibers very interesting for bottom-up approaches and demands further mechanical investigations. However, there are no experimental reports on the effect of the molecular structure on the mechanical properties to date. Investigating the mechanical properties of 1D materials on this scale requires approaches beyond typical macroscopic characterization techniques. Amongst other methods (e.g., indentation and tensile tests), nanomechanical bending experiments are recognized for their reliability, straightforward sample preparation, and applicability to a wide variety of systems.[41,42] In the past, bending experiments were used for the mechanical investigation of polymer nanofibers,[43–45] biological materials,[46–50] carbon nanotubes (CNTs),[51,52] nanowires,[53–55] and even complex structures like particle

bridges.[56,57] In a previous study of BTA fibers, we performed bending experiments using atomic force microscopy (AFM).[40] The presented experiments allowed us to identify the correct type of sample fixation directly from the AFM data, and thus to reliably measure the Young's modulus of the investigated fibers.

Herein, we study the influence of the molecular structure of self-assembled BTA nanofibers on their morphology and mechanical properties. For that purpose, we investigate the fibers of three different BTA structures, with respect to the connectivity of the amide moieties and the size of the alkyl substituents. We briefly discuss morphological aspects and, using AFM bending experiments, determine the stiffness of the fibers and calculate their Young's modulus. Furthermore, we compare our results with predictions and findings in the literature.

2. Results and Discussion

2.1. Morphology

To interpret the mechanical properties of the structurally different BTAs, we first investigated the morphology of the self-assembled nanofibers. A scanning electron microscopy (SEM) overview image of the dried samples is shown in **Figure 1**. The nanofibers of **1a** have an average diameter d of (0.21 ± 0.08) μm. The narrow size distribution (Figure 1a, right) illustrates the homogeneous formation of the stacked structure. Moreover, all self-assembled fibers exhibit an immense aspect ratio of more than 500:1. The inset in Figure 1a shows the morphology of a single nanofiber. The diameter and the straight and uniform structure are maintained over the whole length. Compound **1b** self-assembles into long aggregates with an average diameter of (0.41 ± 0.18) μm. Compound **1a** with substituted cycloaliphatic groups forms smaller fibers than **1b** with branched alkyl substituents, thus demonstrating the influence of the peripheral substituents on the self-assembly behavior. A significantly larger fiber diameter, accompanied by a wider distribution, is formed by **2a** (d = (2 ± 1) μm).

© 2012 Wiley-VCH Verlag GmbH & Co. KGaA, Weinheim

Mechanical Properties of Self-Assembled Benzenetrisamide Nanofibers

small <small>NANO MICRO</small>
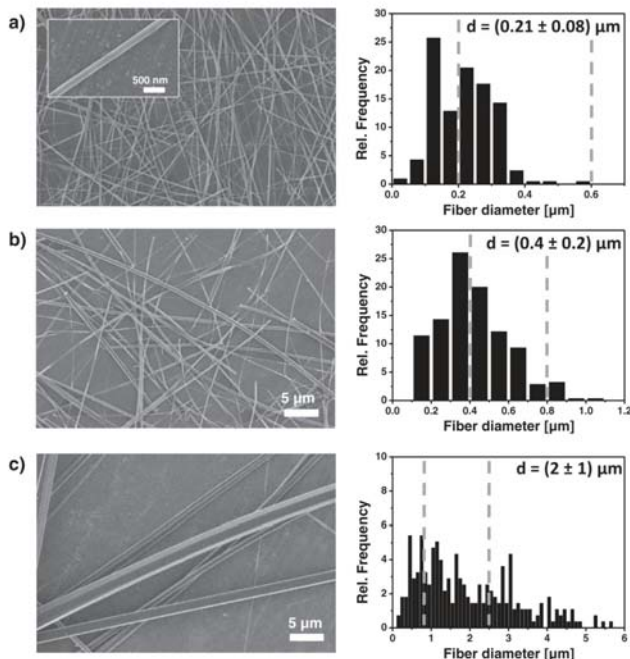
Figure 1. a) SEM image and size distribution of nanofibers of **1a**. The average diameter *d* is (0.21 ± 0.08) μm. The SEM overview image and the inset highlight the narrow size distribution and homogeneous structure of the nanofibers. b) SEM image and size distribution of nanofibers of **1b** (*d* = (0.4 ± 0.2) μm). c) SEM image and size distribution of fibers of **2a** (*d* = (2 ± 1) μm). The vertical dashed lines in the histograms indicate the minimal and maximal size of each fiber type for which successful AFM bending measurements were performed.

2.2. Bending Experiments

For the AFM bending experiments, the nanofibers were transferred to glass substrates structured with lithographically prepared channels to achieve a freestanding configuration. **Figure 2**a shows a schematic representation of the deformation setup. A representative SEM image of suspended fibers can be found in the Supporting Information (SI 1). As a first step, we ensured that there was no indentation or compression of the nanofibers contributing to the bending experiments. Therefore, we recorded force–deformation curves on the supported segments of the samples. A typical measurement can be seen in Figure 2b. There was no significant deformation visible for the typically applied loads.

For the actual bending experiments, we performed force–distance measurements on 30 to 40 positions along the freestanding nanofiber segments. The stiffness at the respective position was calculated from the slope of the force–distance curve. Towards the midpoint of the channel the measured stiffness decreased, and hence we obtained stiffness profiles along the whole freestanding segment (Figure 2c).

From the shape of the profiles, we determined the boundary conditions (i.e., the type of fixation) of each segment and the modulus of the nanofiber using models of classical beam theory.[58] A detailed discussion of the importance of the boundary conditions, of the analytical models, and of the experimental procedure can be found in the literature.[40] The two most commonly applied models are the double-clamped

D. Kluge et al.
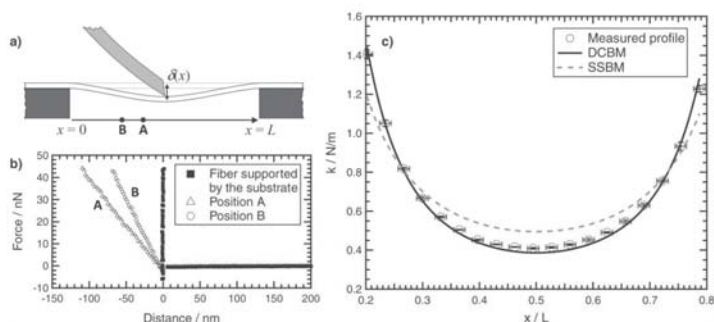
Figure 2. a) Sketch of the experimental setup. b) Force–deformation curves obtained on the bare substrate, around the middle of the supported segment (A), and at an intermediate position between edge and midpoint (B). c) Stiffness profile of a supported segment of **1a**. The data were obtained by averaging over six measurements on the same segment and were fitted with the DCBM (solid line) and SSBM (dashed line). The DCBM is clearly valid.

beam model (DCBM), where the ends of the sample are firmly fixed, and the simply supported beam model (SSBM), where the ends are assumed to rotate freely.[54,58,59]

We observed both types of behavior and could clearly distinguish between both cases. However, effects like a slight slackness of the sample or defects at the fixation points can lead to profiles that resemble a SSBM-type behavior although the ends are clamped, and hence can lead to an inaccurate interpretation of the data. On the contrary, when a profile matches the DCBM, the experimental conditions have to be in perfect agreement with the modeled clamped conditions, and therefore the interpretation is much more reliable. To avoid uncertainties, we decided to use only segments that clearly corresponded to the DCBM for the calculation of the modulus.

For the DCBM, the stiffness $k(x)$ at a given position x is

$$k(x) = \frac{3 L^3 E I}{(L - x)^3 x^3} \tag{1}$$

Here, L is the length of the freestanding segment and x is the position where the load is applied, with $0 \le x \le L$. EI is the flexural rigidity defined as the product of the modulus E and the area moment of inertia I. The measured profiles were fitted with EI as the only free parameter.

To obtain E, we imaged each individual nanofiber with AFM and calculated I from the respective cross sections. This is a highly important step, since the flexural rigidity scales quartic with the diameter of the samples. By imaging each individual investigated nanofiber and calculating the correct area moment of inertia, our evaluation of the mechanical data is not based on any assumptions concerning the size and shape of the cross section. An example cross section can be found in the Supporting Information (SI 2).

It can be seen from Equation (1) that the spring constants of multiple nanofiber segments can be normalized so that one obtains

$$k_{\text{norm}}(x) = \frac{3 E}{(1 - x)^3 x^3} \tag{2}$$

with

$$k_{\text{norm}}(x) = \frac{k(x) L^3}{I} \tag{3}$$

We averaged the normalized spring constants of all investigated nanofiber segments and fitted the data with Equation (2) (**Figure 3**). The resulting modulus for **1a** was (2.3 ± 0.3) GPa. In the same way, we determined the Young's moduli of **1b** $((2.1 \pm 0.1)$ GPa) and **2a** $((3.3 \pm 0.4)$ GPa). The quality of the fit shows the excellent agreement of the deformation profiles with the DCBM. Therefore, the error bars are a direct measure of the uncertainty of the determined Young's modulus which is caused by defects and inhomogeneities of the self-assembled nanofibers and by uncertainties of the measurements. Those may be attributed to the error of the AFM cantilever spring constant (<10%), the channel width (<5%), and the determined area moment of inertia (<20%).

Since the molecular structure suggests highly anisotropic mechanical properties for the nanofibers, the effect of anisotropy should also be discussed. When bent, the upper part of a beam is subjected to compression while the lower part is subject to extension. This leads to additional shear forces within the beam that become important in anisotropic materials when the length-to-radius ratio of the bent segment becomes $\frac{L}{R} \le 4\sqrt{\frac{E}{G}}$.[60] In this case, shearing can be accounted for by defining an apparent bending modulus E_b that is related to the true elastic modulus E and the shear modulus G via[45,47]

Mechanical Properties of Self-Assembled Benzenetrisamide Nanofibers
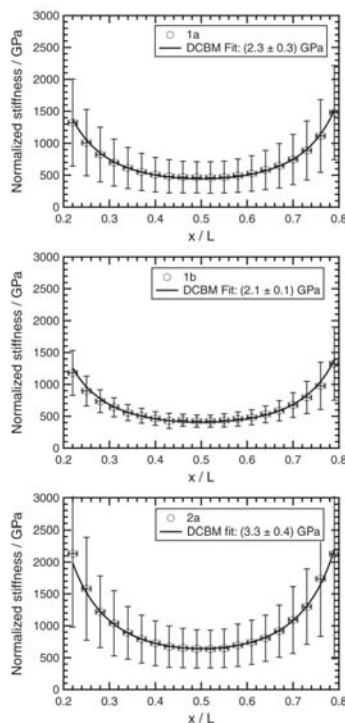
Figure 3. Results of the spatially resolved bending experiments. The shape of all profiles shows excellent agreement with the DCBM. The larger size of the error bars compared to the individual measurements (as seen in Figure 2) is a consequence and a direct measure of the distribution and uncertainty of the determined moduli amongst individual specimens of one sample.

$$\frac{1}{E_b} = \frac{1}{E} + 12 f_s \cdot \frac{R^2}{L^2} \cdot \frac{1}{G} \qquad (4)$$

for samples with a circular cross section. L is the length and R the radius of the freestanding segment, and f_s is the form factor of shear, which is related to the sample's cross section (e.g., 10/9 for a cylinder).[61] For more arbitrary cross sections, the area and second moment of area cannot be expressed by the radius, and therefore

$$\frac{1}{E_b} = \frac{1}{E} + 48 f_s \cdot \frac{I}{AL^2} \cdot \frac{1}{G} \qquad (5)$$

In any case, if shearing plays a dominant role, G and consequently E can be determined from the slope of $1/E_b$ versus $I/(AL^2)$. However, for all investigated systems, no significant influence of shearing was observed (Supporting Information, SI 3). Therefore, the anisotropy is only of minor importance for the bending behavior under our measurement conditions, and the determined values can be regarded as the true Young's moduli in the axial direction of the nanofibers.

2.3. Comparison of the Systems

To determine the effect of the molecular structure on the mechanical properties, we have to differentiate between two effects: the difference arising from the different thicknesses of the individual nanofiber types, and additional changes of the material properties. First, we compared the stiffness of the freestanding nanofiber segments (**Figure 4**a). Since the measurements had to be performed on different channel widths for both samples, we normalized the stiffness with respect to the channel width to obtain the apparent flexural rigidity, irrespective of the boundary conditions found during evaluation of the modulus. The rigidity of the freestanding segments
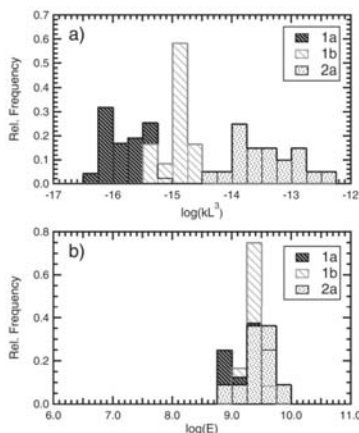
Figure 4. a) Apparent flexural rigidity of all investigated nanofiber segments. The stiffness was measured at the midpoint of the freestanding segments. Please note that the x axis has a logarithmic scaling. The rigidity of **1b** is one to two, and of **2a** is up to three orders of magnitude higher than that of **1a**. b) Distribution of the calculated modulus for all three investigated systems. The results for all systems are comparable.

full papers

of **1b** was one to two orders of magnitude higher than that of **1a**. For **2a**, it was up to three orders of magnitude higher. This increase is a consequence of the increased diameters of the investigated nanofibers, since the rigidity is proportional to the fourth power of the radius.

In contrast, the modulus is comparable for all systems. For **1a**, we found a modulus of (2.3 ± 0.3) GPa, for **1b** (2.1 ± 0.1) GPa, and for **2a** (3.3 ± 0.4) GPa. These values are in good agreement with those found for electrospun polyamide fibers.[62] The result for **2a** also confirms a study where self-assembled aggregates of the same molecule were prepared under different preparation conditions and a modulus of (3 ± 1) GPa was found.[40] Therefore, the change of stiffness by up to three orders of magnitude can clearly be identified as a pure size effect without equivalent changes of the material properties. This is a rather surprising finding, since it suggests that the influence of the investigated molecular structures on the mechanical properties is small. In addition to the absolute value, we also investigated the distribution of the individual moduli, which was also comparable for all systems (Figure 4b).

From a molecular point of view, there are several contributions to the mechanical stability of the BTA aggregates. The formation of intracolumnar hydrogen bonds and the intercolumnar interactions governed by macrodipoles are most important.[15,63] The size and nature of the substituents (linear, branched, cyclic) play an additional role. The calculations of Stals et al. on the effect of the amide connectivity on the aggregate stability suggest that BTAs based on trimesic acid **1** are able to form stronger hydrogen bonds.[11] Therefore one would expect that **1a** and **1b** have a higher elastic modulus than **2a**.

However, our measurements indicate a slightly higher modulus for **2a** compared to **1a** and **1b**. There are two explanations for our findings. If the volume of the substituent is increased, the intercolumnar distance becomes larger. Consequently, the strength of the macrodipole interactions is lowered. Concomitantly, the number of columns per cross-sectional area decreases. Both effects contribute to the lower modulus of **1a** and **1b** compared to **2a**.

3. Conclusion

We have compared self-assembled nanofibers of three BTA derivatives with different molecular structures. We recorded SEM images to investigate their morphological differences and found that **1a** forms nanofibers with an average diameter of (0.21 ± 0.08) μm, followed by the nanofibers of **1b** with an average diameter of (0.4 ± 0.2) μm. The fibers of **2a** had an average diameter of (2 ± 1) μm, with a much wider distribution. We compared the mechanical properties as determined via nanomechanical AFM bending experiments of all systems and found that the flexural rigidity of **1b** is one to two, and of **2a** is up to three orders of magnitude higher than that of **1a**. We calculated the modulus of all three systems and obtained (2.3 ± 0.3) GPa for **1a**, (2.1 ± 0.1) GPa for **1b**, and (3.3 ± 0.4) GPa for **2a**. This showed that the dramatic difference of the stiffness was purely a size effect. In conclusion, our findings

demonstrate that while the molecular structure alters the morphology and therefore the absolute stiffness of the self-assembled nanofibers, the elastic modulus of all systems is similar, even over a large range of sizes from about 100 nm to 3 μm. This allows tuning of the stiffness of the nanofibers. The results of our study are a first step towards the application of self-assembled BTA nanofibers as components for bottom-up functional materials with tailored properties from the nano- to the microscale.

4. Experimental Section

Synthesis of the 1,3,5-Trisamides: **1a**, **1b**, and **2a** were synthesized as described in the literature.[64–66]

Nanofiber Preparation: Compound **1a** or **2a** (600 ppm) in 2,2,4,4,6,8,8-heptamethylnonane (HMN) was dissolved under reflux at 240 °C and cooled to room temperature. This suspension (200 μL) was transferred to a custom-made high-pressure pan and heated to 240 °C for 10 min in the dropping point cell FP83HT from Mettler Toledo. By cooling from 240 to 30 °C at 20 K min⁻¹ (controlled with the Mettler Toledo central processor FP90), a controlled self-assembly into fibers was achieved. For the preparation of **1b**, a solution (500 ppm) was treated as described above. The cooling rate was 5 K min⁻¹.

The samples for the bending experiments were prepared by wetting structured glass substrates (GeSiM GmbH, Grosserkmannsdorf, Germany; channel widths 5 and 10 μm for **1a**, 10 μm for **1b**, and 30 μm for **2a**) with blank HMN (15 μL), adding the nanofiber suspension (0.5 μL), and allowing the samples to dry overnight.

SEM Imaging: For preparation of the SEM samples, the nanofiber suspensions (5 μL) were placed in DSC aluminum pans and the solvent was evaporated under reduced pressure. The samples were sputtered with platinum (2.0 nm) in a Cressington sputter coater 208HR to enhance conductivity. SEM images were recorded on a Zeiss LEO 1530 FESEM instrument (Zeiss, Jena, Germany). For the size distributions, over 200 individual nanofibers of each system were evaluated.

AFM Measurements: All AFM measurements were performed on a Nanowizard I apparatus (JPK Instruments AG, Berlin, Germany), combined with a Zeiss Axiovert 200 microscope and a Zeiss LD A-Plan® Ph1 objective lens (20×, numerical aperture 0.3, working distance 4.3 mm). The bending experiments were performed as previously reported,[40] using tipless NSC12/AIBS cantilevers (μMasch, Tallinn, Estonia). For **1a**, the typical load was 50 nN, which resulted in typical deformations of 100–200 nm at the midpoint. In addition, 50 force–distance measurements with a maximum load of 150 nN were performed on 10 individual nanofibers on segments supported by the substrate, to prove that there was no unwanted compression of the nanofibers during the bending experiments. For the measurements on **1b**, the typical load was around 30 nN. For **2a**, the loads were between 50 and 100 nN to achieve comparable deformations. None of the systems showed unwanted compression under the tested loads of up to 150 nN. The dimensions of the mechanically investigated nanofibers were determined on the segments supported by the substrates in intermittent contact mode with sharp imaging cantilevers (Olympus OMCL-AC160TS, Atomic Force, Mannheim, Germany). All data were

Mechanical Properties of Self-Assembled Benzenetrisamide Nanofibers

small

processed and evaluated using self-written procedures in Igor Pro 6 (Wavemetrics Inc., Portland, USA). For the calculation of Young's modulus, the data from 96 measured profiles on 16 nanofibers of **1a**, 72 profiles on 10 nanofibers of **1b**, and 66 profiles on 10 fibers of **2a** were used.

Supporting Information

Supporting Information is available from the Wiley Online Library or from the author.

Acknowledgements

[1] P. Moriarty, *Rep. Prog. Phys.* **2001**, *64*, 297.
[2] S. Agarwal, J. H. Wendorff, A. Greiner, *Polymer* **2008**, *49*, 5603.
[3] R. S. Barhate, S. Ramakrishna, *J. Membr. Sci.* **2007**, *296*, 1.
[4] P. Fratzl, R. Weinkamer, *Prog. Mater. Sci.* **2007**, *52*, 1263.
[5] Y. N. Xia, P. D. Yang, Y. G. Sun, Y. Y. Wu, B. Mayers, B. Gates, Y. D. Yin, F. Kim, Y. Q. Yan, *Adv. Mater.* **2003**, *15*, 353.
[6] A. Greiner, J. H. Wendorff, *Angew. Chem. Int. Ed.* **2007**, *46*, 5670.
[7] J. H. Fendler, F. C. Meldrum, *Adv. Mater.* **1995**, *7*, 607.
[8] I. A. W. Filot, A. R. A. Palmans, P. A. J. Hilbers, R. A. van Santen, E. A. Pidko, T. F. A. Greef, *J. Phys. Chem. B* **2010**, *114*, 13667.
[9] M. Kristiansen, P. Smith, H. Chanzy, C. Baerlocher, V. Gramlich, L. McCusker, T. Weber, P. Pattison, M. Blomenhofer, H.-W. Schmidt, *Cryst. Growth Des.* **2009**, *9*, 2556.
[10] M. P. Lightfoot, F. S. Mair, R. G. Pritchard, J. E. Warren, *Chem. Commun.* **1999**, 1945.
[11] P. J. M. Stals, J. C. Everts, R. de Bruijn, I. A. W. Filot, M. M. J. Smulders, R. Martin-Rapun, E. A. Pidko, T. F. A. de Greef, A. R. A. Palmans, E. W. Meijer, *Chem. Eur. J.* **2010**, *16*, 810.
[12] M. M. J. Smulders, A. P. H. J. Schenning, E. W. Meijer, *J. Am. Chem. Soc.* **2008**, *130*, 606.
[13] M. Wegner, D. Dudenko, D. Sebastiani, A. R. A. Palmans, T. F. A. Greef, R. Graf, H. W. Spiess, *Chem. Sci.* **2011**, *2*, 2040.
[14] P. J. M. Stals, M. M. J. Smulders, R. Martín-Rapún, A. R. A. Palmans, E. W. Meijer, *Chem. Eur. J.* **2009**, *15*, 2071.
[15] A. Timme, R. Kress, R. Albuquerque, H.-W. Schmidt, *Chem. Eur. J.* **2012**, DOI: 10.1002/chem.201103216.
[16] Y. Harada, Y. Matsunaga, *Bull. Chem. Soc. Jpn.* **1988**, *61*, 2739.
[17] Y. Matsunaga, Y. Nakayasu, S. Sakai, M. Yonenaga, *Mol. Cryst. Liq. Cryst.* **1986**, *141*, 327.
[18] Y. Matsunaga, N. Miyajima, Y. Nakayasu, S. Sakai, M. Yonenaga, *Bull. Chem. Soc. Jpn.* **1988**, *61*, 207.
[19] J. J. van Gorp, J. A. J. M. Vekemans, E. W. Meijer, *J. Am. Chem. Soc.* **2002**, *124*, 14759.
[20] Y. Yasuda, E. Iishi, H. Inada, Y. Shirota, *Chem. Lett.* **1996**, 575.
[21] K. Hanabusa, C. Koto, M. Kimura, H. Shirai, A. Kakehi, *Chem. Lett.* **1997**, 429.
[22] N. Mohmeyer, H.-W. Schmidt, *Chem. Eur. J.* **2007**, *13*, 4499.

[23] S. Y. Ryu, S. Kim, J. Seo, Y.-W. Kim, O.-H. Kwon, D.-J. Jang, S. Y. Park, *Chem. Commun.* **2004**, 70.
[24] A. Bernet, M. Behr, H.-W. Schmidt, *Soft Matter* **2011**, *7*, 1058.
[25] N. E. Shi, H. Dong, G. Yin, Z. Xu, S. H. Li, *Adv. Funct. Mater.* **2007**, *17*, 1837.
[26] D. K. Kumar, D. A. Jose, P. Dastidar, A. Das, *Chem. Mater.* **2004**, *16*, 2332.
[27] N. Shi, G. Yin, M. Han, Z. Xu, *Colloids Surf. B* **2008**, *66*, 84.
[28] J. Roosma, T. Mes, P. Leclere, A. R. A. Palmans, E. W. Meijer, *J. Am. Chem. Soc.* **2008**, *130*, 1120.
[29] T. Mes, M. M. J. Smulders, A. R. A. Palmans, E. W. Meijer, *Macromolecules* **2010**, *43*, 1981.
[30] F. Abraham, H.-W. Schmidt, *Polymer* **2010**, *51*, 913.
[31] N. Mohmeyer, B. Müller, N. Behrendt, J. Hillenbrand, M. Klaiber, X. Zhang, P. Smith, V. Altstädt, G. M. Sessler, H.-W. Schmidt, *Polymer* **2004**, *45*, 6655.
[32] N. Mohmeyer, H.-W. Schmidt, P. M. Kristiansen, V. Altstädt, *Macromolecules* **2006**, *39*, 5760.
[33] N. Mohmeyer, N. Behrendt, X. Zhang, P. Smith, V. Altstädt, G. M. Sessler, H.-W. Schmidt, *Polymer* **2007**, *48*, 1612.
[34] D. P. Erhard, R. Giesa, V. Altstädt, H.-W. Schmidt, *J. Appl. Polym. Sci.* **2010**, *115*, 1247.
[35] D. P. Erhard, D. Lovera, W. Jenninger, J. Wagner, V. Altstädt, H.-W. Schmidt, *Macromol. Chem. Phys.* **2010**, *211*, 2179.
[36] K. Stoll, K. Hoffmann, B. Rotzinger, H.-W. Schmidt, WO 2007039471.
[37] F. Abraham, S. Ganzleben, D. Hanft, P. Smith, H.-W. Schmidt, *Macromol. Chem. Phys.* **2010**, *211*, 171.
[38] J. Varga, K. Stoll, A. Menyhárd, Z. Horváth, *J. Appl. Polym. Sci.* **2011**, *121*, 1469.
[39] M. Blomenhofer, S. Ganzleben, D. Hanft, H.-W. Schmidt, M. Kristiansen, P. Smith, K. Stoll, D. Mäder, K. Hoffmann, *Macromolecules* **2005**, *38*, 3688.
[40] D. Kluge, F. Abraham, S. Schmidt, H. W. Schmidt, A. Fery, *Langmuir* **2010**, *26*, 3020.
[41] E. P. S. Tan, C. T. Lim, *Compos. Sci. Technol.* **2006**, *66*, 1102.
[42] J. R. Withers, D. E. Aston, *Adv. Colloid Interface Sci.* **2006**, *120*, 57.
[43] E. P. S. Tan, C. T. Lim, *Appl. Phys. Lett.* **2004**, *84*, 1603.
[44] M. K. Shin, S. I. Kim, S. J. Kim, S.-K. Kim, H. Lee, *Appl. Phys. Lett.* **2006**, *88*, 193901.
[45] L. Yang, C. F. C. Fitie, K. O. van der Werf, M. L. Bennink, P. J. Dijkstra, J. Feijen, *Biomaterials* **2008**, *29*, 955.
[46] W. Xu, P. J. Mulhern, B. L. Blackford, M. H. Jericho, I. Templeton, *Scanning Microsc.* **1994**, *8*, 499.
[47] A. Kis, S. Kasas, B. Babic, A. J. Kulik, W. Benoit, G. A. D. Briggs, C. Schonenberger, S. Catsicas, L. Forro, *Phys. Rev. Lett.* **2002**, *89*, 4.
[48] C. Guzman, S. Jeney, L. Kreplak, S. Kasas, A. J. Kulik, U. Aebi, L. Forro, *J. Mol. Biol.* **2006**, *360*, 623.
[49] S. Orso, U. Wegst, E. Arzt, *J. Mater. Sci.* **2006**, *41*, 5122.
[50] D. R. Stamov, T. A. K. Nguyen, H. M. Evans, T. Pfohl, C. Werner, T. Pompe, *Biomaterials* **2011**, *32*, 7444.
[51] E. W. Wong, P. E. Sheehan, C. M. Lieber, *Science* **1997**, *277*, 1971.
[52] J. P. Salvetat, G. A. D. Briggs, J. M. Bonard, R. R. Bacsa, A. J. Kulik, T. Stockli, N. A. Burnham, L. Forro, *Phys. Rev. Lett.* **1999**, *82*, 944.
[53] B. Wu, A. Heidelberg, J. J. Boland, *Nat. Mater.* **2005**, *4*, 525.
[54] Y. X. Chen, B. L. Dorgan, D. N. McIlroy, D. E. Aston, *J. Appl. Phys.* **2006**, *100*, 7.
[55] H. Zhang, J. Tang, L. Zhang, B. An, L. C. Qin, *Appl. Phys. Lett.* **2008**, *92*, 3.
[56] X. Y. Ling, I. Y. Phang, W. Maijenburg, H. Schonherr, D. N. Reinhoudt, G. J. Vancso, J. Huskens, *Angew. Chem. Int. Ed.* **2009**, *48*, 983.
[57] X. Y. Ling, I. Y. Phang, H. Schonherr, D. N. Reinhoudt, G. J. Vancso, J. Huskens, *Small* **2009**, *5*, 1428.

full papers

[58] J. M. Gere, B. J. Goodno, in *Mechanics of Materials*, 7th ed., Cengage Learning, Toronto **2008**.

[59] W. J. Mai, Z. L. Wang, *Appl. Phys. Lett.* **2006**, *89*, 073112.

[60] L. Yang, K. O. Van der Werf, C. F. C. Fitie, M. L. Bennink, P. J. Dijkstra, J. Feijen, *Biophys. J.* **2008**, *94*, 2204.

[61] J. M. Gere, S. P. Timoshenko in *Mechanics of Materials*, 3rd ed., Chapman & Hall, London **1991**, p. 692.

[62] C. L. Pai, M. C. Boyce, G. C. Rutledge, *Polymer* **2011**, *52*, 2295.

[63] A. Sakamoto, D. Ogata, T. Shikata, O. Urakawa, K. Hanabusa, *Polymer* **2006**, *47*, 956.

[64] H.-W. Schmidt, P. Smith, M. Blomenhofer, **2002**, WO 02/46300 A2.

[65] D. Mäder, K. Hoffmann, H.-W. Schmidt, **2003**, WO 03102069 A1.

[66] H.-W. Schmidt, M. Blomenhofer, K. Stoll, H.-R. Meier, **2004**, WO 2004072168 A2.

contents

corrigendum

An error was present in Equation 2 on page 2566 of the manuscript. The correct Equation 2 is provided below. The authors wish to note that the error was only typographical–the data, fit, and results presented in the manuscript are unaffected.

Correct Equation (2):

$$K_{\text{norm}}(x) = \frac{3E}{\left(1-\frac{x}{L}\right)^3\left(\frac{x}{L}\right)^3}$$

NANO ‖ MICRO

small

Supporting Information

Influence of the Molecular Structure and Morphology of Self-Assembled 1,3,5-Benzenetrisamide Nanofibers on their Mechanical Properties

Daniel Kluge, Julia C. Singer, Jens W. Neubauer, Frank Abraham, Hans-Werner Schmidt, and Andreas Fery *

Influence of the Molecular Structure and Morphology of Self-Assembled 1,3,5-Benzenetrisamide Nanofibers on their Mechanical Properties

Daniel Kluge, Julia C. Singer, Jens W. Neubauer, Frank Abraham, Hans-Werner Schmidt and Andreas Fery*

Supporting Information
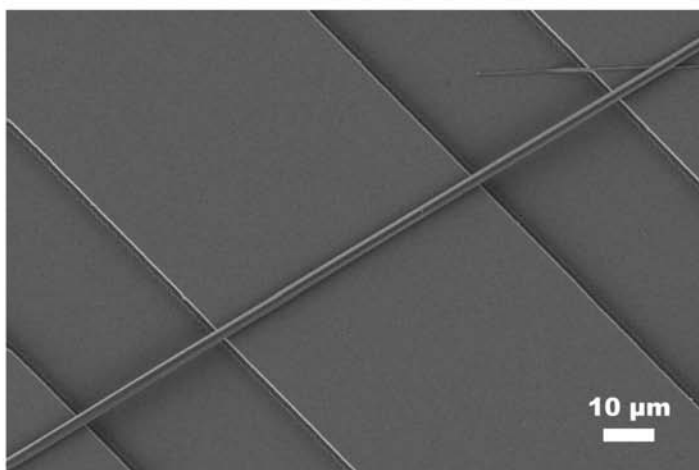
SI 1. Representative SEM image of a fiber of **2a** deposited on a structured glass substrate: The fiber is free-standing in the channel areas, while it is supported on the elevated areas.
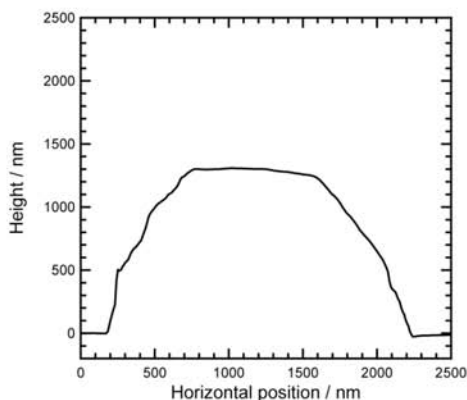
SI 2. Exemplary cross-sections of a fiber of **2a** as obtained by AFM imaging. It can be seen that the cross-section deviates from a cylindrical shape. Therefore, we imaged each individual investigated fiber and calculated the area moment of intertia I directly from the AFM-image in order to calculate Young's modulus.
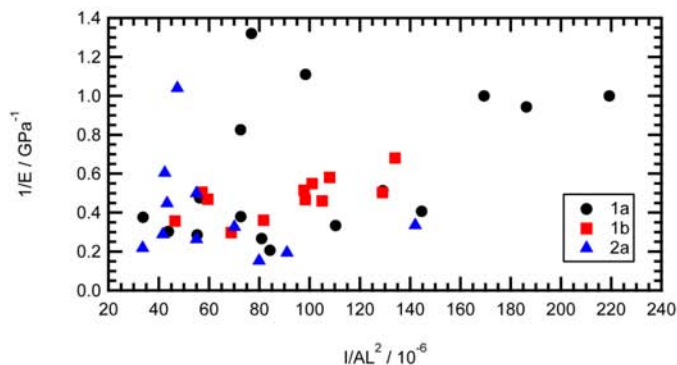
SI 3. Investigation of the shearing influence on the measured moduli. The data was calculated using Equation (5). It can be seen that for **1a** and **2a**, no influence of shearing can be observed. Only for **1b**, a slope of the data points can be seen which – although ill-defined – could be attributed to shearing. However, the contribution is too small for a reliable determination of G which can be seen from the scatter of the data. Therefore, even if shearing contributes to the measurements of **1b**, the contribution is insignificantly small and the calculated bending modulus E_b can be regarded as the true Young's modulus E.

4.4 Shaping Self-Assembling Small Molecules into Fibres by Melt Electrospinning*

The melt electrospinning of low molecular weight trisamides into nano-and microfibres is investigated in dependency on phase behavior, spinning temperature and electric field strength.
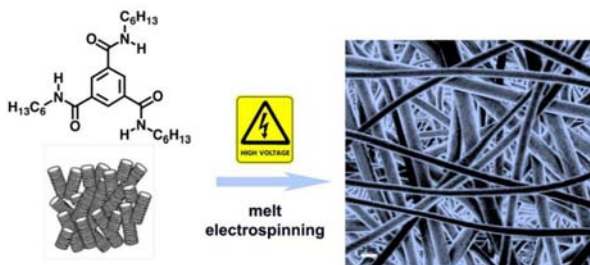
Reproduced with permission;
Copyright © 2012 The Royal Society of Chemistry

---

* Julia C. Singer, Reiner Giesa, Hans-Werner Schmidt; *Soft Matter*, **2012**, *8*, 9972–9976.

Soft Matter

COMMUNICATION

Shaping self-assembling small molecules into fibres by melt electrospinning†

Julia C. Singer, Reiner Giesa and Hans-Werner Schmidt*

Self-assembling small molecules is considered a promising technology for fabricating micro- and nanosized features. Utilization of typical top-down approaches, such as electrospinning, is rare in combination with self-assembly. Here we report for the first time on melt electrospinning of 1,3,5-cyclohexane- and 1,3,5-benzenetrisamides into fibres. The fibre spinning conditions were investigated with respect to the type of mesophase and applied field strength. It is possible to electrospin fibres from the nematic liquid crystalline phase and, most surprisingly, also from the optical isotropic state slightly above the clearing temperature, but not from columnar LC phases. Under optimized conditions it is possible to prepare homogeneous fibres with diameters below 1 μm.

The formation of micro- and nanosized polymer fibres is realized commonly by typical top-down approaches including techniques such as melt blow spinning,[1] centrifugal spinning,[2] or electrospinning.[3] An alternative strategy yielding fibres in the same size range is self-assembly of small molecules as a typical bottom-up approach.[4] Here we report on the combination of both processes by employing electrospinning and self-assembly from the melt of small molecules.

Among top-down approaches, solution electrospinning became a straightforward and versatile fibre spinning technique for polymers.[3,5] In this process, charges are induced to a solution of a high molar weight polymer in the presence of a strong electric field. Due to polymer chain entanglements, breakup into droplets is not observed but a stable jet is formed when electrostatic repulsive forces on the fluid surface overcome the surface tension. For small low molecular weight molecules electrospraying into small spherical droplets is the result. As it was pointed out by Long et al., a high molecular weight polymer is not actually essential for obtaining uniform electrospun fibres from solution.[6] The primary criterion is the presence of sufficient intermolecular interactions which function similar to chain entanglements.[6] Only a few examples are reported where self-assembling small molecules have been electrospun from solution into fibres, for instance phospholipids,[6-8] surfactants,[9] cyclodextrins,[10] ureido-

pyrimidinone moieties,[11] diphenylalanine,[12] or heteroditopic monomers.[13] Long et al. reported also the first case where melt electrospinning at 200 °C of a low molecular weight amphiphilic phospholipid, forming long range aggregates, rendered fibres in the range of 6 μm.[8]

1,3,5-Cyclohexane- and 1,3,5-benzenetrisamides are an important class of self-assembling low molecular weight compounds. The mechanism of self-aggregation of this class of organic compounds into supramolecular structures is well established. Due to strong intermolecular interactions in the form of hydrogen bonds of three amide groups self-assembling takes place to form supramolecular structures such as fibres and networks, and can also induce solvent gelation.[14-16] Depending on the core structure and substituents, trisamides exhibit a complex mesophase phase behavior in the melt.[17-19] It was also shown that compounds of this class of organic molecules form macrodipoles due to columnar stacking.[17,20,21] This was utilized for electric-field assisted alignment of 1,3,5-cyclohexanetrisamides,[22] or remnant polarization studies of thermotropic 1,3,5-benzenetrisamides.[21] Furthermore, solution electrospinning of a liquid crystalline, α-helical poly(α-amino acid) with macroscopic dipoles prealigned in the direction of the helical axis resulted in materials with high thermally stable piezoelectric coefficients.[23] Trisamides were also employed in our group as supramolecular polymer additives to improve the charge storage capability of polypropylene as electret materials.[24] These results were our motivation to explore electrospinning of this class of compounds from the melt. Candidates presented in this communication were selected from a large pool of substances matching certain phase behavior and temperature criteria. Different mesophases and an isotropic melt should be in the experimentally accessible temperature range up to 330 °C, detailed experimental methods are included in the ESI.†

To demonstrate the general electrospinnability of this class of low molecular weight compounds, one 1,3,5-cyclohexane- (**1**) and two types of 1,3,5-benzenetrisamides (**2** and **3**) were selected differing in direction of the linkage of the amide groups to the core and core structure itself. Scheme 1 summarizes chemical structures, phase transition temperatures, type of mesophase, applied spinning temperatures and thermal stability of **1**–**3**. Compounds **1** and **2** exhibit liquid crystalline (LC) phases, denoted as $Cr_1117Cr_2167Col_{rp}254N_c317I$ and $Cr72Col_{hp}172Col_{ho}218I$, respectively.[17] Explicitly, **1** forms a columnar rectangular plastic mesophase (Col_{rp}) between 167 °C and 254 °C followed by a nematic phase (N_c) up to 317 °C.

Macromolecular Chemistry I, Bayreuth Institute of Macromolecular Research (BIMF), and Bayreuth Center for Colloids and Interfaces (BZKG), University of Bayreuth, 95440 Bayreuth, Germany. E-mail: hans-werner.schmidt@uni-bayreuth.de; Fax: +49 (0)921 553206; Tel: +49 (0)921 553200

† Electronic supplementary information (ESI) available. See DOI: 10.1039/c2sm26469b
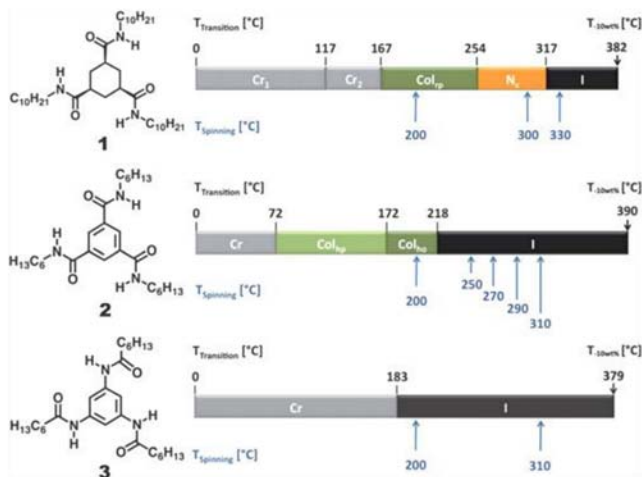
Scheme 1 Representative trisamides subjected to melt electrospinning with phase transition temperatures, type of mesophase, temperature of 10 wt% loss, and the investigated spinning temperatures (vertical arrows) (Cr: crystalline, Col: columnar mesophase, h: hexagonal, r: rectangular, p: plastic crystalline, o: ordered liquid crystalline, N_c: columnar nematic).

Compound **2** forms a columnar hexagonal plastic phase (Col_{hp}) starting at 72 °C, transforming into a columnar hexagonal ordered phase (Col_{ho}) at 172 °C, and changes at 218 °C into an isotropic melt. An exhaustive identification and characterization of all mesophases are reported elsewhere,[17] and the sequence of losing order in discotic mesophases and isotropic phases of trisamides with increasing temperature, which has a direct impact on the melt electrospinning results, is illustrated in Fig. S2 (ESI†). Finally, compound **3** exhibits no mesophase and melts at 183 °C.

In the following, we will discuss fibre morphologies obtained as a function of core structure, spinning temperature, and applied electric field strength. Compound **1**, a derivative of cyclohexane-*cis,cis*-1,3,5-tricarboxylic acid, exhibits a columnar rectangular (Col_{rp}) and a columnar nematic (N_c) phase (Scheme 1), but our efforts to electrospin **1** at 200 °C from its Col_{rp} phase failed due to the high viscosity of this mesophase impeding the elongation and deformation of the droplet at the tip. Instead, a translucent soft strand was extruded at high pressure. In general, nematic phases are less viscous than columnar phases because of reduced secondary interactions.[25] Due to the lower viscosity of the N_c phase, compound **1** was successfully electrospun at 300 °C and, most surprisingly, also from the optical isotropic melt at 330 °C, as illustrated in Fig. 1. Very homogeneous and long fibres with a narrow size distribution of 1.3 ± 0.2 μm were collected at 330 °C. A larger variety of diameters (histograms are included in Fig. S3–S5†) were observed for fibres electrospun from the nematic phase at 300 °C, indicating a more heterogeneous spinning process.

Compound **2**, based on trimesic acid with *n*-hexyl substituents, exhibits a columnar hexagonal plastic (Col_{hp}) and a hexagonal
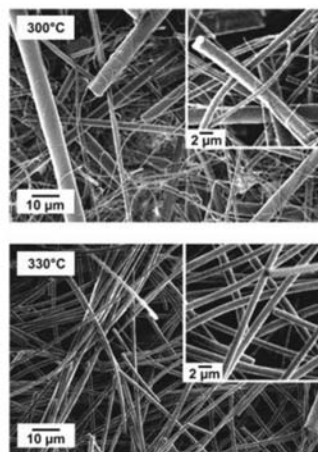
Fig. 1 Comparison of SEM images of melt electrospun fibres of **1** from the nematic phase at 300 °C and optical isotropic phase at 330 °C. In both cases fibre formation is observed, fibres from the isotropic melt are thinner and more homogeneous (spinning conditions: voltage: −40 kV, flow rate: 200 μL h^{-1}, distance needle tip–ground plate: 6 cm, needle ID: 0.6 mm).
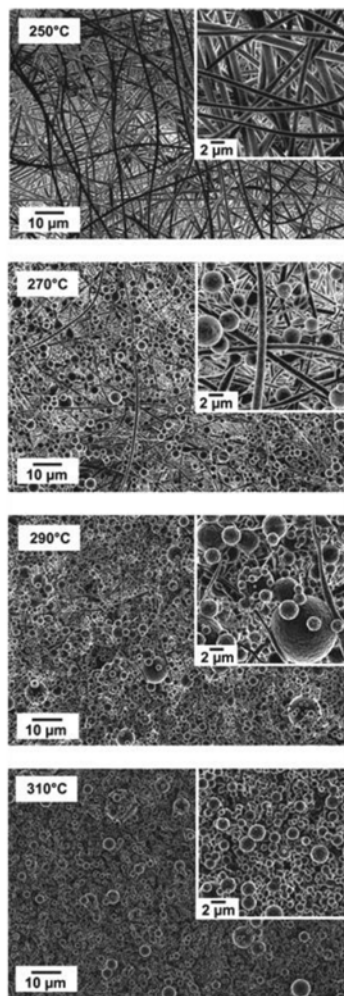
Fig. 2 SEM images of melt electrospun fibres and spheres of **2** as a function of the spinning temperature in the optical isotropic melt. Progressing sphere formation is observed with increasing spinning temperature due to the decreasing H-bond interactions between the molecules (spinning parameters: voltage: −30 kV, flow rate: 200 μL h⁻¹, distance needle tip–ground plate: 6 cm, needle ID: 0.6 mm).

ordered (Col$_{ho}$) mesophase. Our efforts to electrospin **2** at 200 °C from the Col$_{ho}$ phase also failed due its high viscosity. The melt viscosity of **2** as a function of temperature is plotted in Fig. S6† and the viscosity of the Col$_h$ mesophases (10 Pa s) is two magnitudes higher compared to the very fluid optical isotropic phase. The unexpected result that occurred during melt electrospinning of **1**, fibres are also formed from the optical isotropic melt, motivated us to study the influence of spinning temperature on fibre morphology in this phase. Compound **2** is most suitable, since it possesses a broad isotropic phase of around 170 K permitting electrospinning even at 310 °C (Scheme 1). At 250 °C, approx. 30 K above the clearing temperature of 218 °C, **2** was melt electrospun into homogeneous, continuous fibres with a narrow diameter size distribution of 0.9 ± 0.2 μm (Fig. 2). At 270 °C, the fibre diameter decreases to 0.5 ± 0.4 μm and concurrently spheres with a diameter of 2.4 ± 0.7 μm appear. At 290 °C, spheres with an average diameter of 1.8 ± 1.2 μm dominate, whereas the diameter of the few visible fibres reduces to 0.3 ± 0.2 μm. Finally at 310 °C, no fibres and only spheres with a diameter of 0.9 ± 0.2 μm are observed.

The fibre formation even from the optical isotropic melt is very extraordinary and a unique consequence of the supramolecular structure of trisamides. In a temperature range above the transition from the mesophase into the optical isotropic phase, columnar aggregates are still present. This was confirmed by temperature-dependent X-ray diffraction and FTIR investigations.[17] Due to these supramolecular columns, fibre formation is still observed slightly above the clearing temperature. It is feasible that these individual columns of 1,3,5-cyclohexane- and 1,3,5-benzenetrisamides build up a macrodipole,[17,20,21] which in return interacts with the applied electric field. At higher temperatures (for instance at 310 °C) the columnar pre-aggregates, which we consider essential for fibre formation, are reduced in length or completely absent, and only sphere formation is observed.

Compound **3**, based on 1,3,5-triaminobenzene, does not exhibit any LC mesophases and only a melting point at 183 °C. In Fig. 3 the results for electrospinning experiments at 200 °C at different electric field strengths are depicted. The fibre morphologies observed for **3** prove that the existence of a mesophase at lower temperatures is not a prerequisite for fibre formation from the optical isotropic melt. At a low electric voltage (−25 kV), short and thick fibre fragments with an average diameter of 12.0 ± 2.0 μm were collected. At increasing voltage, the diameter of the fragments decreases from 6.5 ± 2.1 μm (−30 kV) to 2.3 ± 0.5 μm (−40 kV) by elongating the fragments to fibres. At −45 kV homogeneous and thin fibres (2.2 ± 0.4 μm) were observed.

Hence, a stronger electrical field is necessary to form long and homogeneous fibres from the melt droplets by inducing additional charges. This phenomenon is also known for several polymers in melt or solution electrospinning.[26]

Additional spinning experiments with **3** at 310 °C and −45 kV revealed besides fibers (0.5 ± 0.3 μm) sphere formation (2.1 ± 1.5 μm, not shown) similar to compound **2** in Fig. 2.

Conclusions

In this communication we demonstrated for the first time that columnar supramolecular structures of self-assembling 1,3,5-cyclo-hexane- and 1,3,5-benzenetrisamides can be melt electrospun from the nematic LC phase and, most surprisingly, even from the optical
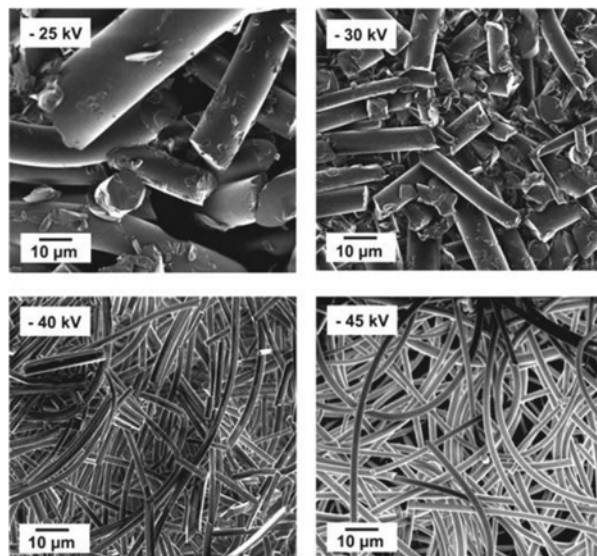
Fig. 3 SEM images of melt electrospun fibres of **3** spun at 200 °C as a function of the electric field strength. Thick fragments are obtained at low field strengths, elongation with increasing field strength to homogeneous long and much thinner fibres is observed (spinning conditions: temperature: 200 °C, flow-rate: 200 μL h^{-1}, distance needle tip–ground plate: 6 cm, needle ID: 0.6 mm).

isotropic melt. Other liquid crystalline phases were too viscous to be electrospun. In future work we will evaluate the nano-mechanical properties[27] of melt electrospun fibres and assess their potential for instance in filters and piezoelectric applications.

Notes and references

1 (a) D. H. Tan, C. Zhou, C. J. Ellison, S. Kumar, C. W. Macosko and F. S. Bates, *J. Non-Newtonian Fluid Mech.*, 2010, **165**, 892; (b) C. J. Ellison, A. Phatak, D. W. Giles, C. W. Macosko and F. S. Bates, *Polymer*, 2007, **48**, 3306.

2 (a) J. Engström and B. Hagström, *Nordic Textile Journal*, 2009, 82; (b) R. T. Weitz, L. Harnau, S. Rauschenbach, M. Burghard and K. Kern, *Nano Lett.*, 2008, **8**, 1187.

3 (a) J. H. Wendorff, S. Agarwal and A. Greiner, *Electrospinning*, Wiley-VCH, Weinheim, 2012, pp. 1–237; (b) D. W. Hutmacher and P. D. Dalton, *Chem.–Asian J.*, 2011, **6**, 44; (c) A. Baji, Y.-W. Mai, S.-C. Wong, M. Abtahi and P. Chen, *Compos. Sci. Technol.*, 2010, **70**, 703.

4 (a) C. C. Lee, C. Grenier and E. W. Meijer, *Chem. Soc. Rev.*, 2009, **38**, 671; (b) N. Kimizuka, *Adv. Polym. Sci.*, 2008, **219**, 1.

5 Y. Dzenis, *Science*, 2004, **304**, 1917.

6 M. G. McKee, J. M. Layman, M. P. Cashion and T. E. Long, *Science*, 2006, **311**, 353.

7 M. T. Hunley, M. G. McKee and T. E. Long, *J. Mater. Chem.*, 2007, **17**, 605.

8 M. T. Hunley, A. S. Karikari, M. G. McKee, B. D. Mather, J. M. Layman, A. Fornof and T. E. Long, *Macromol. Symp.*, 2008, **270**, 1.

9 M. P. Cashion, X. Li, Y. Geng, M. T. Hunley and T. E. Long, *Langmuir*, 2010, **26**, 678.

10 (a) A. Celebioglu and T. Uyar, *Nanoscale*, 2012, **4**, 621; (b) J. L. Manasco, C. D. Saquing, C. Tang and S. A. Khan, *RSC Adv.*, 2012, **2**, 3778.

11 P. Y. Dankers, M. C. Harmsen, L. A. Brouwer, M. J. van Luyn and E. W. Meijer, *Nat. Mater.*, 2005, **4**, 568.

12 G. Singh, A. M. Bittner, S. Loscher, N. Malinowski and K. Kern, *Adv. Mater.*, 2008, **20**, 2332.

13 X. Yan, M. Zhou, J. Chen, X. Chi, S. Dong, M. Zhang, X. Ding, Y. Yu, S. Shaod and F. Huang, *Chem. Commun.*, 2011, **47**, 7086.

14 (a) M. P. Lightfoot, F. S. Mair, R. G. Pritchard and J. E. Warren, *Chem. Commun.*, 1999, 1945; (b) E. Fan, J. Yang, S. J. Geib, T. C. Stoner, M. D. Hopkins and A. D. Hamilton, *J. Chem. Soc., Chem. Commun.*, 1995, 1251; (c) S. Cantekin, T. F. A. de Greef and A. R. A. Palmans, *Chem. Soc. Rev.*, 2012, DOI: 10.1039/c2cs35156k; (d) C. A. Jiménez, J. B. Belmar, L. Ortíz, P. Hidalgo, O. Fabelo, J. Pasán and C. Ruiz-Pérez, *Cryst. Growth Des.*, 2009, **9**, 4987; (e) M. Kristiansen, P. Smith, H. Chanzy, C. Baerlocher, V. Gramlich, L. McCusker, T. Weber, P. Pattison, M. Blomenhofer and H.-W. Schmidt, *Cryst. Growth Des.*, 2009, **9**, 2556; (f) M. Schmidt, J. J. Wittmann, R. Kress, D. Schneider,

S. Steuernagel, H.-W. Schmidt and J. Senker, *Cryst. Growth Des.*, 2012, **12**, 2543.

15 (a) A. Bernet, M. Behr and H.-W. Schmidt, *Soft Matter*, 2011, **7**, 1058; (b) J. Roosma, T. Mes, P. Leclère, A. R. Palmans and E. W. Meijer, *J. Am. Chem. Soc.*, 2008, **130**, 1120; (c) T. Shikata, Y. Kuruma, A. Sakamoto and K. Hanabusa, *J. Phys. Chem. B*, 2008, **112**, 16393; (d) M. M. Smulders, A. P. Schenning and E. W. Meijer, *J. Am. Chem. Soc.*, 2008, **130**, 606.

16 (a) M. Blomenhofer, S. Ganzleben, D. Hanft, H.-W. Schmidt, M. Kristiansen, P. Smith, K. Stoll, D. Mäder and K. Hoffmann, *Macromolecules*, 2005, **38**, 3688; (b) F. Abraham and H.-W. Schmidt, *Polymer*, 2010, **51**, 913; (c) F. Abraham, S. Ganzleben, D. Hanft, P. Smith and H.-W. Schmidt, *Macromol. Chem. Phys.*, 2010, **211**, 171.

17 A. Timme, R. Kress, R. Albuquerque and H.-W. Schmidt, *Chem.–Eur. J.*, 2012, **18**, 8329.

18 I. Tomatsu, C. F. Fitié, D. Byelov, W. H. de Jeu, P. C. Magusin, M. Wübbenhorst and R. P. Sijbesma, *J. Phys. Chem. B*, 2009, **113**, 14158.

19 (a) M. Wegner, D. Dudenko, D. Sebastiani, A. R. Palmans, T. F. Greef, R. Graf and H. W. Spiess, *Chem. Sci.*, 2011, **2**, 2040; (b) P. J. M. Stals, M. M. Smulders, R. Martín-Rapún, A. R. Palmans and E. W. Meijer, *Chem.–Eur. J.*, 2009, **15**, 2071.

20 (a) É. Bayard, S. Hamel and A. Rochefort, *Org. Electron.*, 2006, **7**, 144; (b) A. Sakamoto, D. Ogata, T. Shikata, O. Urakawa and K. Hanabusa, *Polymer*, 2006, **47**, 956.

21 C. F. Fitié, W. S. Roelofs, P. Magusin, M. Wübbenhorst, M. Kemerink and R. P. Sijbesma, *J. Phys. Chem. B*, 2012, **116**, 3928.

22 L. Sardone, V. Palermo, E. Devaux, D. Credgington, M. de Loos, G. Marletta, F. Cacialli, J. van Esch and P. Samori, *Adv. Mater.*, 2006, **18**, 1276.

23 D. Farrar, K. Ren, D. Cheng, S. Kim, W. Moon, W. L. Wilson, J. E. West and S. M. Yu, *Adv. Mater.*, 2011, **23**, 3954.

24 (a) D. P. Erhard, D. Lovera, C. von Salis-Soglio, R. Giesa, V. Altstädt and H.-W. Schmidt, *Adv. Polym.Sci.*, 2010, **228**, 155; (b) J. Hillenbrand, T. Motz, G. M. Sessler, X. Zhang, N. Behrendt, C. von Salis-Soglio, D. P. Erhard, V. Altstädt and H.-W. Schmidt, *J. Phys. D: Appl. Phys.*, 2009, **42**, 065410.

25 C. Destrade, P. Foucher, H. Gasparoux, N. H. Tinh, A. M. Levelut and J. Malthete, *Mol. Cryst. Liq. Cryst.*, 1984, **106**, 121.

26 C. Subramanian, S. C. Ugbolue, S. B. Warner and P. K. Patra, *Mater. Res. Soc. Symp. Proc.*, 2009, **1134**, BB08-18.

27 (a) D. Kluge, J. C. Singer, J. W. Neubauer, F. Abraham, H.-W. Schmidt and A. Fery, *Small*, 2012, **8**, 2563; (b) D. Kluge, F. Abraham, S. Schmidt, H.-W. Schmidt and A. Fery, *Langmuir*, 2010, **26**, 3020.

Shaping self-assembling small molecules into fibers by melt electrospinning

Julia C. Singer, Reiner Giesa and Hans-Werner Schmidt

Macromolecular Chemistry I, Bayreuth Institute of Macromolecular Research (BIMF), and

Bayreuth Center for Colloids and Interfaces (BZKG)

University of Bayreuth, 95440 Bayreuth, Germany

E-mail: hans-werner.schmidt@uni-bayreuth.de

Supporting Information

Content

Experimental Methods

Experimental Methods

Materials

1,3,5-Cyclohexane- and 1,3,5-benzenetrisamides **1-3** were synthesized according to reference 16 and 17. The molecular weight of **1** is 634 g/mol, and of **2** and **3** 460 g/mol. The melting temperature of **3** was determined in a Perkin Elmer Diamond DSC (heating rate: 10 K/min, nitrogen flow: 20 mL/min). Temperature weight loss measurements of **1-3** were performed using a Mettler SDTA 851 TGA at 10 K/min (nitrogen flow: 60 mL/min). **1** shows a 10%-weight loss at 382°C, **2** at 390°C, and **3** at 379°C due to evaporation and not decomposition indicated by a 100% weight loss without any char yield.[16] In isothermal TGA runs at the spinning temperature under nitrogen atmosphere, **1-3** showed evaporation weight loss below 5 wt.% for at least 30 minutes which is much less than the typical time (15 min) for an electrospinning experiment. For each temperature a new sample and syringe was used.

Electrospinning and Characterization

For melt electrospinning a custom designed equipment was utilized (**Figure S1**). An 1 mL glass syringe (3) (Poulten & Graf, Fortuna Optima, luer glass tip) with a shortened (length: 1 mm) hypodermic 20G needle is placed in an electrically heated block (2) which temperature can be set up to 350°C with a fluctuation of ±0.5°C at 250°C. The reported spinning temperature is the temperature of the heated cylinder around the syringe body. The temperature at the needle tip is max. 5 % lower. The plunger of the syringe is driven via a piston, equipped with a pressure transducer, by a precision motor and gear system (1). The entire drive unit can be tilted by 90° and thus the syringe can be easily replaced. Reversely to the most common design for electrospinning, in this setup the syringe needle and consequently all attached electronic components are earthed.[3b,8] The high voltage (HV) power supplies (7) (Schulz Electronic, high voltage units AK0175 and AK1026, +60 and -60 kV,

respectively) were connected to the collector plate (6) in the base plate (5) below the needle (4).

Figure S1. Drawing and details of the melt spinning equipment.
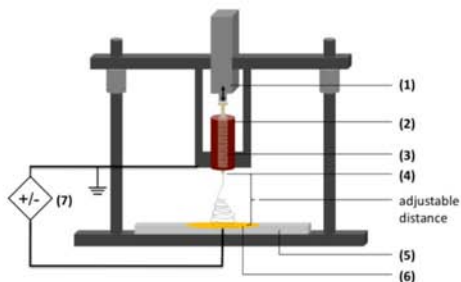
(1) drive unit: DC motor, gear, and pressure transducer, (2) band heater, (3) glass syringe with plunger, (4) metal hollow needle, (5) base plate (Teflon®), (6) collector plate/HV electrode, (7) HV supply max. ±60 kV.

The maximal distance between needle tip and collector is 14 cm, and the feeding rate for a 1 mL syringe can be set from 20 to 1500 µL/h by adjusting the plunger speed. In many preceding spinning experiments the influence of flow rate, needle ID, and distance needle tip-ground plate were optimized, and kept at 200 µL/h, 0.6 mm, and 6 cm, respectively. Before applying HV, each sample was equilibrated for three minutes at the spinning temperature and flow rate. The electrospun material was collected on a single 12 mm diameter aluminum SEM stub which was mounted on the collector plate. To investigate the surface morphology, the stub was sputtered with platinum (2.0 nm) in a Cressington sputter coater 208HR and imaged in a SEM Zeiss LEO 1530 FESEM (Zeiss, Jena, Germany) at 1.5 to 3 keV. From SEM images the thickness distribution from at least 100 individual fibers or spheres was evaluated using AxioVision LE Software (Carl Zeiss AG, Germany). The histograms for all thickness distributions are listed in **Figure S3** to **S5**.

Figure S2. Illustration of loosing order with increasing temperature in a discotic mesophase and optical isotropic melt of trisamides.

In general for discotic mesophases, the order of the liquid crystalline phases decreases with temperature.[see reference 17, and for instance, S. Laschat et al., *Angew. Chem. Int. Ed.*, 2007, **46**, 4832.] Please note that typical and characteristic for trisamides, the isotropic phase still consists of shorter columns but without birefringence, thus called optical isotropic. At higher temperatures the interaction between individual molecules in form of hydrogen bonds is lost resulting in molecular isotropic, single molecules.
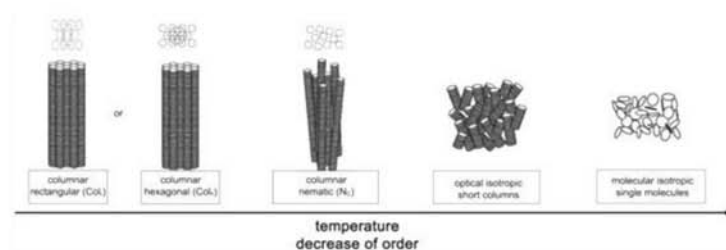
Figure S3. SEM images and fiber histograms of **1**, electrospun as function of the spinning temperature. At 300°C the compound exhibits a nematic mesophase, at 330°C, above the clearing temperature at 317°C, an isotropic melt is formed. Spinning parameters: voltage: -40 kV, flow rate: 200 µL/h; distance needle tip – ground plate: 6 cm; needle ID: 0.6 mm.
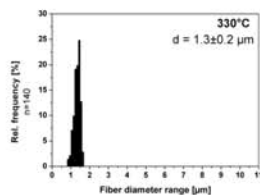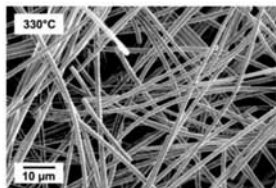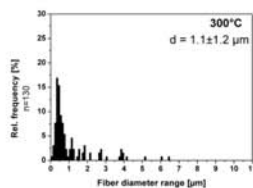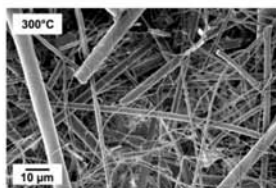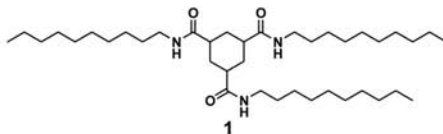
Figure S4. SEM images and fiber/sphere diameter histograms of **2**, electrospun as function of the spinning temperature in the optical isotropic melt. Spinning parameters: voltage: -30 kV; flow rate: 200 µL/h; distance needle tip – ground plate: 6 cm; needle ID: 0.6 mm.

6
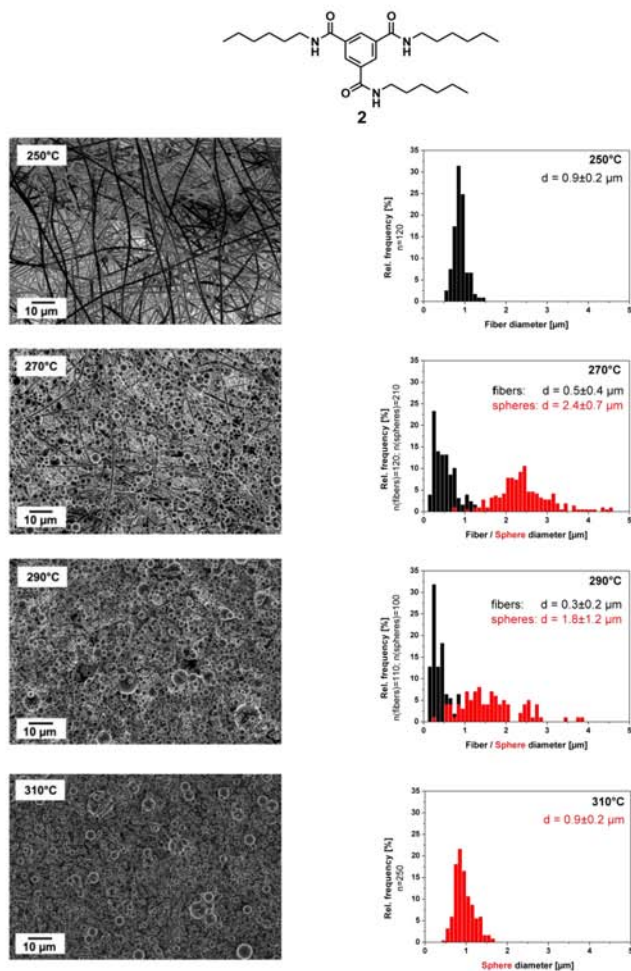
Figure S5. SEM images and fiber diameter histograms of **3** as function of the electric field strength at 200°C in the optical isotropic melt. Spinning parameters: temperature: 200°C; flow rate: 200 µL/h; distance needle tip – ground plate: 6 cm; needle ID: 0.6 mm.
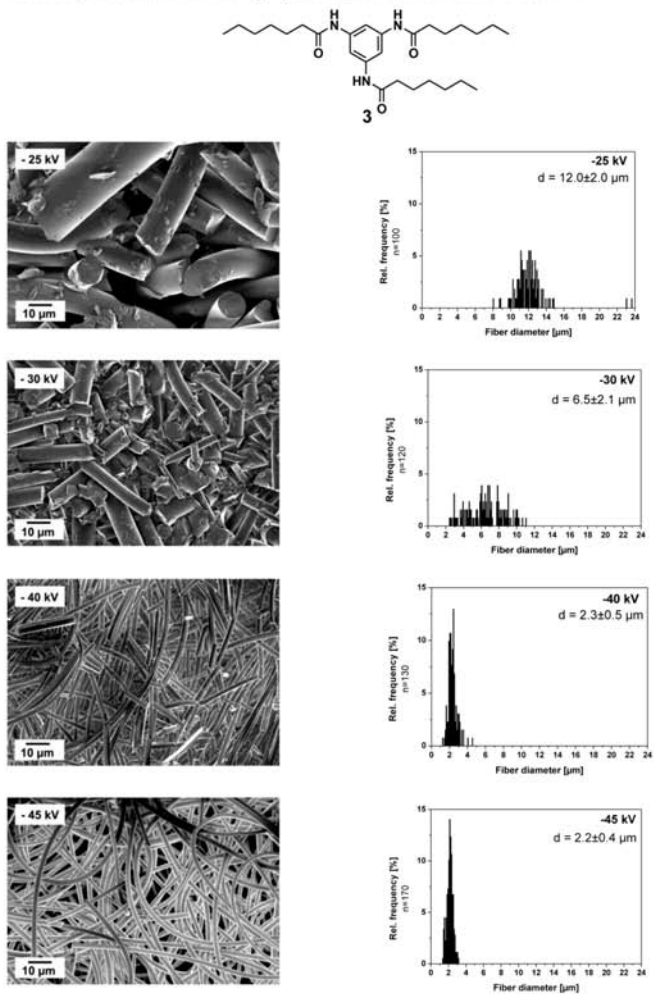
Figure S6. Melt viscosity as function of the temperature of compound **2** for the first cooling run at 2K/min. During cooling, at 207°C the viscosity of the melt dramatically soars during 10 K. Note, that the transition temperatures determined with DSC (Scheme 1) and melt rheology of compound **2** differ by approx. 10 K. (Measured in a CVO150 rheometer (Malvern, Germany) using an oszillating (1 Hz) cone-plate geometry (2.5°/25 mm) at a cooling rate of 2K/min)
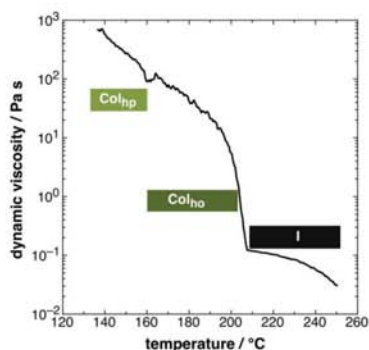
4.5   Melt Electrospinning of Small Molecules*

Electrospinning is an attractive way to prepare nano- and macrofibers. It was demonstrated by our group that trisamides can be melt electrospun into supramolecular fibers. To establish structure–property relationships regarding spinnability and morphology, melt electrospinning experiments were conducted using several classes of compounds. The number of hydrogen bonds was systematically decreased from three for trisamides, to two for bisamide and sorbitols, and to zero for perylene bisimides and tertiary trisamides. As a result, trisamides are readily spun into fibers, whereas for bisamides and sorbitols mainly electrospraying into spheres is observed. Perylene bisimides form well-defined fibers due to strong π–π interactions. This supramolecular fiber is interesting for many scientific disciplines.

Keywords: fibers, melt electrospinning, structure-property relations, supramolecular structures, trisamide

Macromolecular
Materials
and Engineering

3/2015

Feature Article
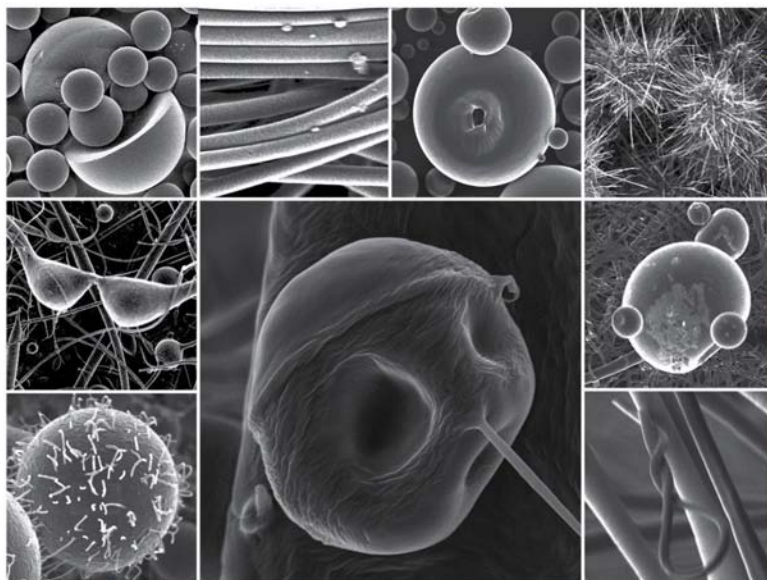
Melt Electrospinning of Small Molecules

Julia C. Singer, Andreas Ringk, Reiner Giesa, Hans-Werner Schmidt*

Electrospinning is an attractive way to prepare nano- and macrofibers. It was demonstrated by our group that trisamides can be melt electrospun into supramolecular fibers. To establish structure–property relationships regarding spinnability and morphology, melt electrospinning experiments were conducted using several classes of compounds. The number of hydrogen bonds was systematically decreased from three for trisamides, to two for bisamide and sorbitols, and to zero for perylene bisimides and tertiary trisamides. As a result, trisamides are readily spun into fibers, whereas for bisamides and sorbitols mainly electrospraying into spheres is observed. Perylene bisimides form well-defined fibers due to strong π–π interactions. This supramolecular fiber is interesting for many scientific disciplines.

R= CH$_2$(OCH$_2$CH$_2$)$_3$OCH$_3$

2 µm

1. Introduction

When a liquid at the tip of a capillary is subjected to an electric field, the created drop is electrostatically charged, deforms from a spherical into a cone-like shape, and a jet is formed out of the elongated droplet. The formation of this cone was first described by Taylor and hence bears his name.[1] Due to the electric charges, the jet breaks up when accelerated in an electric field and bursts into droplets.[2,3] The maximum charge q on a drop depends on the size d and surface tension γ of the droplet and is known as the Rayleigh limit: $q = \sqrt{8\pi^2 \epsilon_0 \gamma d^3}$ where ϵ_0 denotes the vacuum permittivity.[3] An induction of more charges leads to splitting of the drop because repulsive forces between charges on the droplet surface exceed the surface tension. This process is

J. C. Singer, Dr. A. Ringk, Dr. R. Giesa, Prof. H.-W. Schmidt
Macromolecular Chemistry I, Bayreuth Institute of
Macromolecular Research (BIMF) and Bayreuth Center for Colloids
and Interfaces (BZKG), University of Bayreuth, 95440, Bayreuth,
Germany
E-mail: hans-werner.schmidt@uni-bayreuth.de

known as electrospraying, a process used to generate from solution fine and highly monodisperse particles down to 10 nm. After solvent evaporation, the collected powder does not coagulate because the charged aerosol is self-repellent.[2]

During the last two decades, the electrospinning process was established as a versatile method to prepare specialized nano- and microfibers for many different applications. The use of polymer solutions with sufficiently high viscosities in this process prevents the break-up of the jet into droplets; instead, fibers are formed. In the electric field, the droplet at the tip of the capillary is electrostatically charged and shaped into a Taylor cone. As soon as repulsive surface electrostatic forces overcome the surface tension of the droplet, a jet is ejected toward the collector, and is accelerated in the electric field. Instabilities stretch, bend, and introduce a whipping motion of the viscous fluid and the diameter of the jet is extremely reduced.[4]

Polymer type, molecular weight and concentration, type of solvent and possible additives, electric field strength, feeding rate, and ambient conditions are the main parameters which play a crucial role in fiber spinning and control the diameter.[4,5] In particular, the solution viscosity determines the morphology of the collected material. If the solution concentration is too low, beads

are formed during the electrospinning process due to the lack of sufficient polymer chain entanglements and an emerging Rayleigh instability. Additionally, with increasing molecular weight or higher concentration, the necessary amount of chain entanglements is reached. The chain entanglements have to overcome a critical value C_e to keep the jet from breaking up. Beaded fibers are obtained when the polymer chains start to interact with each other, but the chain overlap is still not sufficiently high ($C \leq C_e$). Homogenous fibers are obtained at concentrations above C_e.[6–8] Thus, the link between chain entanglements in polymer solutions and their electrospinnabilty into fibers is evident. Similar arguments hold true for polymer melts. When the viscosity of the melt is too low, breakup of the jet occurs during acceleration in the electric field.[9,10] However, Yu et al. investigated the morphologies of electrospun Newtonian Boger PEO/PEG fluids below concentrations where any entanglement transition is observed. Their results indicate that the presence of entanglements is not required for the formation of uniform fibers but rather a certain degree of fluid elasticity.[11]

Solution electrospinning of small molecules: Compared to solution electrospinning of polymers, only a few studies have been published dealing with the solution electrospinning of small molecules. Mainly, the investigated compounds can be classified as amphiphiles, mono- and dipeptides, or cyclodextrine derivatives. In Table 1, an overview of examples from the literature is presented. It was demonstrated by Long et al.[12–14] and Bittner et al.[15–17] that using different self-assembling compounds with sufficiently strong secondary interactions above a certain solution concentration can act like chain entanglements of polymers and thus electrospraying is avoided. For instance, phospholipids were successfully electrospun into homogenous fibers by using chloroform or dimethylformamide (DMF) solutions at sufficiently high concentrations (Table 1, a).[12]

Electrospun fibers were also obtained from ammonium and phosphonium gemini surfactants in a water/methanol mixture (b),[14] from diphenylalanine (c),[15] other peptide derivatives (d),[16] tetraphenylporphyrin (TPP),[17] and from diphenylalanine coupled with TPP (e).[17] In these cases 1,1,3,3,3-hexafluoro-2-propanol (HFIP) was used as solvent. Moreover, fibers were obtained by solution electrospinning of two bioactive peptide amphiphiles from water (f) at a sufficiently high solution concentration and solution conductivity.[18] Fibers from a crown-ether containing monomer (g) were obtained by Huang et al., suggesting that the formation and entanglement of the supramolecular structures stabilize the electrospinning jet.[19] Solution electrospinning of α-, β-, and γ-cyclodextrins (f) was investigated thoroughly by Celebioglu and Uyar.[20] Here the electrospinning jet seems to be stabilized by hydrogen-bonded cyclodextrin aggregates with sufficient

Julia C. Singer is a PhD student in the graduate school (BayNAT) of the University of Bayreuth, Germany. She received her BSc in chemistry in 2008 and her MSc in material chemistry and catalysis in 2010 at the University of Bayreuth, Germany. Afterwards, Julia joined the group Macromolecular Chemistry I of Prof. Hans-Werner Schmidt at the University of Bayreuth and was awarded with a scholarship of the Elite Network Bavaria (ENB). Her current research focuses on the preparation, characterization, and the comparison of supramolecular nano- and microfibers obtained by self-assembly and melt electrospinning.
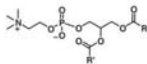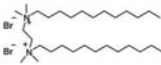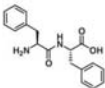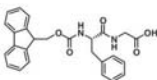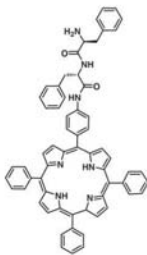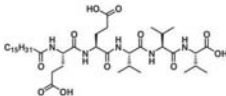
Reiner Giesa is a senior staff chemist at the Department of Macromolecular Chemistry at the University of Bayreuth, Germany. He holds a doctorate (1989) in polymer chemistry from Mainz, Germany. He spent five years as postdoctoral fellow at IBM Almaden Research in San Jose, CA, Materials Department at University of California in Santa Barbara, CA, and at the Polymer Science and Engineering Department at UMass, Amherst, MA. In 1994, he accepted a research position at the University of Bayreuth, Germany. There he is heading the keylab "Small Scale Polymer Processing" which is focused on the development and application of polymer processing and testing techniques on a gram scale. His areas of interest include the synthesis, properties, and processing of high performance polymers, such as polyimides, polyaramides, polyesters, and thermoset materials. Other fields of interest are translating biomimetic principles into polymer materials and melt electrospinning of self-assembling molecules.
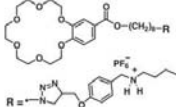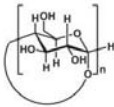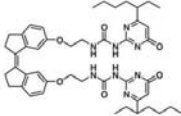
Hans-Werner Schmidt studied Chemistry at the University of Mainz (Germany) and ETH Zürich (Switzerland). He received his Diploma in Chemistry and Dr. rer. nat. degree in Macromolecular Chemistry with Prof. Helmut Ringsdorf at the University of Mainz. After a stay at the DuPont Central Research in Wilmington, Delaware (USA) he moved to the University of Marburg to obtain his Habilitation. From 1989 to 1994, he was Assistant and Associate Professor of Materials with tenure at the Materials Department, College of Engineering at the University of California, Santa Barbara (USA). Since 1994, he has been Full Professor for Macromolecular Chemistry at the University of Bayreuth. He is director of the Bayreuth Institute of Macromolecular Research and founding director of the Bayreuth Centre for Colloids and Interfaces. In 2009, he was appointed as vice president for research of the University of Bayreuth. Since 2004 he is chairman of the 'Elite Study Program Macromolecular Science' within the Elite Network Bavaria and since 2013 director of the University of Bayreuth Graduate School.
His research interest is focused on the synthesis and development of novel organic functional materials in the area of emerging technologies. This includes multifunctional polymers, molecular glasses, and supramolecular polymer additives and gelators. Combinatorial methods to efficiently synthesize and screen materials properties of polymer and supramolecular materials and functions of devices are an additional aspect.

Table 1. Literature overview of selected small molecules processed by solution electrospinning. Presented are the molecular structure, solvent or solvent mixture, solution concentration, resulting morphology, and References.

Entry	Molecular structure	Solvent	Conc. [wt.-%]	Morphology/ fiber diameter	Ref.
a	R, R': fatty acid residues	CHCl₃/DMF(70/30)	<35 35 >35	Beads Beaded fibers Fibers/≈5 μm	12,13
b		Water/MeOH (50/50)	<22 22 >22	Beads Beaded fibers Fibers/≈5 μm	14
c		HFIP	<13.2 13.2 >13.2	Beads Beaded fibers Fibers/≈0.7 μm	15
d		HFIP	≥18	Fibers/0.3–10 μm	16
e		HFIP	9.1	Fibers/0.4 ± 0.3 μm	17
f		Water	3	Fibers/3.8 ± 0.4 μm	18

(Continued)

▌ *Table 1.* Continued

Entry	Molecular structure	Solvent	Conc. [wt.-%]	Morphology/ fiber diameter	Ref.
g		CHCl$_3$	13	Fibers/0.4–4 µm	19
h	n = 6: α-cyclodextrin n = 7: β-cyclodextrin n = 8: γ-cyclodextrin	Water, DMF or DMAc	<100 ≈100 ≈140	Beads Beaded fibers Fibers/0.2–2 µm	20
i		CHCl$_3$	18.1	Fibers/0.3–3 µm	21

CHCl$_3$: chloroform; DMF: *N,N*-dimethylformamide; MeOH: methanol; HFIP: 1,1,1,3,3,3-hexafluoro-2-propanol; TFA: 2,2,2-trifluoroacetic acid; DMAc: *N,N*-dimethylacetamide.

interactions formed only at very high solid concentrations in water or amidic solvent. Recently, a photoresponsive compound (i) was also investigated for solution electrospinning by Yang et al. The fiber formation is driven by the formed supramolecular ring-chain construction.[21] Most used solvents, such as chloroform, DMF, or HFIP are, however, problematic due to their toxicity.

Melt electrospinning of small molecules: In general, melt electrospinning of small molecules results in electrospraying into spheres. In 2008, Long et al. reported on the formation of fibrous morphologies via melt electrospinning of a low molecular weight phospholipid.[13] The well-defined 1-palmitoyl-2-oleoyl-*sn*-glycerol-3-phosphoethanolamine (POPE) with a molecular weight of 718 g · mol^{-1} was melt electrospun around 200 °C at +30 kV and with a needle tip to ground plate distance of 10 cm into fibers

with diameters of 6.5 ± 2.0 µm. We confirmed these results at slightly different melt spinning conditions and obtained uniform fibers with a diameter distribution of $d = 1.8 \pm 0.2$ µm (Figure 1).

However, when a mixture of phospholipids derived from soybean (asolectin) was melt electrospun, solely electrospraying into spheres occurred. In this case, Long et al. assume that asolectin does not associate readily enough to form fibers during the rapid electrospinning process, resulting in droplet formation only.[13]

Recently, we reported for the first time on the melt electrospinning of 1,3,5-benzene- and 1,3,5-cyclohexanetrisamides into long and homogenous fibers.[22,23] Depending on core structure, amide connectivity to the core, and peripheral substituents, trisamides can exhibit thermotropic behavior and form mesophases.[24–27] In the solid

www.MaterialsViews.com
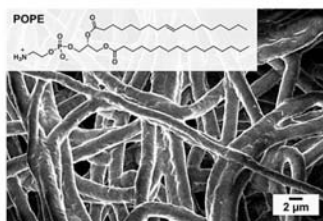
Figure 1. Chemical structure of POPE and an SEM image taken from fibers obtained from melt electrospinning at a spinning temperature of 210 °C, an applied voltage of ~40 kV, a distance from needle tip to ground plate of 6 cm, a flow rate of 200 μL·h⁻¹, and an inner needle capillary diameter of 0.6 mm. The diameter and distribution of the fibers were determined to be $1.8 \pm 0.2\ \mu m$.

state, as well as in dilute non-polar solutions, these organic molecules self-assemble into one-dimensional nanosized rod-like structures stabilized by three hydrogen bonds.[28,29] Along a single columnar structure, a strong macrodipole is formed due to the amide groups pointing in the same direction.[30,31] This macrodipole was used to align and manipulate supramolecular fibers with an electric field.[32]

Encouraged by our initial melt electrospinning results and to systematically establish structure–property relationships with respect to spinnability and fiber morphology, melt electrospinning experiments were conducted on several classes of small molecules. The molecules had molecular weights between 300 and 1 200 g·mol⁻¹. In these different classes, the intermolecular interaction potential was systematically varied by changing type, number, and strength of the secondary interactions, as well as the symmetry of the molecules. In particular, the influence of structural details of the small molecules, such as (i) size and flexibility of substituents, (ii) amide connectivity to the core, (iii) alicyclic or benzene as core structure, and (iv) the amount of hydrogen bonds, was investigated. The number of hydrogen bonds was purposely decreased from three in the class of trisamides to two in bisamide and sorbitol derivatives, then to zero in perylene bisimides and tertiary trisamides. Thus, series of compounds based on 1,3,5-benzene- and 1,3,5-cyclohexanetrisamides, 1,4-bisamides with benzene, naphtyl and cyclohexane cores, sorbitol derivatives, and molecules with an extended π-conjugated core, such as perylene bisimides, and finally tertiary 1,3,5-benzenetrisamides, incapable of any hydrogen bonds, were subjected to melt electrospinning experiments. However, it is not the

objective here to vary all possible electrospinning parameters until fiber formation might occur. Therefore, we kept all spinning parameters constant except the spinning temperature, which is the most critical parameter for small molecules. Solution electrospinning of trisamides is not a topic of this contribution.

2. Experimental Section

2.1. Materials

Starting materials and solvents purchased from ABCR, Acros Organics, and Sigma–Aldrich were purified and dried according to standard procedures. All table and figure numbers with the prefix S and compound numbers specified with (S) refer to the Supporting Information (ESI) available online. The ESI contains comprehensive information for all compounds regarding their chemical structure, molecular weight, phase transition and spinning temperatures, and dynamic thermal weight loss temperatures.

The synthesis of most trisamides used in this study has been previously published. 1,3,5-Benzenetrisamides (**1**(S) to **6**(S)), and 1,3,5-cyclohexanetrisamides (**11–14**) were synthesized according to the literature procedures.[26,33] All other as yet unreported trisamides presented in this article were synthesized according to known literature methods.[27,26,34,35] Full synthetic procedures and analytical data are included in the ESI. Bisamides based on benzene (**16** and **17**) were synthesized according to procedures described elsewhere.[36] Bisamides based on naphtyl (**18**(S)) and cyclohexane core (**19–22**(S)) were synthesized from the amine with the corresponding acid chloride in N-methylpyrrolidone (NMP) as solvent, pyridine as base and lithium chloride to break hydrogen-bonding interactions. The synthesis and characterization of all bisamides can be found in the ESI. The sorbitol derivatives 1,3:2,4-dibenzylidenesorbitol (**23**, DBS, Millad® 3905, Milliken Chemical or Irgaclear® D, Ciba Specialty Chemicals), 1,3:2,4-bis(3,4-dimethyldibenzylidene) sorbitol (**24**(S), DMDBS, Millad® 3988) and 1,2,3-trideoxy-4,6:5,7-bis-O-[(4-propylphenyl) methylene]nonitol (**25**, Millad® NX® 8000) are available from Milliken Chemical. Perylene bisimide **26** was purchased from Aldrich, compounds **27** and **28** were obtained according to literature procedures.[37] POPE was purchased from Sigma–Aldrich.

2.2. Characterization

¹H NMR spectra were recorded on a Bruker Avance 300 spectrometer (300 MHz). Chemical shifts are reported in ppm at room temperature (rt). Mass spectroscopic data were obtained from a FINNIGAN MAT 8500 instrument. Phase transition and melting temperatures were determined with a Perkin Elmer Diamond DSC (heating rate: 10 K·min⁻¹, nitrogen flow: 20 mL·min⁻¹). Reported are data obtained from the second heating curves. Often the term *optical* isotropic melt is used in this work, owing to the observation that even in the melt of trisamides above the isotropic transition recorded by the DSC, shorter aggregates are still present, which was reported by Timme et al.[26] The temperature at 10% weight loss ($T_{-10\%}$) was determined in a Mettler SDTA 851 TGA at 10 K·min⁻¹ (nitrogen flow: 60 mL·min⁻¹) and is included in ESI Table S1–S7.

The material collected on the SEM stub during electrospinning was sputtered with 2.0 nm platinum in a Cressington 208HR sputter coater and analyzed by SEM Zeiss LEO 1530 FESEM (Zeiss, Jena, Germany) at 2.0–3.0 keV. The fiber and sphere diameter distributions were calculated from at least 100 individual fibers or spheres (amount n denoted in the histograms) by evaluating at least three different SEM images taken at different positions within one stub. For structures up to 5 μm, SEM images at a magnification of 2 500 were used; above 5 μm a magnification of 1 000 was chosen. In the main text, SEM images are depicted with a magnification of 2 500; additionally the ESI contains SEM images with a magnification of 1 000. The evaluation software AxioVision LE (Carl Zeiss AG, Germany) was used. In case of the sphere diameters, only single spheres were taken into account without considering elongated objects. The histograms were generated using the software OriginPro 8 G from Origin-Lab; reported are the mean value and the standard deviation. Two histograms shown in Figure 2 as an example and for all other compounds the fiber/sphere diameter histograms can be found in the ESI (Table S1–S7).

2.3. Melt Electrospinning

2.3.1. Spinning Setup

For the melt electrospinning experiments, a custom-designed apparatus was used (see Scheme 1) similar to the one described before.[22] The substances were filled as powder into a 1 mL Fortuna-Optima syringe with luer glass tip (Poulten & Graf). Mounted to this tip with a high temperature adhesive was a hypodermic 20 G (inner diameter: 0.6 mm) metal needle shortened to 1 mm. This assembly was placed in an electrically heated block. The temperature was regulated by an electronic controller up to 400 °C. Compared to the previous setup,[22] two additional cartridge heaters were placed next to the syringe to reduce the temperature loss toward the needle tip. The actual temperature at the tip is about 2% lower than the temperature of the block; the latter is denoted as spinning temperature (T_{sp}). A precision motor and gear system equipped with a force transducer moved the syringe plunger. By adjusting the plunger speed in combination with a 1 mL syringe, the feeding rates ($\dot{V}_{flow}$) can be varied from 20 to 1 500 μL · h^{-1}, in this paper a rate of 200 μL · h^{-1} was set for all experiments. The needle, syringe, and all attached electronic components were grounded. The collector plate below the needle was connected either to +60 or −60 kV power supplies (Schulz Electronic, high voltage units AK0175 and AK1026). In this study, the distance D between needle tip and collector plate was set to 6 cm. In most studies of

solution or melt electro spinning of polymers, the electric field is directed from the needle tip to collector and positive charges are induced into the fluid.[4,6] Since the voltage is applied to the collector in our setup, a negative voltage was chosen to maintain the electric field direction, namely from tip to collector. Unless specified otherwise, the voltage U at the collector was set to −40 kV, resulting in a field strength E of 6.7 kV · cm^{-1}.

Before each electrospinning experiment, the melt in the syringe was equilibrated for at least 3 min at T_{sp} and $\dot{V}_{flow} = 200$ μL · h^{-1}. Then the voltage was turned on and the electrospun material was collected directly on a 12 mm SEM stub (Plano GmbH) covered with a self-adhesive carbon conducting tape. Even with an optimized spinning setup and the experience gained by many spinning experiments, melt electrospinning of highly fluid materials—particularly at temperatures above 300 °C—remains an exper-

$$2: M = 459.7 \text{ g·mol}^{-1}$$
$$\text{Cr } 72 \text{ Col}_{hp} \text{ } 172 \text{ Col}_{ho} \text{ } 218 \text{ I}$$
$$T_{-10\%} = 382 °C$$
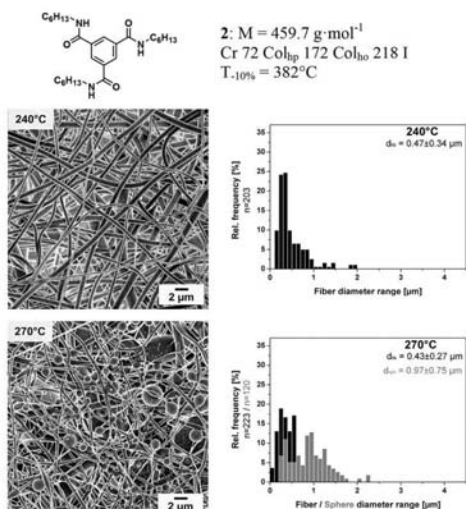
Figure 2. Trisamid **2** was electrospun at 240 and 270 °C from the isotropic melt. With increasing temperature, increasing formation of beaded fibers and spheres is observed. The transition temperatures of **2**, the temperature at 10% weight loss ($T_{-10\%}$), and the diameter distribution of the collected fibers are denoted. Histograms were evaluated from three different SEM images with a magnification of 2 500. (Cr: crystalline, Col: columnar mesophase, h: hexagonal, p: plastic crystalline, o: ordered liquid crystalline, I: isotropic. Spinning parameters: voltage $U = -40$ kV, distance from needle tip to ground plate $D = 6$ cm, flow rate $\dot{V}_{flow} = 200$ μL · h^{-1}; needle capillary ID, $d_{ID} = 0.6$ mm).

264

www.MaterialsViews.com
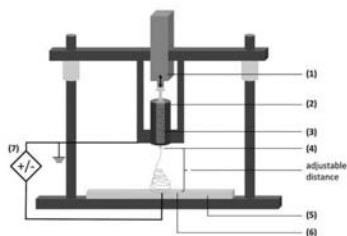
Scheme 1. Drawing of the melt electrospinning setup. (1) Drive unit: DC motor, gear, and force transducer; (2) heating unit: band heater and two cartridge heaters; (3) 1 mL glass syringe with plunger; (4) metal needle 20 G (ID: 0.6 mm); (5) base plate (Teflon®), (6) brass collector plate/HV electrode; (7) HV supply max. ± 60 kV.

imental challenge due to low fluid viscosity and, in some cases, increasing evaporation and decomposition.

2.3.2. Influence of the Spinning Temperature (T_{sp})

The investigation of the electrospun morphology as a function of T_{sp} is exemplarily presented for compound **2**, which is a trisamide based on trimesic acid with *n*-hexyl substituents (Figure 2). It exhibits a columnar hexagonal plastic (Col$_{hp}$) phase from 72 °C to 172 °C followed by a columnar hexagonal ordered (Col$_{ho}$) mesophase until 218 °C. Above this temperature an optical isotropic melt is formed.[26]

As observed before,[22] the high viscosity of columnar phases impedes melt electrospinning from these phases. Therefore, compound **2** was electrospun at higher temperatures (240, 270, and 300 °C) from the optical isotropic melt. The resulting electrospun morphologies and corresponding histograms are shown in Figure 2 and Table S1 (ESI). At a spinning temperature of 240 °C, i.e., 22 K above the transition into the optical isotropic phase, long and homogenous nanofibers (d_{fib} = 0.5 ± 0.3 μm) were obtained. At 270 °C, a mixture of spheres (d_{sph} = 1.0 ± 0.8 μm), beaded fibers, and fibers (d_{fib} = 0.4 ± 0.3 μm) was obtained. The histograms, presented in Figure 2, show the relative frequency of the fiber and sphere diameter distribution with *n* denoting the amount of counted species. At an even higher temperature of 300 °C, the amount of spheres increases and the formation of fibers is suppressed (Table S1). The presence of fibers from the melt is feasible since the optical isotropic phase still consists of short columnar preaggregates which are strong enough to interact with the applied electric field.[22,26]

This experiment shows that T_{sp} has a direct influence on the morphology. However, for each individual compound, the selected T_{sp} depends on the transition into the isotropic state and decomposition onset. In the following experiments, T_{sp} was set around 20 K above the isotropic transition temperature, identical with the temperature at DSC peak maximum temperature. This was done to ensure a fully isotropic melt, with the compromise that decomposition progressed at even higher spinning temperatures, in particular above 300 °C. Exceptions are noted in the text.

2.3.3. Influence of the Electric Field

First, the influence of the electric field direction on the fiber morphology was investigated by applying positive and negative voltages using compound **2**. In our setup, a positive net charge density at the emerging melt droplet is achieved by applying a negative voltage at the collector plate; hence the field direction is the same as in standard electrospinning experiments. When a positive voltage is applied, the melt is negatively charged before being accelerated toward the collector.

A breakdown of the electric field was observed after applying a voltage of +40 kV at a distance of D = 6 cm (E = 6.7 kV · cm^{-1}); thus this is considered the maximum field strength. Therefore, a lower voltage of +35 kV (E = 5.8 kV · cm^{-1}) was applied to achieve fiber formation. Fibers with a diameter of 0.9 ± 0.5 μm were obtained by melt electrospinning from the isotropic phase (250 °C) with a voltage of +35 kV; sporadic bead formation also occurred (Figure 3 left). When applying a negative voltage, no spinning process was observed at voltages below −30 kV (E = 5.0 kV · cm^{-1}). In Figure 3, right image, electrospun nanofibers (d_{fib} = 0.5 ± 0.2 μm) of **2** are depicted using a voltage of −40 kV (E = 6.7 kV · cm^{-1}).

In summary, lower electric field strength is necessary to collect fibers when positive voltage is applied. At negative voltages, meaning a positively charged melt, thinner and more uniform fibers were obtained and the melt electrospinning process was more homogeneous.
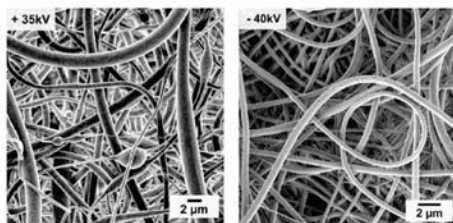
Figure 3. SEM images of the melt electrospun fibers obtained from compound **2** at T_{sp} = 250 °C for similar field strengths, but with reversed field direction. Left: at a positive voltage of +35 kV (E = 5.8 kV · cm^{-1}) the field direction is from ground plate to needle tip: d_{fib} = 0.9 ± 0.5 μm. Higher voltages resulted in electric breakdowns. Right: a negative voltage of −40 kV (E = 6.7 kV · cm^{-1}) is applied, the field direction is reversed and now from needle tip to collector,: d_{fib} = 0.5 ± 0.2 μm. (Spinning parameters: T_{sp} = 250 °C, D = 6 cm, V_{flow} = 200 μL · h^{-1}, d_{ID} = 0.6 mm).

Materials Views
www.MaterialsViews.com

Macromol. Mater. Eng. **2015**, 300, 259–276
© 2015 WILEY-VCH Verlag GmbH & Co. KGaA, Weinheim

Macromolecular
Journals

265

Furthermore, the influence of the electric field strength E on the morphology was investigated by applying a negative voltage. Exemplarily, compound **14**, a trisamide based on cyclohexane-cis-cis-1,3,5-carboxylic acid with branched side chains was chosen (Figure 4). It exhibits a columnar hexagonal ordered (Col_{ho}) phase from 121 °C to 338 °C. For the experiment T_{sp} was kept at 345 °C. This temperature is just 7 K above the isotropic transition, but at higher temperatures electrospinning of **14** was impeded by evaporation and decomposition. The distance between the needle tip and the ground plate was kept at 6 cm and U was varied from −25, −30, −40, to −45 kV (Figure 4).

At a voltage of −25 kV ($E = 4.2$ kV · cm^{-1}), fibers with a broad size distribution of 0.9 ± 0.5 µm, beaded fibers, and spheres of several micrometers were collected. With a higher electric field of 5.0

kV · cm^{-1} (−30 kV), the electrospinning process also resulted in a heterogeneous mixture of fibers, beaded fibers, and spheres. At a voltage of −40 kV (6.7 kV · cm^{-1}) mostly fibers were observed. Then, with a very strong electric field of 7.5 kV cm^{-1} (−45 kV), solely long and homogeneous fibers ($d_{fib} = 1.6 \pm 0.2$ µm) were collected.

Spheres and beaded fibers were mainly observed at applied voltages of −25 and −30 kV, whereas at higher voltages only fibers were observed. This example shows that a higher electric field strength increases the net charge density on the surface of the melt droplet and thus facilitates the formation of long and homogenous fibers and in turn prevents the formation of spheres.[10]

Since a voltage of −40 kV at a distance of 6 cm ($E = 6.7$ kV · cm^{-1}) is optimal for the fabrication of long and homogenous fibers from compounds **2** (Figure 3) and **14** (Figure 4) and avoids the breakdowns more often observed at −45 kV, the electric field was set to $E = 6.7$ kV · cm^{-1} ($U = -40$ kV, $D = 6$ cm) for all subsequent experiments.

Hence, in this work the optimal melt electrospining parameters were set to a voltage $U = -40$ kV (needle grounded), the distance from needle tip to ground plate at $D = 6$ cm, a flow rate of $\dot{V}_{flow} = 200$ µL · h^{-1} and a needle capillary ID, $d_{ID} = 0.6$ mm).

2.3.4. Taylor Cone Formation

The electrospinning process of small molecules was studied further using a high speed camera to gain more details about Taylor cone formation, the accelerated melt, and instabilities occurring within the fluid jet. The formation of the Taylor cone (Figure 5) and the acceleration of the fluid jet in the electric field (Figure 5, right image) were tracked using compound **2** at 250 °C again. Imaging of the emerging jet at the capillary was performed with an Optronis CR5000 × 2 High Speed Camera (Optronis, Germany) with a Navitar 1−60135 6.5× Zoom Objective (Navitar, USA) from the outside of the electrospinning apparatus.[38] For illumination, a Jansjö LED lamp (IKEA, Germany) was used, image acquisition was controlled by Optronis CamControl V5.0 software.

The jet shows a straight path before it starts to move rapidly in lateral directions; instabilities occur and lead to unstable motions which are critical for the creation of fibers during electrospinning. A spherical fluid drop emerges from the capillary die (Figure 5, 0 ms) and is electrically charged in the electric field. The interaction of the charged fluid with the electric field results in a cone-like deformation of the drop shape, and with increasing electric field the drop is elongated (1.05−2.15 ms). For 2.15 ms the half-angle of the cone is 34°. The applied electric field overcomes the surface tension of the drop when the half-angle of the cone reaches 30° and a jet is ejected toward

14: M=643.0 g/mol
Cr 121 Col_{ho} 338 I
T_{sp}= 345 °C
$T_{10\%}$= 378 °C

R=

- 25kV

d_{fib} =0.8±0.5 µm; d_{sph} = 4.4±2.3 µm

- 30kV

d_{fib}= 0.6±0.4 µm; d_{sph} = 2.8±2.1 µm

- 40kV

d_{fib} = 1.6±0.9 µm

- 45kV

d_{fib} = 1.6±0.7 µm

Figure 4. SEM images of fibers of **14** melt electrospun as a function of the applied voltage of −25, −30, −40, to −45 kV and thus electric field strength E [kV · cm^{-1}] of 4.2, 5.0, 6.7, and 7.5, respectively. (Field direction from needle tip to ground plate. Spinning parameters: T_{sp}= 345 °C, D = 6 cm, V_{flow} = 200µL · h^{-1}, d_{ID} = 0.6 mm).

266

Macromolecular
Journals

Macromol. Mater. Eng. **2015**, 300, 259–276
© 2015 WILEY-VCH Verlag GmbH & Co. KGaA, Weinheim

Materials
Views

www.MaterialsViews.com

Figure 5. Images taken from a high-speed video of the formation of the Taylor cone (left with elapsed time) and the acceleration of the jet in the electric field (right) are shown for compound **2**. Images were taken with a frame rate of 20 000 frames · s⁻¹ (left with elapsed time) and 10 000 frames · s⁻¹ (right), respectively. Scale bars reflect 1mm. (Spinning parameters: $U = -30$ kV, $T_{sp} = 250\,°C$, $D = 6$ cm, $V_{flow} = 200\mu L \cdot h^{-1}$, $d_{ID} = 0.6$ mm).

the collector (images at 2.35° and 2.50 ms). The images reveal that a stable jet is generated by melt electrospinning of **2** and intermolecular forces are sufficient to prevent breakup of the fluid jet into droplets.

For polymer solutions and melts, the formation of the Taylor cone has been studied in detail. At a critical point, the conical shape exhibits a characteristic half-angle of the cone in the range of 30° and above before a jet is ejected.[39] As pointed out by Shin et al. for any given fluid, and also for simple molecules such as glycerol, the electric field and flow rate (operating conditions) affect the shape of the jet. As the electric field is increased, the jet thins more rapidly and the cone region becomes shorter and more concave in profile.[40]

3. Results and Discussion

To ensure comparability of the morphologies, the electro-spinning parameters, such as electric field strength and direction, flow rate, and capillary diameter, were kept constant for all experiments. As the main parameter, the spinning temperature (T_{sp}) was adjusted for each compound with respect to its melting point or transition into the optical isotropic phase. To keep this article to a reasonable length, substances with an S following the compound number—for instance, **1**(S)—are discussed only briefly in this main text, but detailed information can be found in the ESI. Moreover, the ESI contains comprehensive information for all compounds regarding their chemical structure, molecular weight, phase transition and spinning temperatures, thermal degradation, and additional SEM

images at a lower magnification of 1 000, complemented with fiber and sphere histograms.

3.1. Benzenetrisamides

Benzenetrisamides are versatile molecules in supramolecular chemistry and are becoming more and more important in several scientific areas. Recently this class of supramolecular building blocks was reviewed by Palmans et al.[29] 1,3,5-Benzenetrisamides are accessible with a few synthetic steps and their structure can be tailored for a broad range of applications including nanotechnology, polymer additives, and biomaterials. Benzenetrisamides can be applied, for example, as nucleating agents for poly (vinylidene fluoride),[41] poly(butylene terephthalate) (PBT),[42] poly(ethylene-co-propylene),[43] polylactides,[44] and isotactic poly(propylene) (i-PP).[34,35,45,46] In some cases trisamides are also efficient clarifiers.[35,45] Furthermore, they can control the cell nucleation and foam morphology during foaming of injection molded i-PP,[47] and additionally are known as additives to improve the electret performance of i-PP.[48] They also have been applied as metal complexation reagents,[49] as organogelators,[50] hydrogelators,[51] and as supramolecular nanofibers in non-woven scaffolds for filter media.[52]

In the following, several benzenetrisamides were selected to study their melt electrospinning behavior and establish structure–morphology relations. The first series encompasses 1,3,5-benzenetrisamides with linear alkyl substituents and branched alkyl substituents. In a second

Materials
Views
www.MaterialsViews.com

Macromol. Mater. Eng. **2015,** *300,* 259–276
© 2015 WILEY-VCH Verlag GmbH & Co. KGaA, Weinheim

Macromolecular
Journals

267

series, the influence of the connectivity of the amide bond to the benzene core was studied while keeping the substituents unchanged.

3.1.1. Benzenetricarboxamides with Linear and Branched Substituents

The trisamides **1**(S) to **6**(S) are based on trimesic acid (benzene-1,3,5-tricarboxylic acid) and thus referred to as C-centered trisamides. Compound **1**(S) features a propyl substituent, **2** and **3** *n*-hexyl and *n*-octyl chains, respectively. Trisamides **4**(S), **5**, and **6**(S) are substituted with branched alkyl chains of various lengths up to seven C-atoms, as shown in Figure 6 and Table S1.

Electrospinning of **1**(S) has been discussed briefly before.[23] Due to the progressing evaporation of **1**(S) at temperatures above 290 °C, the spinning temperature (T_{sp}) was set at 290 °C, only 1 K above the melting transition of 289 °C, and uniform nanofibers ($d_{fib} = 0.5 \pm 0.2 \,\mu m$) were obtained as depicted in Table S1 (ESI). As described in detail in the Experimental section and there in Figure 2 and 3, trisamide **2** with hexyl substituents was used to study the influence of T_{sp}. As shown in Figure 2, at a spinning temperature of 240 °C uniform nanofibers with $d_{fib} = 0.5 \pm 0.3$ were obtained. Also the influence of the electric field direction and the formation of the Taylor cone were investigated using this trisamide as depicted in Figure 3 and 5, respectively.

Trisamide **3** exhibits a columnar hexagonal ordered phase with a transition to the optical isotropic phase at 207 °C.[26] From the isotropic phase, **3** was melt electrospun at $T_{sp} = 230$ °C into long, uniform fibers with a narrow diameter distribution of $d_{fib} = 1.0 \pm 0.3 \,\mu m$. The surface of the fibers is slightly structured and the fibers adhere together, indicating that incompletely solidified fibers reached the collector during the fast electrospinning process.

In the following, the melt electrospinning of trisamides **5** and **6**(S) with branched substituents will be discussed as to whether this structural feature has any impact. Compound **4**(S) with a 3-methyl-butyl group exhibits a plastic crystalline phase from 211 to 272 °C.[26] From the isotropic melt at $T_{sp} = 300$ °C, thin fibers were obtained ($d_{fib} = 0.7 \pm 0.4 \,\mu m$). Besides fibers, many spheres with a diameter of $d_{sph} = 2.1 \pm 0.8 \,\mu m$ were observed, which was not the case for linear substituted analogs **2** and **3** under comparable conditions. Substituted with a 5-methyl-hexyl group trisamide **5** forms a columnar hexagonal plastic (Col$_{hp}$) phase at rt, followed at higher temperatures by a Col$_{ho}$ phase. The transition into the isotropic phase is at 291 °C. Electrospinning of **5** at 310 °C resulted in a mixture of fibers, spheres, and some indication of beaded fibers. Fibers of **5** exhibit a size distribution of $d_{fib} = 0.8 \pm 0.5 \,\mu m$ and spheres a distribution of $d_{sph} = 2.4 \pm 1.0 \,\mu m$. Trisamide **6**(S) with 2-ethyl-hexyl substituents (Table S1) exhibits a very similar phase behavior as to **5**. Also the electrospinning results are very similar; fibers, spheres, and beaded fibers are formed in a comparable size range.

A comparison of 1,3,5-benzenetrisamides with linear and branched substituents reveals how very slight changes in the molecular structure govern morphology during melt electrospinning. With branched substituents more and more the formation of spheres and beaded fibers can be observed. The linear substituents induce the formation of uniform supramolecular nanofibers.

3: Cr 117 Col$_{ho}$ 207 I; T_{sp} = 230 °C;
d_{fib} = 1.0±0.3 μm

5: Col$_{hp}$ 204 Col$_{ho}$ 291 I; T_{sp} = 310 °C;
d_{fib} = 0.8±0.5 μm; d_{sph} = 2.4±1.0 μm
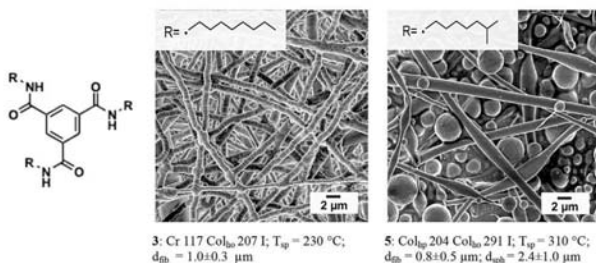
Figure 6. Chemical structures of 1,3,5-tricarboxamides **3** and **5**, based on trimesic acid with linear and branched substituents. Phase transitions, melt electrospinning temperatures (T_{sp}), and fiber/sphere diameters (d_{fib}/d_{sph}) are listed. A representative fiber morphology obtained from the spinning experiment is depicted in the SEM images. (Cr: crystalline, Col: columnar mesophase, h: hexagonal, p: plastic crystalline, o: ordered liquid crystalline, I: isotropic. Spinning parameters: $U = -40$ kV, $D = 6$ cm, $\dot{V}_{flow} = 200\,\mu L \cdot h^{-1}$, $d_{ID} = 0.6$ mm).

3.1.2. Influence of the Connectivity of the Amide Linkage to the Benzene Core

The benzentrisamides discussed so far are based on trimesic acid and are thus C-centered. In this series, we systematically change the connectivity while keeping n-hexyl groups as the linear peripheral substituent. Compared to trisamide **2** with three C-centered amide bonds (Figure 2), one amide connectivity is reversed, resulting in trisamide **7** (based on 5-amino isophthalic acid), and in trisamide **8** (based on 3,5-diamino benzoic acid) two amide bonds are reversed. Finally, trisamide **9** is based on 1,3,5-triaminobenzene with three N-centered amide bonds. The chemical structures of **7–9** are shown in Figure 7. The melting temperature for all three compounds is around 180 °C and thus lower than the 218 °C of **2**. Compounds **7–9** do not exhibit LC phases.

For all three compounds, T_{sp} was set at 200 °C. With one N-centered amide bond (**7**), electrospun fibers exhibit larger diameters ($d_{fib} = 1.4 \pm 0.4$ μm), several fiber ends are visible. From **8**, with one C-centered and two N-centered amide bonds, fibers ($d_{fib} = 1.7 \pm 0.9$ μm), beaded fibers, and large spheres ($d_{sph} = 6.6 \pm 2.0$ μm) are obtained. The melt electrospinning of **9** resulted in a homogenous non-woven of nanofibers ($d_{fib} = 0.7 \pm 0.3$ μm) without any evidence of spheres or beaded fibers.

The strength of the macrodipoles formed by triple helical hydrogen bonds along the column axis can be considered as an explanation for the different morphologies observed depending on the connectivity. A theoretical investigation of 1,3,5-benzenetrisamides shows that macrodipoles are formed by all four isomers **2**, **7**, **8**, and **9**.[26] The strongest macrodipole is formed by C-centered trisamides, the lowest in N-centered representatives. Electrospinning of the sym-

metrical C-centered trisamide **2** and N-centered **9** results in very homogenous fibers. For trisamides **7** and **8**, with mixed amide connectivities, the formation of fibers, beaded fibers, and spheres is observed.

Hence, it can be concluded that the electrospinning results cannot be caused solely by different macrodipole strengths. Generally, a stable electrospinning jet results in the formation of fibers, whereas a disturbance of the jet during electrospinning can lead to a partial breakup of the accelerated melt and results in beads, beaded fibers, or a heterogeneous mixture of morphologies. Therefore, for trisamides **7** and **8** the electrospinning jet is not stabilized in the same way as for **2** and **9**. Reasons might be slower packing of the columns from the melt owing to mixed amide connectivity and the resulting asymmetry in **7** and **8**.

Trisamide **10**(S) is based on 1,3,5-triamino-2,4,6-trimethylbenzol and belongs to a class of ultra-efficient supramolecular nucleating agents for i-PP.[35] Its benzene core additionally features a triple methyl substitution (ESI, Table S2). The core substitution influences the supramolecular packing, resulting in higher transition temperatures.[34,27] Here, n-octyl substituents were chosen to lower the transition temperatures instead of n-hexyl ones. Trisamide **10**(S) was successfully electrospun at 375 °C into thin uniform fibers with a narrow size distribution of $d_{fib} = 1.0 \pm 0.3$ μm.

3.2. Cyclohexanetrisamides

Cyclohexanetrisamides are structurally similar to benzenetrisamides but their alicyclic core strongly affects their stacking behavior; consequently their phase transition

7: Cr 176 I;
T_{sp} = 200 °C;
d_{fib} = 1.4 ± 0.4μm

8: Cr 184 I;
T_{sp} = 200 °C;
d_{fib} = 1.7±0.9 μm; d_{sph} = 6.6±2.0 μm

9: Cr 183 I;
T_{sp} = 200 °C;
d_{fib} = 0.7±0.3 μm
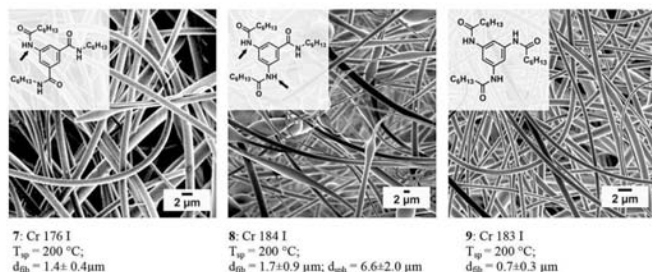
Figure 7. The amide connectivity to the benzene core is systematically changed in trisamides **7** to **9**. The arrows indicate the position of the changed connectivity; in **9** all three substituents are N-centered. The chemical structures and phase transition temperatures are listed, the spinning temperature was 200 °C. The morphology of the melt electrospun materials is shown in the SEM images and complemented with the corresponding fiber/sphere diameters d_{fib}/d_{sph}. (Cr: crystalline, I: isotropic. Spinning parameters: $U = -40$ kV, $D = 6$ cm, $V_{flow} = 200$ μL · h^{-1}, $d_{iD} = 0.6$ mm).

Materials
Views
www.MaterialsViews.com

Macromol. Mater. Eng. **2015**, 300, 259–276
© 2015 WILEY-VCH Verlag GmbH & Co. KGaA, Weinheim

Macromolecular
Journals

269

temperatures are generally higher.[24,26] For 1,3,5-cyclo-hexanetrisamides substituted with n-hexyl and longer alkyl chains, columnar rectangular plastic (Col_{rp}) meso-phases and columnar nematic (N_c) phases have been observed[26]; they form columnar aggregates with much higher dipole moments than similar benzene trisamides.[31] Using conventional melt fiber spinning equipment, Japa-nese researchers succeeded in fabricating thick fibers with diameters in the range of 100–300 μm from a 1,3,5-cyclohexanetrisamide derivative.[53] Their self-assembly behavior distinguishes cyclohexanetrisamides as efficient gelators for organic solvents and water.[26,54]

In our preliminary work, the electrospinnability of cyclohexanetrisamide **13**(S), with three n-decyl substitu-ents (ESI, Table S3), was demonstrated. Starting at a $T_{sp} = 300\,°C$ in its N_c phase, fibers were obtained with diameters of $d_{fib} = 2.8 \pm 0.8\,μm$. Electrospinning in its isotropic phase at 330 °C led to thinner fibers with $d_{fib} = 2.0 \pm 0.6\,μm$.[22]

In this work, the melt electrospinnability of 1,3,5-cyclohexanetrisamides from the N_c and isotropic phases was verified by spinning five trisamides with different connectivities and alkyl substituent lengths. Compound **11**(S) (Table S3), with n-heptyl substituents, forms a columnar rectangular plastic (Col_{rp}) phase between 218 and 290 °C, followed by an N_c phase up to 319 °C. At $T_{sp} = 310\,°C$, and thus in the N_c phase, fibers with $d_{fib} = 2.8 \pm 0.8\,μm$ were observed, whereas in the isotropic phase at a spinning temperature of 340 °C, long and homogenous fibers ($d_{fib} = 1.9 \pm 0.6\,μm$) were collected; hence fibers from the N_c phase are slightly thicker. Trisamide **12** (Figure 8), with n-octyl substituents,

exhibits a broad Col_{rp} phase from 189 to 276 °C and an N_c phase up to 320 °C. For trisamide **12**, melt electrospun fibers in the micrometer range ($d_{fib} = 2.3 \pm 1.2\,μm$) were collected from the N_c phase at $T_{sp} = 300\,°C$, and from the isotropic phase at $T_{sp} = 340\,°C$, fibers in the same thick-ness range ($d_{fib} = 2.6 \pm 1.2\,μm$) were obtained.

In addition, a cyclohexanetrisamide with branched substituents (**14**) was investigated by melt electrospinning, as shown already in Figure 4 in the Experimental section. This trisamide possesses a columnar hexagonal ordered (Col_{ho}) phase but no N_c phase. As shown in Figure 4 for −40 kV, at $T_{sp} = 345\,°C$ in the isotropic phase, a mixture of fibers ($d_{fib} = 1.6 \pm 0.9\,μm$) and spheres ($d_{sph} = 2.6 \pm 1.7\,μm$) was obtained. Similar to trisamides based on a benzene core, melt electrospinning of cyclohexane with branched substituents results in a mixture of fibers and spheres, indicating distorted column packing. It seems conclusive that steric effects are the reason for slower packing of the resulting columns during the fast cooling of the melt, causing a more unstable electrospinning jet and an increase in the amount of beads.

To study the influence of the amide connectivity, cyclohexanetrisamide **15** (Figure 8) with three N-centered amide bonds was synthesized. Trisamide **15** is based on 1,3,5-cyclohexanetriamine with n-octyl substituents. It possesses a melting point of 272 °C without an LC phase and thus shows a simpler thermal behavior than C-centered cyclohexanetrisamides. Trisamide **15** was melt electrospun at 285 °C into fibers with a size distribution of $d_{fib} = 1.2 \pm 0.5\,μm$. Compared to **12** with C-centered amide bonds electrospun from the isotropic phase, **15** forms thinner fibers.

12: Cr_1 43 Cr_2 189 Col_{rp} 276 N_c 320 I;
$T_{sp} = 300\,°C$ nematic phase
$d_{fib} = 2.3 \pm 1.2\,μm$

12
$T_{sp} = 340\,°C$, isotropic phase
$d_{fib} = 2.6 \pm 1.2\,μm$

15: Cr 272 I
$T_{sp} = 285\,°C$
$d_{fib} = 1.2 \pm 0.5\,μm$
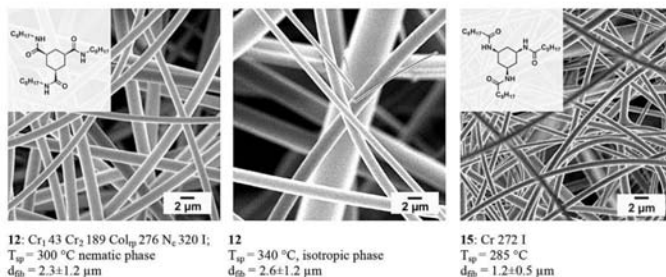
Figure 8. Chemical structures of 1,3,5-cis,cis-cyclohexanetrisamides **12** and **15** with n-octyl substituents, their phase transition, and spinning temperatures (T_{sp}). Note that for trisamide **15** the connectivity of the amide bonding is all N-centered. SEM images of melt electrospun fibers are shown. (Cr: crystalline, Col: columnar mesophase, h: hexagonal, r: rectangular, p: plastic crystalline, o: ordered liquid crystalline, N_c: columnar nematic, I: isotropic. Spinning parameters: $U = -40$ kV, $D = 6$ cm, $\dot{V}_{flow} = 200\,μL \cdot h^{-1}$, $d_{ID} = 0.6$ mm).

270

Macromolecular
Journals

Macromol. Mater. Eng. **2015**, *300*, 259–276
© 2015 WILEY-VCH Verlag GmbH & Co. KGaA, Weinheim

Materials
Views

www.MaterialsViews.com

These experiments show that smooth and homogeneous fibers without any defects can be prepared from 1,3,5-cyclohexanetrisamides with linear substituents. The resulting fiber diameters are slightly thicker than those based on benzene cores. The connectivity has a minor impact on the fiber morphology but the spinning temperature is lower for N-centered compounds.

3.3. Bisamides Based on Aromatic and Cyclohexane Cores

In order to gain a better understanding of the influence of the amount of hydrogen bonds on the electrospun morphology, the number of amide hydrogen bonds was successively decreased and furthermore the amide connectivity changed. 1,4-Bisamides can function as nucleating agents, as charge storage modifiers for i-PP,[55] and as organogelators.[56] Bisamides are also known for self-assembling into two-dimensional nanosheets.[57]

In this section, bisamides based on different benzene, naphtyl, and cyclohexane cores were synthesized and electrospun. For cyclohexane systems cis- and $trans$-isomers were also considered. To achieve better comparability and lower melting points, again n-octyl groups were chosen as substituents. In addition, we also investigated monoamides based on phenylamine, benzoic acid, cyclohexaneamine, or cyclohexanecarboxylic acid with n-octyl substituents for melt electrospinning. However, under the applied electrospinning parameters, none of these monoamides led to fiber formation but rather undefined, unstructured morphologies and hence more detailed results and SEM images are omitted here.

3.3.1. Bisamides Based on Aromatic Cores

1,4-Bisamide **16**, referred to as being N-centered since it is based on 1,4-diaminobenzene, exhibits a melting point at 209 °C. By electrospinning at $T_{sp} = 230$ °C mainly beaded fibers were obtained, along with spheres and very few fibers (Figure 9). Also, the analogous C-centered bisamide based on terephthalic acid **17** (mp = 206 °C) was synthesized and spun at 225 °C. Electrospinning of **17** rendered solely spheres with a diameter distribu-

tion of $2.4 \pm 1.0\,\mu m$. To study the influence of a larger aromatic system, bisamide **18**(S) (Table S4, mp = 232 °C), based on naphthalene-2,6-dicarboxylic acid, was synthesized and electrospun at 260 °C. Only spheres ($d_{sph} = 2.7 \pm 0.8\,\mu m$) were observed.

These electrospinning experiments show that the secondary interactions formed in benzene bisamides are considered too weak to form a stable jet within the electric field, and electrospraying occurs due to the breakup of the jet. The larger naphtyl core in **18**(S) cannot induce fiber formation for aromatic bisamides either.

3.3.2. Bisamides Based on Cyclohexane Cores

To study the influence of the cyclohexyl core, bisamide **19** (mp = 271 °C), based on $trans$-cyclohexane-1,4-diamine, as

16: Cr 209 I; $T_{sp} = 230$ °C
$d_{fib} = 0.6 \pm 0.3\,\mu m$; $d_{sph} = 3.4 \pm 2.1\,\mu m$

17: Cr$_1$ 79 Cr$_2$ 115 Cr$_3$ 190 Cr$_4$ 206 I
$T_{sp} = 225$ °C; $d_{sph} = 2.4 \pm 1.0\,\mu m$

19: Cr 271 I; $T_{sp} = 290$ °C
$d_{fib} = 1.4 \pm 1.2\,\mu m$; $d_{sph} = 2.9 \pm 1.6\,\mu m$

20: Cr 85 I; $T_{sp} = 110$ °C
$d_{fib} = 2.0 \pm 0.6\,\mu m$
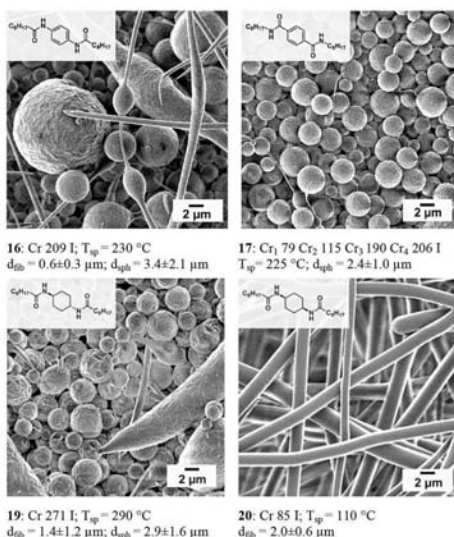
Figure 9. 1,4-Bisamides based on benzene (**16** and **17**) and cyclohexane (**19** and **20**) were investigated by melt electrospinning. Their phase transition, spinning temperatures (T_{sp}), and diameters are listed. The melt electrospun morphologies are shown in the SEM images. Only for **20** was a fibrous morphology observed. (Cr: crystalline, I: isotropic. Spinning parameters: $U = \sim 40$ kV, $D = 6$ cm, $V_{flow} = 200\,\mu L \cdot h^{-1}$, $d_{iD} = 0.6$ mm).

well as the *cis*-isomer **20** (mp = 85 °C) were synthesized (Figure 9). Electrospinning of **19** at 290 °C resulted in a mixture of spheres and fiber fragments. However, the *cis*-isomer **20** can be melt electrospun at 110 °C into homogenous, long fibers with a diameter distribution of $2.0 \pm 0.6 \, \mu m$ (Figure 9). Next, the amide connectivity was reversed from N-centered to C-centered by investigating compounds based on cyclohexane-1,4-dicarboxylic acid. *Trans*-bisamide **21**(S) (mp = 255 °C) and *cis*-isomer **22**(S) (mp = 70 °C) (Table S4) were chosen for spinning experiments. From **21**(S), at $T_{sp} = 275$ °C, spheres with a diameter distribution of $2.3 \pm 1.0 \, \mu m$ were collected, whereas from *cis*-1,4-bisamide **22**(S) at $T_{sp} = 100$ °C, a vitrified, featureless glass was obtained (ESI, Table S4).

For cyclohexane-based compounds **19** and **21**(S) with their melting points above 250 °C, a fiber spinning process resulted in a mixture of beads and fiber fragments, indicating a heterogeneous electrospinning process. Surprisingly and for reasons yet unknown, homogeneous microfibers could only be collected for the N-centered 1,4-*cis*-bisamide **20** (mp = 85 °C). A clear influence of the *trans*- or *cis*-configuration on the melting points and electrospun morphologies of the cyclohexane-based compounds is observed.

3.4. Sorbitol Derivatives

Sorbitol derivatives are butterly-shaped compounds composed of a hydrophilic sorbitol moiety with two hydrophobic phenyl wings which are often additionally substituted. Their self-assembly behavior into fibrillar structures is based on intermolecular hydrogen bonds

between acetal oxygens and protons of the terminal hydroxyl groups.[58] Sorbitols serve as efficient nucleation and clarifying agents for *i*-PP. In polymer melts, they self-assemble upon cooling into fine fibrils and induce nucleation.[59] In solvents they can act as organogelators, where the physical gelation is promoted by the formation of a three-dimensional network.[58,60,61]

For melt electrospinning experiments we selected derivatives such as dibenzylidene sorbitol, (DBS, **23**), 3,4-dimethyl-dibenzylidene sorbitol (DMDBS, **24**(S)), and a nonitol derivative **25**. DBS (**23**) exhibits a melting point at 225 °C. By introducing two methyl substituents at each aromatic ring in 3,4-position, the melting point is increased to 275 °C for **24**(S). Nonitol derivative **25**, a recently commercialized clarifier for *i*-PP, features one propyl substituent at each aromatic ring and one at the core and melts at 245 °C.[58,59]

By electrospinning DBS (**23**) at 245 °C, a mixture of fibers and spheres was collected (Figure 10). The very few visible fibers are often connected to spheres and exhibit a diameter range of $0.7 \pm 0.3 \, \mu m$. For nonitol derivative **25**, the spinning temperature was first selected 20 K above the melting point with $T_{sp} = 265$ °C. Electrospraying occurred and solely spheres in the 2–5 μm diameter range were observed (Figure 10, center). As shown for 1,3,5-benzene-trisamides (Figure 2), higher spinning temperatures typically lead to an increased formation of spheres. Thus, we conducted spinning experiments at 245 °C, to suppress sphere formation. However, also at this lower temperature larger spheres of **25** ($d_{sph} = 6.1 \pm 2.9 \, \mu m$) with a broad diameter distribution and dented surface reminiscent of blueberries were collected but no fibers were formed

23 (DBS): Cr 225 I; T_{sp} = 245 °C;
d_{fib} = 0.7±0.3 μm; d_{sph} = 7.0±3.0 μm

25: Cr 245 I; T_{sp} = 265 °C;
d_{sph} = 3.4±1.5 μm

25: T_{sp} = 245 °C;
d_{sph} = 6.1±2.9 μm
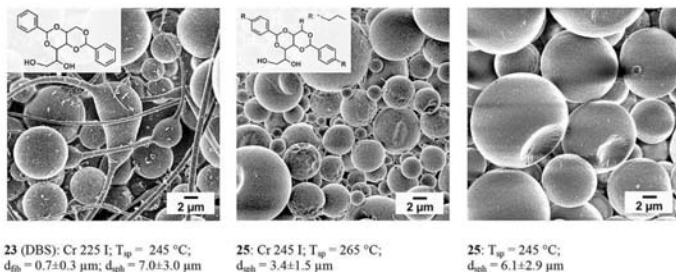
Figure 10. SEM images of melt electrospun morphologies of sorbitol **23** (DBS) and nonitol **25**. The chemical structures, their phase transition, and spinning temperatures (T_{sp}) are given. (Cr: crystalline, I: isotropic. Spinning parameters: $U = -40$ kV, $D = 6$ cm, $\dot{V}_{flow} = 200 \mu L \cdot h^{-1}$, $d_{ID} = 0.6$ mm).

(Figure 10, right). Electrospinning of DMDBS (**24**(S)) at 295 °C resulted also in spheres with a smooth surface and a diameter range of $3.9 \pm 2.3 \, \mu m$ (ESI, Table S5).

VanderHart et al. reported for sorbitol **23** the formation of weak and inhomogeneous hydrogen bonds upon rapid cooling from the melt.[62] This observation can provide an explanation for the formation of spheres during melt electrospinning. The formed hydrogen bonds are not strong enough to stabilize the fluid jet into fibers, the jet breaks up during electrospinning and the melt returns to its energetic favorable state as a droplet and thus electrospraying occurs.

3.5. Perylene Bisimide Derivatives

To shed further light on the role of interactions on the electrospinning behavior of small molecules into fibers, also molecules with extended π-conjugated structures were investigated. One prominent class are perylene bisimides which exhibit a strong self-assembling behavior and are, for example, applied as electron transporting material in functional devices.[63] Here π–π interactions act as intermolecular force and neither hydroxy nor amide hydrogen bonds are present.

Three perylene bisimides with different types of substituents, such as linear n-octyl alkyl chains **26**(S) (ESI, Table S6), a swallow tailed n-heptyl alkyl chains **27** (Figure 11), and substituted with polar swallow tailed oligo(ethylene glycol) substituents **28** were selected. Perylene bisimide **26**(S) is known as a high performance organic semiconductor and utilized in organic field-effect transistors.[64] It exhibits a liquid crystalline phase from 220 to 375 °C. Electrospinning of **26**(S) at $T_{sp} = 385$ °C led to very inhomogeneous fibers (ESI, Table S6) with a ribbon-like structure and some beads. At such high spinning temper-atures just slightly above the extreme isotropic transition temperature of 375 °C, substantial evaporation and degradation occurred. Consequently, a poor and non-uniform fiber quality was observed.

To lower the transition temperature and thus reach feasible spinning temperatures, perylene bisimides substituted with swallow tail substituents were selected.[37] Bisimide **27** (Figure 11) possesses a melting point of 163 °C and forms no LC phase. Long, thick, and very homogeneous fibers ($d_{fib} = 6.8 \pm 0.3 \, \mu m$) were obtained at a spinning temperature of 180 °C.

Perylene bisimide **28** with branched oligo(ethylene glycol) tails and shows an LC columnar hexagonal ordered phase from 64 to 123 °C, followed by the isotropic phase. This substance forms at $T_{sp} = 140$ °C homogeneous fibers ($d_{fib} = 3.2 \pm 1.2 \, \mu m$) lacking bead formation. Electrospinning at 185 °C, now 62 K above the isotropization, resulted solely in thick spheres ($d = 11.7 \pm 4.1 \, \mu m$, Figure 11), indicating that now the higher thermal energy suppresses fiber formation, similar to the previously discussed behavior for trisamides (Figure 2).

For the first time, it was demonstrated that electron transporting materials—namely perylene bisimides **27** and **28**—can be processed by melt electrospinning into fibers. The result demonstrates that fibers can be obtained not only from molecules with amide hydrogen bonds but also from those with strong π–π interactions. Melt electrospinning of perylene bisimides is an alternative solvent-free technique to shape organic semiconductors into fibers.

3.6. Tertiary Benzenetrisamides

Finally we investigated tertiary 1,3,5-benzenetrisamides. In this class of compounds all amide nitrogen atoms are fully

27: Cr 163 I; $T_{sp} = 180$ °C;
$d_{fib} = 6.8 \pm 3.0 \, \mu m$

28: Cr 64 Col$_{ho}$ 123 I; $T_{sp} = 140$ °C;
$d_{fib} = 3.4 \pm 1.2 \, \mu m$

28: $T_{sp} = 185$ °C;
$d_{sph} = 11.7 \pm 4.1 \, \mu m$
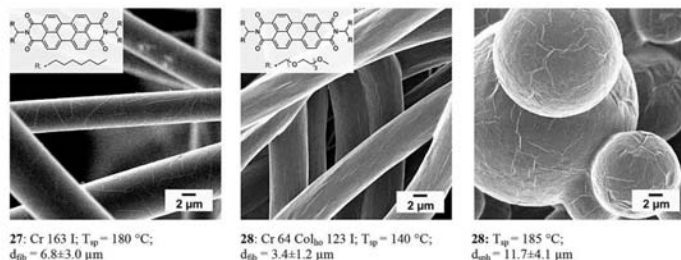
Figure 11. SEM images of melt electrospun morphologies of perylene bisimides **27** and **28**. The chemical structures, their phase transition, and spinning temperatures (T_{sp}) are given. (Cr: crystalline, Col: columnar mesophase, h: hexagonal, o: ordered, LC: liquid crystalline, I: isotropic. Spinning parameters: $U = -40$ kV, $D = 6$ cm, $V_{flow} = 200 \mu L \cdot h^{-1}$, $d_{ID} = 0.6$ mm).

substituted. Consequently, these molecules cannot form intermolecular interactions via amide hydrogen bonds.

Three benzenetrisamides (**29–31**) based on trimesic acid and reacted with cycloaliphatic and aliphatic secondary amines were synthesized. Trisamide **29** (Figure 12) is substituted with methyl and hexyl groups and only exhibits a glass transition at 65 °C. The stability of this glass was followed over three months by annealing experiments using DSC without any indication of crystallization.

As depicted in Figure 12, tertiary trisamide **29** electrospun at 140 °C forms thick, but very homogenous fibers with a narrow size distribution of 12.9 ± 1.3 µm. Compound **30**(S) with two cyclohexyl groups exhibits a melting temperature at 295 °C. At $T_{sp} = 305$ °C, a mixture of thinner fibers ($d_{fib} = 3.6 \pm 1.7$ µm) and large spheres ($d_{sph} = 12.3 \pm 8.2$ µm) was collected (ESI, Table S7). Compound **31** with one methyl and one tert-butyl substituent at each amide nitrogen melts at 220 °C. At a spinning temperature of 230 °C very different beaded fibers with fine, short structures several nanometers in length growing on the surface were obtained. Dynamic TGA measurements revealed a two-step weight loss around 228 and 310 °C. The unusual surface morphology of **31** as depicted in Figure 12 is caused most likely by vapor phase deposition on the fiber surface.

In summary, also fibers were unexpectedly collected from tertiary 1,3,5-benzene tricarboxamides investigated, regardless melt electrospinning was performed using a glassy or a crystalline compound. Since these compounds are not able to form amide hydrogen bonds similar to perylene bisimides, we conclude the presence of hydrogen bonds is not a prerequisite for fiber formation during melt electrospinning of small molecules.

4. Summary and Conclusion

In this feature article, we discuss morphologies such as fibers, beaded fibers, and spheres observed from melt electrospinning of small molecules. Another aspect of this research is the avoidance of the hazardous solvents commonly used for solution electrospinning.

In order to reveal structure–property relations with respect to spinnability and fiber morphology, we synthesized 30 substances with different molecular structures. In particular, the influence of structural details, such as size and flexibility of substituents, amide connectivity to the core, alicyclic or aromatic rings as core, and amount of hydrogen bonds, were explored. These structural features govern the intermolecular interaction potential of each substance. Classes of compounds based on 1,3,5-benzene- and 1,3,5-cyclohexanetrisamides, 1,4-bisamides, and tertiary 1,3,5-benzenetrisamides were investigated by melt electrospinning. Additionally, sorbitol derivatives forming hydroxyl hydrogen bonds, and molecules with an extended π-conjugated structure, such as perylene bisimides, were subjected to melt electrospinning experiments.

1,3,5-Benzene- and 1,3,5-cyclohexanetrisamides comprise three strong hydrogen bonds and thus exhibit a distinguished self-assembly behavior. As shown over the course of this work, these two classes form fibers most often and most reliably during melt electrospinning. Linear substituents facilitate the formation of uniform supramolecular nanofibers, however, with branched substituents spheres and beaded fibers were increasingly obtained.

Bisamides based on benzene, naphthyl, and cyclohexane cores were also melt electrospun. The experiments revealed that interactions in bisamides are too weak to form stable jets and mainly electrospraying occurred. Similar results were observed for the three tested sorbitol derivatives.

To answer the question, whether amide hydrogen bonds are essential for fiber formation, melt electrospinning experiments were also performed with perylene bisimides and tertiary trisamides. Perylene bisimides are characterized by an extended π-conjugated structure. As it was shown for the first time, these materials can be successfully shaped into fibers by melt electrospinning. The strong

29: glass, $T_g = 65$°C; $T_{sp} = 140$ °C;
$d_{fib} = 12.9 \pm 1.3$ µm

31: Cr 220 I; $T_{sp} = 230$ °C;
$d_{fib} = 1.6 \pm 0.7$ µm
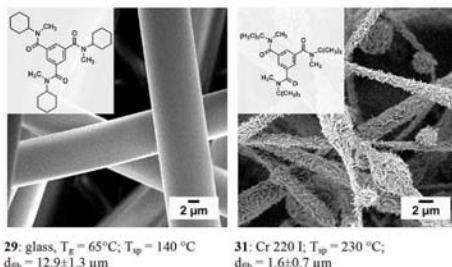
Figure 12. Compound **29** forms a glass whereas **31** is crystalline and exhibits a melting point. The electrospinning temperatures (T_{sp}) are denoted and representative SEM images of melt electrospun morphologies are shown. (Cr: crystalline, I: isotropic, T_g: glass transition temperature. Spinning parameters: $U = -40$ kV, $D = 6$ cm; $V_{flow} = 200$ µL · h⁻¹, $d_{iD} = 0.6$ mm).

274

Macromolecular
Journals

Macromol. Mater. Eng. **2015**, *300*, 259–276
© 2015 WILEY-VCH Verlag GmbH & Co. KGaA, Weinheim

www.MaterialsViews.com

π–π-interactions are sufficient for jet stabilization and thus fiber formation. Unexpectedly, also tertiary trisamides formed fibers and beaded fibers. Both examples confirm that amide hydrogen bonds are not essential for fiber formation of small molecules via melt electrospining.

In conclusion, small molecules can be successfully shaped into nano- and microfibers via melt electrospinning. As advanced nano materials they offer promising potential, for example in device preparation or filter or medical applications.

Appendix/Nomenclature/Abbreviations

Col	columnar mesophase
Cr	crystalline
D	distance between needle tip and ground plate
d_{fib}	fiber diameter complemented with diameter distribution
d_{sph}	sphere diameter and distribution
d_{ID}	inner capillary/needle diameter used for electro-spinning
h	hexagonal
I	isotropic
mp	melting point
N_c	columnar nematic
o	ordered liquid crystalline
p	plastic crystalline
$\dot{V}_{flow}$	flow rate
r	rectangular
T_{sp}	spinning temperature
U	applied voltage

[1] G. I. Taylor, R. Proc., *Soc. Lond. A.* **1964**, *280*, 383.

[2] a) A. Jaworek, A. T. Sobczyk, *J. Electrostat.* **2008**, *66*, 197; b) A. Jaworek, *Powder Tech.* **2007**, *176*, 18; c) O. V. Salata, *Curr. Nanosci.* **2005**, *1*, 25.

[3] J. M. Deitzel, J. Kleinmeyer, D. Harris, N. C. B. Tan, *Polymer* **2001**, *42*, 261.

[4] a) A. V. Subbotin, V. G. Kulichikhin, *Polym. Sci. Ser. A.* **2014**, *56*, 213; b) B. Sun, Y. Z. Long, H. D. Zhang, M. M. Li, J. L. Duvail, X. Y. Jiang, H.-L. Yin, *Prog. Polym. Sci.* **2014**, *39*, 862; c) N. Bhardwaj, S. C. Kundu, *Biotech. Adv.* **2010**, *28*, 325; d) D. W. Hutmacher, P. D. Dalton, *Chem. Asian J.* **2011**, *6*, 44; e) E. Zhmayev, D. Cho, Y. L. Yoo, *Polymer* **2010**, *51*, 274; f) A. Greiner, J. H. Wendorff, *Angew. Chem. Int. Ed.* **2007**, *46*, 5670; g) G. C. Rutledge, S. V. Fridrikh, *Adv. Drug Deliv. Rev.* **2007**, *59*, 1384; h) T. Han, D. H. Reneker, A. L. Yarin, *Polymer* **2007**, *48*, 6064; i) P. D. Dalton, D. Grafahrend, K. Klinkhammer, D. Klee, M. Möller, *Polymer* **2007**, *48*, 6823.

[5] C. J. Thompson, G. G. Chase, A. L. Yarin, D. H. Reneker, *Polymer* **2007**, *48*, 6913.

[6] a) A. Baji, Y.-W. Mai, S.-C. Wong, M. Abtahi, P. Chen, *Compos. Sci. Technol.* **2010**, *70*, 703; b) S. L. Shenoy, W. D. Bates, H. L. Frisch, G. E. Wnek, *Polymer* **2005**, *46*, 3372.

[7] a) M. T. Hunley, A. Harber, J. A. Orlicki, A. M. Rawlett, T. E. Long, *Langmuir* **2008**, *24*, 654; b) P. Gupta, C. Elkins, T. E. Long, G. L. Wilkes, *Polymer* **2005**, *46*, 4799; c) M. G. McKee, G. L. Wilkes, R. H. Colby, T. E. Long, *Macromolecules* **2004**, *37*, 1760; d) M. G. McKee, C. L. Elkins, T. E. Long, *Polymer* **2004**, *45*, 8705.

[8] A. A. Vetcher, R. Gearheart, V. N. Morozov, *Polym. J.* **2007**, *39*, 878.

[9] P. D. Dalton, J. L. Calvet, A. Mourran, D. Klee, M. Möller, *Biotechnol. J.* **2006**, *1*, 998.

[10] C. Subramanian, S. C. Ugbolue, S. B. Warner, P. K. Patra, *Mater. Res. Soc. Symp. Proc.* **2008**, *1134*, BB08.

[11] J. H. Yu, S. V. Fridrikh, G. C. Rutledge, *Polymer* **2006**, *47*, 4789.

[12] a) M. G. McKee, J. M. Layman, M. P. Cashion, T. E. Long, *Science* **2006**, *311*, 353; b) M. T. Hunley, M. G. McKnee, T. E. Long, *J. Mater. Chem.* **2007**, *17*, 605.

[13] a) M. T. Hunley, A. S. Karikari, M. G. McKnee, B. D. Mather, J. M. Layman, A. R. Fornof, T. E. Long, *Macromol. Symp.* **2008**, *270*, 1; b) M. T. Hunley, M. G. McKee, P. Gupta, G. L. Wilkes, T. E. Long, *Mater. Res. Soc. Symp. Proc.* **2007**, *948*, 0948–B02.

[14] a) S. T. Hemp, A. G. Hudson, M. H. Allen, Jr., S. S. Pole, R. B. Moore, T. E. Long, *Soft Matter* **2014**, *10*, 3970; b) M. P. Cashion, X. Li, Y. Geng, M. T. Hunley, T. E. Long, *Langmuir* **2010**, *26*, 678.

[15] G. Singh, A. M. Bittner, S. Loscher, N. Malinowski, K. Kern, *Adv. Mater.* **2008**, *20*, 2332.

[16] a) W. Nuansing, D. Frauchiger, F. Huth, A. Rebollo, R. Hillenbrand, A. M. Bittner, *Faraday Discuss.* **2013**, *166*, 209; b) W. Nuansing, A. Rebollo, J. M. Mercero, J. Zumiga, A. M. Bittner, *J. Raman Spectrosc.* **2012**, *43*, 1397.

[17] W. Nuansing, E. Georgilis, T. V. A. G. de Oliveira, G. Charalambidis, A. Eleta, A. G. Coutsolelos, A. Mitraki, A. M. Bittner, *Part. Part. Syst. Charact.* **2014**, *31*, 88.

[18] A. S. Tayi, E. T. Pashuck, C. J. Newcomb, M. T. McClendon, S. I. Stupp, *Biomacromolecules* **2014**, *15*, 1323.

[19] X. Yan, M. Zhou, J. Chen, X. Chi, S. Dong, M. Zhang, X. Ding, Y. Yu, S. Shao, F. Huang, *Chem. Comm.* **2011**, *47*, 7086.

[20] a) O. Celebioglu, T. Uyar, *J. Colloid Interface Sci.* **2013**, *404*, 1; b) A. Celebioglu, T. Uyar, *RSC Adv.* **2013**, *3*, 22891; c) C. Asli, U. Tamer, *Nanoscale* **2012**, *4*, 621; d) J. L. Manasco, C. D. Saquin, C. Tang, S. A. Khan, *RSC Adv.* **2012**, *2*, 3778; e) W. Zhang, M. Chen, B. Zha, G. Diao, *Phys. Chem. Chem. Phys.* **2012**, *14*, 9729.

[21] J.-F. Xu, Y.-Z. Chen, D. Wu, L.-Z. Wu, C.-H. Tung, Q.-Z. Yang, *Angew. Chem.* **2013**, *125*, 9920.

[22] J. C. Singer, R. Giesa, H.-W. Schmidt, *Soft Matter* **2012**, *8*, 9972.

[23] D. Kluge, J. C. Singer, B. R. Neugrig, J. W. Neubauer, H.-W. Schmidt, A. Fery, *Polymer* **2012**, *53*, 5754.

[24] I. Tomatsu, C. F. C. Fitié, D. Byelov, W. H. de Jeu, P. C. M. M. Magusin, M. Wübbenhorst, R. P. Sijbesma, *J. Phys. Chem. B* **2009**, *113*, 14158.

[25] a) P. J. M. Stals, M. M. J. Smulders, R. Martín-Rapún, A. R. A. Palmans, E. W. Meijer, *Chem. Eur. J.* **2009**, *15*; b) Y. Matsunaga, N. Miyajima, Y. Nakayasu, S. Sakai, M. Yonenaga, *Bull. Chem. Soc. Jpn.* **1988**, *61*, 207.

[26] A. Timme, R. Kress, R. Q. Albuquerque, H.-W. Schmidt, *Chem. Eur. J.* **2012**, *18*, 8329.

[27] Y. Harada, Y. Matsunaga, *Bull. Chem. Soc. Jpn.* **1988**, *61*, 2739.

[28] a) M. P. Lightfoot, F. S. Mair, R. G. Pritchard, J. E. Warren, *Chem. Comm.* **1999**, 1945; b) E. Fan, J. Yang, S. J. Geib, T. C. Stoner, M. D. Hopkins, A. D. Hamilton, *J. Chem. Soc. Chem. Comm.* **1995**, 1251.

[29] S. Cantekin, T. F. A. de Greef, A. R. A. Palmans, *Chem. Soc. Rev.* **2012**, *41*, 6125.

[30] a) M. Schmidt, J. J. Wittmann, R. Kress, D. Schneider, S. Steuernagel, H.-W. Schmidt, J. Senker, *Cryst. Growth Des.* **2012**, *12*, 2543; b) A. Sakamoto, D. Ogata, T. Shikata, O. Urakawa, K. Hanabusa, *Polymer* **2007**, *47*, 956; c) A. Sakamoto, D. Ogata, T. Shikata, K. Hanabusa, *Macromolecules* **2005**, *38*, 8983.

[31] R. Q. Albuquerque, A. Timme, R. Kress, J. Senker, H.-W. Schmidt, *Chem. Eur. J.* **2013**, *19*, 1647.

[32] a) C. F. C. Fité, W. S. C. Roelofs, R. P. Sijbesma, J. Phys. Chem. B **2012**, *116*, 3928; b) C. F. C. Fité, W. S. C. Roelofs, M. Kemerink, R. P. Sijbesma, *J. Am. Chem. Soc.* **2010**, *132*, 6892; c) L. Sardone, V. Palermo, E. Devaux, D. Credgington, M. de Loos, G. Marletta, F. Cacialli, J. van Esch, P. Samorì, *Adv. Mater.* **2006**, *18*, 1276.

[33] C. A. Jiménez, J. B. Belmar, L. Ortíz, P. Hidalgo, O. Fabelo, J. Pasán, C. Ruiz-Pérez, *Cryst. Growth Des.* **2009**, *9*, 4987.

[34] F. Abraham, S. Ganzleben, D. Hanft, P. Smith, H.-W. Schmidt, *Macromol. Chem. Phys.* **2010**, *211*, 171.

[35] F. Abraham, R. Kress, P. Smith, H.-W. Schmidt, *Macromol. Chem. Phys.* **2013**, *214*, 17.

[36] J. P. Larocca, M. A. Y. Sharkawi, *J. Pharm. Sci.* **1967**, *56*, 916.

[37] A. Wicklein, A. Lang, M. Muth, M. Thelakkat, *J. Am. Chem. Soc.* **2009**, *131*, 14442.

[38] T. Yoshioka, R. Dersch, A. Greiner, M. Tsuji, A. K. Schaper, *Macromol. Mater. Eng.* **2010**, *295*, 1082.

[39] a) W. Greiner, *Adv. Polym. Sci.* **2008**, *219*, 107; b) H. Fong, D. H. Reneker, in *Structure Formation in Polymeric Fibers*, D. R. Salem Eds., Hanser Publishing, Munich, Germany **2000**, 225; c) L. Larrondo, S. J. Manley, *J. Polym. Sci. Polym. Phys, Ed.* **1981**, *19*, 921.

[40] Y. M. Shin, M. M. Hohman, M. P. Brenner, G. C. Rutledge, *Polymer* **2001**, *42*, 9955.

[41] F. Abraham, H.-W. Schmidt, *Polymer* **2010**, *51*, 913.

[42] F. Richter, H.-W. Schmidt, *Macromol. Mater. Eng.* **2013**, *298*, 190.

[43] J. Wang, Q. Dou, X. Chen, L. Di, *J. Polym. Sci. B: Polym. Phys.* **2008**, *46*, 1067.

[44] a) P. Song, Z. Wei, J. Liang, G. Chen, W. Zhang, *Polym. Eng. Sci.* **2012**, *52*, 1058; b) H. Bai, W. Zhang, H. Deng, Q. Zhang, Q. Fu, *Macromolecules* **2011**, *44*, 1233; c) H. Nakajima, M. Takahashi, Y. Kimura, *Macromol. Mater. Eng.* **2010**, *295*, 460.

[45] a) K. P. Magnus, A. Gress, P. Smith, D. Hanft, H.-W. Schmidt, *Polymer* **2006**, *47*, 249; b) M. Blomenhofer, S. Ganzleben, D. Hanft, H.-W. Schmidt, M. Kristiansen, P. Smith, K. Stoll, D. Mäder, K. Hoffmann, *Macromolecules* **2005**, *38*, 3688.

[46] M. Gahleitner, C. Grein, S. Kheirandish, J. Wolfschwenger, *Internat. Polym. Proc.* **2011**, *26*, 2.

[47] a) M. Kersch, L. Pischke, H.-W. Schmidt, V. Altstädt, *Polymer* **2014**, *55*, 3227; b) M. Stumpf, A. Spörrer, H.-W. Schmidt, V. Altstädt, *J. Cell. Plast.* **2011**, *47*, 519.

[48] D. P. Erhard, D. Lovera, C. von Salis-Soglio, R. Giesa, V. Altstädt, H.-W. Schmidt, *Adv. Polym. Sci.* **2010**, *228*, 155.

[49] M. Gelinsky, R. Vogler, H. Vahrenkamp, *Inorg. Chem.* **2002**, *41*, 2560.

[50] a) H. Cao, P. Duan, X. Zhu, J. Jiang, Liu, *Chem. Eur. J.* **2012**, *18*, 5546; b) T. Shikata, Y. Kuruma, A. Sakamoto, K. Hanabusa, *J. Phys. Chem. B* **2008**, *112*, 16393; c) J. J. van Gorp, J. A. J. M. Vekemans, E. W. Meijer, *J. Am. Chem. Soc.* **2002**, *124*, 14759; d) K. Hanabusa, C. Koto, M. Kimura, H. Shirai, A. Kakehi, *Chem. Lett.* **1997**, *26*, 429; e) Y. Yasuda, E. Iishi, H. Inada, Y. Shirota, *Chem. Lett.* **1996**, *25*, 575.

[51] a) A. Bernet, R. Q. Albuquerque, M. Behr, S. T. Hoffmann, H.-W. Schmidt, *Soft Matter* **2012**, *8*, 66; b) N. Shi, H. Dong, G. Yin, Z. Xu, S. Li, *Adv. Funct. Mater.* **2007**, *17*, 1837.

[52] H. Misslitz, K. Kreger, H.-W. Schmidt, *Small* **2013**, *9*.

[53] R. Takasawa, K. Murota, I. Yoshikawa, K. Araki, *Macromol. Rapid Commun.* **2003**, *24*, 335.

[54] M. de Loos, J. H. van Esch, R. M. Kellogg, B. L. Feringa, *Tetrahedron* **2007**, *63*, 7285.

[55] N. Mohmeyer, H.-W. Schmidt, P. M. Kristiansen, V. Altstädt, *Macromolecules* **2006**, *39*, 5760.

[56] a) N. Mohmeyer, H.-W. Schmidt, *Chem. Eur. J.* **2007**, *13*, 4499; b) N. Mohmeyer, H.-W. Schmidt, *Chem. Eur. J.* **2005**, *11*, 863.

[57] a) M. Schmidt, C. S. Zehe, R. Siegel, J. U. Heigl, C. Steinlein, H.-W. Schmidt, J. Senker, *Cryst. Eng. Comm.* **2013**, *15*, 8784; b) H.-Z. Guo, G.-D. Yin, N.-F. She, A.-X. Wu, *Acta Cryst.* **2005**, *E61*, 4062; c) P. G. Jones, J. Ossowski, P. Kus, *Z. Naturforsch.* **2002**, *57b*, 914.

[58] E. A. Wilder, C. K. Hall, S. A. Khan, R. J. Spontak, *Langmuir* **2003**, *19*, 6004.

[59] a) K. Bernland, T. Tervoort, P. Smith, *Polymer* **2009**, *50*, 2460; b) J. Lipp, M. Schuster, A. E. Terry, Y. Cohen, *Langmuir* **2006**, *22*, 6398; c) M. Kristiansen, M. Werner, T. Tervoort, P. Smith, M. Blomenhofer, H.-W. Schmidt, *Macromolecules* **2003**, *36*, 5150; d) C. Marco, G. Ellis, M. A. Gomez, J. M. Arribas, *J. Appl. Polym. Sci.* **2002**, *84*, 2440; e) T. A. Shepard, C. R. Delsorbo, R. M. Louth, J. L. Walborn, D. A. Norman, N. G. Harvey, R. J. Spontak, *J. Polym. Sci., Part B: Polym. Phys.* **1997**, *35*, 2617.

[60] M. Watase, Y. Nakatani, H. Itagaki, *J. Phys. Chem. B* **1999**, *103*, 2366.

[61] a) A. S. Krishnan, P. H. Vargantwar, R. J. Spontak, *Soft Matter* **2012**, *8*, 12025; b) E. A. Wilder, C. K. Hall, R. J. Spontak, *J. Colloid Interface Sci.* **2003**, *267*, 509;

[62] D. L. VanderHart, J. F. Douglas, S. D. Hudson, J. M. Antonucci, E. A. Wilder, *Langmuir* **2011**, *27*, 1745.

[63] a) A. Ringk, X. Li, F. Gholamrezaie, E. C. P. Smits, A. Neuhold, A. Moser, C. van der Marel, G. H. Gelinck, R. Resel, D. M. de Leeuw, P. Strohriegl, *Adv. Funct. Mater.* **2013**, *23* 2016; b) A. Ringk, W. S. C. Roelofs, E. C. P. Smits, C. van der Marel, I. Salzmann, A. Neuhold, G. H. Gelinck, R. Resel, D. M. de Leeuw, P. Strohriegl, *Org. Electron.* **2013**, *14*, 1297; c) H. Huang, S. Barlow, S. R. Marder, *J. Org. Chem.* **2011**, *76*, 2386; d) F. Würthner, *Chem. Comm.* **2004**, 1564; e) P. Ranke, I. Bleyl, J. Simmerer, D. Haarer, A. Bacher, H.-W. Schmidt, *Appl. Phys. Lett.* **1997**, *71*, 1332.

[64] B. A. Jones, A. Facchetti, M. R. Wasielewski, T. J. Marks, *J. Am. Chem. Soc.* **2007**, *129*, 15259.

Melt electrospinning of small molecules

Julia C. Singer, Andreas Ringk, Reiner Giesa, and Hans-Werner Schmidt[*]

Macromolecular Chemistry I, Bayreuth Institute of Macromolecular Research (BIMF), and Bayreuth Center for Colloids and Interfaces (BZKG), University of Bayreuth,

95440 Bayreuth, Germany, E-mail: hans-werner.schmidt@uni-bayreuth.de

_____

Supporting Information

Content:

I. Synthesis of 1,3,5-Benzenetrisamides **7-10**

General procedure: To a mixture of dry *N*-methylpyrrolidone (NMP) or tetrahydrofuran (THF) as solvent, pyridine or triethylamine as base, lithium chloride (LiCl) and the corresponding amine, 1,3,5-benzenetricarboxylic acid chloride was added at 0 °C under nitrogen. Over night the reaction mixture was stirred at 60 °C and after cooling to room temperature (rt) precipitated into ice water. If THF was used as solvent, it was evaporated from the cold reaction mixture and the residue was stirred with water. The precipitate was filtered, dried in vacuum and purified by recrystallisation, reprecipitation, or column chromatography.

5-Heptanoylamino-N,N'-dihexyl-isophthalamide (7): Heptanoylchloride was reacted under the above described conditions with the corresponding 5-aminoisophthalic acid *N,N*-dihexyl-diamide. Isolation of the product and purification was performed in the same way as described in the general procedure. 5-Aminoisophthalic acid *N,N*-dihexyldiamide (3.9 g, 11 mmol), heptanoylchloride (1.8 g, 12.2 mmol), NMP (100 mL), pyridine (20 mL), LiCl (0.1 g). Recrystallization from methanol. Yield: 3.8 g (74%).^{1}H NMR (300 MHz, DMSO-d$_6$, δ [ppm]): 0.86 (t, J = 6.54 Hz, 9H, 3x CH$_3$); 1.22-1.35 (m, 18H, 9x CH$_2$); 1.47-1.61 (m, 6H, 1x CO-CH$_2$CH$_2$, 2x NH-CH$_2$CH$_2$); 2.32 (t, J = 7.34 Hz, 2H, 1x CO-CH$_2$); 3.24 (dd, J = 6.53 Hz, 4H, 2x NH-CH$_2$); 7.86 (s, 1H, 1x Ar H); 8.12 (s, 2H, 2x Ar H);8.48(t, J = 5.57 Hz, 2H, 2x NH); 10.13 (s, 1H, 1x NHCO-CH$_2$). MS (70 eV), *m/z* (%): 459 (M$^+$, 100); 389 (71); 347 (99); 247 (36); 163 (12); 100 (14); 43 (56).

3,5-Bis-heptanoylamino-N-hexyl-benzamide (8): Heptanoylchloride was reacted according to the general procedure with the corresponding 3,5-diamino-*n*-hexyl-benzamide. Isolation of the product and purification was performed in the same way as described in the general procedure. 3,5-diamino-*n*-hexyl-benzamide (2.7 g, 11.6 mmol), heptanoylchloride (3.8 g, 25.5 mmol), NMP (100 mL), pyridine (20 mL), LiCl (0.1 g). Recrystallization from methanol. Yield: 2.2 g (41 %).^{1}H NMR (300 MHz, DMSO-d$_6$, δ [ppm]): 0.85 (t, J = 6.54 Hz, 9H, 3x CH$_3$); 1.19-1.35 (m, 18H, 9x CH$_2$); 1.46-1.60 (m, 6H, 2x CO-CH$_2$CH$_2$, 1x NH-CH$_2$CH$_2$); 2.25-2.31 (m, 4H, 2x CO-CH$_2$); 3.16-3.21 (m, 2H, 1x NH-CH$_2$); 7.61 (s, 2H, 2x Ar H); 8.04 (s, 1H, 1x Ar H); 8.33 (s, 1H, 1x NH); 9.97 (s, 2H, 2x NHCO-CH$_2$).MS (70 eV), *m/z* (%): 459 (M$^+$, 68); 347 (100); 322 (39); 220 (19); 109 (12); 43 (33).

Heptanoic acid (3,5-bis-heptanoylamino-phenyl)-amide (9): Heptanoylchloride was reacted according to the general procedure with 1,3,5-triaminobenzene. Isolation of the product and purification was performed in the same way as described in the general procedure. 1,3,5-

2

triaminobenzene (2.0 g, 16.0 mmol), heptanoylchloride (8.0 g, 54.0 mmol), NMP (150 mL), pyridine (20 mL), LiCl (0.1 g). Recrystallization from cyclohexane and THF. Yield: 4.1 g (56%).^{1}H NMR (300 MHz, DMSO-d$_6$,δ [ppm]): 0.86 (t, J = 5.75 Hz, 9H, 3x CH$_3$); 1.22-1.31 (m, 18H, 9x CH$_2$); 1.50-1.60 (m, 6H, 3x CO-CH$_2$CH$_2$); 2.27 (t,J = 7.34 Hz, 6H, 3x CO-CH$_2$); 7.63 (s, 3H, 3x Ar H); 9.34 (s, 3H, 3x NH). MS (70 eV), *m/z* (%): 495 (M$^+$, 64); 347 (100); 260 (23); 235 (51); 123 (19); 44 (27).

Nonanoic acid (2,4,6-trimethyl-3,5-bis-nonanoylamino-phenyl)-amide (10): Nonanoic acid chloride was reacted according to the general procedure with 1,3,5-trisamino-2,4,6-trimethylbenzene (provided by Ciba Specialty Chemicals, now BASF SE, Basel, Switzerland). Isolation of the product and purification was performed in the same way as described in the general procedure. 1,3,5-trisamino-2,4,6-trimethylbenzene (2.0 g, 12.0 mmol), nonanoic acid chloride (8.0 g, 40.0 mmol), NMP (150 mL), pyridine (20 mL), LiCl (0.1 g). Recrystallization from methanol and dichloromethan. Yield: 1.0 g (14 %).^{1}H NMR (300 MHz, CF$_3$COOD/CDCl$_3$ 5:1, δ [ppm]): 0.90 (t, J = 7.59 Hz, 9H,3x CH$_3$); 1.22-1.44 (m, 30H, 15x CH$_2$); 1.73-1.81 (m, 6H, 3x NH-CH$_2$CH$_2$); 2.09-2.51 (m, 9H, 3x CH$_3$-Ar); 2.60 (t, J = 7.73 Hz, 4H, 2x NH-CH$_2$). MS (70 eV), *m/z* (%): 585 (M$^+$, 11); 446 (100); 305 (25); 164 (20); 58 (9).

II. 1,3,5-Cyclohexanetrisamide 15

General procedure: To a mixture of dry NMP as solvent, triethylamine as base, LiCl and *cis,cis*-1,3,5-triaminocyclohexane, nonanoic acid was added at 0 °C under nitrogen. Over night the reaction mixture was stirred at 60 °C and after cooling to rt precipitated in ice water. The precipitate was filtered, dried under vacuum and purified by recrystallisation.

Nonanoic acid (3,5-bis-nonanoylamino-cyclohexyl)-amide (15): Nonanoic acid chloride was reacted with *cis,cis*-1,3,5-triaminocyclohexane. Isolation of the product and purification was performed in the same way as described in the general procedure. *cis,cis*-1,3,5-triaminocyclohexane (0.93 g, 2.5 mmol), nonanoic acid chloride (1.5 g, 8.3 mmol), NMP (50 mL), triethylamine (5 mL), LiCl (0.1 g). Recrystallization from methanol. Yield: 0.25 g (18 %).^{1}H NMR (300 MHz, CF$_3$COOD/CDCl$_3$ 5:1, δ [ppm]): 0.72 (t, J = 6.66 Hz, 9H, 3x CH$_3$); 1.11 (s, 30H, 15x CH$_2$); 1.28-1.58 (m, 6H, 3x CH$_2$ cyclo); 1.99-2.13 (m, 6H, 3x CO-CH$_2$CH$_2$); 2.29 (t, J = 7.89 Hz, 6H, 3x CO-CH$_2$); 3.80-3.89 (m, 3H, 3x NH-CHcyclo). MS (70 eV), *m/z* (%): 549 (M$^+$, 14); 393 (38); 236 (100); 158 (59); 94 (43); 44 (55).

III. Tertiary 1,3,5-benzenetrisamides **29-31**

To a mixture of dry THF as solvent, pyridine or triethylamine as base, LiCl and the corresponding amine, 1,3,5-benzenetricarboxylic acid chloride was added at 0 °C under nitrogen. Over night the reaction mixture was stirred at 70 °C. After cooling to rt, THF was evaporated from the cold reaction mixture and the residue was stirred with water. The precipitate was filtered, dried under vacuum, and purified by recrystallisation, reprecipitation, or column chromatography.

Benzene-1,3,5-tricarboxylicacid tris-(cyclohexyl-methyl-amide) **(29)**:   1,3,5-Benzenetricarboxylic acid chloride (3.0 g, 11 mmol), dicyclohexylamine, *N-tert*-butylmethylamine (3.2 g, 37 mmol), THF (150 mL), pyridine (20 mL), LiCl (0.1 g). Recrystallization from hexane. Yield: 2.5g (55 %). ^{1}H NMR (300 MHz, DMSO-d_6, δ [ppm]): 1.45 (s, 27H, 3x N-C-(CH$_3$)$_3$)); 2.81 (s, 9H, 3x N-CH$_3$); 7.37 (s, 3H, 3x Ar H). MS (70 eV), *m/z* (%): 418 (M$^+$, 9); 402 (88); 331 (100); 275 (39); 220 (16); 136 (9); 59 (12).

*Benzene-1,3,5-tricarboxylic acid tris-dicyclohexylamide***(30)**: 1,3,5-Benzenetricarboxylic acid chloride (3.0 g, 11 mmol), dicyclohexylamine (6.8 g, 37 mmol), THF (150 mL), pyridine (20 mL). Column chromatography (Alox neutral) from hexane and THF (4:1). Yield: 1.3 g (17 %). ^{1}H NMR (300 MHz, CDCl$_3$, δ [ppm]): 0.95-1.87 (m, 54H,27x CH$_2$); 2.42-2.71 (m, 6H, 3x CH$_2$); 2.99-3.44 (m, 6H, 6x N-CH); 7.28 (s, 3H, 3x Ar H). MS (70 eV), *m/z* (%): 698 (M$^+$, 46); 616 (37); 340 (12); 284 (30); 180 (100); 161 (32); 55 (99); 41 (39).

Benzene-1,3,5-tricarboxylicacid tris(tert-butyl-methyl-amide) **(31)**:   1,3,5-Benzenetricarboxylic acid chloride (3.0 g, 11 mmol), *N*-methylcyclohexylamine (4.3 g, 37 mmol), THF (150 mL), pyridine (20 mL), LiCl (0.1 g). Recrystallization from hexane. Yield: 3.2 g (59 %). ^{1}H NMR (300 MHz, CDCl$_3$, δ [ppm]): 0.97-1.23 (m, 6H, 3x CH$_2$ cyclo); 1.47-1.84 (m, 24H, 12x CH$_2$ cyclo); 2.90 (d, J = 46.16 Hz, 9H, 3x N-CH$_3$); 3.42 (axial), 4.47 (equatorial) (s, 1H, 1x N-CH cyclo) 7.42 (s, 3H, 3x Ar H). MS (70 eV), *m/z* (%): 495 (M$^+$, 100); 412 (60); 356 (58); 216 (49); 112 (85); 55 (33).

4

IV. Bisamides based on aromatic and cyclohexane cores **16-22**

General procedure: To a mixture of dry NMP as solvent, pyridine as base, LiCl and the corresponding amine, carboxylic acid chloride was added under nitrogen atmosphere and at 0°C. After stirring over night at 80 °C, the reaction mixture was cooled to rt and precipitated in ice water, filtered, dried under vacuum, and purified by recrystallization. In case the carboxylic acid chloride was not commercial available it was synthesized by adding oxalyl dichloride at 0 °C under nitrogen drop wise to a mixture of dry dichloromethane and the carboxylic acid. The reaction mixture was stirred over night at 40 °C. After cooling to rt the remaining oxalyl dichloride and dichloromethane were evaporated under vacuum. The obtained solid was used for further synthesis without purification.

Nonanoic acid (4-nonanoylamino-phenyl)amide (16): Phenylenediamine (5.0 g, 46 mmol), nanonylchloride (18.8 g, 106 mmol), NMP (150 mL), pyridine (30 mL), LiCl (0.1 g). Recrystallization from dimethylformamide (DMF). Yield: 13.0 g (73 %).^{1}H NMR (300 MHz, CF$_3$COOD/CDCl$_3$ 5:1, δ [ppm]): 0.90 (t, J = 6.69 Hz, 6H,2x CH$_3$); 1.23-1.42 (m, 20H, 10x CH$_2$); 1.69-1.79 (m, 4H, 2x CO-CH$_2$CH$_2$); 2.50 (t, J = 7.76 Hz, 4H, 2x CO-CH$_2$); 7.42 (s, 4H, 4x Ar H). MS (70 eV), *m/z* (%): 388 (M$^+$, 60); 290 (9); 248 (100); 108 (80); 43 (14).

N,N'-Dioctyl-terephthalamide (17): N-Octylamine (6.2 g, 48 mmol); terephthalic acid dichloride (4.4 g, 22 mmol), NMP (150 mL), pyridine (30 mL), LiCl (0.1 g). Recrystallization from methanol. Yield: 2.5 g (29 %).^{1}H NMR (300 MHz, CF$_3$COOD/CDCl$_3$ 5:1, δ [ppm]): 0.90 (t, J = 6.73 Hz, 6H,2x CH$_3$); 1.30-1.42 (m, 20H, 10x CH$_2$); 1.63-1.71 (m, 4H, 2x NH-CH$_2$CH$_2$); 3.52(t, J = 7.31 Hz, 4H, 2x NH-CH$_2$); 7.81 (s, 4H, 4x Ar H). MS (70 eV), *m/z* (%): 388 (M$^+$, 35); 331 (25); 290 (43); 260 (100); 147 (12); 104 (15).

Naphthalene-2,6-dicarboxylic acid bisoctylamide (18): N-Octylamine (6.6 g, 51 mmol), naphtalen-2,6-dicarboxylic acid chloride (5.0 g, 20 mmol), NMP (150 mL), pyridine (30 mL), LiCl (0.1 g). Recrystallization from methanol. Yield: 6.2 g (71 %).^{1}H NMR (300 MHz, CF$_3$COOD/CDCl$_3$ 5:1, δ [ppm]): 0.91 (t, J = 6.78 Hz, 6H,2x CH$_3$); 1.32-1.43 (m, 20H, 10x CH$_2$); 1.70-1.79 (m, 4H, 2x CO-CH$_2$CH$_2$); 3.60 (t, J = 7.26 Hz, 4H, 2x CO-CH$_2$); 7.82 (d, J = 7.56 Hz, 2H, 2x Ar H), 8.05 (d, J = 8.76 Hz, 2H, 2x Ar H); 8.32 (s, 2H, 2x Ar H). MS (70 eV), *m/z* (%): 438 (M$^+$, 79); 321 (84); 340 (74); 310 (100); 198 (31); 154 (53); 126 (15); 41 (9).

Nonanoic acid (4-nonanoylamino-trans-cyclohexyl)amide (19): Trans-1,4-cyclohexylamine (3.3 g, 28 mmol), nonanoic acid chloride (11.23 g, 64 mmol), NMP (160 mL), pyridine

5

(40 mL), LiCl (0.1 g). Recrystallization from THF. Yield: 8.0 g (72 %).^{1}H NMR (300 MHz, CF$_3$COOD/CDCl$_3$ 5:1, δ [ppm]): 0.89 (t, J = 6.68 Hz, 6H, CH$_3$); 1.28-1.41 (s, 20H, 10x CH$_2$); 1.43-1.55 (m, 4H, 2x CH$_2$ cyclo); 1.63-1.74 (m, 4H, 2x CH$_2$ cyclo); 2.06-2.13 (m, 4H, 2x CO-CH$_2$CH$_2$);2.53 (t, J = 7.82 Hz,4H, 2x CO-CH$_2$); 3.92 (s,2H, 2x NH-CH cyclo). MS (70 eV), m/z (%): 395 (M$^+$, 2); 253 (24); 237 (100); 158 (99); 140 (11); 96 (26); 81 (14); 44 (18).

Nonanoic acid (4-nonanoylamino-cis-cyclohexyl-amide (20): *Cis*-1,4-cyclohexylamine (3.3 g, 28 mmol), nonanoic acid chloride (11.23 g, 64 mmol), NMP (100 mL), pyridine (40 mL), LiCl (0.1 g). Recrystallization from ethyl acetate. Yield: 6.0 g (54 %).^{1}H NMR (300 MHz, DMSO-*d$_6$*, δ [ppm]): 0.85 (t, J = 6.69 Hz, 6H, CH$_3$); 1.23 (s, 20H, 10x CH$_2$); 1.44-1.57 (m, 12H, 4x CH$_2$ cyclo/ 2x CO-CH$_2$CH$_2$); 2.05 (t, J = 7.32 Hz,4H, 2x CO-CH$_2$); 3.56 (s,2H, 2x NH-CH cyclo), 7.62 (d, J = 6.69 Hz, NH). MS (70 eV), m/z (%): 395 (M$^+$, 5); 238 (16); 159 (30); 142 (38); 96 (25); 81 (23); 71 (36); 56 (70); 56 (70); 43 (100); 41 (73).

Trans-cyclohexane-1,4-dicarboxylic acid bisoctylamide (21): *N*-Octylamine (5.7 g, 44 mmol), *trans*-cyclohexane-1,4-dicarboxylic acid chloride (4.0 g, 19 mmol), NMP (100 mL), pyridine (25 mL), LiCl (0.1 g). Recrystallization from THF. Yield: 5.5 g (73 %).^{1}H NMR (300 MHz, CF$_3$COOD/CDCl$_3$ 5:1, δ [ppm]): 0.89 (t, J = 7.61 Hz, 6H, 2x CH$_3$); 1.28-1.32 (m, 20H, 10x CH$_2$); 1.58-1.71 (m, 8H, 4x CH$_2$ cyclo); 2.03-2.09 (m, 4H, 2x NH-CH$_2$CH$_2$), 2.79-2.85 (m,2H, 2x CO-CH cyclo), 3.42 (t, J = 7.43 Hz, 4H, 2x NH-CH$_2$). MS (70 eV), m/z (%): 395 (M$^+$, 11); 239 (37); 82 (7); 72 (10); 57 (100); 43 (58).

Cis-cyclohexane-1,4-dicarboxylic acid bisoctylamide (22): *N*-Octylamine (4.8 g, 36 mmol), *cis*-cyclohexane-1,4-dicarboxylic acid chloride (3.6 g, 17 mmol), NMP (60 mL), pyridine (25 mL), LiCl (0.1 g). Recrystallization from ethyl acetate. Yield: 3.9 g (58 %).^{1}H NMR (300 MHz, DMSO-*d$_6$*, δ [ppm]): 0.85 (t, J = 6.56 Hz, 6H, 2x CH$_3$); 1.23 (s, 20H, 10x CH$_2$); 1.29-1.44(m, 4H, 2x CH$_2$ cyclo); 1.73-1.82 (m, 4H, 2x CH$_2$ cyclo);2.18 (s, 2H, 2x CO-CH cyclo); 2.99 (q, J = 6.35 Hz, 4H 2x NH-CH$_2$); 7.60(t, J = 5.45 Hz, NH). MS (70 eV), m/z (%): 395 (M$^+$, 9); 305 (20); 239 (100); 232 (27); 185 (35); 154 (46); 139 (35); 71 (90); 57 (55); 43 (83); 41 (42).

V. SEM images and fiber/sphere diameter histograms of compounds **1-31**

The fiber and sphere diameter distributions were calculated from at least 100 individual fibers or spheres (exact amount denoted by *n*) by evaluating at least three different SEM images taken at different positions within one SEM stub. For structures above to 5 µm SEM images at a magnification of 1000 were chosen.

Table S1: *Benzenetricarboxamides with linear and branched substituents* **1-6**.

(M: molecular weight; Cr: crystalline, Col: columnar mesophase, h: hexagonal, p: plastic crystalline, o: ordered liquid crystalline, I: isotropic. Spinning parameters: voltage: -40 kV, flow rate: 200 µL h^{-1}, distance needle tip to ground plate: 6 cm, needle ID: 0.6 mm, spinning temperature T_{sp} as specified).
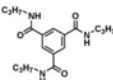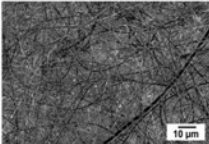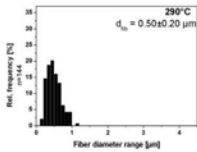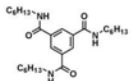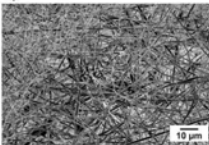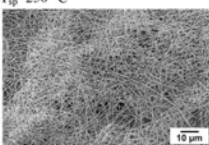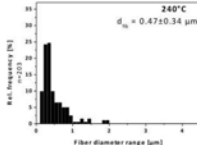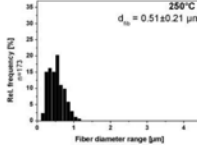
Entry	Chemical structure / phase transition temp./ temp. at 10% weight loss	SEM of melt electrospun morphologies	Fiber and sphere diameter histograms
1	$M = 333.43$ g·mol^{-1} Cr 289 I T_{sp}=290 °C $T_{-10 wt\%}$=351 °C		
2	$M = 459.66$ g·mol^{-1} Cr 72 Col$_{hp}$ 172 Col$_{ho}$ 218 I $T_{-10 wt\%} = 382$ °C	T_{sp}=240 °C T_{sp}=250 °C 	

7

Table S1, continued.

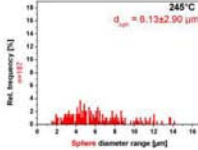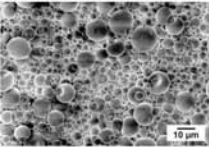|	Structure	SEM images	Histograms
2		T_{sp}=270 °C	270°C d_{fib} = 0.43±0.27 µm d_{sph} = 0.97±0.75 µm
		T_{sp}=300 °C	300°C d_{fib} = 0.39±0.24 µm d_{sph} = 1.15±0.98 µm
3	M = 543.82 g·mol^{-1} Cr 117 Col$_{ho}$ 207 I T_{sp}=230 °C $T_{-10\ wt\%}$=384 °C		230°C d_{fib} = 0.97±0.28 µm
4	M = 417.58 g·mol^{-1} Cr 211 M$_p$ 272 I T_{sp}=300 °C $T_{-10\ wt\%}$=347 °C		300°C d_{fib} = 0.68±0.44 µm d_{sph} = 2.14±0.81 µm

8

Table S1, continued.

5	M = 542.82 g·mol^{-1} Col$_{hp}$ 204 Col$_{ho}$ 291 I T$_{sp}$=310 °C T$_{-10 wt\%}$=365 °C	10 µm	
6	M = 542.82 g·mol^{-1} Col$_{hp}$ 241 Col$_{ho}$ 291 I T$_{sp}$=310 °C T$_{-10 wt\%}$=376 °C	10 µm	

9

Table S2: *Influence of the connectivity of the amide linkage to the benzene core **7-10**.*
(M: molecular weight; Cr: crystalline, I: isotropic. Spinning parameters: voltage: -40 kV, flow rate: 200 μL h^{-1}, distance needle tip to ground plate: 6 cm, needle ID: 0.6 mm, spinning temperature T$_{sp}$ as specified).
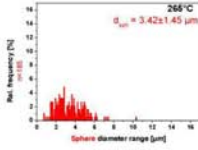
Entry	Chemical structure / phase transition temp. / temp. at 10% weight loss	SEM of melt electrospun morphologies	Fiber and sphere diameter histograms
7	M = 459.66 g·mol^{-1} Cr 176 I T$_{sp}$=200 °C T$_{-10\,wt\%}$=375 °C		
8	M = 459.66 g·mol^{-1} Cr 184 I T$_{sp}$=200 °C T$_{-10\,wt\%}$=372 °C		
9	M = 459.66 g·mol^{-1} Cr 183 I T$_{sp}$=200 °C T$_{-10\,wt\%}$=379 °C		
10	M = 589.90 g·mol^{-1} Cr 356 I T$_{sp}$=375 °C T$_{-10\,wt\%}$=392 °C		

Table S3: *Cyclohexanetrisamides* **11-15**.

(M: molecular weight; Cr: crystalline, Col: columnar mesophase, h: hexagonal, r: rectangular, p: plastic crystalline, o: ordered liquid crystalline, N_C: columnar nematic, I: isotropic. Spinning parameters: voltage -40 kV, flow rate: 200 μL h^{-1}, distance needle tip to ground plate: 6 cm, needle ID: 0.6 mm, spinning temperature T_{sp} as specified).
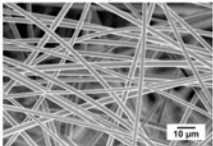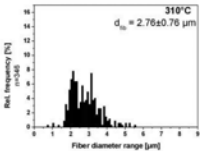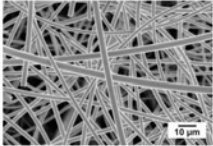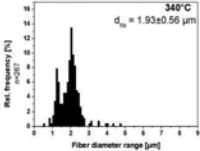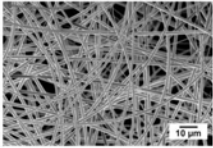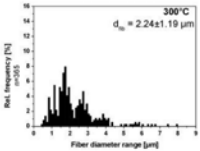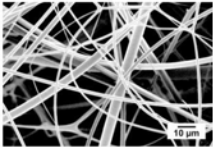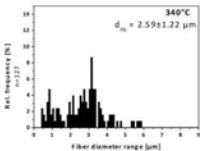
Entry	Chemical structure / phase transition temp. / temp. at 10% weight loss	SEM of melt electrospun morphologies	Fiber and sphere diameter histograms
11	M = 507.79 g·mol^{-1} Cr$_1$ 200 Cr$_2$ 218 Col$_{rp}$ 290 N$_c$ 319 I T$_{-10 wt\%}$=377 °C	Nematic phase: T$_{sp}$= 310 °C Isotropic phase: T$_{sp}$= 340 °C	
12	M = 549.87 g·mol^{-1} Cr$_1$ 43 Cr$_2$ 189 Col$_{rp}$ 276 N$_c$ 320 I T$_{-10 wt\%}$=373 °C	Nematic phase: T$_{sp}$= 300 °C Isotropic phase: T$_{sp}$= 340 °C	
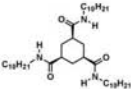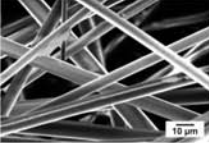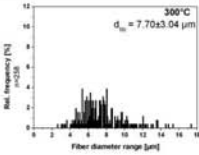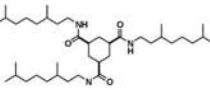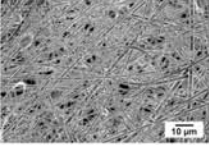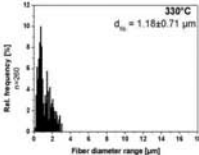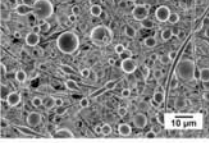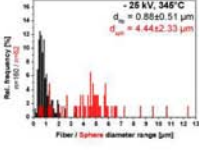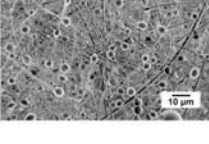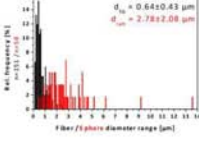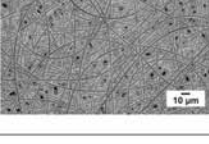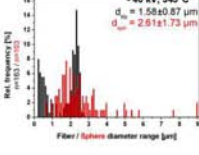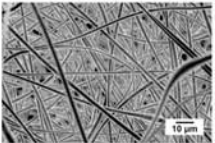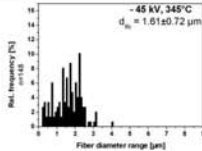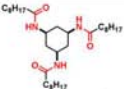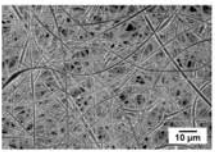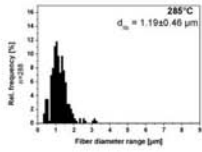
11

Table S3, continued.

13 M = 634.03 g·mol⁻¹ Cr₁ 117 Cr₂ 167 Col_rp 254 N_c 317 I T₋₁₀ wt% = 382 °C	Nematic phase: T_sp = 300 °C Isotropic phase: T_sp = 330 °C 	

$M = 634.03 \text{ g·mol}^{-1}$
$\text{Cr}_1\ 117\ \text{Cr}_2\ 167\ \text{Col}_{rp}\ 254\ \text{N}_c\ 317\ \text{I}$
$\text{T}_{-10\ wt\%} = 382\ °C$

$M = 643.03 \text{ g·mol}^{-1}$
$\text{Cr}\ 121\ \text{Col}_{ho}\ 338\ \text{I}$
$\text{T}_{sp} = 345\ °C$
$\text{T}_{-10\ wt\%} = 378\ °C$

14

-25 kV; E = 4.2 kV cm⁻¹

-30 kV; E = 5 kV cm⁻¹

-40 kV; E = 6.7 kV cm⁻¹

Table S3, continued.

14	- 45 kV; E = 7.5 kV cm^{-1}	
15 $M = 549.87$ g·mol^{-1} Cr 272 I $T_{sp} = 285\ ^\circ C$ $T_{-10\ wt\%} = 358\ ^\circ C$		

Table S4: *Bisamides based on aromatic and cyclohexane cores* **16-22**.

(M: molecular weight; Cr: crystalline, I: isotropic. Spinning parameters: voltage: -40 kV, distance needle tip to ground plate: 6 cm, flow rate: 200 μL h⁻¹, needle capillary ID: 0.6 mm, spinning temperature T$_{sp}$ as specified).
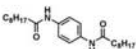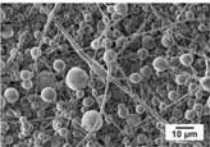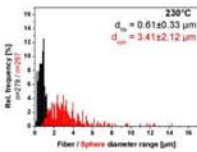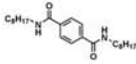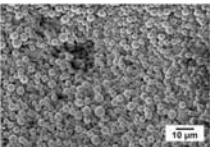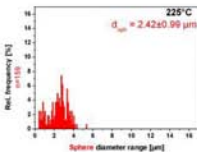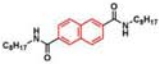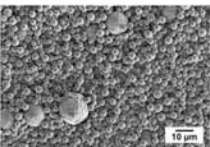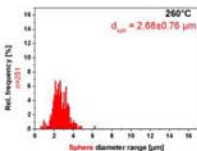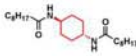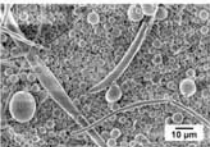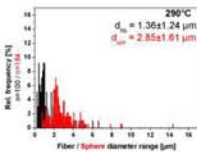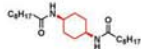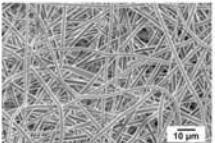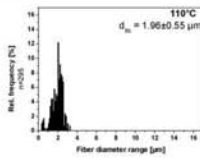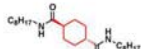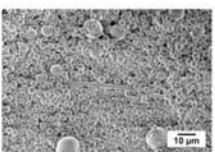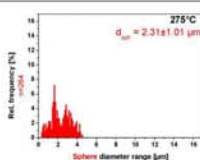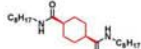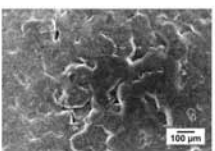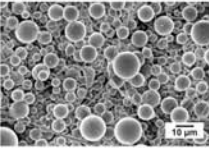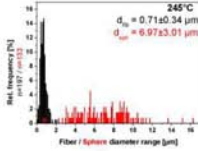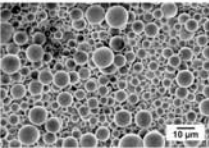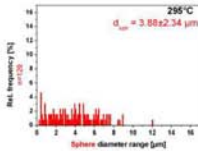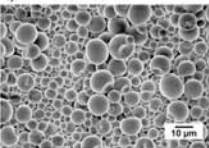
Entry	Chemical structure / phase transition temp. / temp. at 10% weight loss	SEM of melt electrospun morphologies	Fiber and sphere diameter histograms
16	M = 388.59 g·mol⁻¹ Cr 209 I T$_{sp}$=230 ° T$_{-10\ wt\%}$=350 °C		
17	M = 388.59 g·mol⁻¹ Cr₁ 79 Cr₂ 115 Cr₃ 190 Cr₄ 206 I T$_{sp}$=225 °C T$_{-10\ wt\%}$=345 °C		
18	M = 438.65 g·mol⁻¹ Cr₁ 72 Cr₂ 103 Cr₃ 232 I T$_{sp}$=260 °C T$_{-10\ wt\%}$=392 °C		
19	M = 394.63 g·mol⁻¹ Cr 271 I T$_{sp}$=290 °C T$_{-10\ wt\%}$=344 °C		

Table S4, continued.

20	C_8H_{17} structure $M = 394.63 \text{ g·mol}^{-1}$ Cr 85 I $T_{sp} = 110 °C$ $T_{-10 \text{ wt\%}} = 284 °C$		
21	C_8H_{17} structure $M = 394.63 \text{ g·mol}^{-1}$ Cr 255 I $T_{sp} = 275 °C$ $T_{-10 \text{ wt\%}} = 344 °C$		
22	C_8H_{17} structure $M = 394.63 \text{ g·mol}^{-1}$ Cr 70 I $T_{sp} = 100 °C$ $T_{-10 \text{ wt\%}} = 334 °C$		
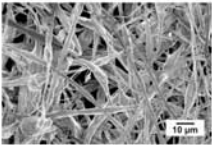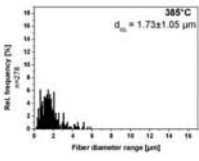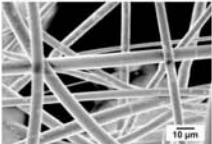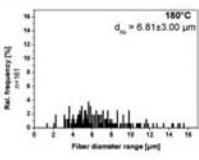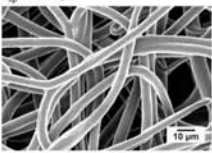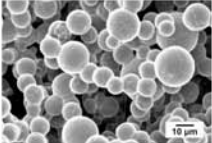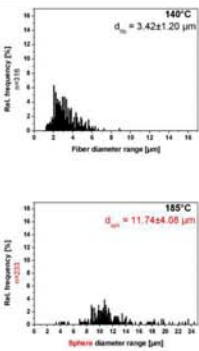
Table S5: *Sorbitole and nonitol derivatives* **23-25**.

(M: molecular weight; Cr: crystalline, Col: columnar mesophase, h: hexagonal, o: ordered liquid crystalline, I: isotropic, LC: liquid crystalline. Spinning parameters: voltage: -40 kV, distance needle tip to ground plate: 6 cm, flow rate: 200 µL h^{-1}, needle capillary ID: 0.6 mm, spinning temperature T$_{sp}$ as specified).

Entry	Chemical structure / phase transition temp. / temp. at 10% weight loss	SEM of melt electrospun morphologies	Fiber and sphere diameter histograms
23 DBS	M = 358.39 g·mol^{-1} Cr 225 I T$_{sp}$=245 °C T$_{-10\,wt\%}$=311 °C		
24 DMDBS	M = 414.49 g·mol^{-1} Cr 275 I T$_{sp}$=295 °C T$_{-10\,wt\%}$=340 °C		
25	M = 484.62 g·mol^{-1} Cr 245 I T$_{-10\,wt\%}$=329 °C	T$_{sp}$=245 °C T$_{sp}$= 265 °C	

Table S6: *Perylene bisimides* **26-28**.

(M: molecular weight; Cr: crystalline, Col: columnar mesophase, h: hexagonal, o: ordered liquid crystalline, I: isotropic, LC: liquid crystalline. Spinning parameters: voltage: -40 kV, distance needle tip to ground plate: 6 cm, flow rate: 200 mL h^{-1}, needle capillary ID: 0.6 mm, spinning temperature T_{sp} as specified).
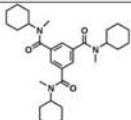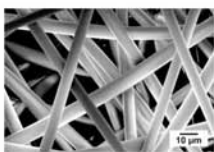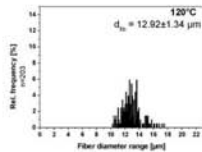
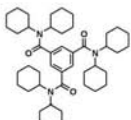| Entry	Chemical structure / phase transition temp. / temp. at 10% weight loss	SEM of melt electrospun morphologies	Fiber and sphere diameter histograms
26	$M = 614.77$ g·mol^{-1} Cr 220 LC 375 I $T_{sp}= 385$ °C $T_{-10\ wt\%} = 480$ °C		
27	$M = 811.14$ g·mol^{-1} Cr 163 I $T_{sp}=180$ °C $T_{-10\ wt\%}=410$ °C		
28	$M = 1123.24$ g·mol^{-1} Cr 64 Col$_{ho}$ 123 I $T_{-10\ wt\%}=376$ °C	$T_{sp}=140$ °C $T_{sp}= 185$ °C	

Table S7: *Tertiary benzenetrisamides **29-31** and POPEa.*

(M: molecular weight; Cr: crystalline, I: isotropic, T_g: glass transition temperature. Spinning parameters: voltage: - 40 kV, distance needle tip to ground plate: 6 cm, flow rate: 200 µL·h⁻¹, needle capillary ID: 0.6 mm, spinning temperature T_{sp} as specified).
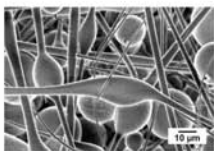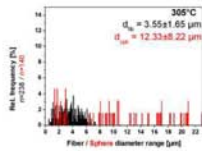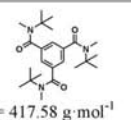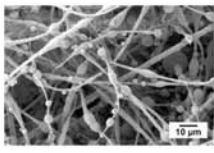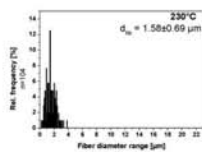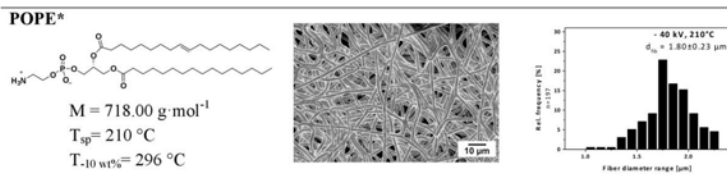
Entry	Chemical structure / phase transition temp. / temp at 10% weight loss	SEM of melt electrospun morphologies	Fiber and sphere diameter histograms
29	M = 495.70 g·mol⁻¹ glass: T_g= 65 °C T_{sp}= 140 °C $T_{-10\ wt\%}$=374 °C		
30	M = 700.05 g·mol⁻¹ Cr 295 I T_{sp}= 305 °C $T_{-10\ wt\%}$ = 400 °C		
31	M = 417.58 g·mol⁻¹ Cr 220 I T_{sp}= 230 °C $T_{-10\ wt\%}$= 289 °C		

Table S7, continued.

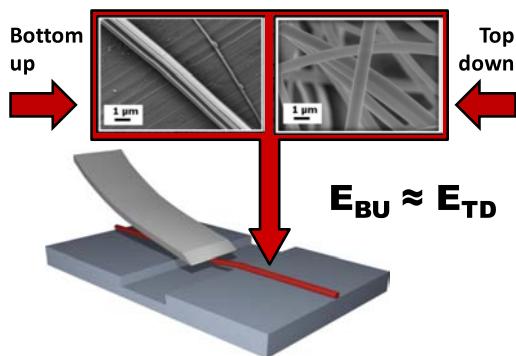| POPE*		
$M = 718.00 \text{ g·mol}^{-1}$ $T_{sp} = 210 \text{ °C}$ $T_{-10 \text{ wt%}} = 296 \text{ °C}$		

*1-palmitoyl-2-oleoyl-*sn*-glycerol-3-phosphoethanol-amine.

4.6 **Top-Down Meets Bottom-Up: A Comparison of the Mechanical Properties of Melt Electrospun and Self-Assembled 1,3,5-Benzenetrisamide Fibers ***

Keywords: 1,3,5-benzenetrisamides, melt electrospinning, self-assembly

Top–down meets bottom–up: A comparison of the mechanical properties of melt electrospun and self-assembled 1,3,5-benzenetrisamide fibers

Daniel Kluge [a,1,2], Julia. C. Singer [b,2], Benedikt R. Neugirg [a,1], Jens W. Neubauer [a,1], Hans-Werner Schmidt [b], Andreas Fery [a,*]

[a] Physical Chemistry II and Bayreuth Center for Colloids and Interfaces, University of Bayreuth, Universitaetsstrasse 30, D-95440 Bayreuth, Germany
[b] Macromolecular Chemistry I, Bayreuth Institute of Macromolecular Research and Bayreuth Center for Colloids and Interfaces, University of Bayreuth, Universitaetsstrasse 30, D-95440 Bayreuth, Germany

ARTICLE INFO

ABSTRACT

1,3,5-Benzenetrisamides (BTAs) are a prominent class of low-molecular weight compounds in supramolecular chemistry. They are well-known to self-assemble into micro- and nanofibers in a bottom–up approach. At the same time, BTAs are also suitable for top-down processing by melt electrospinning. In this work, we demonstrate for the first time that both approaches lead to mechanically robust BTA fibers. We compare self-assembled and electrospun fibers of N,N,N″-tripropyl-1,3,5-benzenetricarboxamide on multiple length scales. X-ray diffraction (XRD) reveals the same crystal structure independently from the preparation method. Using scanning electron microscopy (SEM), we observe significantly different morphologies of both fiber types on the sub-micron-scale. However, atomic force microscopy (AFM) bending experiments show that despite differences in morphology, Young's modulus is comparable for both types and in the lower GPa range (3–5 GPa). Thus, both top–down and bottom–up techniques with their complementary features in terms of accessible structures and potential applications are available for this class of materials.

© 2012 Elsevier Ltd. All rights reserved.

1. Introduction

The controlled fabrication of well-defined microscopic fibrillar structures has become one of the main topics in materials science [1–3]. Networks and nonwovens based on these structures possess exceptional properties, such as high surface area, possibility for easy functionalization and superior mechanical strength [4]. These are promising features for applications such as tissue engineering, drug delivery, sensors, micro-/nanoelectromechanical systems (MEMS/NEMS), and filtration [3–7]. Especially fibers of sub-micron or nanoscale diameters are of interest due to their surface to volume ratio and the possibility to form structures with small mesh-sizes. Two approaches are feasible to access these length scales: Bottom–up approaches rely on the self-assembly of smaller units (even single molecules) to hierarchical structures [8,9]. Top–down approaches, such as electrospinning, shape the materials directly into the desired structure. Especially for fibers and nonwovens, a great variety of structures has been demonstrated [10].

Both techniques are complementary in various ways: Since self-assembly allows simultaneous formation and growth of many fibers in a given volume, it is preferable in terms of processing times, especially for upscaling. In addition, if the processing conditions are chosen well, smaller fiber diameters are accessible in a more simple fashion than in electrospinning [9,11]. On the downside, self-assembled fibers have smaller length and random orientation since they grow from many nuclei.

The advantage of electrospinning is that fibers can easily be formed with macroscopic length and well-defined orientation on macroscopic length scales. This even allows the controlled formation of superstructures at the micrometer level and above. However, the processing times are longer since electrospinning is a sequential process, in which the time necessary to form fibers is proportional to the total fiber length.

To offer the highest flexibility, it would be desirable to switch from one to the other approach for the same class of materials — especially for the formation of hierarchically organized structures which span multiple length scales.

* Corresponding author. Tel.: +49 921 55 27 51; fax: +49 921 55 20 59.
  E-mail addresses: hans-werner.schmidt@uni-bayreuth.de (H.-W. Schmidt), andreas.fery@uni-bayreuth.de (A. Fery).
[1] Tel.: +49 921 55 27 51; fax: +49 921 55 20 59.
[2] Julia C. Singer and Daniel Kluge contributed equally to this work.

Lately, the self-assembly of 1,3,5-benzenetrisamides (BTAs) into fibrillar structures has attracted increasing research interest [12,13]. The benzene core realizes a planar and symmetric moiety and three amide groups allow the formation of strong hydrogen bonds between adjacent molecules resulting in supramolecular architectures [14]. BTAs are well-known as nucleating agents for polyvinylidene fluoride and polypropylene [15–18]. Moreover, they are applied as organo- and hydrogelators [19–22], as additives to improve the charge storage capability of electret materials [23] and as supramolecular materials [24,25].

In addition to their bottom–up properties, we recently reported on the melt electrospinning of various BTAs and 1,3,5-cyclohexanetrisamides into defined fine fibers with a narrow size distribution [26]. Although a high molecular mass polymer is not essential for obtaining uniform electrospun fibers [27], electrospinning of low molecular weight substances is still unusual. BTAs form macrodipoles along the main axis of the column during the supramolecular assembly process within external electric fields and consequently offer excellent pre-conditions for electrospinning [28–30]. The melt electrospinning of BTAs is an exciting new top–down approach for self-assembling systems. It offers the possibility to overcome the strict limitation of the self-assembly conditions and consequently opens up a wide field of new applications for BTAs.

For all applications, a reasonable mechanical stability is an essential prerequisite. However, regardless by which means the BTA fibers are prepared, the mechanical characterization on a micron- or sub-micron scale requires sophisticated methods. A powerful technique is nanomechanical bending experiments, which have been used for the mechanical investigation of polymer nanofibers [31–33], biological materials [34–38], CNTs [39,40], and nanowires [41–43]. In previous studies, we performed bending experiments on BTA micro- and nanofibers obtained via controlled self-assembly from nonpolar solvents. The experiments demonstrated that their molecular architecture allows control over the fiber morphology without decreasing their mechanical stability [44,45].

In this work, we address the question whether the properties of BTA fibers are affected by using a top–down approach instead of a bottom–up approach. For that purpose, we prepare fibers of the same 1,3,5-benzenetrisamide via self-assembly from solution and melt electrospinning. This allows us for the first time to compare crystal structure, morphology and nano-mechanical properties of BTA fibers prepared from the same material.

2. Results and discussion

For the comparison, we prepared fibers of N,N',N''-tripropyl-1,3,5-benzenetricarboxamide **1** (Scheme 1) via bottom–up (in the following termed SA-fibers) as well as top–down techniques (in
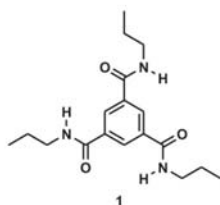
the following termed ES-fibers). The SA-fibers were produced via controlled self-assembly by cooling of a solution of **1** in 2,2,4,4,6,8,8-heptamethylnonane (HMN). As top–down approach, we used melt electrospinning.

In order to investigate structural features on the Ångström-scale, we performed XRD measurements on chopped fibers. The X-ray diffractograms of both systems are identical, indicating the same crystal structure (Fig. 1, see also Supplementary material S1). The peaks of the SA fibers show a narrower full width at half maximum, what is expected since a higher degree of crystallinity is typically achieved by the bottom–up process. Due to hydrogen bonds, **1** packs in a primitive cubic $[4^6]$-pcu supramolecular three-dimensional network. The molecules are located in planes, which are stacked along the c axis [46]. While it is on first glance surprising that the electrospun material shows an as well-developed crystalline order as the self-assembled material, we demonstrated in previous work that ES-fibers are not formed from a molecular liquid state but from a melt which still consists of short columnar pre-aggregates [26,47]. Thus the crystallization process is greatly accelerated due to the pre-aggregation of single molecules and leads to a poly-crystalline state.

The microscopic morphology of the fibers was investigated via SEM. The average diameter of the SA- and ES-fibers, respectively, was $1.2 \pm 0.7\ \mu m$ and $0.8 \pm 0.2\ \mu m$ (size distribution diagrams see S2 and S3). Although the diameters of SA- and ES-fibers are comparable, the morphology of both systems shows significant differences. SA-fibers possess a hierarchical structure: they consist of bundles of individual strands that have an average diameter of about 100 nm (see inset of Fig. 2, top, left). This bundle substructure is also visible in the irregular fracture sections of the SA-fibers (Fig. 2, top, right). In contrast, ES-fibers exhibit a homogenous, smooth surface without defects or pronounced surface features (Fig. 2, bottom, left). Even fracture sections of the ES-fibers are very smooth without any detailed sub-structure or obvious defects (Fig. 2, bottom, right).

These differences in the microscopic morphology arise from the significantly different methods used to generate the two investigated fiber types. The crystallization process of the SA-fibers is much slower, allowing the development of larger crystals which then bundle into fibers. This explains the broader diameter distribution found for SA-fibers. In contrast, during electrospinning, ES-fibers are obtained from molten material, resulting in a homogenous strand.

Scheme 1. Chemical structure of N,N',N''-tripropyl-1,3,5-benzenetricarboxamide (**1**).
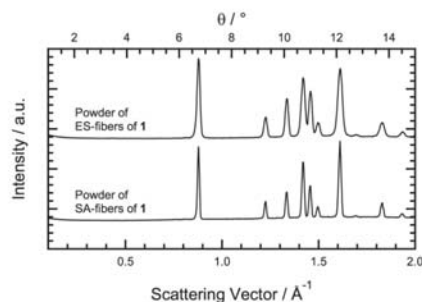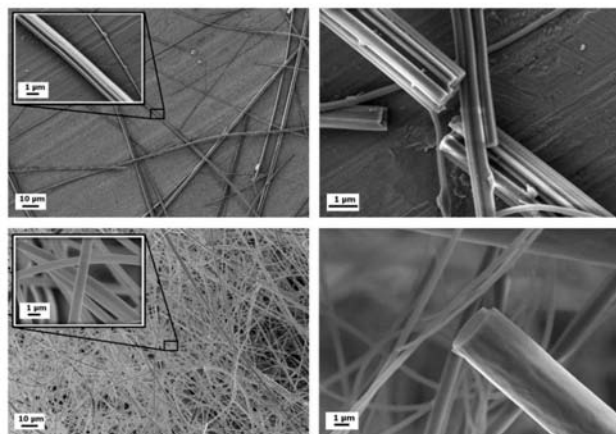

Fig. 1. X-ray diffractograms of SA- and ES-fibers in powder form.

Fig. 2. Top: SEM micrograph of the SA-fibers (left) and of a fracture section (right). Bottom: SEM micrograph of the ES-fibers of **1** (left) and of a fracture section (right). More detailed structures of the fibers are shown in the insets.

In order to evaluate the mechanical properties of both systems, we performed nanomechanical bending experiments using an atomic force microscope (AFM). A detailed description of the theoretical background and experimental procedures can be found elsewhere [44]. Both fiber types were transferred to micro-structured glass substrates (Fig. 3) to achieve a free-standing configuration (Fig. 4a). In this configuration, no deformation was observed when applying a vertical load to the segments supported by the substrate (Fig. 4b). Therefore, only bending deformations are measured when applying a load to the free-standing segments over the gap and the results can be evaluated with classical beam theory [48].

We recorded stiffness profiles by measuring the stiffness $k(x)$ at several positions x along the free-standing segment (Fig. 4c) and calculated Young's modulus E of each investigated segment by fitting the profiles with the double-clamped beam model (Equation (1)) [42,44,48].

$$k(x) = \frac{3L^3 EI}{(L-x)^3 x^3} \qquad (1)$$

Here, L is the length of the free-standing segment and I is the area moment of inertia. We imaged each investigated sample with

the AFM to obtain the correct fiber thickness and shape to avoid errors as I shows quartic scaling with the radius.

Since Young's modulus is a material property, it is possible to normalize the profiles of all investigated SA- and ES-fibers, respectively, to calculate the averaged values [45]. The resulting Young's moduli were $E_{SA} = 3.6 \pm 0.4$ GPa and $E_{ES} = 4.7 \pm 0.6$ GPa (see S4 for more detailed data). In addition, we calculated the modulus of each fiber individually and determined the distributions (Fig. 4d). While the ES-fibers show a slightly higher average modulus than the SA-fibers, the distributions are similar for both systems. We also investigated if shearing affects the measurements, but found no influence (see S5).

Our experiments show that the moduli of SA- and ES-fibers are in the same range and comparable to those of (semi) crystalline or glassy polymers like PVC and PMMA, common fiber materials like nylon and electrospun collagen fibers [33,49]. The elastic properties of the fibers are also in good agreement with BTAs with different molecular structure where Young's moduli between 2 and 4 GPa have been observed [44,45]. In order to understand the mechanical similarity of these morphologically quite different SA- and ES-fibers, one has to look at the underlying principles behind the mechanics. In both systems, intermolecular hydrogen bonds and π-
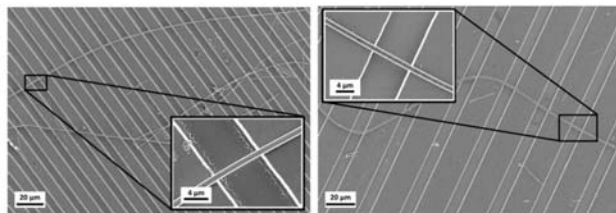
Fig. 3. SA-fibers (left) and ES-fibers (right) on micro structured glass substrates for AFM bending experiments.
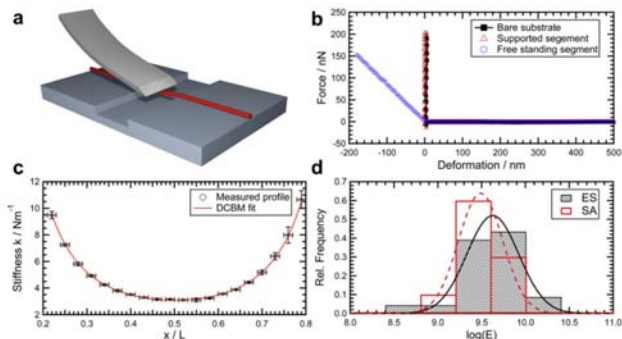
Fig. 4. a) Schematic setup of the bending experiments. b) Force-deformation measurements on bare glass substrates (black squares), substrate-supported (red triangles) and free-standing segments (blue circles) of ES-fibers. c) Stiffness profile of a free-standing ES-fiber segment fitted with the DCBM. d) Distribution of the Young's moduli of SA-fibers (open bars, dashed line) and ES-fibers (hatched bars, solid line). (For interpretation of the references to color in this figure legend, the reader is referred to the web version of this article.)

stacking are responsible for the formation and cohesion of the fibers. Likewise, the ensemble of these noncovalent interactions determines the response to mechanical stresses. Therefore, despite differences in their morphology, it is reasonable that SA- and ES-fibers posses comparable elastic properties. Although the distributions of the moduli are rather broad, we observed a tendency toward a slightly lower modulus of the SA-fibers compared to the ES-fibers. This can be explained by their bundle-substructure which is more likely prone to defects. However, the effect is small and within the range of sample deviations and the error of the measurements. The important finding is that both fiber types show a remarkable mechanical stability despite the small molecule size and the absence of covalent interactions.

3. Conclusions

In this study we demonstrated for the first time that mechanically robust BTA fibers can be accessed via bottom–up- and top–down-approaches. We prepared self-assembled (SA) and melt electrospun (ES) fibers from the same compound **1** and obtained fibers with an average diameter of 1.2 ± 0.7 μm and 0.8 ± 0.2 μm for SA- and ES-fibers, respectively. On the Ångström-scale, XRD measurements show the same crystal structure of the fibers, independently of the preparation method. On the microscopic scale, SEM measurements however clearly revealed morphological differences: The self-assembled fibers possessed a hierarchical structure, consisting of firmly connected bundles of individual strands, while melt electrospun fibers showed a smooth and homogenous structure. AFM bending experiments, which probe the mechanical behavior on the length scale of the whole assembly, revealed that Young's modulus E was not significantly affected by changing the preparation process. While the order of magnitude and distributions of the moduli were comparable, the average values suggested that E_{SA} (3.6 ± 0.4 GPa) was slightly lower than E_{ES} (4.7 ± 0.6 GPa) due to the bundle-substructure of the SA-fibers which is more likely prone to defects. However, the difference was small and within the error range of measurements. Still, our results prove that mechanically robust BTA fibers can be obtained by bottom–up as well as top–down approaches.

These findings open interesting perspectives for structure formation from BTAs. First, the relatively high elastic constants in the lower GPa range that are found for both approaches demonstrate that the fibrillar structures are mechanically robust regardless of how they are formed, qualifying them as a platform for hierarchical structure formation. Second, the results show that BTAs are shapeable into fibers with both approaches. This is interesting, since bottom–up and top–down approaches have complementary advantages and disadvantages, as discussed in the introduction. Now with this system, the best of the bottom–up and top–down approaches can be combined for one materials class and used for creating hierarchically structured nonwovens for example for filter applications.

4. Experimental section

4.1. Material

N,N′,N″-tripropyl-1,3,5-benzenetricarboxamide **1** was synthesized according to the literature [50]. The melting temperature of **1** is 289 °C and was determined in a Perkin Elmer Diamond DSC (heating rate: 10 K/min, nitrogen flow: 20 mL/min). The temperature at a 10% weight loss was 351 °C. The measurement was performed in a Mettler SDTA 851 TGA at 10 K/min (nitrogen flow: 60 mL/min). Isothermal TGA runs under nitrogen atmosphere were performed to verify the thermal stability of **1** during the period of the electrospinning process. **1** shows a weight loss below 5 wt.% for 55 min.

4.2. SA-fiber preparation

In 2,2,4,6,8,8-heptamethylnonane (HMN) 600 ppm of **1** were dissolved under reflux at 240 °C and cooled to room temperature. To ensure a controlled self-assembly behavior, 200 μL of the suspension were heated in a custom designed high pressure pan to 240 °C for 10 min in the Dropping Point Cell FP83HT from METTLER TOLEDO followed by cooling to 30 °C with 5 K/min (controlled with the METTLER TOLEDO Central Processor FP90). For the bending experiments, identical structured glass substrates were wetted

with 10 μL of blank HMN, 0.5 μL of the fiber suspension were added and the samples were allowed to dry overnight.

4.3. ES-fiber preparation

The melt electrospinning experiments were carried out as described elsewhere [26]. **1** was equilibrated in a syringe with an inner needle diameter of 0.6 mm for 3 min at its melting point at 290 °C (temperature of the heated cylinder around the syringe body in the melt electrospinning set-up) before applying high voltage of −30 kV. The distance between needle tip and collector was 6 cm and the feeding rate 500 μL/h. The electrospun material was collected on a single 12 mm diameter aluminum SEM stub with a carbon tab which was mounted on top of the collector plate. The melt electrospinning experiment was carried out during 15 min. For the bending experiments, the fibers were transferred to structured glass substrates (GeSiM GmbH, Grosserkmannsdorf, Germany; channel widths 20, 30 and 40 μm, respectively) by gently bringing the SEM stub and the substrates in contact.

4.4. XRD-measurements

The XRD-measurements in the angle range of $\theta = 0.5° - 15°$ were carried out on a Huber Guinier diffractometer 600. To get Cu $K_{\alpha 1}$ radiation ($\lambda = 154.051$ pm) it is equipped with a Huber germanium monochromator 61. An extra slit diaphragm reduces the broadening of the primary beam due to scattering in air. The samples were prepared in soda glass capillaries (1.5–2 mm diameter) from powder.

4.5. Scanning electron microscopy

For preparation of the SA-fiber SEM samples, 5 μL of the HMN-suspension was put in aluminum pans and the solvent was evaporated under reduced pressure. ES-fibers of **1** were directly spun onto a SEM specimen stub with a carbon tab. All samples were sputtered with platinum (2.0 nm) in a Cressington sputter coater 208HR. The SEM micrographs were recorded on a Zeiss ULTRA plus FESEM (Zeiss, Jena, Germany). To obtain a reliable size distribution, 250 individual SA- and ES-fibers, respectively, were evaluated using AxioVision LE Software (Carl Zeiss AG, Germany). The histograms can be found in the Supplementary material S2 and S3.

4.6. AFM measurements

All AFM measurements were performed on a Nanowizard I (JPK Instruments AG, Berlin, Germany). The bending experiments were performed as previously reported [44]. Details about the used cantilever types and applied loads can be found in the Supplementary material S6.

Acknowledgments

Appendix A. Supplementary data

Supplementary data related to this article can be found, in the online version, at http://dx.doi.org/10.1016/j.polymer.2012.10.016.

References

[1] Xia YN, Yang PD, Sun YG, Wu YY, Mayers B, Gates B, et al. Advanced Materials 2003;15(5):353–89.
[2] Kuttner C, Tebbe M, Schlaad H, Burgert I, Fery A. ACS Applied Materials & Interfaces 2012;4:3485–92.
[3] Agarwal S, Wendorff JH, Greiner A. Polymer 2008;49(26):5603–21.
[4] Jayaraman K, Kotaki M, Zhang YZ, Mo XM, Ramakrishna S. Journal of Nanoscience and Nanotechnology 2004;4(1–2):52–65.
[5] Moriarty P. Reports on Progress in Physics 2001;64(3):297–381.
[6] Barhate RS, Ramakrishna S. Journal of Membrane Science 2007;296(1–2): 1–8.
[7] Lutolf MP, Hubbell JA. Nature Biotechnology 2005;23(1):47–55.
[8] Palmer LC, Stupp SI. Accounts of Chemical Research 2008;41(12):1674–84.
[9] Kimizuka N. Self-assembly of supramolecular nanofibers. In: Shimizu T, editor. Self-assembled nanomaterials I: nanofibers, vol. 219. Berlin: Springer-Verlag Berlin; 2008. p. 1–26.
[10] Greiner A, Wendorff JH. Angewandte Chemie-International Edition 2007; 46(30):5670–703.
[11] Hutmacher DW, Dalton PD. Chemistry-an Asian Journal 2011;6(1):44–56.
[12] Filot IAW, Palmans ARA, Hilbers PAJ, van Santen RA, Pidko EA, Greef TFA. The Journal of Physical Chemistry B 2010;114(43):13667–74.
[13] Kristiansen M, Smith P, Chanzy H, Baerlocher C, Gramlich V, McCusker L, et al. Crystal Growth & Design 2009;9(6):2556–8.
[14] Lightfoot MP, Mair FS, Pritchard RG, Warren JE. Chemical Communications 1945–1946;1999(19).
[15] Abraham F, Schmidt H-W. Polymer 2010;51(4):913–21.
[16] Abraham F, Ganzleben S, Hanft D, Smith P, Schmidt H-W. Macromolecular Chemistry & Physics 2010;211:171–81.
[17] Blomenhofer M, Ganzleben S, Hanft D, Schmidt H-W, Kristiansen M, Smith P, et al. Macromolecules 2005;38(9):3688–95.
[18] Schmidt M, Wittmann JJ, Kress R, Schneider D, Steuernagel S, Schmidt HW, et al. Crystal Growth & Design 2012;12(5):2543–51.
[19] Yasuda Y, Iishi E, Inada H, Shirota Y. Chemistry Letters 1996;7:575–6.
[20] Hanabusa K, Koto C, Kimura M, Shirai H, Kakehi A. Chemistry Letters 1997;5: 429–30.
[21] Kumar DK, Jose DA, Dastidar P, Das A. Chemistry of Materials 2004;16(12): 2332–5.
[22] Bernet A, Behr M, Schmidt H-W. Soft Matter 2011;7(3):1058.
[23] Mohmeyer N, Behrendt N, Zhang X, Smith P, Altstädt V, Sessler GM, et al. Polymer 2007;48(6):1612–9.
[24] Roosma J, Mes T, Leclere P, Palmans ARA, Meijer EW. Journal of the American Chemical Society 2008;130(4):1120–1.
[25] Mes T, Smulders MMJ, Palmans ARA, Meijer EW. Macromolecules 2010;43(4): 1981–91.
[26] Singer JC, Giesa R, Schmidt H-W. Soft Matter 2012;8:9972–6.
[27] Hunley MT, McKee MG, Gupta P, Wilkes GL, Long TE. MRS Proceedings 2006; 948.
[28] Sakamoto A, Ogata D, Shikata T, Urakawa O, Hanabusa K. Polymer 2006;47(4): 956–60.
[29] Tomatsu I, Fitié CFC, Byelov D, Jeu WH, Magusin PCMM, Wübbenhorst M, et al. The Journal of Physical Chemistry B 2009;113(43):14158–64.
[30] Kulkarni C, Reddy SK, George SJ, Balasubramanian S. Chemical Physics Letters 2011;515(4–6):226–30.
[31] Tan EPS, Lim CT. Applied Physics Letters 2004;84(9):1603–5.
[32] Shin MK, Kim SI, Kim SJ, Kim S-K, Lee H. Applied Physics Letters 2006;88(19): 193901–3.
[33] Yang L, Fitie CFC, van der Werf KO, Bennink ML, Dijkstra PJ, Feijen J. Biomaterials 2008;29(8):955–62.
[34] Xu W, Mulhern PJ, Blackford BL, Jericho MH, Templeton I. Scanning Microscopy 1994;8(3):499–506.
[35] Kis A, Kasas S, Babic B, Kulik AJ, Benoit W, Briggs GAD, et al. Physical Review Letters 2002;89(24):4.
[36] Guzman C, Jeney S, Kreplak L, Kasas S, Kulik AJ, Aebi U, et al. Journal of Molecular Biology 2006;360(3):623–30.
[37] Orso S, Wegst U, Arzt E. Journal of Materials Science 2006;41(16):5122–6.
[38] Stamov DR, Nguyen TAK, Evans HM, Pfohl T, Werner C, Pompe T. Biomaterials 2011;32(30):7444–53.
[39] Wong EW, Sheehan PE, Lieber CM. Science 1997;277(5334):1971–5.
[40] Salvetat JP, Briggs GAD, Bonard JM, Bacsa RR, Kulik AJ, Stockli T, et al. Physical Review Letters 1999;82(5):944–7.
[41] Wu B, Heidelberg A, Boland JJ. Nature Materials 2005;4:525–9.
[42] Chen YX, Dorgan BL, McIlroy DN, Aston DE. Journal of Applied Physics 2006; 100(10):104301.
[43] Zhang H, Tang J, Zhang L, An B, Qin LC. Applied Physics Letters 2008; 92(17):3.
[44] Kluge D, Abraham F, Schmidt S, Schmidt HW, Fery A. Langmuir 2010;26(5): 3020–3.

[45] Kluge D, Singer JC, Neubauer JW, Abraham F, Schmidt H-W, Fery A. Small 2012;8(16):2563–70.

[46] Jimenez CA, Belmar JB, Ortiz L, Hidalgo P, Fabelo O, Pasan J, et al. Crystal Growth & Design 2009;9(12):4987–9.

[47] Timme A, Kress R, Albuquerque RQ, Schmidt H-W. Chemistry – A European Journal 2012;18(27):8329–39.

[48] Gere JM, Goodno BJ. Mechanics of materials. 7th ed. Toronto: Cengage Learning; 2008.

[49] Brandrup J, Immergut EH, Grulke EA, Abe A, Bloch DR. In: Polymer handbook, vol. 1. Hoboken, New Jersey: John Wiley & Sons, Inc; 1999. p. V/162–7.

[50] Schmidt H-W, Smith P, Blomenhofer M. In: Inc. CSCH, editor. vol. WO 02/46300 A2, 2002.

Top-down meets bottom-up: A comparison of the mechanical properties of melt electrospun and self-assembled fibers of 1,3,5-benzenetrisamide.

Daniel Kluge,[‡,§] Julia. C. Singer,[‡,§] Benedikt Neugirg,[‡] Jens W. Neubauer,[‡] Hans-Werner Schmidt,[,†]*

Andreas Fery[,‡]*

[‡] Physical Chemistry II and Bayreuth Center for Colloids and Interfaces; University of Bayreuth, Universitaetsstrasse 30, D-95440 Bayreuth (Germany)
E-mail: andreas.fery@uni-bayreuth.de

[†] Macromolecular Chemistry I, Bayreuth Institute of Macromolecular Research and Bayreuth Center for Colloids and Interfaces; University of Bayreuth, Universitaetsstrasse 30, D-95440 Bayreuth (Germany)
E-mail: hans-werner.schmidt@uni-bayreuth.de

[§] Julia C. Singer and Daniel Kluge contributed equally to this work.
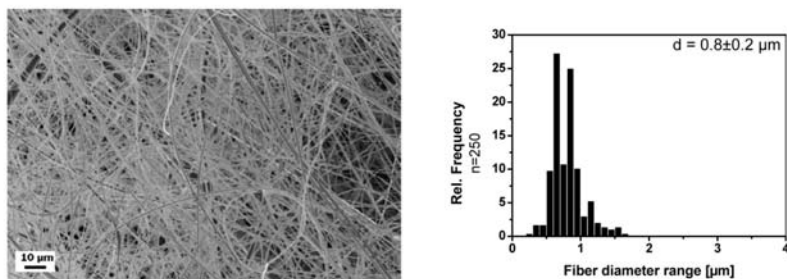
Supplementary material
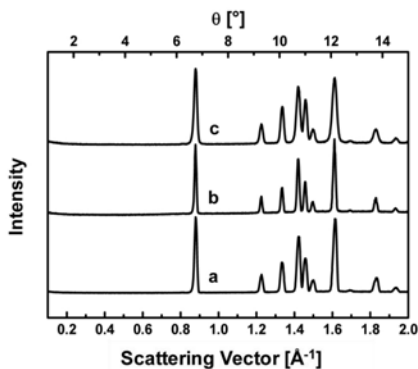
Figure S1. X-ray diffractograms of **1**: a) powder obtained by recrystallization from dimethylformamide; b) powdery self-assembled fibers and c) powdery melt electrospun fibers.
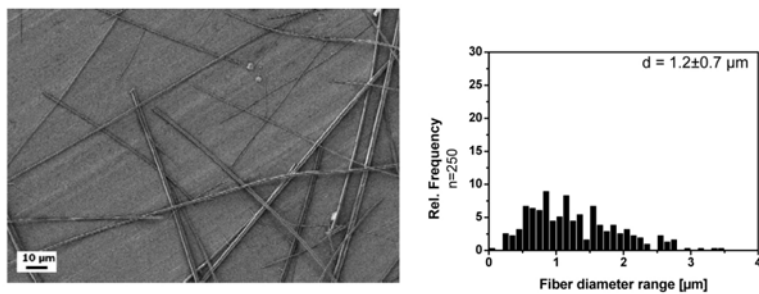
Figure S2. SEM image and histogram of self-assembled fibers of **1**, obtained by self-assembly from 2,2,4,4,6,8,8-heptamethylnonane (600 ppm of **1**).

Figure S3. SEM image and histogram of melt electrospun fibers of **1**. Spinning parameters: applied voltage: -30 kV; temperature: 290°C; flow rate: 500 µL/h; distance needle tip – ground plate: 6 cm; needle ID: 0.6 mm.
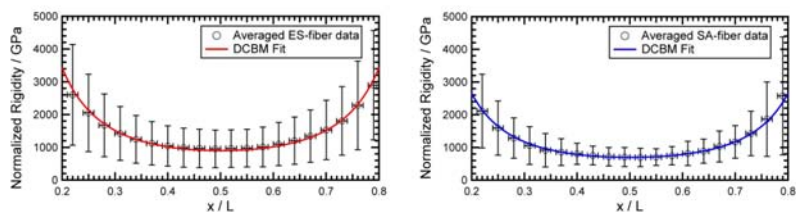
Figure S4. Evaluation of all normalized ES-fiber and SA-fiber bending profiles and fit with the double clamped beam model. Detailed information about the normalization procedures can be found in Kluge et al., *Small*, **2012**, 8 (16): 2563-2570.
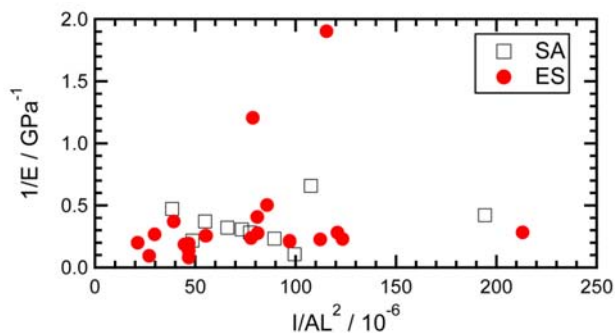
Figure S5. Shearing influence. More details on the theoretical background of the shearing investigation can be found in e.g. in Yang et al., *Biomaterials*, **2008**, 29 (8): 955-962 and Kluge et al., *Small*, **2012**, 8 (16): 2563-2570. Briefly, if shearing occurs, the apparent measured modulus decreases with increasing ratio of fiber thickness to fiber length. Therefore, one would expect to see a linear increase in the plot of $1/E$ versus I/AL^2 (where the second is a measure for the thickness-to-length ratio for fibers with arbitrary cross sections). Since we found no such dependence, we can conclude that shearing does not significantly affect our measurements

S6. Experimental parameters of the AFM measurements. For the bending experiments, we used tipless NSC12/AlBS cantilevers (μMasch, Tallinn, Estonia). The typical loads were 50 nN (SA-fibers) and 150 nN (ES-fibers), which resulted in typical deformations of 100 nm (SA-fibers) and 200 nm (ES-fibers) at the midpoint of the free standing segment. In addition, force-distance measurements with a maximum load of 50 nN (SA-fibers) and 150 nN (ES-fibers) were performed on sample segments supported by the substrate to proof that there was no unwanted compression of the fibers during the bending experiments. The systems showed no unwanted compression under the tested loads. The dimensions of the mechanically investigated samples were determined on the segments supported by the substrates in intermittent contact mode with sharp imaging cantilevers (Olympus OMCL-AC160TS, Atomic Force, Mannheim, Germany). All data was processed and evaluated using self-written procedures in Igor Pro 6 (Wavemetrics Inc., Portland, USA). For the calculation of Young's modulus, the data from 10 free-standing segments on a total of 9 SA-fibers and 23 segments on a total of 18 ES-fibers and were used.

Danksagung

An dieser Stelle möchte ich mich herzlich bei allen Personen bedanken, die mich bei der Erstellung dieser Arbeit unterstützt haben.

Mein besonderer Dank gilt meinem Doktorvater Herrn Prof. Dr. Schmidt für die interessante Aufgabenstellung, die hervorragende Betreuung dieser Arbeit und die Freiheit, die Arbeit nach eigener Vorstellung zu entwickeln. Seine stetige Diskussionsbereitschaft, seine zahlreichen Anregungen, seine Motivation sowie seine Wertschätzung trugen maßgeblich zum Gelingen dieser Arbeit bei. Dank meines perfekt ausgestatteten Arbeitsplatzes konnte ich jederzeit begeistert arbeiten und forschen.

Meinen Mentoren im Promotionsprogramm „Polymer Science", Professor Dr. Andreas Fery und Professor Dr. Stephan Förster, danke ich herzlichst für die vielen wissenschaftlichen Diskussionen, ihre Motivation und die erfolgreiche Bearbeitung von gemeinsamen Forschungsprojekten.

Großer Dank gebührt vor allem Herrn Dr. Reiner Giesa für seine bemerkenswerte Unterstützung, sowie für die vielen hilfreichen Denkanstöße und sein großes Vertrauen in meine Arbeit. Danke, dass du mir immer mit Rat und Tat zur Seite stehst.

Liebe Petra, vielen Dank für dein immer offenes Ohr und deine tolle Unterstützung bei allen administrativen und organisatorischen Fragen.

Jutta Failner, Sandra Ganzleben, Doris Hanft und Rika Schneider danke ich für ihre unermüdliche Hilfsbereitschaft, die gute und engagierte Zusammenarbeit im Labor und für die Synthesen der Verbindungen.

Mein weiterer Dank gilt Alexander Kern, der für jedes Computer- und Software-Problem eine Lösung fand und bei schweren Arbeiten immer kräftig zupackte.

Für die Aufnahme von 8995 (!) Bildern habe ich viele Stunden dieser Arbeit am Rasterelektronenmikroskop verbracht. Für dessen Wartung, ihren unermüdlichen Einsatz und die wertvollen Tipps und Tricks möchte ich mich herzlich beim REM-Team, Dr. Beate Förster, Martina Heider und Werner Reichstein, bedanken.

Des Weiteren danke ich allen Mitarbeitern des Lehrstuhls Makromolekulare Chemie I für die zahlreichen Anregungen, die immerwährende Hilfsbereitschaft und die schönen gemeinsamen Aktivitäten. Vielen Dank für die vertraute Arbeitsatmosphäre!

Ein besonderer Dank geht an Dr. Klaus Kreger, der durch seine fundierte Expertise und Erfahrung immer weiterhelfen und unterstützen konnte.

Ein großer Dank gebührt auch Dr. Cosima Freiin von Salis-Soglio und Roman Kress, die mir v.a. zu Beginn der Promotion jeder Zeit mit Rat und Tat zur Seite standen und auf deren Forschungsergebnisse ich aufbauen konnte.

Besonders meinen Laborkollegen Doris Hanft, Astrid Rauh, Dr. Kai Claussen, Steffen Czich, Andreas Schedl und Dr. Andreas Timme danke ich für die konstruktive und fröhliche Zusammenarbeit, den freundschaftlichen Umgang und den regen Austausch.

Meinen ehemaligen Studenten Leonard Kaps, Alexander Daniel, Benedikt Neugirg, Georg Schlageter, Christoph Zehe, Sarah Jessl, Miriam Mauer, Mareike Stenglein und Katharina Jörg, danke ich für ihre Mitarbeit auf meinem Themengebiet im Rahmen von Mitarbeiterpraktika.

Ein großer Dank gilt Daniel Kluge für die außerordentlich tolle und entspannte Zusammenarbeit in gemeinsamen Forschungsprojekten und für die daraus entwickelte gute Freundschaft.

Bei der Deutschen Forschungsgemeinschaft (DFG) möchte ich mich für die finanzielle Unterstützung meiner Arbeit und die großzügige Bereitstellung von finanziellen Mitteln zur Bearbeitung des Sonderforschungsbereichs 840, Teilprojekt B8 „Struktur-Eigenschaftskorrelation und Anwendung von faserförmigen Nanoaggregaten und Nanofasernetzwerken" herzlich bedanken.

Besonders möchte ich mich auch beim Elitestudiengang „Macromolecular Science" innerhalb des Elitenetzwerks Bayern (ENB) für die Finanzierung meines Auslandsaufenthalts bedanken. Dr. Andreas Bernet und Christina Wunderlich gebührt größter Dank für die Organisation und Koordination der interessanten Seminare und Workshops, sowie für die schnelle Erledigung aller administrativen Arbeiten.

Danke darf ich auch meinen Freunden sagen, die immer für mich da sind und mir beim Sport und Weggehen den nötigen Ausgleich zur Arbeit geben. Schön, dass es euch gibt!

Ein großes Dankeschön gebührt meiner Familie. Ihr unterstützt mich auf jede erdenkliche Art und Weise, motiviert mich, glaubt an mich und gebt mir immer den nötigen Rückhalt, damit ich meine Ziele erreichen kann. Ich hab euch lieb!

Lieber Kevin, für dein Lachen, für die Kraft, die du mir gibst, für das Ertragen meiner Launen, für deine Motivation, für deine Liebe - Danke!

(Eidesstattliche) Versicherungen und Erklärungen

Promotionsordnung (PromO) der Bayreuther Graduiertenschule für Mathematik und Naturwissenschaften (BayNAT) vom 20. März 2014.

(§ 8 S. 2 Nr. 6 PromO)

Hiermit erkläre ich mich damit einverstanden, dass die elektronische Fassung meiner Dissertation unter Wahrung meiner Urheberrechte und des Datenschutzes einer gesonderten Überprüfung hinsichtlich der eigenständigen Anfertigung der Dissertation unterzogen werden kann.

(§ 8 S. 2 Nr. 8 PromO)

Hiermit erkläre ich eidesstattlich, dass ich die Dissertation selbständig verfasst und keine anderen als die von mir angegebenen Quellen und Hilfsmittel benutzt habe.

(§ 8 S. 2 Nr. 9 PromO)

Ich habe die Dissertation nicht bereits zur Erlangung eines akademischen Grades anderweitig eingereicht und habe auch nicht bereits diese oder eine gleichartige Doktorprüfung endgültig nicht bestanden.

(§ 8 S. 2 Nr. 10 PromO)

Hiermit erkläre ich, dass ich keine Hilfe von gewerbliche Promotionsberatern bzw. -vermittlern in Anspruch genommen habe und auch künftig nicht nehmen werde.

Bayreuth, den 22. Juli 2014

Julia Singer

This thesis focuses on the preparation, characterization and comparison of supramolecular nano- and microfibers of 1,3,5-benzene- and 1,3,5-cyclohexanetrisamides using two routes: self-assembly from solution as bottom-up approach and melt electrospinning as top-down approach.

The results of this thesis reveal that trisamides can be shaped into nano- and microfibers using powerful bottom-up and top-down approaches. Their interesting morphology combined with their mechanical properties make this class of low molecular weight substances suitable for constructing new materials.